

Crosstalk between Drp1 phosphorylation sites during mitochondrial dynamics and metabolic adaptation

Présentée le 9 octobre 2020

à la Faculté des sciences de la vie
Programme doctoral en approches moléculaires du vivant

pour l'obtention du grade de Docteur ès Sciences

par

Miriam VALERA ALBERNI

Acceptée sur proposition du jury

Prof. V. Simanis, président du jury
Dr C. Canto Alvarez, Prof. E. Meylan, directeurs de thèse
Prof. B. Kornmann, rapporteur
Dr T. Wai, rapporteur
Prof. G. D'Angelo, rapporteur

“It’s like in the great stories, Mr. Frodo. The ones that really mattered. Full of darkness and danger they were. And sometimes you didn’t want to know the end. Because how could the end be happy? How could the world go back to the way it was when so much bad had happened? But in the end, it’s only a passing thing, this shadow. Even darkness must pass. A new day will come. And when the sun shines it will shine out the clearer. Those were the stories that stayed with you. That meant something, even if you were too small to understand why. But I think, Mr. Frodo, I do understand. I know now.

Folk in those stories had lots of chances of turning back, only they didn’t. They kept going, because they were holding on to something.

That there is some good in this world, and it’s worth fighting for.”

— Samwise Gamgee’s Speech in *The Lord of the Rings: The Two Towers*, J. R. R. Tolkien

Acknowledgements

The work of this thesis would have been impossible without so the support of many people. First of all, special thanks to the one-and-only Carles, for being the best boss any PhD could wish for. Words will never make justice for how immensely honored I am that I got the chance of pursuing this PhD adventure with you as my supervisor. For all the great advices, great scientific and non-scientific chats, for all the laughs while on ChroMe retreats, for all the memories, gràcies. Thank you for all the mentorship and for helping me becoming a better scientist. Moltes gràcies!

While Carles helped me to think like a scientist, Magali helped me to work like a scientist. Merci, merci et mille mercis Magali, pour toute la patience, pour tous les bons conseils, pour l'assistance pratique pour les expériences scientifiques, et pour le soutien moral que tu m'as donné, surtout lors de ces difficiles derniers mois. Sans toi et sans Carles, ni le projet Drp1 ni moi-même ne seraient dans le bon état dans lequel nous sommes aujourd'hui. Vos conseils resteront toujours avec moi. Moreover, this PhD experience has been extra especial thanks to our incredible Metabolic Sensing group. To the rest of the Canto team, you are my scientific family and I am very fortunate I had the chance to witness the amazing people you are. To Asia, who not only was a role model when she was in the lab but also helped me with with any question I had after she left. To Angelique, oh girl, this ride would not have been the same without you! Thank you for always willing to lend an ear to my issues and for your moral support. To Eleonora, Marie, Sameer and all past members of the Canto team, thank you so much for nourishing our amazing group towards a fun, helping and happy team!

Going to the institute every day was a blessing because of all the amazing people I had the chance of interacting with. Starting with my favorite PhD warriors. AK and Phillip, we started this adventure together like naïve students during the EDMS PhD hiring days, and (ay!) the trip has been bumpy, but we have come so far! To Margie, for being the most resilient kick-ass scientist and human being. Together with AK and Angelique, our “Coffee sessions” group will always have a special place in my heart. To Christopher, for making every chat a funny moment. To Katia, Caterina, Isabelle, Tanja and every other PhD that made our amazing PhD community even though circumstances were sometimes very challenging. Special thanks to all the colleagues and friends from NIHS. À Steve, qui est un autre membre du groupe Canto. To Maria, Robin, Matthew and all the incredible people who are continuously providing PhD students great advice on science, life and, literally, any issue.

I would also like to acknowledge our collaborators from NIHS and the Lausanne universities that helped me build up this astonishing research story. To Roy Combe, José-Luis Sanchez Garcia, and the rest of the EPFL Animal Facility caretakers, for helping with the mouse experiments. To Jean Daraspe, from UNIL, who provided critical assistance for the imaging of the mouse tissues. To Jessica and Gianni, for their help with histology. To Tatiana Dubi, who is the backbone of our doctoral programs and has an iron patience.

Moving on, my heart has a special place for all my ChroMes. ESRs, PIs and other mentors. To CJ, for making us the amazing family we are today. We started talking about science and now we come to cherish life events with one another, like weddings and baby births. I am extremely thankful to Joan, Jordi, Sandra and Oscar for welcoming me to their group and teaching me metabolomics. To the Munich team, ChroMes Iva and Haris, you guys are so amazing! To Flavia, who helped me to master the art of making mitochondria look beautiful and with whom I truly enjoyed discussing about mitochondria. Special thanks to Laura, Berta and Paula, for being wonderful friends with whom to share the ChroMe adventure!

I would like to express my deepest gratitude to my Ohana. We first met 10 years ago and now you are my family. Regardless of where in the globe, we stay truly united and we are always counting on each other for everything. To Alejandra, Lucy and Alba.... the best video entertainers to the endless lab practices during the bachelor. To Jose, our lovely panda, who is also an amazing cook (though curry much?). To Alejandro, for always making me smile. To Evy, words cannot express how grateful I am to the universe I met you. Thanks you guys for always staying by my side in the good but specially in the bad moments.

A mis padres Mila y Toni. Os agradezco de todo corazón todos los sacrificios que habéis hecho para que tanto yo como Sofia lleguemos tan lejos. Nos hicisteis soñar con todo lo que podíamos alcanzar, y luego nos disteis alas para lograr nuestros sueños. Con Sofia y Scotty, a pesar de que estemos lejos, os tengo muy cerca. Esta tesis también va dedicada al resto de mi familia, en especial a mi tía Geli y a mi primo David, así como a mi tía Vicky, quien además ha sido de increíble ayuda con los gráficos de esta tesis. También quiero dedicar unas últimas palabras a la yaya Milagros, quien me enseñó a mirar los problemas no como obstáculos, sino como retos para aprender y mejorar.

Dimi, mes derniers mots de remerciement vont être pour toi, mon petit chevalier. Sans toi, je n'aurais jamais terminé cette thèse. Tu es la lumière au bout du tunnel ou le réconfort d'un feu brûlant après une journée froide et pluvieuse. Tu es mon Samwise Gamgee. Merci de m'écouter avec tous mes problèmes, d'être très compréhensif. Merci pour tous les éclats de rire et merci de toujours rester avec moi. J'attends avec impatience toutes les aventures qui nous attendent pour le reste de nos vies.

Abstract

Mitochondria are highly dynamics organelles that undergo coordinated cycles of fission and fusion, referred to as mitochondrial dynamics. Mitochondrial dynamics regulate mitochondrial bioenergetics and allow cells to adapt to changing cellular stresses and physiological challenges. The balance between different GTPase enzymes dictates the shift from interconnected tubular networks to fragmented individual units. Among them, mitochondrial fission is regulated by the mitochondrial fission orchestrator, Drp1. Drp1 function is modulated by post-translational modifications, of which the phosphorylation at two specific sites have gained most attention. Drp1 phosphorylation at the S579 site results in Drp1 recruitment to mitochondria to promote fission, whereas the research investigating the role of the S600 phosphorylation has yielded contradictory results on whether it promotes fission or fusion. Importantly, the crosstalk and physiological impact of these phosphorylations is poorly understood. In this project, we focused first on elucidating the interplay between Drp1 S600 and Drp1 S579 phosphorylations. We described how Drp1 S600 phosphorylation promotes S579 phosphorylation by protecting against its dephosphorylation. The activation at both S600 and S579 sites is required to, then, promote mitochondrial fragmentation. To explore the physiological relevance of these phosphorylations, we generated a Drp1 S600A knock-in (Drp1KI) mouse model. Drp1KI mice displayed enhanced lipid oxidation rates and respiratory capacity, granting improved glucose tolerance and thermogenic capacity upon high-fat feeding. Housing mice at thermoneutrality blunted these differences, suggesting a role for the brown adipose tissue in the protection of Drp1KI mice against metabolic damage.

Therefore, this work unveils for the first time the crosstalk between Drp1 phosphorylation sites and their relationship to impact on mitochondrial architecture. Moreover, we demonstrate that targeting the Drp1 S600 site can grant protection against diet-induced insulin resistance, suggesting that the modulation of these phosphorylations could be used in the treatment and prevention of metabolic diseases.

Keywords

Mitochondria, mitochondrial dynamics, Drp1, phosphorylation, metabolic syndrome, brown adipose tissue

Résumé

Les mitochondries sont des organelles hautement dynamiques qui subissent des cycles coordonnés de fission et de fusion, connus sous le nom de dynamique mitochondriale. La dynamique mitochondriale régule la bioénergétique mitochondriale et permet aux cellules de s'adapter aux changements de stress cellulaire et aux réponses physiologiques. L'équilibre entre les différentes enzymes GTPase mitochondriales dicte la transition des réseaux tubulaires interconnectés aux unités individuelles fragmentées. Parmi eux, la fission mitochondriale est régulée par Drp1. La fonction de Drp1 est modulée par des modifications post-traductionnelles, dont la phosphorylation de deux sites spécifiques qui ont été particulièrement étudiés. La phosphorylation de Drp1 au site S579 entraîne l'utilisation de Drp1 dans les mitochondries pour promouvoir la fission. Au contraire, la recherche montre des résultats contradictoires concernant la fonction de la phosphorylation de Drp1 S600, notamment sur le fait de savoir si elle favorise la fission ou la fusion. De plus, la relation et l'impact physiologique de ces phosphorylations sont inconnus. Dans cette thèse, nous avons décrit l'interaction entre les phosphorylations sur Drp1 S600 et Drp1 S579. Nous avons démontré comment la phosphorylation de Drp1 S600 favorisait la phosphorylation de S579 en prévenant sa déphosphorylation. Par conséquent, l'activation des deux sites S600 et S579 est nécessaire pour favoriser la fragmentation mitochondriale. Afin d'explorer l'impact physiologique de ces phosphorylations, nous avons généré le modèle de souris Drp1 S600A knock-in (Drp1 KI). Ces souris utilisent de façon préférentielles les lipides comme source d'énergie et montrent une capacité respiratoire mitochondriale supérieure, offrant une tolérance au glucose et une capacité thermogénique améliorées lors d'un régime riche en graisses. Lorsque ces souris ont été mises dans des conditions de thermoneutralité, ces différences ont été atténuées, suggérant un rôle du tissu adipeux brun dans la protection des souris Drp1 KI contre les maladies métaboliques.

En conclusion, ce travail dévoile pour la première fois la relation entre les sites de phosphorylation de Drp1 et leur impact sur l'architecture mitochondriale. De plus, nous démontrons que le ciblage du site Drp1 S600 peut conférer une protection contre la résistance à l'insuline induite par l'alimentation, suggérant que la modulation de ces phosphorylations pourrait être utilisée dans le traitement et la prévention des maladies métaboliques.

Mots clés

Mitochondrie, dynamique mitochondriale, Drp1, phosphorylation, syndrome métabolique, tissu adipeux brun

Table of Contents

Acknowledgements.....	i
Abstract.....	iii
Keywords.....	iii
Résumé	v
Mots clés.....	v
List of Figures.....	xi
List of Appendices.....	xii
List of Tables.....	xii
List of Abbreviations	xiii
Chapter 1. Introduction	1
1.1 History on mitochondrial research	1
1.1.1 First insights on mitochondrial function and form	1
1.1.2 More than just powerhouses.....	3
1.2 Mitochondrial dynamics	4
1.2.1 Concept of mitochondrial dynamics	4
1.2.2 Mitochondrial dynamics: quality control and cellular communication	5
1.3 Regulation of mitochondrial fusion	7
1.3.1 Mitofusin 1 and Mitofusin 2.....	7
1.3.2 Opa1.....	9
1.4 Regulation of mitochondrial fission	10
1.4.1 Initial insights into Drp1 function.....	10
1.4.2 Drp1 receptors	11
1.4.3 Inter-organelle communication in mitochondrial fission	12
1.5 Drp1 regulation	16
1.5.1 Drp1 structure.....	16
1.5.2 Drp1 isoforms.....	17
1.5.3 Drp1 post-translational modifications	18
1.6 Metabolic regulation and mitochondrial dynamics	22
1.6.1 Mitochondrial alterations in metabolic disease	22
1.6.2 Role of cellular metabolism in shaping mitochondrial dynamics	23
1.6.3 Drp1 in the regulation of nutrient utilization: Lessons from mouse models.....	25

1.7	Mitochondrial dynamics in human diseases.....	31
1.7.1	Familial disorders arising from defects in mitochondrial dynamics proteins.....	31
1.7.2	Cancer: a novel role for mitochondrial fission.....	33
1.8	Goals of the project.....	36
Chapter 2.	Drp1 phosphorylation pattern in mammalian cells and mouse tissues	37
2.1	Drp1 phosphorylation landscape in cultured cells	37
2.2	Drp1 phosphorylation at S579 is independent to ERK activation.....	39
2.3	Drp1 P-S579 and P-S600 occur simultaneously in mouse tissues.....	40
2.4	Conclusions	41
Chapter 3.	Drp1 S600 phosphorylation boosts S579 activation to promote mitochondrial fragmentation.....	47
3.1	P-S600 protects against Drp1 S579 dephosphorylation	47
3.2	Both S579 and S600 phosphorylations are required to trigger mitochondrial fission	48
3.3	Conclusions	49
Chapter 4.	Drp1 S600A KI mice display higher lipid utilization and respiratory capacity	55
4.1	Generation of a Drp1 S600A knock-in mouse model.....	55
4.2	The Drp1 S600A mutation blunts Drp1 P-S579 levels.....	56
4.3	Drp1 KI mice display a tendency towards mitochondrial elongation	57
4.4	Glucose metabolism is not altered in Drp1 KI mice on LFD	58
4.5	Drp1 KI mice on LFD exhibit increased mitochondrial respiration and lipid oxidation rates	58
4.6	Conclusions	58
Chapter 5.	Drp1 KI mice are protected against high-fat-diet-induced insulin resistance.....	65
5.1	Drp1 KI mice display improved insulin sensitivity.....	65
5.2	Drp1 KI mice exhibit increased thermogenesis	66
5.3	Conclusions	67
Chapter 6.	Drp1 KI mice display a unique BAT-specific phenotype.....	71
6.1	Drp1 KI BAT displays enhanced fatty acid oxidation and mitochondrial function	72
6.2	Drp1 KI BAT exhibits increased ER stress.....	74
6.3	Conclusions	75
Chapter 7.	Thermoneutrality blunts the phenotype of the Drp1 KI mice	83
7.1	Thermoneutrality blunts the BAT-specific features of the Drp1 KI mice.....	83
7.2	Thermoneutrality prevents the improved insulin sensitivity of the Drp1 KI mice	84
7.3	Conclusions	85

Chapter 8. Mitochondrial dynamics in the progression of the epithelial-mesenchymal transition..	91
8.1 Mitochondrial dynamics proteins increase upon EMT in a NSCLC cell line	93
8.2 Discussion and conclusions.....	95
Chapter 9. General discussion and future perspectives	99
9.1 Crosstalk of Drp1 phosphorylation sites	100
9.2 Role of the Drp1 S600 phosphorylation in mammalian physiology	104
9.3 Mitochondria & Co.....	106
9.4 Future perspectives	108
Chapter 10. Materials & Methods	111
10.1 Materials	111
10.2 Plasmid generation	111
10.3 Cell culture	112
10.4 Live imaging	112
10.5 Generation of the Drp1 knock-in mice	113
10.6 Animal care	113
10.7 Animal phenotyping.....	113
10.8 <i>In vivo</i> measurement of brown adipose tissue activity	114
10.9 Electron microscopy on mouse brown adipose tissue	114
10.10 Histology	115
10.11 Respirometry studies on mouse tissue homogenates.....	115
10.12 Respirometry studies on isolated mitochondria.....	116
10.13 Mitochondria isolation.....	116
10.14 Primary hepatocyte isolation.....	117
10.15 Primary muscle culture	117
10.16 Primary brown adipocyte isolation.....	118
10.17 Antibody generation	119
10.18 Protein extraction and Western Blotting.....	119
10.19 RNA extraction and qPCR.....	120
10.20 Measurement of acyl-carnitines in BAT.....	120
10.21 Adipokine profiling.....	121
10.22 Plasma Biochemistry	121
10.23 Statistical Analyses.....	122
Annex 1. Table of materials	123

Annex 2. Primers for site-directed mutagenesis.....	124
Annex 3. Table of antibodies	125
Annex 4. Primers for qPCR	126
Appendices	127
References.....	133
Curriculum Vitae	153

List of Figures

Figure 1.1. First electron microscopy images of mitochondria.	3
Figure 1.2. The events of mitochondrial dynamics.....	5
Figure 1.3. Mitochondrial dynamics as a quality control mechanism.	7
Figure 1.4. Model for mitochondrial fission in mammals.....	15
Figure 1.5. Drp1 structure and phosphorylation sites.	18
Figure 1.6. Drp1 regulation by post-translational modifications.....	22
Figure 1.7. Diversity of the mitochondrial shape in different tissues.....	25
Figure 1.8. Role of mitochondrial dynamics in cancer.....	35
Figure 2.1. Drp1 phosphorylation pattern on cultured cells.	42
Figure 2.2. Drp1 S579 phosphorylation occurs independently of ERK.	44
Figure 2.3. Drp1 phosphorylation at S600 and S579 occur simultaneously in mouse tissues.	45
Figure 3.1. Drp1 S600 phosphorylation protects against S579 dephosphorylation.	51
Figure 3.2. Efficiency of CDK and ERK inhibitors.....	52
Figure 3.3. Both S579 and S600 phosphorylations are required for mitochondrial fragmentation.....	53
Figure 3.4. Starvation shapes mitochondrial morphology differently upon Drp1 phosphorylation.	54
Figure 4.1. Generation of the Drp1 KI mouse model.....	60
Figure 4.2. The Drp1 KI mouse model presents impaired S579 phosphorylation.	61
Figure 4.3. The Drp1 KI mouse model displays increased mitochondrial elongation.....	62
Figure 4.4. Drp1 KI mice fed on a LFD do not exhibit differences in glucose homeostasis.	63
Figure 4.5. Drp1 KI mice display higher rates of lipid utilization and mitochondrial respiration.	64
Figure 5.1. Drp1 KI mice are protected against diet-induced glucose intolerance and insulin resistance.	68
Figure 5.2. Muscle and heart performance are not impaired in Drp1 KI mice.	69
Figure 5.3. Drp1 KI mice have increased thermogenic function.....	70
Figure 6.1. Increased fatty acid oxidation capacity in the BAT of Drp1 KI mice.	76
Figure 6.2. Characterization of eWAT from HFD-fed Drp1 KI mice.	78
Figure 6.3. Characterization of liver from HFD-fed Drp1 KI mice.	79
Figure 6.4. Supplementary BAT-specific features of the HFD-fed Drp1 KI mice.....	80
Figure 6.5. Drp1 KI BAT exhibits increased ER stress-induced unfolded protein response.....	81
Figure 7.1. Housing mice at 30°C hinders BAT thermogenic tone.	87
Figure 7.2. Thermoneutrality blunts the BAT-specific features of the Drp1 KI mice.....	88

Figure 7.3. Thermoneutrality blunts the improved insulin sensitivity phenotype of the Drp1 KI mice.	89
Figure 8.1. Mitochondrial dynamics upon EMT in a H727 transformed cell line.	97
Figure 9.1. Crosstalk between Drp1 S579 and Drp1 S600 phosphorylation sites.....	103
Figure 9.2. Phenotype of the Drp1 S600A KI mice.	106
Figure 10.1. Primary muscle culture.	118
Figure 10.2. Primary BAT isolation and culture.	119

List of Appendices

Appendix 1. Time-course for Drp1 phosphorylations <i>in vitro</i> and <i>in vivo</i>	128
Appendix 2. Drp1 isoforms in different tissues.	129
Appendix 3. Muscle data from the Drp1 KI mice.	130
Appendix 4. Primary cultures of liver, muscle and BAT.	131
Appendix 5. Adrenergic stimuli in brown adipose tissue leads to mitochondrial fragmentation.	132

List of Tables

Table 1. Drp1 mouse models.	30
Table 2. Table of materials.....	123
Table 3. Primers for site-directed mutagenesis.....	124
Table 4. Table of antibodies.....	125
Table 5. Primers for qPCR.	126

List of Abbreviations

ACADM	Acyl-CoA Dehydrogenase Medium Chain
ACADL	Acyl-CoA Dehydrogenase Long Chain
ACC1	Acetyl-CoA Carboxylase 1
ACC2	Acetyl-CoA Carboxylase 2
ADP	Adenosine Diphosphate
ANGPT-L3	Angiopoietin-Like 3
cAMP	cyclic Adenosine Monophosphate
ATF4	Activating Transcription Factor 4
ATF6	Activating Transcription Factor 6
ATP	Adenosine Triphosphate
BAT	Brown Adipose Tissue
BIP	Binding Immunoglobulin Protein
CLAMS	Comprehensive Lab Animal Monitoring System
CPT1b	Carnitine Palmitoyltransferase 1b
CPT2	Carnitine Palmitoyltransferase 2
CRP	C-Reactive Protein
DRP1	Dynamin Related-Protein 1
EDL	Extensor Digitorum Longus
EV	Empty Vector
eWAT	epididymal White Adipose Tissue
EIF2 α	Eukaryotic Translation Initiation Factor 2 α
FAS	Fatty Acid Synthase
FBS	Fetal Bovine Serum
FCCP	Carbonyl Cyanide-4-(Trifluoromethoxy)Phenylhydrazone
FFA	Free Fatty Acid
GAPDH	Glyceraldehyde 3-Phosphate Dehydrogenase
GTT	Glucose Tolerance Test

HFD	High-Fat Diet
ICAM1	Intercellular Adhesion Molecule 1
IMM	Inner Mitochondrial Membrane
ITT	Insulin Tolerance Test
IRE1	Inositol Requiring Enzyme 1
KI	Knock-In
KO	Knock-Out
LC-MS	Liquid Chromatography – Mass Spectrometry
LFD	Low-Fat Diet
MEFs	Mouse Embryonic Fibroblasts
MFN1	Mitofusin 1
MFN2	Mitofusin 2
OMM	Outer Mitochondrial Membrane
OPA1	Optic Atrophy 1
PKA	Protein Kinase A
PGC1 α	Peroxisome Proliferator-Activated Receptor Gamma Coactivator 1-alpha
PPAR γ	Peroxisome Proliferator-Activated Receptor gamma
PRDM16	PR Domain containing 16
RBP4	Retinol Binding Protein 4
RER	Respiratory Exchange Ratio
ROCK1	Rho Associated Coiled-Coil Containing Protein Kinase 1
scWAT	subcutaneous White Adipose Tissue
SREBF1	Sterol Regulatory Element Binding Transcription Factor 1
SREBF2	Sterol Regulatory Element Binding Transcription Factor 2
TG	Triglycerides
UCP1	Uncoupling Protein 1
WT	Wild Type
$\Delta\Psi_m$	Mitochondrial Membrane Potential

Chapter 1. Introduction

1.1 History on mitochondrial research

1.1.1 First insights on mitochondrial function and form

The earliest records on intracellular structures that probably represent mitochondria date from the 1840s, only a few years after the discovery of the cell nucleus. Richard Altmann in 1890 described these structures as “bioblasts”, cytoplasmic entities of ubiquitous occurrence, which resembled bacteria and functioned as “elementary organisms” (Ernster & Schatz, 1981). In 1898, the microbiologist Carl Brenda, who stained the organelles with alizarin and crystal violet to observe their internal structure, renamed Altmann’s bioblasts as “mitochondria” (from Greek *mitos*, ‘thread’, and *chondros*, ‘granule’), referring to their appearance during spermatogenesis (Ernster & Schatz, 1981).

The first insights on the functional role of mitochondria were provided by Benjamin Kingsbury (1912), who suggested that mitochondria serve as the sites for cellular respiration. In the following years, most groups attempted to identify the components of the respiratory chain, although the subcellular localization of the events in cellular respiration was still unknown (Ernster & Schatz, 1981). To solve this, Albert Claude devised the first reliable cellular fractionation procedure using differential centrifugation, allowing the isolation of intact and functional mitochondria (Claude, 1946). This came to be of fundamental importance for the elucidation of enzymes and biochemical processes specific to mitochondria. For instance, Eugene Kennedy and Albert Lehninger (1949) demonstrated that fatty acid oxidation and the citric acid cycle occurred exclusively in mitochondria and that these events were linked to the synthesis of ATP via NADH.

All these discoveries paved the way for Peter Mitchell to introduce his radical new theory of “chemiosmotic coupling” (Mitchell, 1961). Essentially, Mitchell proposed that the energy derived from the oxidation of fuels was used to pump protons from the mitochondrial matrix to the intermembrane space, creating what he called the “proton motive force”. His theory explained that it was the energy captured from those protons returning to the matrix that was then used to drive ATP synthesis (Mitchell, 1961). This hypothesis, while rejected by the field for a decade, would be later confirmed with seminal

experiments by André Jagendorf and others (Jagendorf & Uribe, 1966). Finally, Mitchell got the Nobel Prize in 1978 "for his contribution to the understanding of biological energy transfer through the formulation of the chemiosmotic theory". Interestingly, Philip Siekevitz faithfully depicted the functional role of mitochondria in an article for the magazine *Scientific American* titled "Powerhouse of the Cell" (Siekevitz, 1957).

The discoveries on mitochondrial function occurred in parallel to a detailed characterization of mitochondrial structure. Initially, the Swiss anatomist Albert von Kölliker identified granule-like structures in the sarcoplasm of insect muscle cells. He then showed that these granules swelled in water and owned a membrane (Ernster & Schatz, 1981). MR. Lewis and WH. Lewis (1915) performed a novel procedure for mitochondrial staining and described extensive changes in the position and morphology of mitochondria in living muscle cells (Lewis & Lewis, 1915). These observations were later extended by several scientists using phase-contrast microscopy in combination with time-lapse imaging. These studies were pioneered by J. Frédéric and M. Chèvremont (1952), who obtained the first pictures of morphology changes and mitochondrial movements in cultured fibroblasts in various phases of cell activity (including mitosis), as well as in response to varied physiological, pathological and experimental conditions. Detailed studies of mitochondrial ultrastructure became possible only after the development of thin-sectioning techniques in the early 1950s. In this regard, the pioneering electron microscopy of George Palade (1953) and Fritiof Sjostrand (1953) revealed the unique morphology of these organelles, including the characteristic double-membrane structure and the convoluted invaginations that Palade termed "cristae" (Figure 1.1). These cristae were found to be different among tissues and organism, and although the functional implications of these variations were then poorly understood, it was evident that a high respiratory activity was linked to an abundance of cristae (Palade, 1953). Later, Jürgen Bereiter-Hahn (1978) described the remarkable variety of shapes and motile nature of mitochondria in living cells and first characterized the interaction of mitochondria with other elements of the cell, such as the cytoskeleton or microtubules. However, the mechanism and physiological significance of these movements remained largely unknown. These insights led to the start of the research field of mitochondrial dynamics. Since then, aided by the development of mitochondria-specific probes and advances in light microscopy, numerous groups have studied mitochondrial dynamics in living cells and model organisms.

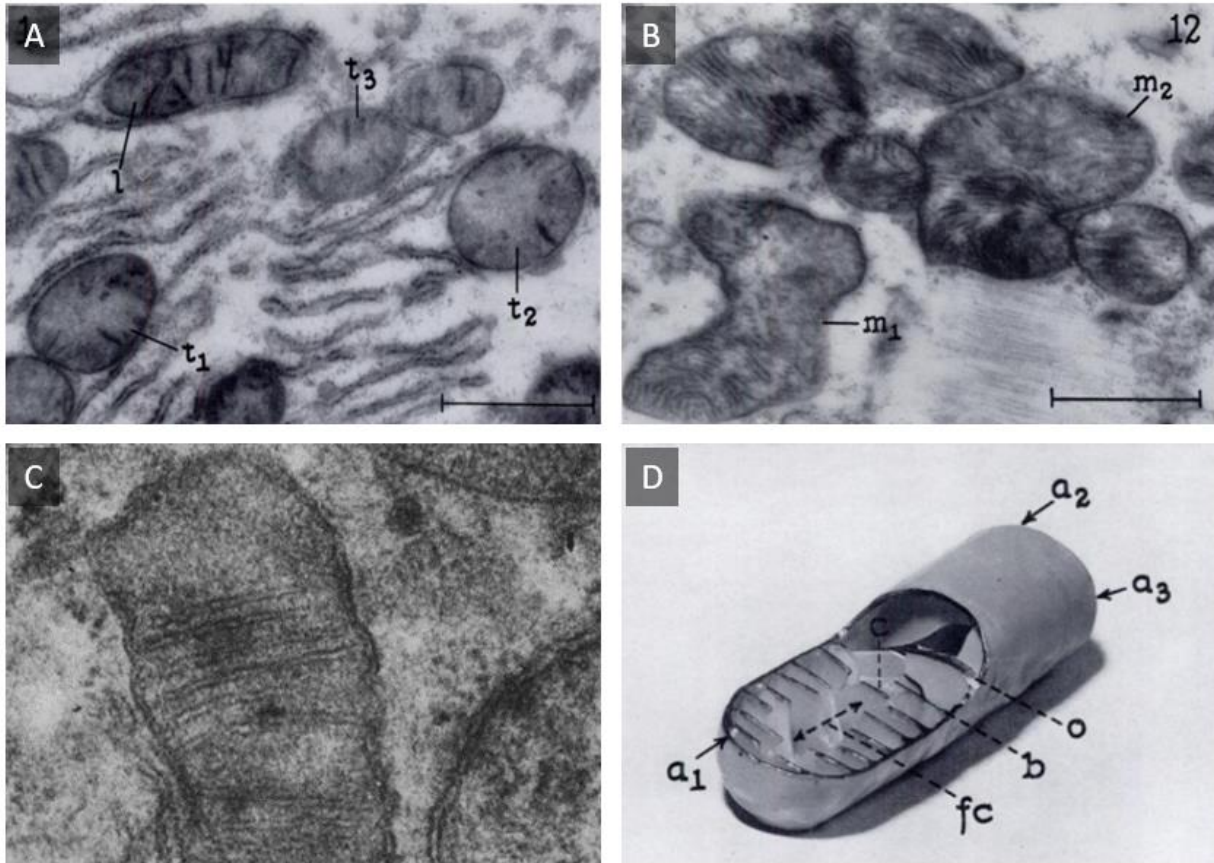


Figure 1.1. First electron microscopy images of mitochondria.

(A-B) From Palade (1953), image of mitochondrial in rat liver (A) and under the sarcolemma of a striated muscle fiber (B). (C) From Sjostrand (1953), electron image of kidney mitochondria. (D) Representation of the tridimensional model of mitochondria by Palade.

1.1.2 More than just powerhouses

In the late 1960s, mitochondrial DNA was identified and quantified from yeast, while mitochondrial ribosomes were first isolated from *Neurospora*, indicating that mitochondria retain their own genome and transcription/translation machineries (Ephrussi, 1950) (Küntzel & Noll, 1967). In the 1990s, the discovery that mitochondrial release of Cytochrome C initiates a cascade that leads to cell death dramatically changed how cell biologists perceived mitochondria (Liu *et al.*, 1996). Formerly viewed as sites of bioenergetic production, these organelles could now also be thought of as regulators of signal transduction.

Over the past decades, mitochondria were demonstrated to participate in multiple roles, such as heme biosynthesis, calcium buffering, iron homeostasis, or antiviral responses (Sano *et al.*, 1959) (Koshiba *et al.*,

2011) (Anderson *et al.*, 2019). Therefore, it has been increasingly appreciated that mitochondria have developed mechanisms to communicate their biosynthetic and bioenergetics fitness to the rest of the cell and thus have signaling functions beyond their purely metabolic ones. This mitochondrial communication ensures that cells do not commit to a biological process without input on the fitness of mitochondria, risking a discrepancy between the metabolic demands of the cell and the ability of the mitochondria to meet them (Chandel, 2014). Therefore, mitochondria are intimately embedded in the signaling cascades that operate within cells and act as quality control entities to ensure cellular homeostasis.

These studies led the way to decades of research focusing on mitochondria as an essential, yet independent, functional component of the cell. However, the conceptual view of mitochondria as a collection of isolated structures has been profoundly altered with the discovery that mitochondria function within an integrated network that is continually remodeled by fusion and fission events.

1.2 Mitochondrial dynamics

1.2.1 Concept of mitochondrial dynamics

Mitochondria within cells exist as a dynamic network that rapidly modulate their morphology to adapt to the cellular environment. Mitochondrial dynamics refers to the highly orchestrated cycles of fusion and fission between mitochondria that take place in response to a variety of physiological and metabolic cues. Mitochondrial fission is characterized by the division of a single mitochondrion into two daughter organelles, while mitochondrial fusion results in the union of two mitochondria in one single organelle. The deregulation of the balance in mitochondrial dynamics results in either a fragmented network characterized by a large number of small round-shape mitochondria or a hyperfused network with elongated and highly connected mitochondria (Figure 1.2).

Mitochondria fission and fusion events require specialized enzymes that physically alter the mitochondrial membrane. The components of the core machinery regulating mitochondrial dynamics are large GTPase proteins belonging to the Dynamin family (Tilokani *et al.*, 2018). These mechanoenzymes can oligomerize and change conformation to drive membrane remodeling, constriction and fragmentation (fission) or fusion. Mitochondrial constriction and fission are initiated by the Dynamin-related protein 1 (Drp1). Mitochondrial fusion is ensured by Mitofusins 1 and 2 (Mfn1 and Mfn2) and Optic Atrophy 1 (Opa1), which mediate fusion of the outer mitochondrial membrane (OMM) and inner mitochondrial membrane (IMM), respectively. Knockout (KO) of either of these GTPases is embryonically lethal in mice, and mouse embryonic fibroblasts (MEFs) derived from these mice harbor drastic mitochondrial morphology defects

(Ishihara *et al.*, 2009) (Chen *et al.*, 2003) (Davies *et al.*, 2007). For example, MEFs deficient in Mfn1 display a completely fragmented mitochondrial morphology. In contrast, Drp1 deficient MEFs exhibit a largely elongated mitochondrial network (Tilokani *et al.*, 2018). The relevance of mitochondrial dynamics has also been highlighted in human disease, with the identification of mutations in mitochondrial dynamics-related genes leading to neurological disorders. Altogether, this emphasizes the importance of understanding how mitochondrial morphology is regulated, in order to decipher how mitochondrial shape meets the function.

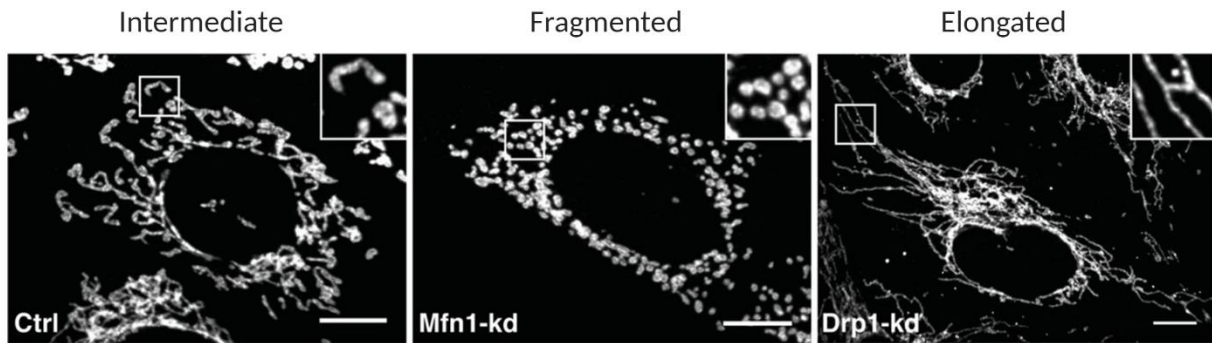


Figure 1.2. The events of mitochondrial dynamics.

Representative confocal microscopy images of mouse embryonic fibroblast (MEF) cells undergoing different mitochondrial morphological changes. Control cells exhibit a balance of the fragmented and elongated mitochondrial forms, thus an intermediate morphological state. The predominance of the fission machinery or the inhibition of fusion components, as validated by Mfn1 knockdown (kd), leads to fragmented mitochondria. Contrarily, impairment of mitochondrial fission, testified by the Drp1 kd cells, or increase in the activity of the mitochondrial fusion core results in mitochondrial elongation. Scale bars: 10 μ m. Images adapted from Tilokani *et al.* (2018).

1.2.2 Mitochondrial dynamics: quality control and cellular communication

Mitochondrial dynamics were initially proposed to act as a quality control mechanism that preserves cellular homeostasis (Valera-Alberni & Canto, 2018). On the one hand, mitochondrial fission ensures an even distribution of mitochondria between daughter cells upon cell division. Moreover, fission events exclude dysfunctional mitochondria that will be separated from the healthy mitochondrial pool and eliminated by mitophagy, the selective removal of mitochondria by the autophagic machinery (Figure 1.3). On the other hand, mitochondrial fusion is suggested as a complementary mechanism by which mitochondria equilibrate matrix metabolites, intact mitochondrial DNA (mtDNA) copies and membrane

components. Therefore, fusion recruits mitochondria into the active pool, instead of being segregated by fission and targeted for elimination.

Then, what determines whether mitochondria should be rescued by fusion or channeled for mitophagy? To answer this question, one has to consider that random redistribution would have an impact upon mitochondria function. Non-selective fusion would contribute to damaged mitochondria impairing the activity and efficiency of the healthy population. Therefore, most fusion/fission events do not occur in a random fashion. As demonstrated by Twig *et al.* (2008), after a fission event, fusion occurs preferentially between mitochondria with higher mitochondrial membrane potential ($\Delta\psi_m$), as compared to the subpopulation of non-fusing mitochondria that were depolarized. Depolarization below a certain $\Delta\psi_m$ is associated with impaired mitochondrial function, thus acting as a trigger for mitophagy. The long time gap between depolarization of an individual mitochondrion and its autophagy indicates that mitochondria lose their fusion capability prior to elimination, validated by the increased Opa1 cleavage in these non-fusing mitochondria (Twig *et al.*, 2008) (see section 1.3.2 for information on Opa1 cleavage). These findings would indicate that fusion is a selective and exclusive process for hyperpolarized mitochondria, rather than an unselective rescue mechanism. The selectivity of mitochondrial fusion not only prevents the migration of damaged components into the healthy mitochondrial pool, but is also an isolation step that creates a segregated population that is available for autophagy (Figure 1.3) (Twig & Shirihai, 2011).

Following mitochondrial fission and depolarization, Parkin and PINK1 (PTEN-induced putative kinase 1) are recruited to the OMM to tag the organelle for mitophagy (Figure 1.3). Healthy mitochondria maintain a stable membrane potential that facilitates the import of the serine/threonine kinase PINK1 into the mitochondrial matrix, where it is cleaved and degraded (McWilliams & Muqit, 2017). However, impaired $\Delta\psi_m$ alters mitochondrial protein import, leading to PINK1 accumulation in the OMM. This promotes the recruitment of the E3 ubiquitin ligase Parkin from the cytosol, which then ubiquitinates substrates Mfn1 and Mfn2, preventing the fusion of damaged mitochondria with the healthy mitochondrial network (Gegg *et al.*, 2010). Ubiquitination of the damaged mitochondrial also signals for the recruitment of autophagosomes, which finally degrade the engulfed mitochondria by the action of acid hydrolases.

Overall, the interplay between mitochondrial dynamics and mitophagy ensures the correct functioning of the mitochondrial network, which in turn determines the homeostasis of the cell. When one of these elements fails, dysfunctional mitochondria are not properly removed from the cellular pool, generally leading to higher amounts of reactive oxygen species (ROS) production and increased susceptibility to the release of Cytochrome C and cell death (Valera-Alberni & Canto, 2018).

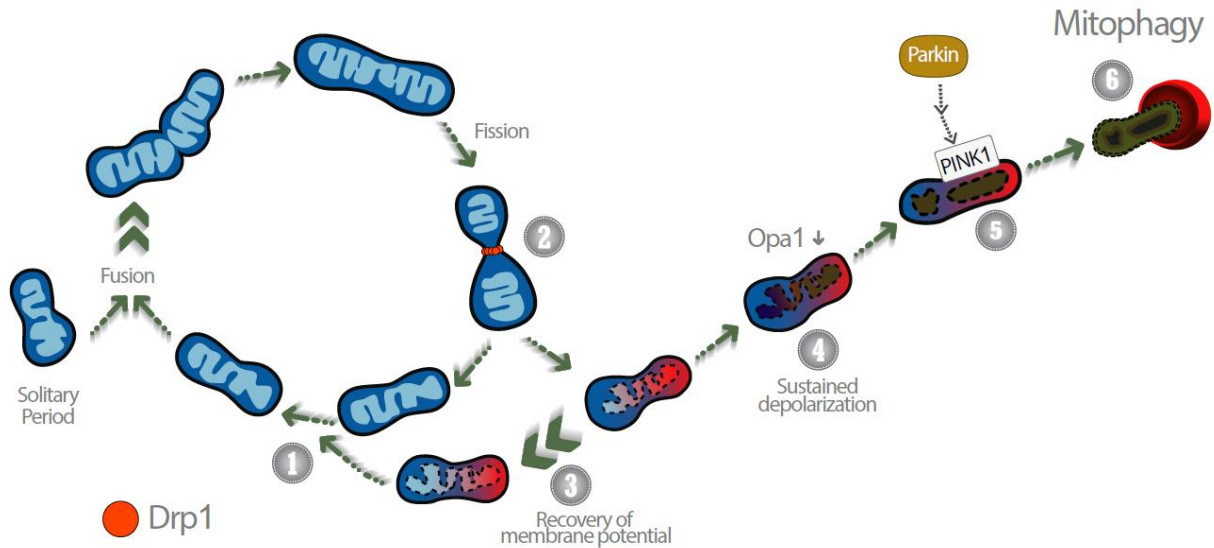


Figure 1.3. Mitochondrial dynamics as a quality control mechanism.

The mitochondrial network shifts between continuous cycles of fusion and fission. Fission of mitochondria (2) is carried out by the Drp1 GTPase. Fission events often generate daughter units with different $\Delta\psi_m$: on the one hand, some mitochondria are depolarized, but the $\Delta\psi_m$ can be restored (3) by fusion with other mitochondria (1). After solitary periods, mitochondria might also fuse if the membrane potential is above a certain threshold. On the other hand, sustained $\Delta\psi_m$ depolarization triggers Opa1 cleavage (4), rendering impossible for the damaged mitochondria to be fused back with the healthy mitochondria population. The impaired mitochondrial protein import facilitates the recruitment and accumulation of the mitophagy markers Parkin and PINK1 (5). This targets single dysfunctional mitochondrion to mitophagy (6), where it is engulfed by the autophagosome. Image adapted from Twig & Shirihai (2011).

1.3 Regulation of mitochondrial fusion

1.3.1 Mitofusin 1 and Mitofusin 2

The first characterization of the mitochondrial fusion machinery was provided by Hales and Fuller (1997) from studies in *Drosophila* spermatogenesis. In this model, mitochondria aggregated beside each haploid nucleus forming concentric circles that resembled an onion slice when viewed by transmission electron microscopy (TEM) (Hales & Fuller, 1997). Moreover, flies with a mutation in an OMM-located GTPase displayed altered concentric structures due to prevented fusion of the mitochondrial population (Hales & Fuller, 1997). Because of this, the gene encoding this GTPase was then named fuzzy onions (*Fzo*). The *Fzo* gene has homologues in yeast (*Fzo1*) and mammals (*Mfn1* and *Mfn2*), performing similar function in controlling outer membrane fusion (Hermann *et al.*, 1998) (Santel & Fuller, 2001). Interestingly, although

mitochondrial fusion also occurs in plants, functional orthologs of the mitochondrial fusion proteins have not been found so far in any plant, which indicates that a separate system must have evolved in this kingdom (Arimura *et al.*, 2004).

In mammals, OMM fusion is carried out by the Mfn1 and Mfn2 proteins, which accumulate at contact areas between two adjacent mitochondria. Both mitofusins can consequently interact homotypically (Mfn1-Mfn1, Mfn2-Mfn2) or heterotypically (Mfn1-Mfn2) forming dimers and leading to mitochondrial fusion (Chen *et al.*, 2003). Mitochondrial fusion occurs in a series of consecutive events: tethering of two mitochondria, docking of the two respective mitochondrial membranes and accumulation of Mfn1-Mfn1, Mfn1-Mfn2 and Mfn2-Mfn2 dimers and, finally, GTP hydrolysis and fusion of the two OMMs due to conformational changes in the mitofusins (Brandt *et al.*, 2016).

Although Mfn1 and Mfn2 are both essential for mitochondrial fusion, they exhibit distinct GTPase activity and mitochondrial membrane tethering capacity. Indeed, Mfn1 has higher GTPase and organelle fusion activity while Mfn2 has greater affinity for GTP (Ishihara *et al.*, 2004) (Gouspillou & Hepple, 2016). In addition, Mfn2, but apparently not Mfn1, is involved in the interaction of mitochondria with other organelles, such as the endoplasmic reticulum (ER) (de Brito & Scorrano, 2008), the lipid droplet (Boutant *et al.*, 2017) or the lysosomes (Wong *et al.*, 2019) (Deus *et al.*, 2020). For example, Mfn2 deficient MEF cells exhibited disrupted ER morphology and ER-mitochondria interactions (de Brito & Scorrano, 2008). Complementarily, ablation of Mfn2 in mouse adipose tissue (Mfn2-adKO) reduced mitochondria-lipid droplet interaction (Boutant *et al.*, 2017). Moreover, Mfn2, but not Mfn1, has a direct impact on the integrity and function of the electron transport chain. Indeed, Mfn2 has been suggested to directly interact with oxidative phosphorylation (OXPHOS) elements such as Complex I or Complex III (Segalés *et al.*, 2013), and also sustain the mitochondrial coenzyme Q pool (Mourier *et al.*, 2015).

In fact, the functional redundancy between Mfn1 and Mfn2 is very partial, as can be exemplified by the different genetic mouse models deficient in either of these proteins. For example, while ablation of Mfn2 in adipose tissue (Mfn2-adKO) in mice led to impaired thermogenic function and glucose homeostasis, Mfn1-adKO mice did not display differences in energy expenditure nor in response to cold exposure (Boutant *et al.*, 2017). This certifies that the alterations in Mfn2-adKO mice are not simply due to impaired mitochondrial fusion, but also to the alternative pleiotropic functions of Mfn2. Indeed, the liver-specific deletion of Mfn2 in mice (Mfn2-LKO) triggered the ER stress response (Sebastián *et al.*, 2012), whereas this was not observed in Mfn1-LKO mice (Kulkarni *et al.*, 2016). Therefore, the genetic ablation of *Mfn2* in mice results in ER-mitochondria miscommunication, which triggers the ER stress response in tissues such

as brown adipose tissue (BAT), liver or muscle, eventually leading to alterations in the metabolism of these tissues (Sebastián *et al.*, 2012) (Boutant *et al.*, 2017). This could explain why Mfn2 loss often results in more dramatic physiological changes than Mfn1, despite its minor role as a pure mitochondrial fusion protein.

1.3.2 Opa1

Inner mitochondrial membrane fusion generally occurs downstream of outer membrane fusion and is mediated by the large GTPase Opa1. Indeed, genetic loss of *Opa1* in cultured cells leads to mitochondrial fragmentation whereas Opa1 overexpression induces mitochondrial elongation. Originally described in yeast as Mgm1p, Opa1 is evolutionary conserved and was named after its genetic mutation was shown to be the main cause of autosomal dominant optic atrophy in humans (ADOA) (Alexander *et al.*, 2000) (Delettre *et al.*, 2000). Opa1 is inserted within the IMM via an approximately 100 residue N-terminal fragment, exposing most of the protein to the intermembrane space (Olichon *et al.*, 2002). Importantly, Opa1 is a complex protein with eight identified splice-variants that results from the proteolytic cleavage in at least two sites of the protein, which generate shorter and soluble fragments. This cleavage is mediated by two membrane-bound metalloproteases, Oma1 and Yme1 (Head *et al.*, 2009) (Ehse *et al.*, 2009) (Song *et al.*, 2007). The cleavage of Opa1 downstream the transmembrane domain results in five Opa1 fragments detectable by immunoblot. In this regard, the two higher molecular weight forms are referred as L-Opa1 while the three shorter as S-Opa1.

The abundance of the different forms of Opa1 has a direct effect on mitochondrial dynamics regulation. Uncleaved L-Opa1 forms promote mitochondrial fusion whereas the accumulation of cleaved S-Opa1 forms accelerate mitochondrial fission (Anand *et al.*, 2014) (Ruan *et al.*, 2013). In addition to this, the activity of the proteases Yme1 and Oma1 is highly sensitive to external stimuli. For example, Yme1-mediated processing of Opa1 is metabolically stimulated by increased OXPHOS activity (Mishra *et al.*, 2014). Furthermore, Oma1-mediated cleavage of Opa1 is strongly enhanced in response to various stress insults, such as mitochondrial membrane depolarization (Zhang *et al.*, 2014) or heat stress (Baker *et al.*, 2014).

Importantly, Opa1 responds dynamically to changes in energetic conditions to regulate cristae structure (Patten *et al.*, 2014). This cristae regulation was then demonstrated essential for the cellular adaptation to metabolic demands, mediated by the maintenance of ATP synthase assembly and the regulation of mitochondrial respiration (Patten *et al.*, 2014). In line with this, muscle-specific Opa1 KO mice displayed aberrant mitochondria with dilated cristae, which induced mitochondrial dysfunction and triggered ER

stress (Tezze *et al.*, 2017). This eventually led to protein synthesis inhibition, muscle atrophy and systemic aging in the muscle-specific Opa1 KO mice. Of note, age-related muscle loss in humans and mice is associated with decreased Opa1 expression, whereas regular exercise was probed to counteract this decline (Tezze *et al.*, 2017).

In most cases fusion of the outer membrane is coordinated with inner membrane fusion. However, dissipation of the mitochondrial membrane potential or mutations in Opa1 selectively block inner membrane fusion. Under these conditions, outer membrane fusion proceeds in the absence of inner membrane fusion and, therefore, the fusion machineries at the OMM and IMM operate independently. Finally, other factors not directly involved in the pro-fusion machineries have also been demonstrated to aid in the double-membrane fusion. For example, the nucleus-encoded mitochondrial protein Chchd2 has recently been reported to regulate mitochondrial morphology and tissue homeostasis in flies by fine-tuning the levels of Opa1 (Liu *et al.*, 2020a). Indeed, Opa1 expression levels were reduced in Chchd2 mutant flies, leading to a decrease in cristae number and a tendency towards mitochondrial fragmentation, whereas Chchd2 overexpression rescued Opa1 levels (Liu *et al.*, 2020a).

1.4 Regulation of mitochondrial fission

1.4.1 Initial insights into Drp1 function

Mitochondrial fission is a multi-step process involving the recruitment of the large GTPase Drp1 (Dnm1 in yeasts) from the cytosol to mitochondria. Because of its homology to the well-characterized mammalian Dynamin, a GTP-binding protein that promotes membrane scission during endocytosis, it was originally suggested that Dnm1 was involved in endosomal trafficking in yeasts (Gammie *et al.*, 1995). However, subsequent studies indicated that *Dnm1* mutations did not affect endocytosis, and that Dnm1 was largely localized to the mitochondrial surface. The first evidence that Dnm1 was a component required for mitochondrial fragmentation was provided by Janet Shaw and collaborators in 1998. In yeast, mitochondria are normally found in a broadly branched network that is evenly spread around the cellular periphery (Otsuga *et al.*, 1998) (Bleazard *et al.*, 1999). However, mutation of the *Dnm1* gene disrupted this mitochondrial network to collapse to one side of the cell, due to the impaired function of the GTP-binding domain (Otsuga *et al.*, 1998). In the absence of Dnm1, mitochondria in yeast formed highly fenestrated, net-like structures. Interestingly, endocytosis defects did not induce changes in yeast mitochondrial morphology, validating an independent role of Dnm1 to that of the mammalian Dynamin. Further consolidating its pro-fission role, immunofluorescence imaging was used to localize Dnm1 at

mitochondrial branch points or at the tips of newly formed mitochondrial fragments, sites of mitochondrial division (Otsuga *et al.*, 1998) (Sesaki & Jensen, 1999). Dnm1 was then described as the antagonist to the pro-fusion factor Fzo1 in maintaining the balance in mitochondrial shape (Sesaki & Jensen, 1999). In parallel to the research in yeast, studies in *C. elegans* (Labrousse *et al.*, 1999) and mammals (Smirnova *et al.*, 1998) further consolidated the role of Drp1 as the main contributor to mitochondrial fragmentation.

1.4.2 Drp1 receptors

Subcellular fractionation experiments demonstrate that Drp1 is largely cytosolic, with only 3% being localized to mitochondria as foci in basal conditions (Smirnova *et al.*, 2001). In contrast to the classical Dynamin, Drp1 lacks the specialized pleckstrin-homology domain required for membrane binding and insertion (Achiriloaie *et al.*, 1999) (Otera *et al.*, 2013) (Dar & Pucadyil, 2017). Therefore, in order to be recruited to mitochondria, Drp1 requires the assistance of adaptor proteins, as well as the mitochondrial lipid cardiolipin. In mammals, the docking of Drp1 to mitochondria can occur via up to four integral membrane proteins of the OMM: mitochondrial fission 1 protein (Fis1), mitochondrial fission factor (Mff), and mitochondrial dynamics protein of 49 and 51 kDa (MiD49 and MiD51, respectively).

Fis1 was the first proposed receptor, based on genetic and biochemical data from yeast. In mammals, the role of Fis1 as a Drp1 receptor has been controversial. Some reports support that mammalian Fis1 interacts with Drp1 (James *et al.*, 2003) (Yoon *et al.*, 2003) (Yu *et al.*, 2005), whereas other studies reveal that Fis1 is largely dispensable for Drp1 recruitment (Suzuki *et al.*, 2003) (Lee *et al.*, 2004) (Stojanovski *et al.*, 2004) (Osellame *et al.*, 2016). Indeed, analysis of Fis1 KO MEFs indicated a minor role of Fis1 in Drp1 recruitment and mitochondrial fission as compared to Mff or MiD49/MiD51 (Osellame *et al.*, 2016). Rather than promoting mitochondrial fission, a recent report by Yu *et al.* (2019a) suggests that Fis1 inhibits mitochondrial fusion. Consistent with this, crosslinking experiments demonstrated that Fis1 robustly interacted with Mfn1, Mfn2 and Opa1 and this, in turn, inhibited their GTPase activity (Yu *et al.*, 2019a). Despite its critical role in determining yeast mitochondrial architecture, the relative importance of Fis1 in mammals might be cell-type or stimuli dependent (Losón *et al.*, 2013). In agreement with this, Fis1 was proposed to contribute to Drp1-dependent mitochondrial fission in cellular stress responses, such as mitophagy, apoptosis or pathophysiological conditions (Qi *et al.*, 2013) (Wang *et al.*, 2012a) (Joshi *et al.*, 2018).

MiD49 and MiD51 were identified as part of a random cellular localization screening of uncharacterized human proteins (Palmer *et al.*, 2011). MiD49 and MiD51 share 45% sequence identity and anchor to the

OMM through N-terminal transmembrane domains, while exposing C-terminal segments to the cytoplasm. At basal expression levels, MiD49/ MiD51 are found at discrete foci in the OMM and form rings around mitochondria, similar to those observed for Drp1 (Palmer *et al.*, 2011). Paradoxical views exist on the mechanism of action of MiD49 and MiD51. While some observations indicate that the double MiD49/ MiD51 deletion results in mitochondrial elongation and impairment of Drp1 recruitment to mitochondria (Palmer *et al.*, 2011), overexpression of either MiD49 or MiD51 also causes mitochondrial elongation (Palmer *et al.*, 2011) (Zhao *et al.*, 2011). This might be explained by the requirement for MiD49 or MiD51 receptor dissociation before Drp1 ring constriction. Indeed, GTP-binding facilitates Drp1 stabilization and recruitment by MiD49 and MiD51, which then initiates Drp1 oligomerization (Kalia *et al.*, 2018).

Mff is a tail-anchored OMM receptor that interacts with Drp1 during mitochondrial fragmentation (Otera *et al.*, 2010) (Gandre-Babbe & van der Bliek, 2008). Whereas MiD49 and MiD51 are exclusively found on the OMM, Mff is additionally located on peroxisomes, where it can also recruit Drp1 for peroxisomal fission (Otera *et al.*, 2010) (Palmer *et al.*, 2013). Opposite to MiD49/ MiD51, Mff overexpression results in increased mitochondrial fission. Using genetic and biochemical assays, Liu and Chan (2015) demonstrated how Mff is unable to bind to assembly-deficient mutants of Drp1, suggesting that Mff selectively interacts with higher-order complexes of Drp1.

Nevertheless, how these adaptors interact with each other to coordinate mitochondrial fission is still a topic under investigation. Experiments with Drp1-adaptor KO MEFs by Osellame *et al.* (2016) provided evidence of the cooperativity and contribution of MiD49/MiD51 and Mff to Drp1-mediated mitochondrial fission. While MiD51 and Mff were proposed to assemble with Drp1 at the same fission foci (Elgass *et al.*, 2015), Drp1 GTPase activity was inhibited by MiDs and stimulated by Mff (Osellame *et al.*, 2016). In this sense, Mff and MiDs could have distinct but complementary roles in mitochondrial fission where MiDs recruit GTP-bound Drp1 to facilitate its oligomerization while Mff selectively recruits oligomeric and active forms of Drp1.

1.4.3 Inter-organelle communication in mitochondrial fission

Mitochondria and peroxisomes

Besides its role in promoting mitochondrial fragmentation, Drp1 can also drive peroxisomal fission. Peroxisomes, while sharing a dual origin from both the ER and mitochondria (Sugiura *et al.*, 2017), are single-membrane organelles that catalyze the breakdown of long chain fatty acids through beta-oxidation. Initial experiments in COS7 and HepG2 cells proved that expression of a dominant-negative Drp1 mutant

inhibited peroxisomal fission and caused elongation of peroxisomes (Koch *et al.*, 2003). Interestingly, Mff and Fis1 localize to peroxisomes in addition to mitochondria, and aid in the peroxisomal targeting of Drp1 to promote peroxisomal fission in a mechanism dependent on the peroxisome factor Pex11 (Gandre-Babbe & van der Blik, 2008) (Kobayashi *et al.*, 2007) (Koch *et al.*, 2005) (Koch & Brocard, 2012). Furthermore, peroxisomes have been suggested to regulate mitochondrial morphology in a Drp1-dependent manner, validated by the increased mitochondrial fragmentation in MEF cells depleted of the peroxisome markers Pex3 and Pex5 (Tanaka *et al.*, 2019).

The ER and the initial steps of mitochondrial scission

Mitochondrial fragmentation is a complex process involving the participation of Drp1 and its receptors, but also of the crosstalk with different organelles. A groundbreaking discovery by Friedman *et al.* (2011) identified the endoplasmic reticulum as a trigger for the initial step of mitochondrial division. The diameter of Drp1 rings (16-20 nm) is significantly narrower than that of mitochondria (0.5–1 μm). Thus, ER tubules physically wrap around and constrict mitochondria, and this decreases the mitochondrial diameter to a size that allows for Drp1-oligomeric ring formation (Basu *et al.*, 2017) (Kalia *et al.*, 2018) (Figure 1.4). Interestingly, immunolocalization experiments showed that the ER is recruited to mitochondria independently of Drp1 and Mff, as mitochondria-ER constriction sites were still observed in COS7 cells depleted of these factors (Friedman *et al.*, 2011). Therefore, ER contact and constriction of mitochondria is an upstream event in the mitochondrial fission process that defines the position for Mff localization, Drp1 recruitment and oligomerization, leading to Drp1 ring formation. Nevertheless, of the many ER-mitochondria contacts, only a subset undergoes fragmentation.

Therefore, what defines the ER-mitochondrial contact site that will pursue fragmentation? Lewis *et al.* (2016) demonstrated that nucleoids actively engaged in mtDNA synthesis in mammalian cells were spatially and temporally linked to a subset of ER-mitochondria contacts engaged for mitochondrial division. Indeed, replicating mtDNA nucleoids localized to mitochondrial tips before mitochondrial constriction by the ER tubules and assembly of the Drp1 division machinery (Lewis *et al.*, 2016). These findings suggest that ER-mitochondria contacts coordinate mtDNA replication with downstream mitochondrial division to segregate nascent mtDNA to daughter mitochondria.

Besides the ER, actin polymerization at the mitochondrial surface has also been suggested to aid in the initial constriction of mitochondria (Hatch *et al.*, 2014). This is controlled by the actin regulatory proteins inverted formin 2 (INF2), which is located in the membrane of the ER, and the mitochondrial Spire1C.

Silencing either of these results in mitochondrial elongation and defects in actin polymerization at the mitochondria-ER interface (Korobova *et al.*, 2013) (Manor *et al.*, 2015). At the ER-mitochondria contact sites, INF2 cooperates with Spire1C to regulate actin assembly required for mitochondrial constriction before Drp1 recruitment and oligomerization (Figure 1.4) (Tilokani *et al.*, 2018).

After the ER-mediated constriction of mitochondria, MiD49 and MiD51 recruit and stabilize GTP-bound Drp1 in the OMM. Then, Drp1 polymerizes with other GTP-bound Drp1 forms, and GTP hydrolysis leads to MiD49/MiD51 receptor dissociation and curling of the Drp1 filaments into closed rings (Kalia *et al.*, 2018). Finally, the Drp1 ring is stabilized by its interaction with Mff and Fis1. Therefore, different receptor proteins recruit and stabilize a specific nucleotide-bound conformation of Drp1, which enables Drp1 to perform mechanical work around the mitochondrial tubule to induce scission.

Final steps of mitochondrial division

The ubiquitously expressed classical Dynamin 2 (Dnm2) has been suggested to be involved in the final mitochondrial constriction. As demonstrated by Lee *et al.* (2016) using live-cell and electron microscopy imaging in PtK1 and COS7 cells, mitochondrial membrane constriction occurs in a sequential manner where Drp1 assembles first and constricts mitochondria to a final diameter that is conducive for Dnm2 assembly to complete fission (Figure 1.4). However, the molecular details of Dnm2 function remain unclear, and opposite views exist on this topic (Fonseca *et al.*, 2019). This could indicate that Dnm2 function promoting the final mitochondria scission could be organism or cell-type specific.

Finally, the Golgi apparatus has also been recently described to participate in the late steps of mitochondrial division. Nagashima *et al.* (2020) found that microdomains of phosphatidylinositol 4-phosphate [PI(4)P] on Golgi vesicles were recruited to mitochondria-ER contact sites and facilitated mitochondrial division downstream of Drp1. Deletion of the ADP-ribosylation factor 1 (Arf1) or its effector, phosphatidylinositol 4-kinase IIIb [PI(4)KIIIb], in different mammalian cell lines, prevented PI(4)P generation and led to a hyperfused and branched mitochondrial network marked with extended mitochondrial constriction sites (Nagashima *et al.*, 2020).

Overall, these findings reveal a collaborative participation of different cellular organelles on driving mitochondrial fragmentation. From the initial selective marking of the sites of mitochondrial fission by the ER and actin filaments to the recruitment of Drp1 and the final mitochondrial scission aided by the Golgi, these findings highlight the complexity of mitochondrial fragmentation and the requirement for inter-organellar communication.

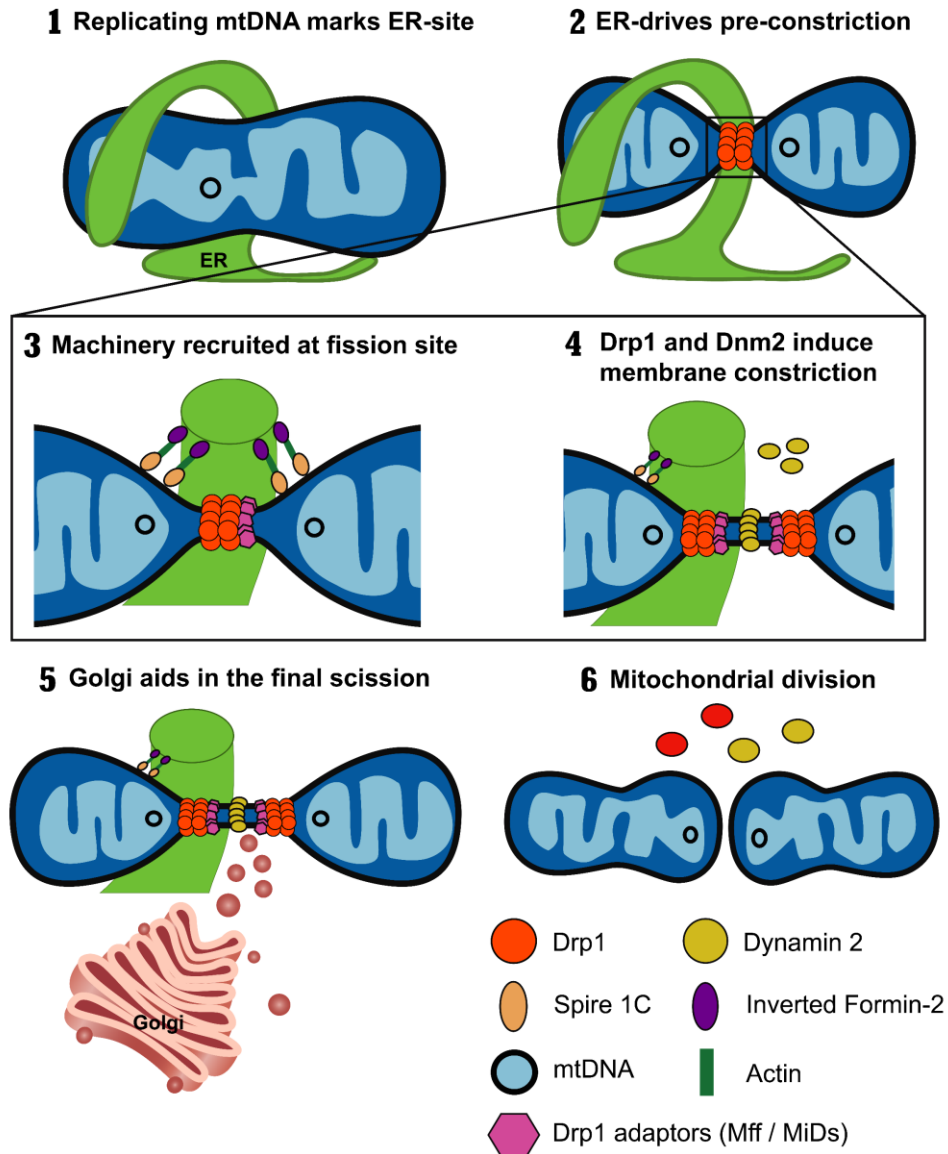


Figure 1.4. Model for mitochondrial fission in mammals.

(1) Replication of the mtDNA marks the site for the ER recruitment and first constriction of mitochondria. (2) Oligomeric forms of Drp1 accumulate at ER-mitochondria contact where the mtDNA nucleoids were replicated. The zoomed area highlights the factors regulating mitochondrial division. (3) The ER-bound INF2 and mitochondrial Spire1C induce actin polymerization at mitochondria–ER contact sites. At these sites, Mff and MiDs recruit Drp1 where it oligomerizes in a ring-like structure, and GTP hydrolysis leads to conformational change, enhancing pre-existing mitochondrial constriction. (4) Dnm2 is recruited to the Drp1-mediated mitochondrial constriction site where it assembles and intensifies membrane scission. (5) Golgi-derived vesicles accumulate at Drp1 foci. (6) The dynamic activity of all components results in complete division and separation of the daughter mitochondria, with Golgi-derived vesicles and the fission machinery dissociating from the fission site. Adapted from Tilokani *et al.* (2018).

1.5 Drp1 regulation

The human Drp1 protein is encoded by the *Dnm1l* gene, located in chromosome 12 and contains 21 exons. Drp1 homologs are found in yeast (Otsuga *et al.*, 1998) (Bleazard *et al.*, 1999), and in all metazoans, including *C. elegans* (Imoto *et al.*, 1998) (Labrousse *et al.*, 1999), *Drosophila* (Verstreken *et al.*, 2005) (Aldridge *et al.*, 2007) or rodents (Yoon *et al.*, 1998), and share a high degree of sequence similarity (Rosdah *et al.*, 2020). Furthermore, the alternative splicing of *Dnm1l* mRNA generates different variants that include or exclude amino acid residues in the encoded isoform. This, in turn, impart conformational constraints of the protein (Yang *et al.*, 2016) or modify the variations in Drp1 post-translational modifications (Merkin *et al.*, 2012).

1.5.1 Drp1 structure

The vast majority of studies use the classical (sequential) Drp1 structure nomenclature for the four domains, namely (1) the N-terminal GTP-binding domain (GTPase); (2) the middle domain; (3) the variable domain; and the (4) C-terminal GTPase effector domain (GED) (Figure 1.5). Nevertheless, X-ray structural studies of Drp1 human isoform 2 identified three distinct (non-sequential) structural domains: the GTPase domain, the bundle signaling elements (BSE) and the stalk region (Fröhlich *et al.*, 2013). A fourth domain, the variable domain, could not be resolved due to its dynamic nature, which allows it to act as a flexible hinge. Therefore, two different nomenclatures (sequential or non-sequential) can be used to refer to Drp1 structure (Figure 1.5). For simplicity, this document will refer to the classical (sequential) Drp1 nomenclature.

GTPase domain. The GTPase domain is essential for GTP binding and to provide the mechanical force to drive membrane scission. For instance, mutations that impair Drp1 GTPase activity (i.e.: K38A in the GTPase domain) generate extremely long and interconnected mitochondria by inhibiting mitochondrial division. Indeed, the Drp1-K38A mutant binds but does not hydrolyze or release GTP. Therefore, the affinity of Drp1-K38A for mitochondrial membranes is increased, but instead forms inactive aggregates unable to carry out the final mitochondrial scission (Yoon *et al.*, 2001) (Whitley *et al.*, 2018).

GTPase Effector Domain (GED). The GED or assembly domain of Drp1, in addition to being crucial for the regulation of the GTPase activity, mediates both intra- and intermolecular Drp1 interactions. Indeed, mutations within the GED (e.g.: K679A) inhibit its intramolecular backfolding onto the middle domain, which leads to a markedly decrease in Drp1 GTPase activity and mitochondrial fission in mammalian cells (Zhu *et al.*, 2004).

Middle domain. The Drp1 middle domain facilitates tetramer formation as well as higher order assembly on membranes. In line with this, overexpression of middle domain mutants (A395D, A350D, A363D) in HeLa cells inhibited mitochondrial division by impairing Drp1 ring formation (Chang *et al.*, 2010). In an analogous paradigm, peroxisomal and mitochondrial division in CHO cells were impaired by the Drp1 G363D middle domain mutation (Tanaka *et al.*, 2006).

Variable domain. Upon higher-order assembly, the variable domain of Drp1 functions as a pivot to direct a helical conformation (Francy *et al.*, 2017) (Lu *et al.*, 2018). Flexibility in the variable domain is necessary for optimal geometry during oligomerization. Specifically, the helical assembly of oligomers is required for cooperative GTPase activity and fine-tuning of the diameter of Drp1 rings encircling the mitochondrial tubule (Macdonald *et al.*, 2016) (Lu *et al.*, 2018). Furthermore, the variable domain facilitates Drp1 helical polymers to attach to cardiolipin-rich membranes (Lu *et al.*, 2018).

Overall, the coupled functionality of the different Drp1 domains is essential for its assembly, recruitment to mitochondria and activity to perform mitochondrial fission.

1.5.2 Drp1 isoforms

Alternative splicing of the *Dnm1l* transcript generally takes place in exon 3 (encoding the A-insert within the GTPase domain) and exons 16 and 17 (encoding the B-insert within the variable domain). This alternative splicing then gives rise to nine Drp1 isoforms in mammalian cells (Rosdah *et al.*, 2020). The various Drp1 isoforms differ in their tissue distribution (Strack *et al.*, 2013), and can influence Drp1 activity (Macdonald *et al.*, 2016) and subcellular localization (Strack *et al.*, 2013) (Itoh *et al.*, 2018). For example, mouse Drp1 isoform 1 (comprising 742 aa) is highly expressed in neurons, while the shorter isoform 3 (only ranging 699 aa) is expressed ubiquitously (Strack *et al.*, 2013). In addition, isoform 1 lacks the A-insert but contains the B-insert, whereas isoform 3 lacks both A- and B-inserts (Rosdah *et al.*, 2020).

However, a limitation on most published studies on Drp1 is that these have not explicitly indicated which Drp1 isoform was under investigation, or have favored an isoform that might not be the most suitable to address the hypothesis in question (Itoh *et al.*, 2018). Referring to Drp1 according to the species under study and splice isoform will be crucial for understanding Drp1 function in different organisms and tissues.

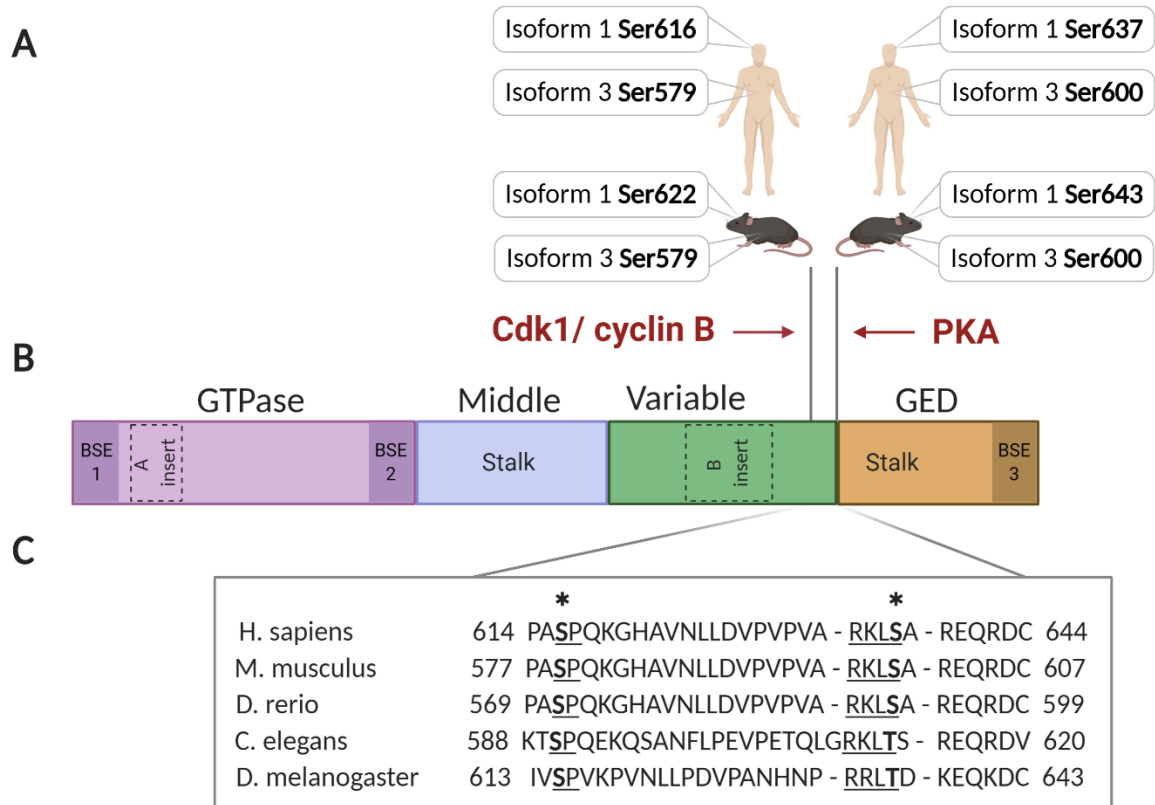


Figure 1.5. Drp1 structure and phosphorylation sites.

(A) CDK1/cyclin B phosphorylates Drp1 at a serine residue within the variable domain. Drp1 is also phosphorylated by cAMP-dependent PKA at a serine residue situated at the interface of the variable domain and the stalk of the GED. The different nomenclatures for these sites are isoform-dependent and are indicated for the neuron-specific Isoform 1 and ubiquitously expressed Isoform 3. **(B)** Linear schematic shows the domain structure of Drp1. Labelled above the schematic is the classical (sequential) domain boundaries, while the structural (non-sequential) domains are labelled within the schematic. **(C)** Alignment of Drp1 protein sequences from different metazoan species. Asterisks and bold letter mark the serine phosphorylation sites for Cdk1/cyclin B and PKA, respectively. Underline indicates the conserved consensus motif.

1.5.3 Drp1 post-translational modifications

The modulation of Drp1 function has been a topic of great interest. Many studies overexpressing the Drp1 WT form in cells have not reported an increase in fission, but rather intermediate mitochondrial shapes (Rambold *et al.*, 2011) (Chang & Blackstone, 2010), indicating that simply altering Drp1 protein levels would not significantly change mitochondrial fission. Instead, Drp1 activity is regulated by intrinsic modifications of the protein structure that ultimately determine Drp1 translocation to mitochondria, its assembly capability and its GTPase activity. Indeed, Drp1 function is regulated by post-translational

modifications, including phosphorylation, SUMOylation, ubiquitination, S-nitrosylation, acetylation, and O-GlcNAcylation.

Drp1 **phosphorylation** is one of the most widely reported post-translational modifications, due to the implication of different kinases and phosphatases that link mitochondrial fission to different cellular processes. Two phospho-sites, in particular Serine 616 and Serine 637, are shared among all Drp1 isoforms and have been most extensively studied (Rosdah *et al.*, 2020). The first described Drp1 phosphorylation came from the Mihara group in 2007, who reported that Cdk1/cyclin B could phosphorylate Drp1 at the Serine 616 residue (corresponding to human Drp1 isoform 1; S579 in mouse isoform 3), and this resulted in Drp1 recruitment to the OMM, and subsequent mitochondrial fragmentation (Taguchi *et al.*, 2007). Thus, the phosphorylation at this site establishes a link between mitochondrial dynamics and cell division during mitosis, which ensures the proper distribution and segregation of mitochondria into daughter cells. The S616 site is located in the variable domain of Drp1 (Figure 1.5). Moreover, Drp1 S616 has been shown to also be targeted by the Protein Kinase C δ (PKC δ) or the mitogen-activated protein kinase family (ERK1/2) to induce mitochondrial fragmentation (Qi *et al.*, 2011) (Kashatus *et al.*, 2015). In fact, many human tumors display increased levels of Drp1 phospho-S616 due to the hyperactivation of ERK1/2, making this site of great interest for the development of anti-tumorigenic therapeutic strategies (Kashatus *et al.*, 2015).

Later in 2007, two different groups identified a second Drp1 phosphorylation site at Serine 637 (as in Drp1 human isoform 1; equivalent to S600 in mouse variant 3) (Cribbs & Strack, 2007) (Chang & Blackstone, 2007). This site is situated at the interface of the variable domain and the stalk within the GED and is part of a consensus site highly conserved among metazoans (Figure 1.5). All evolutionary substitutions preserve the consensus motif (R-[R/K]- × -[S/T]) (Figure 1.5). It was originally discovered as a substrate of the cAMP-dependent Protein Kinase A (PKA). Drp1 phosphorylation at S637 by PKA was reported to inhibit its GTPase activity, thereby impeding mitochondrial fission (Cribbs & Strack, 2007) (Chang & Blackstone, 2007) (Gomes *et al.*, 2011). Similarly, the mitochondrial A-kinase anchoring protein 1 (AKAP1) was described to facilitate S637 phosphorylation by targeting PKA to the OMM, thus inhibiting Drp1-mediated mitochondrial fission and leading to unopposed mitochondrial elongation (Merrill *et al.*, 2011). Moreover, the phosphatase calcineurin dephosphorylates S637, and this regulates Drp1 translocation to mitochondria to execute fragmentation (Cereghetti *et al.*, 2008) (Edwards *et al.*, 2020). However, conflicting reports have emerged demonstrating that phosphorylation of this same site can, in fact, promote mitochondrial fission. Indeed, AKAP1-mediated phosphorylation of S637 promoted Drp1

recruitment to mitochondria in high-glucose-stimulated podocytes, inducing mitochondrial fragmentation (Chen *et al.*, 2020). Furthermore, phosphorylation at the Drp1 S637 by Ca^{+2} -calmodulin-dependent protein kinase I α (CaMKI α) has been documented to facilitate Drp1 recruitment and mitochondrial fission in neurons (Han *et al.*, 2008). Similarly, Rho-associated protein kinase 1 (ROCK1) mediates hyperglycemia-induced Drp1 recruitment to mitochondria by phosphorylation of Drp1 at S600 of mouse isoform 3, which eventually leads to mitochondrial fission in podocytes (Wang *et al.*, 2012b). In addition, Drp1 phosphorylation in the mouse Ser600 (isoform 3) in response to norepinephrine triggers mitochondrial fragmentation in primary brown adipocytes (Wikstrom *et al.*, 2014). Altogether, the effects of S637 phosphorylation on Drp1 function may be highly cell type and stimuli dependent, and also could vary depending on the Drp1 isoform under study. For instance, since Drp1 isoform 3 lacks both the A- and B-inserts, the phosphorylation at S637 may confer conformational changes that favor fission in this particular paradigm (Rosdah *et al.*, 2020).

Other Drp1 phosphorylations have also been described, but are less studied (Figure 1.6). Phosphorylation of the GTPase domain sites Serine 40/44 by glycogen synthase kinase 3 β (GSK3 β) induces mitochondrial fragmentation in cultured neurons, which were then more vulnerable to amyloid- β (A β)–induced apoptosis (Yan *et al.*, 2015). Contrarily, GSK3 β -mediated phosphorylation of Drp1 at the Serine 693 site decreases its GTPase activity leading to mitochondrial elongation, which protected neuronal cells against oxidative stress-induced apoptosis (Chou *et al.*, 2012).

The small ubiquitin-like modifier (SUMO) protein is also involved in Drp1 modification (Anderson & Blackstone, 2013). Pioneering discoveries on the role of **SUMOylation** on Drp1 function and mitochondrial dynamics have been provided by the McBride group. Initially, they described that Drp1 was a substrate of SUMO1, which was often found at the sites of mitochondrial fission and colocalized with endogenous Drp1 in mammalian cells (Harder *et al.*, 2004). Interestingly, SUMO1 was suggested to specifically protect Drp1 from degradation, resulting in a more stable, active pool of Drp1 (Harder *et al.*, 2004). Recently, SUMO1 has been suggested to facilitate the phosphorylation of Drp1 at S616 via regulating the catalytic activity of the phosphatase DUSP6 (Ma *et al.*, 2020). Furthermore, Drp1 SUMOylation by MAPL/MUL1 functionally stabilizes ER-mitochondrial contact sites, leading to mitochondrial constriction, calcium flux and Cytochrome C release during the onset of apoptosis (Prudent *et al.*, 2015). Alternative enzymes described in mediating Drp1 SUMOylation are the SUMO transferase Ubc9 or the proteases SENP3 and SENP5 (Harder *et al.*, 2004) (Figueroa-Romero *et al.*, 2009) (Zunino *et al.*, 2007) (Guo *et al.*, 2013). Critical

SUMO-acceptor residues of Drp1 are located in the B-insert of the variable domain, specifically Lys532, 535, 558 and 568 (Figueroa-Romero *et al.*, 2009).

Drp1 can also be modified by **ubiquitination**. Membrane associated RING finger 5 (MARCH5, also known as MITOL) is an OMM E3 ligase that ubiquitinates Drp1 on the OMM. MARCH5-mediated ubiquitination of Drp1 was originally reported to mark Drp1 for proteolytic degradation, leading to reduced fission and elongated mitochondrial network (Nakamura *et al.*, 2006) (Yonashiro *et al.*, 2006). In later reports, MARCH5-mediated Drp1 ubiquitination was shown to enhance mitochondrial fission by regulating the subcellular trafficking of Drp1 (Karbowski *et al.*, 2007). To address these contradictory findings, it was suggested that inhibition or delay of a final step of the mitochondrial fission process could lead to increased colocalization of MARCH5 and Drp1, resulting in MARCH5-mediated degradation of Drp1 (Karbowski *et al.*, 2007). Parkin is another E3 ubiquitin ligase demonstrated to ubiquitinate Drp1 for degradation, leading to suppression of mitochondrial fission in neurons (Lutz *et al.*, 2009) (Wang *et al.*, 2011).

S-nitrosylation is a redox-related modification of cysteine residues by nitric oxide (NO), which in normal conditions acts as a signaling molecule, but in excess can lead to cellular damage. S-nitrosylation of Drp1 at Cysteine 644 has been linked to excessive mitochondrial fission in neuronal injury models (Barsoum *et al.*, 2006) and neurodegenerative diseases, including Alzheimer's disease (Cho *et al.*, 2009), Parkinson's disease (Zhang *et al.*, 2016) or Huntington's disease (Haun *et al.*, 2013). In line with this, Drp1 S-nitrosylation was described to promote cell senescence and aging in mammals (Rizza *et al.*, 2018). In these models, NO overproduction induces Drp1 phosphorylation at S616, leading to its activation and recruitment to mitochondria (Zhang *et al.*, 2016) (Lee & Kim, 2018). These observations emphasize the role of Drp1 S-nitrosylation in neurodegenerative disorders and suggests of an interplay between Drp1 S-nitrosylation and Drp1 phosphorylation.

Drp1 **acetylation** has been the newest reported post-translational modification, which occurs at Lysine 642 (K642) and promotes Drp1 oligomerization and recruitment to mitochondria to promote fission (Hu *et al.*, 2020). In an analogous paradigm to Drp1 S-nitrosylation, acetylation at K642 was linked to increased Drp1 phosphorylation at S616 in adult cardiomyocytes treated with palmitate (Hu *et al.*, 2020). However, it is still not clear whether this increased phosphorylation was the consequence of lipid overload or a downstream direct effect of Drp1 acetylation. This latter hypothesis seems more likely, since treatment of adult cardiomyocytes with oleate – which is the most abundant unsaturated fatty acid in the plasma of HFD-fed mice – had no effect on Drp1 acetylation or Drp1 phosphorylation at S616 (Hu *et al.*, 2020).

Finally, Drp1 undergoes **O-GlcNAcylation** in cardiomyocytes at Threonine 585 and 586, respectively, which augments the levels of GTP-bound active form of Drp1 and induces Drp1 translocation from the cytosol to mitochondria (Gawłowski *et al.*, 2012). Increased O-GlcNAcylation has been associated to a reduction in the phosphorylation at the S637 site. In this regard, O-GlcNAcylation could directly affect the activity of other enzymes (such as PKA and/or calcineurin) or proximal residues within Drp1, which in turn affect the phosphorylation of S637.

Overall, these findings demonstrate that various post-translational modifications can regulate Drp1 activity, function and localization (Figure 1.6). Moreover, these modifications are not exclusive, but can occur in combination, directly influencing each other.

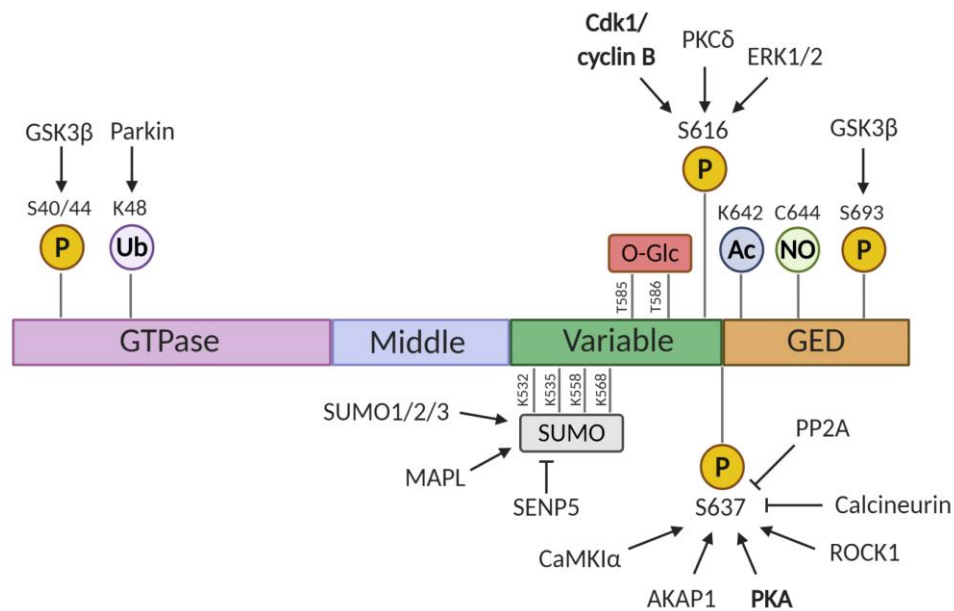


Figure 1.6. Drp1 regulation by post-translational modifications.

Drp1 activity is regulated by various post-translational modifications, namely phosphorylation (P), ubiquitination (Ub), O-GlcNAcylation (O-Glc), SUMOylation (SUMO), acetylation (Ac) and S-nitrosylation (NO). The amino acid numbering is based on the reference literature. Indicated are the GTPase domain, middle domain, variable domain and GTPase effector domain (GED).

1.6 Metabolic regulation and mitochondrial dynamics

1.6.1 Mitochondrial alterations in metabolic disease

As the primary platform controlling metabolic and energy homeostasis, mitochondria show aberrant function during metabolic dysregulation. The World Health Organization estimated that in 2016 more than 650 million adults worldwide were obese, reaching pandemic proportions globally (WHO 2020©).

This reflects the profound changes in lifestyle largely attributed to the overconsumption of energy-dense foods combined with reduced physical activity (Cheng & Almeida, 2014). Consequently, obesity increases the risk of type 2 diabetes mellitus (T2DM), cardiovascular disease or cancer. Many studies demonstrated a link between these diseases and mitochondrial dysfunction. Indeed, nutrient surplus hyperpolarizes mitochondria, leading to a decrease in metabolic substrate oxidation (particularly fatty acids) and ROS overproduction (Cheng & Almeida, 2014). In addition, ROS induces mitochondrial dysfunction and leads to impaired insulin secretion in pancreatic β -cells, thereby deteriorating metabolic homeostasis.

Defects in insulin signaling impair the response of the cell to insulin and thus trigger insulin resistance (Beale, 2013). As such, insulin resistance refers to the pathological condition in which insulin-dependent cells, such as skeletal muscle cells or adipocytes, fail to properly respond to normal insulin circulatory levels (Samuel & Shulman, 2016). In conditions of insulin resistance, severe hyperglycemia, hyperinsulinemia and dyslipidemia can occur after a glucose load, giving rise to glucose intolerance. Therefore, impaired insulin signaling affects systemic insulin-stimulated glucose disposal, albeit it can also impair specifically insulin function in tissues including liver, adipose tissue or the heart (Shimobayashi *et al.*, 2018) (Ormazabal *et al.*, 2018) (Samuel & Shulman, 2016).

Since mitochondrial form and function are tightly linked, metabolic perturbations associated to obesity-related disorders will also impact mitochondrial architecture. Mitochondrial dynamics is a crucial quality control mechanism to maintain a healthy mitochondrial network, particularly allowing cells to adapt and respond to metabolic challenges.

1.6.2 Role of cellular metabolism in shaping mitochondrial dynamics

One of the first evidences linking mitochondrial dynamics and cellular metabolism was reported by the Zorzano group in 2003. Using a differential mRNA screen, the *Mfn2* gene turned out to be one of the most significantly downregulated in skeletal muscles of obese diabetic rats (Bach *et al.*, 2003). Electron microscopy from these muscles showed a reduced mitochondrial size in line with a fragmented mitochondrial network (Bach *et al.*, 2003). Similarly, *Mfn2* mRNA levels were also reduced in obese humans and patients with T2DM (Bach *et al.*, 2005). Interestingly, weight loss in the obese patients resulted in a substantial recovery in *Mfn2* levels in skeletal muscle, and this was directly correlated with improved insulin sensitivity (Bach *et al.*, 2005). These observations suggested that increased adiposity was linked to repression of mitochondrial fusion, albeit this could be reversed by weight loss. In line with this, mitochondrial fission has been described in the metabolic response to nutrient surplus. Indeed, increased mitochondrial fragmentation was observed after treatment with palmitate in INS-1 and MEF cells, as well

as in AML12 hepatocytes (Molina *et al.*, 2009) (Kulkarni *et al.*, 2016). Stimulation of mitochondrial fission upon nutrient overload occurs by fine-tuning of Drp1 post-translational modifications aimed to enhance Drp1 GTPase activity. For instance, diabetic mice display increased Drp1 S616 phosphorylation in brain (Huang *et al.*, 2015) and Drp1 O-GlcNAcylation in heart (Gawlowski *et al.*, 2012), both of which activate Drp1 to trigger mitochondrial fragmentation.

The opposite condition to nutrient excess, starvation, causes an acute inhibition of mitochondrial fission by preventing Drp1 recruitment to mitochondria, hence promoting unopposed mitochondrial tubulation (Gomes *et al.*, 2011) (Rambold *et al.*, 2011) (Liesa & Shirihai, 2013). Mitochondrial elongation then leads to increased number of cristae, which facilitates the dimerization of the ATPase F0/F1 enzyme (Gomes *et al.*, 2011). This maximizes the efficiency of energy conversion and aids maintaining ATP production to allow the survival of the starving cell, thus sparing it from autophagic elimination (Gomes *et al.*, 2011) (Strauss *et al.*, 2008). Conversely, blocking fusion prevents mitochondria to maintain ATP production upon starvation, prompting cell death. Therefore, these observations suggest that nutrient depletion promotes mitochondrial elongation to increase ATP synthesis capacity, thus sustaining the ATP demand required for cell survival.

Altogether, the examples reviewed here illustrate that nutrient excess is associated with mitochondrial fragmentation while the opposite nutrient paradigm, starvation, is associated with mitochondrial elongation. This comparison emphasizes the role of mitochondrial dynamics in changes in mitochondrial bioenergetic efficiency.

Beyond nutrients, other hormonal inputs can have a strong impact on mitochondrial function. In this sense, and of particular interest for this thesis, the brown adipocyte represents a model in which a large shift in bioenergetic efficiency can be acutely induced through hormonal stimulation. Activation of non-shivering thermogenesis in human brown adipocytes by cold exposure is the result of norepinephrine (NE) - induced lipolysis (reviewed in (Cannon & Nedergaard, 2004) and (Ouellet *et al.*, 2012)). In fact, NE-stimulation triggers mitochondrial fission in the BAT via Drp1 phosphorylation at S637 (Wikstrom *et al.*, 2014). This forced mitochondrial fragmentation enhances mitochondrial uncoupling capacity in brown adipocytes by increasing fatty acid availability to UCP1 and promoting BAT energy expenditure. In fact, the rapid fatty acid uptake into BAT resulted in improved dyslipidemia and insulin resistance in mice, thereby testifying for the mitochondrial function in brown adipocytes in modulating glucose metabolism and energy homeostasis. Accordingly, inhibiting mitochondrial fission jeopardized thermogenic function

in primary brown adipocytes, as validated by the decreased energy expenditure of brown adipocytes expressing an inactive dominant form of Drp1 (Wikstrom *et al.*, 2014).

1.6.3 Drp1 in the regulation of nutrient utilization: Lessons from mouse models

Mitochondrial morphology varies significantly across tissues, as the mitochondrial network adapts to their particular metabolic needs (Figure 1.7). Thus, the genetic ablation of mitochondrial fusion and fission components can elicit different responses that vary between tissues and organs.

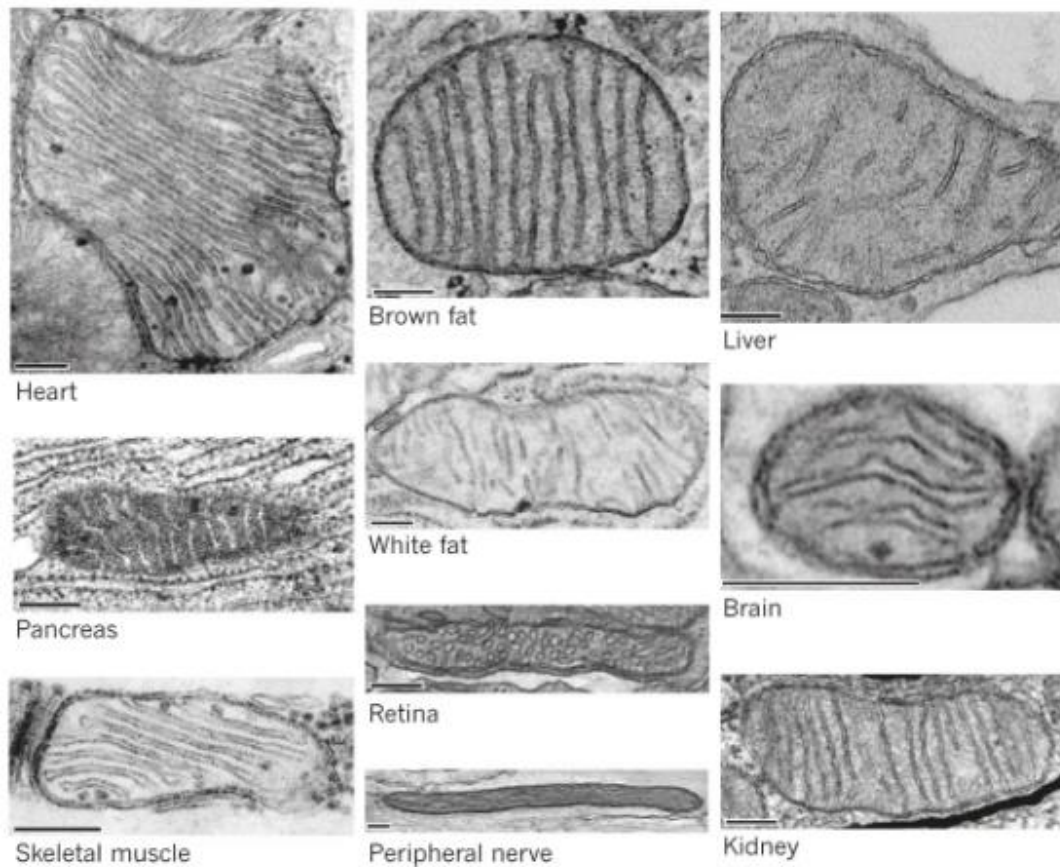


Figure 1.7. Diversity of the mitochondrial shape in different tissues.

Electron micrographs of mitochondria from various tissues (scale bar, 200 nm) (Vafai & Mootha, 2012).

Early attempts to evaluate the impact of mitochondrial dynamics on mitochondrial function were based on classical gain- or loss-of-function approaches through overexpression or genetic knockdown/ablation, respectively, of the mitochondrial fission or fusion machinery. In line with the homozygous deletion of either *Mfn1*, *Mfn2* or *Opa1* in mice, whole-body ablation of the *Dnm1* gene is embryonically lethal (Chen *et al.*, 2003) (Davies *et al.*, 2007) (Wakabayashi *et al.*, 2009). Accordingly, Drp1 homozygote knockout (KO)

mice have developmental abnormalities, particularly in the forebrain, and die shortly after E12.5 from brain hypoplasia (Wakabayashi *et al.*, 2009). Primary cultures from Drp1KO forebrain showed a decrease in neurites and the presence of defective synapse formation, as mitochondria formed aggregates and exhibited impaired trafficking to synapses (Ishihara *et al.*, 2009). In line with this, Drp1-mediated synaptic degeneration has also been described as a causative factor in human neurodegenerative disorders such as Alzheimer's, Parkinson's or Huntington's disease (Qi *et al.*, 2019). Therefore, the modulation of Drp1 function has been a topic of increasing interest, also because Drp1 is involved in other age-related pathologies such as metabolic disorders (obesity and T2DM), cardiovascular diseases or cancer (Serasinghe & Chipuk, 2017). In this section, we will thus focus on the metabolic implications upon alteration of the mitochondrial fission machinery, particularly Drp1. For this, we will summarize the evidences learned from Drp1 mouse models in a tissue-specific case manner. A resume of the animal models described can be found on Table 1.

Liver

Deletion of Drp1 in mouse liver (Drp1-LKO) impairs mitochondrial fission and results in reduction in the number of mitochondria, which appear more tubulated (Wang *et al.*, 2015). The increased swelling of mitochondria and the aberrant morphology of the endoplasmic reticulum (ER) prevented mitochondria-ER contacts and triggered the ER stress response in the Drp1-LKO mice via the induction of the eIF2 α axis. Consequently, this elicited an increase in downstream targets CHOP and ATF4, which promoted the transcription of *Fgf21* in liver and increased the levels of circulating Fgf21 in plasma of the Drp1-LKO mice (Wang *et al.*, 2015). These effects were observed on a normal diet and were further exacerbated on a high-fat feeding. Of note, Fgf21 has been proposed as a marker of mitochondrial dysfunction, validated by the fact that pathological conditions that impair mitochondrial respiration and cause a reduction in ATP synthesis lead to the increase in Fgf21 levels in plasma (Suomalainen, 2013). Thus, the elevated Fgf21 levels in the Drp1-LKO mice likely testify for defective mitochondrial function. Nevertheless, the Drp1-LKO mice were protected from diet-induced obesity due to reduced adiposity and increased whole-body energy expenditure (Wang *et al.*, 2015). Liver-derived Fgf21 contributes in the regulation of thermogenesis in adipose tissues (Ameka *et al.*, 2019). Accordingly, the expression of UCP1 was significantly higher in the Drp1-LKO BAT, and also in WAT, thereby suggesting an Fgf21-induced browning of the adipose tissue. Despite the fact that Drp1-LKO mice showed improved systemic glucose metabolism, the levels of AKT phosphorylation, which is a marker of insulin sensitivity and glucose clearance, were significantly reduced in the livers of Drp1-LKO mice (Wang *et al.*, 2015). This could hint an

alternative mechanism for energy homeostasis that includes the compensation by other tissue-specific signaling pathways. Globally, these results suggest that defects in the inter-organellar communication between the ER and mitochondria directly modulate Fgf21 signaling as a compensatory mechanism to maintain metabolic homeostasis (Wang *et al.*, 2015)

Thus, Drp1 in the liver regulates the communication between the ER and the mitochondrial network and demonstrates that, when disrupted, leads to hepatic insulin resistance.

Muscle

The skeletal muscle-specific overexpression of Drp1 in mice prevented the formation of the inner pool of inter-myofibrillar mitochondria, and this impaired postnatal muscle development (Touvier *et al.*, 2015). Similar to the previous Drp1-LKO model described, transgenic mice overexpressing Drp1 displayed a persistent activation of the eIF2 α /ATF4 axis of the ER stress-response cascade that interfered with muscle anabolism by preventing protein synthesis (Touvier *et al.*, 2015). Thus, this demonstrates that Drp1 overexpression in muscle inhibits cytosolic protein translation and results in reduced growth hormone signaling. Interestingly, the phenotype observed upon genetic ablation of *Dnm1l* in muscle is identical to that of Drp1 overexpression. Indeed, skeletal muscle-specific Drp1 KO mice (Drp1-skmKO) exhibited an enhanced ER stress response and inhibition of protein translation via eIF2 α activation, eventually resulting in reduction of muscle growth (Favaro *et al.*, 2019). This muscle growth degeneration in the Drp1-skmKO mice consequently led to body weight loss and mice died within 30 days of postnatal life. One of the peculiarities of the loss-of-function approach is the great induction of Fgf21 in muscle, which could give an explanation to the observed metabolic changes in the Drp1-skmKO mice (Favaro *et al.*, 2019).

Given that Drp1-related fission activity is controlled by post-translational modifications, strategies altering Drp1 phosphorylation could also provide clues on the physiological role of Drp1. In this sense, the muscle-specific ablation of calcineurin, the phosphatase that dephosphorylates Drp1 at S637, attenuated exercise capacity but protected mice against diet-induced obesity (Pfluger *et al.*, 2015). Interestingly, overexpression of calcineurin in mouse skeletal muscle has also been reported to protect against diet-induced obesity (Jiang *et al.*, 2010).

The fact that the ablation and gain-of-function of calcineurin (or Drp1), respectively, evoke in a similar phenotype suggests that unopposed fusion or fission might be equally deleterious, due to the altered dynamic remodeling of mitochondria and the impaired quality control.

Heart

The description of Drp1 function in heart relies on heterozygous or inducible cardiac-specific mouse models (for more information, see (Dorn, 2015)). Even though the consequences of cardiac Drp1 ablation differ between studies (Table 1), some conclusions are similar. First, Drp1 is essential for normal homeostatic functioning of neonatal and adult hearts. Indeed, either postnatal or conditional adult cardiomyocyte-specific ablation of Drp1 compromised heart function. Second, enhanced mitochondrial fusion is not necessarily cardioprotective, testified by the fact that mitochondrial elongation by Drp1 deletion in mouse hearts can be as detrimental as the fragmentation elicited upon fusion impairment. Finally, Drp1 plays a crucial role in cardiac mitophagy. All of the studies with cardiac-specific Drp1 KO mouse models uncovered abnormalities in mitophagy. Furthermore, as part of a large scale mutagenesis screen, Ashrafian *et al.* (2010) identified a dominant mutation in the middle domain of the *Dnm1l* gene, which was named Python mutation, that led to inherited dilated cardiomyopathy in mice. While the homozygous mutation is embryonically lethal, the Python heterozygous mutation resulted in abnormally elongated mitochondria and peroxisomes in cultured neonatal skin fibroblasts. In addition to this, hearts from heterozygous Python mice showed reduced mitochondria enzyme complexes and ATP levels, respectively, leading to impaired cardiac energy metabolism (Ashrafian *et al.*, 2010). Overall, Drp1-mediated mitochondrial fission is essential to mitochondrial quality control in the heart.

Brain

In neurons, mitochondrial fission facilitates both axonal mitochondrial transport and mitophagic elimination (Shields *et al.*, 2015). In particular, Drp1 has been reported to control postsynaptic endocytosis, neuronal morphology and brain function (Itoh *et al.*, 2019). The inducible Drp1 deletion from adult forebrain neurons in mice triggered ER stress via the integrated stress response (ISR), resulting in increased circulating Fgf21 in plasma and mRNA levels in the Drp1 deficient neurons (Restelli *et al.*, 2018). Interestingly, no changes were observed in the canonical Fgf21 sources (liver and adipose tissue), indicating that Fgf21 was indeed produced in neurons upon mitochondrial dysfunction. Moreover, the Drp1 deficient neurons displayed synaptic dysfunction, which prompted the development of memory deficit and hippocampal atrophy in these forebrain neuron-specific Drp1 KO mice (Oettinghaus *et al.*, 2016). Of note, the activation of the ISR has also been suggested to be the retrograde response mechanism to widespread mitochondrial dysfunction in Alzheimer's disease (Weidling & Swerdlow, 2019). These observations indicate that Drp1-mediated mitochondrial fission is required for brain development and mature neuronal function. Similar observations were reported upon the ablation in mice of Drp1 in

CA1 hippocampal neurons, a neuronal population affected by Alzheimer's disease, stroke, and seizure disorders (Shields *et al.*, 2015). These CA1-specific Drp1 KO mice had impaired memory and synaptic function due to compromised ability of mitochondria in axons to produce ATP. These deficits occurred specifically at the nerve terminal, not at the cell body, and were sufficient to impair synaptic vesicle cycling (Shields *et al.*, 2015). Further sustaining the critical role of fission for mitochondrial trafficking in neurons, Drp1 ablation in mouse dopamine neurons led to axonal degeneration specifically in these neurons (Berthet *et al.*, 2014).

Therefore, these data reveal a crucial role of Drp1 in dendrite formation, neuronal morphology and brain function, which has broad implications for understanding the role of mitochondrial fission in the context of brain diseases and places it as an attractive therapeutic target.

Pancreas

The specific ablation of Drp1 in pancreatic β cells in mice (Drp1 β -KO) led to glucose intolerance due to impaired glucose-stimulated insulin secretion (GSIS) (Hennings *et al.*, 2018). Moreover, β -cells from the Drp1 β -KO mice exhibited hyperfused perinuclear mitochondria, and also increased peroxisomal elongation as compared with the spherical peroxisomes of control β cells. Nevertheless, the Drp1 β -KO islets displayed normal oxygen consumption (Hennings *et al.*, 2018). This differs from experiments using pancreatic β -cell lines overexpressing a dominant negative Drp1 form, where impaired ATP-linked oxygen consumption was reported (Kabra *et al.*, 2017) (Reinhardt *et al.*, 2016). This discrepancy could reflect a difference between the proliferative β -cells *in vitro* and the quiescent adult mouse islets, or could be the result of the effects of acute loss of Drp1 *in vitro* by siRNA as compared to the chronic *in vivo* deletion. Regardless, these observations provide evidence that changes in Drp1 function and mitochondrial fission can directly disrupt β -cell function and lead to whole body metabolic dysfunction.

Kidney

In the last years, the Danesh group has provided novel insights in the implications of Drp1 deletion in kidney from diabetic mice. For instance, ultrastructure analysis of podocytes revealed a marked amelioration in mitochondrial structure of the podocyte-specific Drp1 KO diabetic mice (db/db;Drp1^{Pod-ff}), compared to the marked mitochondrial fragmentation of control diabetic mice (Ayanga *et al.*, 2016). This granted Drp1-PodKO mice improved mitochondrial function, validated by the enhanced mitochondrial respiration and reduced ROS production, ultimately leading to systemic albuminuria decrease (Ayanga *et al.*, 2016). Interestingly, a separate study from the same group reported that ROCK1

plays a critical role in the progression of diabetic nephropathy by triggering mitochondrial fission via the direct phosphorylation of Drp1 at Ser600 (Wang *et al.*, 2012b). In line with this research, they recently described a Drp1 S600A knock-in (KI) mouse model in the development of kidney injury (Galvan *et al.*, 2019). This mutation prevented Drp1 translocation to the mitochondria, thus explaining the reduced mitochondrial fission in the diabetic Drp1 S600A mice (Galvan *et al.*, 2019). Podocytes of diabetic Drp1 S600A KI mice exhibited reduced mitochondrial ROS, along with improved histological and biochemical features that protected mice against the progression of diabetic nephropathy (Galvan *et al.*, 2019).

Mitochondrial fragmentation contributes to the development of kidney injury via release of pro-apoptotic factors by the mitochondria (Gall *et al.*, 2012). Hence, inhibition of mitochondrial fragmentation protects against tubular cell apoptosis and renal injury, suggesting a possible novel therapeutic strategy for the prevention and treatment of acute renal failure.

Table 1. Drp1 mouse models.

Tissue	Mouse model	Response	Reference
Liver	Drp1 KO	ER stress, Fgf21, improved glucose metabolism	Wang <i>et al.</i> , Diabetologia, 2015
Muscle	Drp1 overexpression	ER-stress via eIF2 α , Fgf21, muscle mass loss	Touvier <i>et al.</i> , Cell Death Dis, 2015
Muscle	Drp1 KO	ER-stress via eIF2 α	Favaro <i>et al.</i> , Nat Comms, 2019
Heart	Drp1 KO	MPTP-induced mitophagy	Song <i>et al.</i> , Cell Metabolism, 2015
Heart	Drp1 KO	Autophagy inhibition, I/R injury	Ikedo <i>et al.</i> , Circulation Research, 2015
Heart	Drp1 KO	Defective mitophagy	Kageyama <i>et al.</i> , EMBO J., 2014
Brain	CA1 hippocampal neuron Drp1 KO	Defective synaptic transmission, memory loss	Shields <i>et al.</i> , Cell Death Dis, 2015
Brain	Forebrain neuron Drp1 KO	ISR activation, Fgf21 induction	Restelli <i>et al.</i> , Cell Reports, 2018
Brain	Forebrain neuron Drp1 KO	Impaired memory function, hippocampal atrophy	Oettinghaus <i>et al.</i> , Cell Death Differ., 2016
Brain	Midbrain dopamine neuron Drp1 KO	Axon degeneration, parkinsonism	Berthet <i>et al.</i> , J Neurosci., 2014
Pancreas	β cell-specific Drp1 KO	Glucose intolerance, islets impaired GSIS	Hennings <i>et al.</i> , Endocrinology, 2018
Kidney	Podocyte-specific Drp1 KO	Protection against diabetic nephropathy	Ayanga <i>et al.</i> , JASN, 2016
Kidney	Podocyte-specific Drp1 S600A	Protection against diabetic nephropathy	Galvan <i>et al.</i> , JCI, 2019

Overall, here we reviewed the role of Drp1 in the function of different tissues, as well as the impact of its gain- or loss- of function on systemic metabolic adaptation. Yet, the interpretation from these studies still lacks the molecular definition that is at the root for the mitochondrial and cellular dysfunction. For instance, are the cellular and systemic adaptations a result of disturbed mitochondrial dynamics? Or, contrarily, is this a secondary effect from faulty mitochondrial turnover or mitochondrial contact with other organelles?

Thus, understanding whether the structural remodeling of mitochondria in many pathological conditions is cause or consequence of disease requires that we establish the sequence of events that follows the disruption or imbalance of mitochondrial dynamics within the cell, tissue, and ultimately, the whole organism.

1.7 Mitochondrial dynamics in human diseases

Research on mitochondrial dynamics came in the spotlight when it was discovered that mutations in the genes encoding for the components of the mitochondrial fission/fusion machinery were the cause for different human neurodegenerative disorders. Since then, the pathophysiological role of mitochondrial dynamics has been described on the progression of a wide range of human disorders. Throughout this Chapter 1, we have briefly depicted the role of mitochondrial dynamics in age-related pathologies, including metabolic disorders, as well as in cardiovascular and neurological diseases. In this final section, we will describe the first discoveries on the relation between mitochondrial dynamics and human disease, and will bring special emphasis to the crucial role of mitochondrial morphology in tumorigenesis.

1.7.1 Familial disorders arising from defects in mitochondrial dynamics proteins

In 2000, two simultaneous studies reported Opa1 mutations in patients affected by autosomal dominant optic atrophy (ADOA), which is the most common form of inherited optic neuropathy (Delettre *et al.*, 2000) (Alexander *et al.*, 2000). This neuropathy is characterized by a loss of retinal ganglion cells in the optic nerve, leading to a gradual and progressive loss of vision. Almost 50% of the mutations cause truncation of the Opa1 protein and while these can be found scattered along the Opa1 structure, the majority (approx. 41%) are detected in the GTPase domain (Thiselton *et al.*, 2002) (Ferré *et al.*, 2005). Some data indicate that ADOA develops as a consequence of a dominant negative mechanism, testified by the capacity of mutant Opa1 to oligomerize with wild-type proteins and, thus, interfere with GTPase activity (Olichon *et al.*, 2006). Recessive mutations in Opa1 have also been reported in the pathogenesis

of Behr syndrome, a complex neurological disorder characterized by early-onset optic atrophy, ataxia, and spasticity (Marelli *et al.*, 2011).

In 2004, Mfn2 mutations were reported in patients affected by Charcot-Marie-Tooth neuropathy Type 2A (CMT2A; OMIM #609260) in an autosomal dominant inheritance pattern (Züchner *et al.*, 2004). CMT2A disease belongs to the hereditary motor and sensory neuropathies, caused by heterozygous mutations in the gene encoding Mfn2. Clinically, patients exhibit progressive degeneration of peripheral sensory and motor axons, which eventually leads to distal sensory loss, muscle atrophy and weakness. More than 100 mutant forms of Mfn2 have been reported in CMT2A disease patients, most of which are missense mutations detected in the GTPase domain (>50%) (Beręsewicz *et al.*, 2018). Moreover, recent observations suggest that ER-mitochondria contacts are altered in CMT2A patients, and this correlates with disease severity (Larrea *et al.*, 2019). Morphological studies of nervous tissue and fibroblasts from CMT2A patients showed altered mitochondrial morphology, including swelling, degeneration and altered distribution of mitochondria (Verhoeven *et al.*, 2006).

Afterwards, a report published on *The New England Journal of Medicine* on 2007 described a newborn girl with microcephaly, abnormal brain development, optic atrophy and hypoplasia, and also persistent lactic acidemia, and a mildly elevated plasma concentration of very-long-chain fatty acids (Waterham *et al.*, 2007). Fibroblasts obtained from this patient showed defective mitochondrial and peroxisomal fission. Genetic analysis revealed a heterozygous missense mutation in Drp1 (A395D), mapping to a conserved residue in the middle domain of the protein (Waterham *et al.*, 2007). This mutation behaves as a dominant form and results in Drp1 inhibition through impairment of its initial oligomerization to form high-order assembly structures (Chang *et al.*, 2010). The Drp1 A395D mutation was lethal, possibly linked to the accumulation of defects on mitochondrial and peroxisome function. In 2016, the group of David Chan reported a novel missense mutation (R403C) in Drp1 in two unrelated patients who experienced normal development for 4-5 years of age before presenting with refractory focal status epilepticus and subsequent rapid neurological decline (Fahrner *et al.*, 2016). Similar to the A395D mutation, the R403C mutation impacts the middle domain of Drp1, which leads to reduced self-assembly and impaired recruitment to the mitochondrial surface. The R403C mutation also exhibits a common dominant-negative pattern, although the cellular and clinical phenotype observed with the A395D mutation was more severe (Fahrner *et al.*, 2016). In addition to this, Gerber *et al.* (2017) identified dominant mutations in the *Dnm1l* gene in three large families with isolated optic atrophy. Analyses of patient fibroblasts revealed accumulation of Drp1 aggregates on the cytoplasm and on highly tubulated mitochondria, although the

mechanism as to how these missense alleles result in disease remains to be explored. Hence, these observations suggest that, in addition to Opa1, mutations in Drp1 could contribute to inherited optic neuropathies.

Defects involving components of the fission machinery, such as Mff, have also been linked to human diseases. Indeed, patients harboring mutations in Mff became symptomatic within the first year of life, exhibiting seizures, developmental delay and acquired microcephaly (Koch *et al.*, 2016). Despite the fact that mitochondrial respiration was unchanged, skeletal muscle from these patients revealed elongated mitochondria and peroxisomes, as well as increased mitochondrial branching and an abnormal distribution of Drp1 (Koch *et al.*, 2016).

1.7.2 Cancer: a novel role for mitochondrial fission

In 1925 Dr. Otto Warburg linked for the first time mitochondria to tumorigenesis by observing that cancer cells undergo aerobic glycolysis, which offers a more rapid means of generating ATP (Warburg, 1925). Renovated interest in the role of mitochondria in cancer manifested in the mid-1990s with the demonstration that the permeabilization of the outer mitochondrial membrane and the release of Cytochrome C constitutes a decisive step in the execution of apoptosis (Liu *et al.*, 1996). It is now becoming clear that many oncogenic and tumor suppressor networks converge on mitochondria and alter cellular metabolism to support excessive tumor cell proliferation.

Interestingly, recent studies have revealed that hyper-activated oncogenic pathways act as potent signals to remodel mitochondrial dynamics during tumorigenesis (Trotta & Chipuk, 2017). According to the close link between mitochondrial function and morphology, oncogene-mediated metabolic reprogramming will induce changes in mitochondrial architecture to support changing metabolism. For example, B-RAF^{V600E}-driven melanoma cells contain fragmented mitochondria in line with increased glycolytic metabolism (Serasinghe *et al.*, 2015) (Ferretta *et al.*, 2016). Furthermore, changes in the expression of mitochondrial dynamics that promote mitochondrial fission have been discovered in many cancer patient samples. Indeed, lower Mfn2 expression is observed in breast cancer (Xu *et al.*, 2017), lung cancer (Rehman *et al.*, 2012), or hepatocellular carcinoma (Wu *et al.*, 2016). These cases also correlated with increased Drp1 levels, suggesting that a fragmented mitochondrial network is essential to many tumors (Zhao *et al.*, 2013) (Rehman *et al.*, 2012) (Li *et al.*, 2017).

Many tumors exhibit an upregulation of the mitogen activated protein kinase (MAPK) pathway, of which ERK1/2 has been described to directly promote Drp1 phosphorylation at the S616 site (Serasinghe *et al.*,

2015) (Kashatus *et al.*, 2015). Consequently, this elicits Drp1 GTPase activation and mitochondrial fragmentation. Accordingly, Drp1 phospho-S616 levels are enhanced in human pancreatic cancer (Kashatus *et al.*, 2015) and brain tumor initiating cells (Xie *et al.*, 2015). Interestingly, human lung cancer cell lines A549 and H1993 were characterized by increased S616 phosphorylation and reduced S637 phosphorylation, in agreement with excessive mitochondrial fission (Rehman *et al.*, 2012). Of note, restoring mitochondrial fusion in these cell lines by overexpression of Mfn2 or Drp1 inhibition, resulted in a marked reduction of cancer cell proliferation and an increase in spontaneous apoptosis (Rehman *et al.*, 2012). The requirement for Drp1 by MAPK-driven tumorigenesis can be related to the metabolic reprogramming that is needed by the cancer cells during transformation. In line with this, Drp1-mediated fragmentation results in decreased OXPHOS, forcing cellular metabolism towards glycolysis (Serasinghe *et al.*, 2015). Furthermore, Drp1 phosphorylation at S616 promotes mitochondrial division and segregation in rapidly proliferating cells, and is required for tumor growth (Kashatus *et al.*, 2015). Altogether, these observations place Drp1 as a potential therapeutic target for cancer treatments.

Two additional signaling pathways have also been described to directly impact mitochondrial dynamics. On the one hand, the PI3K-AKT signaling is hyper-activated in many solid tumors with loss of the PI3K inhibitor PTEN (Yang *et al.*, 2019). Tumors with constitutive activation of the PI3K-AKT pathway increase glucose uptake to fuel glycolysis which then triggers mitochondrial fragmentation (Tondera *et al.*, 2004) (Kim *et al.*, 2016) (Nagdas & Kashatus, 2017). On the other hand, MYC signaling is an activator of mitochondrial biogenesis by upregulating PGC1 β expression, thus coupling increased mitochondrial mass with rapid cell proliferation and suggesting a link with mitochondrial dynamics. For example, MYC signaling in triple-negative breast cancer cells induces mitochondrial fusion via phospholipase D Family member 6 (PLD6 also known as mitoPLD), which localizes at the outer mitochondrial membrane and facilitates the cleavage of cardiolipin to phosphatidic acid (von Eyss *et al.*, 2015) (Huang *et al.*, 2011). Some observations suggest that Drp1 GTPase activity is blocked following the interaction with phosphatidic acid and mitoPLD (Adachi *et al.*, 2016), potentially explaining how MYC is able to couple lipid metabolism and mitochondrial dynamics.

The fact that these signaling pathways result in different mitochondrial phenotypes might be due to their mechanistic differences (Figure 1.8) (Trotta & Chipuk, 2017). On the one hand, MYC acts downstream to regulate gene expression, which culminates in the upregulation of the metabolic capacity of cancer cells to support rapid proliferation, and this is coupled to mitochondrial fusion. On the other hand, MAPK regulates upstream protein activity by integrating plasma membrane receptor signals with multiple

subsequent kinase effector proteins, including ERK-mediated activation of Drp1 to promote mitochondrial fission.

Thus, mitochondrial plasticity in response to specific oncogenic stresses might be dependent on the cell type, tissue affected or stimuli in action. Understanding how these signaling pathways differentially influence mitochondrial shape and the mechanism that couples mitochondrial dynamics to other carcinogenic events (i.e. tumor microenvironment, metastasis, etc.) will be an exciting field for the development of cancer therapies.

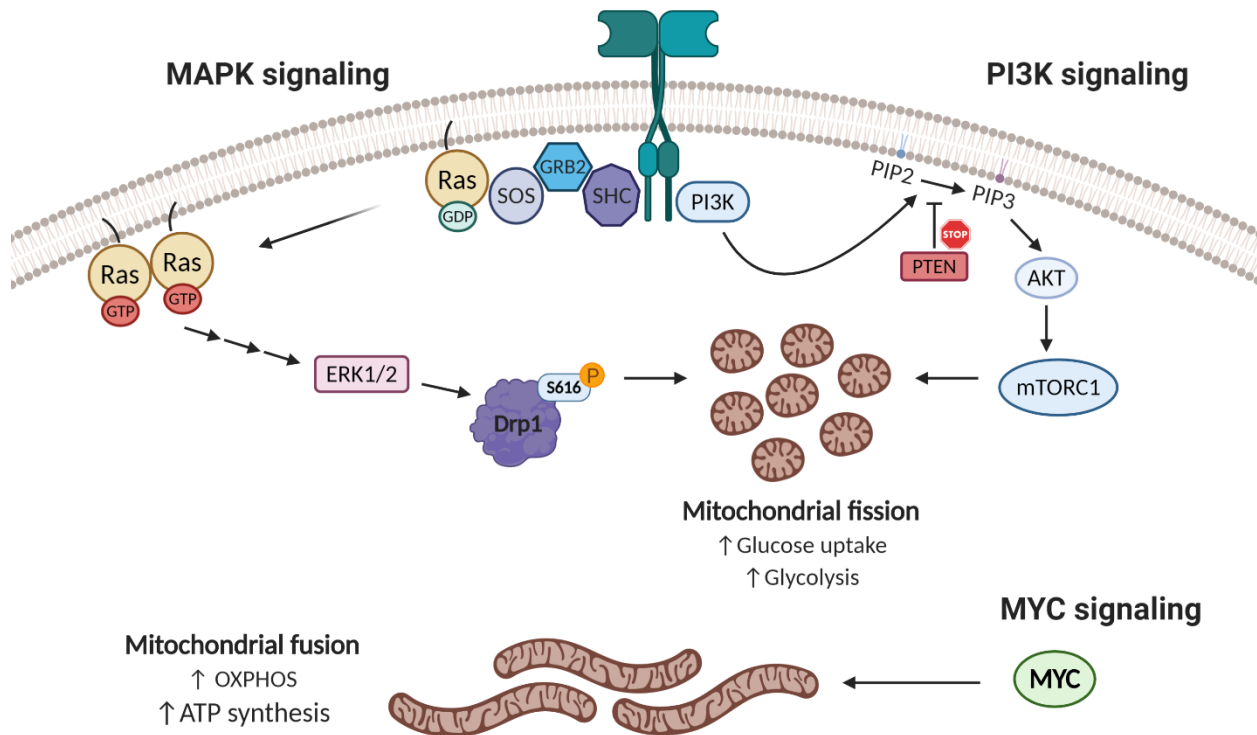


Figure 1.8. Role of mitochondrial dynamics in cancer.

Three different signaling pathways directly modulate mitochondrial dynamics: MAPK, PI3K and MYC signaling, respectively. Activation of ERK1/2 in the MAPK signaling pathway results in Drp1 phosphorylation at S616, leading to increased mitochondrial fission. Hyperactivation of the oncogenic PI3K signaling occurs upon loss or silencing of the PI3K inhibitor PTEN. Then, constitutive PI3K signaling leads to mTORC1 activation via AKT to inhibit autophagy and fragments the mitochondrial network. Oncogenic signaling that fragments mitochondria increases glucose uptake and decreases OXPHOS, which leads to a metabolic switch to glycolysis. Contrarily, oncogenic MYC promotes the expression of pro-fusion and mitochondria biogenesis proteins. Fused mitochondria, in turn, have increased oxidative metabolism and ATP production.

1.8 Goals of the project

While it is clear that mitochondrial dynamics critically influence mitochondrial quality control and metabolic adaptation, most of our knowledge on this area comes from genetic strategies ablating one or more components of the mitochondrial dynamics machinery. These approaches fail to accurately reflect the complex interplay between regulatory mechanisms and physiological responses at the organism level. Moreover, the key components in mitochondrial dynamics are regulated by post-translational modifications. In particular, Drp1 phosphorylation at S600 and S579 determines its activity and recruitment to mitochondria to perform fission. Yet the interrelation between these phosphorylation sites and their physiological impact remain unclear. Given that altered mitochondrial architectures can be at the root of multiple metabolic complications, including obesity and T2DM, understanding the acute regulation of Drp1 fission activity through phosphorylation would provide new avenues to tackle diseased states.

Therefore, the main goal of this research project was to study the role of Drp1 phosphorylation on metabolic and transcriptional pathways. This can be subdivided as follows:

- ✓ Understanding the crosstalk between the two main phosphorylation sites of Drp1 in cultured cells and mouse tissues.
- ✓ Defining how the Drp1 phosphorylation crosstalk modulates the change in mitochondrial shapes.
- ✓ Evaluating how the defective phosphorylation at Drp1 S600 impacts the sensitivity to develop metabolic disease by characterizing the Drp1 S600A knock-in (KI) mouse model.
- ✓ Exploring how mitochondrial dynamics could directly influence human disease in tumorigenesis by means of a model of epithelial-mesenchymal transition (EMT) in cultured cells.

Chapter 2. Drp1 phosphorylation pattern in mammalian cells and mouse tissues

Drp1 activity and recruitment to mitochondria is mediated by post-translational modifications, of which Drp1 phosphorylations have gained most research interest. While the role of the Drp1 phosphorylation at S579 is quite consistent in promoting translocation to mitochondria and mitochondrial fragmentation, the functional readout of the S600 phosphorylation on Drp1 activity remains controversial. In this Chapter, we aimed to investigate Drp1 phosphorylations in our culture cell system, as well as having some first insights into the relationship between Drp1 P-S579 and Drp1 P-S600 in mouse tissues.

2.1 Drp1 phosphorylation landscape in cultured cells

An initial caveat that we encountered when working on Drp1 phosphorylations was the quality of commercially available antibodies, which poorly detected endogenous Drp1 phosphorylation levels. In our hands, commercial antibodies only detected changes in S600 phosphorylation if Drp1 was overexpressed, but not at endogenous levels (M. Joffraud and C. Canto, personal observations). For this reason, we generated homemade rabbit polyclonal antibodies (provided by YenZym®) for total Drp1, as well as for the Drp1 phospho-Ser600 and Drp1 phospho-Ser579 sites, respectively (see Methods section for more information on antibody generation).

We first validated the two antibodies provided by YenZym® for total Drp1, and compared them against the Drp1 commercial antibody from Cell Signaling Technology® (CST). For this, we used mouse embryonic fibroblasts (MEFs) either from WT mice or from Drp1KO mice. This model also allows us to reintroduce Drp1 forms in the KO MEFs through regular transfection methods. In WT MEFs, total Drp1 was well detected by the three antibodies. As expected, we did not observe any signal in Drp1KO MEFs transfected with pcDNA3 (empty vector, EV) (Figure 2.1A). Drp1 expression was greatly intensified in Drp1KO MEFs overexpressing a FLAG-tagged wild-type (WT) Drp1 vector, and the detection was also comparable between the commercial and homemade antibodies (Figure 2.1A). Therefore, we next validated these

antibodies in mouse tissues. Drp1 bands displayed weaker intensity with the commercial and Drp1 (A) antibodies in brown adipose tissue (BAT) from control mice, as compared to the Drp1 (B) antibody, which showed a strong signal for the same blot exposition time (Figure 2.1A). We thus selected the Drp1 total (B) homemade antibody for further analyses.

Drp1 activity can be modulated by increasing intracellular cAMP levels, leading to the activation of the cAMP-dependent Protein Kinase A (PKA) and the consequent phosphorylation of Drp1 at the S600 site. Thus, we used this paradigm to analyze Drp1 S600 phosphorylation in two different cell culture models. We first made use of 3T3 fibroblasts, as they are easy to manipulate and transfect (Figure 2.1B). We transfected 3T3 cells with either Drp1 WT or with a S600A phospho-null mutant plasmid (Drp1 S600A), both of which were YFP-tagged. Both forms were equally expressed, as validated by the homogenous levels of total Drp1 detected at ~100 kDa (Figure 2.1B). Regardless, we could also observe endogenous total Drp1 bands at 75 kDa. When pcDNA3-transfected fibroblasts (empty vector, EV) were treated with Forskolin (Fsk; an activator of the adenylyl cyclase enzyme, leading to increased cAMP production), we could observe an increase in the endogenous Drp1 P-S600 form (~75 kDa). Moreover, Fsk treatment increased the Drp1 P-S600 signal on cells transfected with the Drp1 WT form, but not with the Drp1 S600A mutant, testifying for the specificity of our homemade antibody (Figure 2.1B). However, we could also see a spectrum of non-specific bands, ranging from 75 to 100 kDa.

In order to evaluate the specificity of this signal to Drp1, we used a second cell culture model with the Drp1KO MEFs. As expected, Drp1KO MEFs do not display endogenous Drp1 protein (EV-transfected KO MEFs), while the WT and S600A forms can be expressed and detected (Figure 2.1C). Thus, we took advantage of this system to validate the two antibodies provided by YenZym® against the Drp1 Ser600 phosphorylation (A, B). When cells were treated with Fsk, we could see an increase in Drp1 P-S600 levels only in Drp1KO MEFs overexpressing the Drp1 WT form, as opposed to the cells expressing the Drp1 S600A phospho-null plasmid. We concluded that the Drp1 P-S600 (A) antibody gave us increased band resolution, decreased background and non-specific bands, thus we selected this antibody for further analysis. Moreover, the Drp1 P-S600 (A) antibody could also detect some levels of endogenous Drp1 S600 activation in the Drp1 WT MEFs, which was not the case with the Drp1 P-S600 (B) antibody. Interestingly, when the cells were treated with Fsk, a decrease in the S579 phosphorylation was observed in Drp1 WT overexpressing cells, and this reduction was further exacerbated with the Drp1 S600A form (Figure 2.1C). Therefore, this suggests that Fsk treatment leads to an opposing phosphorylation pattern on S600 and S579 in MEF cells.

Finally, we validated the homemade Drp1 phospho-S579 antibodies. In this case, 3T3 and Drp1KO MEFs were transfected with the FLAG-tagged Drp1 WT form and treated with Fsk, after which Drp1 P-S579 levels were analyzed with the commercial (CST) or with the two homemade antibodies (A, B) (Figure 2.1D). Drp1 P-S579 (A) antibody demonstrated a comparable signal level to that of the commercial antibody in cultured cells and in mouse control BAT treated with vehicle or with the cAMP inducer in BAT, CL316,243 (Figure 2.1D). However, the Drp1 P-S579 (B) form displayed non-specific bands in cell culture and an increased background signal in mouse BAT (Figure 2.1D). Therefore, we selected the Drp1 P-S579 (A) homemade antibody for the following experiments as it displays a signal ratio comparable to the commercial antibody in both cultured cell lines and mouse tissues.

2.2 Drp1 phosphorylation at S579 is independent to ERK activation

We next wondered why the phosphorylation of S600 could downregulate S579 in the cell models we tested. The mitogen-activated protein kinase (MAPK) pathway has been previously documented to promote mitochondrial fragmentation through the direct phosphorylation of Drp1 at the Ser579 site by ERK1/2 in samples characterized by increased cell proliferation, such as tumours and cells derived from cancer patients (Kashatus *et al.*, 2015). Moreover, PKA activation can prompt ERK inhibition through the uncoupling of Raf1 from Ras signaling, either through the direct blocking of Raf1 by PKA or by the GTPase Rap1 (Schmitt & Stork, 2002) (Guerrero *et al.*, 2002) (Figure 2.2A). Based on this, cAMP induction, for instance by Forskolin, would lead to PKA activation and Drp1 S600 phosphorylation while inhibiting the Raf-1/ERK axis and decreasing Drp1 P-S579 levels (Figure 2.2A). Indeed, this mechanism would explain the inversely proportional phosphorylation levels in our mouse fibroblast model.

To evaluate this hypothesis, we transfected Drp1KO MEFs with the Drp1 WT vector to recover the protein expression, and then the transfected cells were treated with H89, a PKA inhibitor. Thus, if the model is correct, the addition of H89 would result in the increased phosphorylation of both ERK1/2 and Drp1 S579 (Figure 2.2A). When the Drp1 WT overexpressing MEFs were treated with Fsk, we could again observe the negative correlation between Drp1 P-S600 and P-S579 (Figure 2.2B). In this condition, there were no visible changes in the phosphorylation of ERK. When these cells were pre-treated with H89, Fsk action on Drp1 P-S600 levels was completely blocked, which correlates with PKA inhibition. Upon PKA inhibition, a slight but significant increase in P-ERK1/2 could be detected in cells transfected with the Drp1 WT form (Figure 2.2B and Figure 2.2C), in line with the model proposed by Guerrero *et al.* (2002). Despite the increase of phosphorylated ERK in Drp1 WT overexpressing KO MEFs, the blockage of PKA signaling did

not increase Drp1 P-S579 levels (Figure 2.2B and Figure 2.2C). These results suggest that PKA activity leads to ERK blockage, and that Drp1 S579 phosphorylation in our model is not dramatically influenced by ERK activation.

2.3 Drp1 P-S579 and P-S600 occur simultaneously in mouse tissues

The potential crosstalk between Drp1 phosphorylation sites has never been explored in animal models. Hence, our next goal was to analyse Drp1 phosphorylation in mouse tissues, and evaluate whether they reflected the negative co-regulation between S600 and S579 phosphorylations observed in cultured cell lines. To evaluate the impact of PKA activation on Drp1 S600 phosphorylation in mouse tissues, we treated WT mice with the adrenergic β 3-selective agonist CL316,243 (CL). This led to an increase in Drp1 P-S600 in BAT which, strikingly, was accompanied by an increase in Drp1 S579 phosphorylation (Figure 2.3A). To rule out tissue-specific effects, we also analysed the response to PKA activation in other tissues. For this, we treated control mice with glucagon and isoproterenol, in order to promote Drp1 P-S600 in liver and muscle, respectively (Figure 2.3A). The results in these two additional tissues corroborated that cAMP induction triggered the phosphorylation of both S600 and S579 (Figure 2.3A). Therefore, Drp1 S600 and Drp1 S579 occur in parallel upon PKA activation in mouse tissues, which contradicts the observations in cultured cells.

To further document the different Drp1 phosphorylation landscape between cultured cells and mouse tissues, we performed a time-course experiment where we analysed Drp1 phosphorylation status upon CL treatment in cultured brown adipocytes (Appendix 1A) as compared to the response in BAT from WT mice (Appendix 1B). Interestingly, the results *in vitro* suggest that P-S579 levels decrease rapidly after treatment, while the increase in P-S600 is more persistent with time. Contrarily, the increase in Drp1 P-S600 and P-S579 levels occurred simultaneously *in vivo*. These observations further support the discrepancy between cultured immortalized cell models and the paradigm in mouse tissues.

We next aimed to modulate Drp1 phosphorylation through a physiological challenge, which could complement the results obtained in the previous pharmacological treatment with cAMP inducers in mice. Prolonged fasting times (>24h) induce the increase of cAMP levels in muscle (Lavine *et al.*, 1975) and lead to Drp1-mediated mitochondrial fission and muscle atrophy in mice (Romanello *et al.*, 2010). Thus, we exposed WT mice to a fasting/refeeding challenge by fasting mice for 24 h and then refeeding a subgroup for 6 h. Our results in muscle illustrated a significant increase in Drp1 P-S600 levels in fasted mice, as compared to the refed group (Figure 2.3B). As it also occurred for the pharmacological challenge,

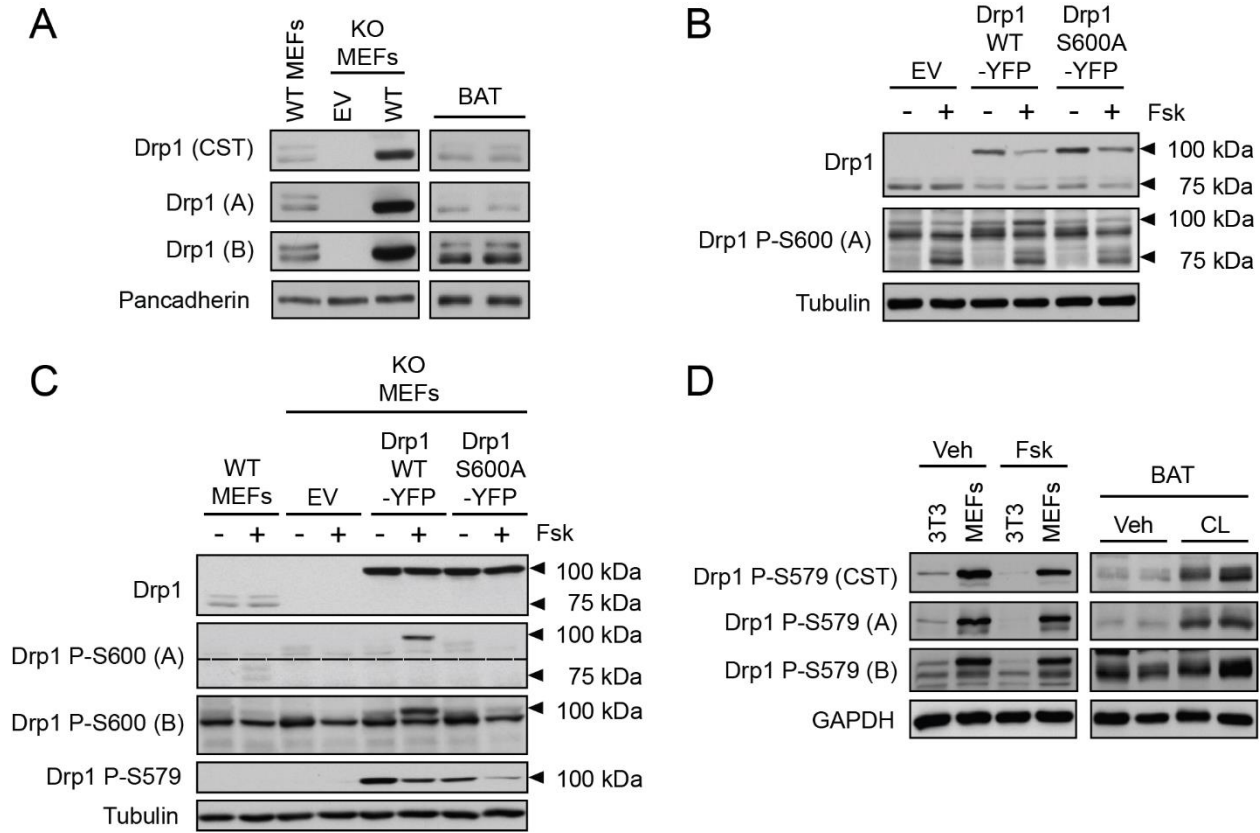
increased Drp1 P-S600 was correlated to upregulated Drp1 P-S579 levels in the muscle from fasted mice (Figure 2.3B).

We also analysed the Drp1 phosphorylation landscape on a second physiological challenge, for which we used the response of the BAT to cold temperatures. In this paradigm, we exposed WT mice to a cold challenge for 4 h, and compared the Drp1 S579 and S600 phosphorylation levels to those of control mice habituated to normal housing conditions (room temperature, RT, 22°C). In line with the results from Wikstrom *et al.* (2014), we observed higher Drp1 P-S600 levels in the BAT from cold-exposed mice. Similar to the fasting/refeeding challenge, the increase in Drp1 S600 phosphorylation was correlated to the upregulation in Drp1 P-S579 levels in the BAT samples from cold-exposed mice (Figure 2.3C).

2.4 Conclusions

Overall, this Chapter describes the differential expression of Drp1 phosphorylation at the Ser579 and Ser600 sites in cell culture lines compared to mouse tissues. Contrary to what is observed in cultured cell lines, we describe for the first time that P-S600 and P-S579 occur simultaneously in mouse tissues upon pharmacological and physiological challenges. This emphasizes a critical point in mitochondrial research, which is the contradictory results sometimes gathered between *in vitro* and *in vivo* settings.

In the next Chapter, we will further investigate the crosstalk between Drp1 phosphorylations by means of Drp1 phospho-mutant forms that mimic the activation of the Drp1 phospho-sites in the absence of cAMP stimulation.

Figure 2.1**Figure 2.1. Drp1 phosphorylation pattern on cultured cells.**

(A) Validation of homemade total Drp1 antibodies in a cell culture system and in mouse brown adipose tissue (BAT). Drp1KO MEFs were transfected with empty vector (pcDNA3, EV) or with a Flag- tagged Drp1 WT form (WT), and total Drp1 protein levels were evaluated alongside the endogenous Drp1 from WT MEFs. Further, Drp1 protein levels were measured from BAT of control mice. In both settings, Western Blot analysis compared the detection of total Drp1 with either the commercial antibody from Cell Signaling Technology (CST) or two different homemade antibodies (A and B). **(B)** 3T3 cells were transfected with a control vector (pcDNA3, EV), an YFP-tagged WT Drp1 form (Drp1 WT - YFP) or an YFP-tagged S600A Drp1 mutant form (Drp1 S600A - YFP). Then, 48 h later, cells were treated with DMSO (-) or Forskolin (20 μ M; +) for 2 h after which protein extracts were obtained. Drp1 total protein was analyzed with our homemade antibody, while the Drp1 S600 phosphorylation was measured with one of our homemade antibodies (A). **(C)** Validation of homemade Drp1 P-S600 antibodies in an overexpression system. Drp1KO MEFs were transfected with pcDNA3, Drp1 WT-YFP or Drp1 S600A-YFP. Then, cells were treated and processed as in (B). Endogenous Drp1 molecular weight is 75 kDa, while the recombinant Drp1-YFP is 100 kDa approximately. Drp1 P-S600 levels were evaluated with two different homemade antibodies (A and B). Total Drp1 was detected with our homemade antibody, while the Drp1 P-S579 antibody was from CST. **(D)** Validation of homemade Drp1 P-S579

antibodies in a cell culture system and in mouse brown adipose tissue (BAT). 3T3 or Drp1KO cells were both transfected with a Flag-tagged Drp1 WT plasmid and, after 48 h, cells were treated with DMSO (Veh) or Forskolin (Fsk) for 2 h. Also, control C57Bl/6NTac male mice were intraperitoneally injected with either saline (vehicle, Veh) or CL316,243 (CL, 1mg/kg) for 1 hour, and then BAT was collected and snap frozen. In both settings, protein extracts were obtained to evaluate Drp1 P-S579 levels with two different homemade antibodies (A and B) as compared to the commercial antibody from Cell Signaling Technology (CST).

Figure 2.2

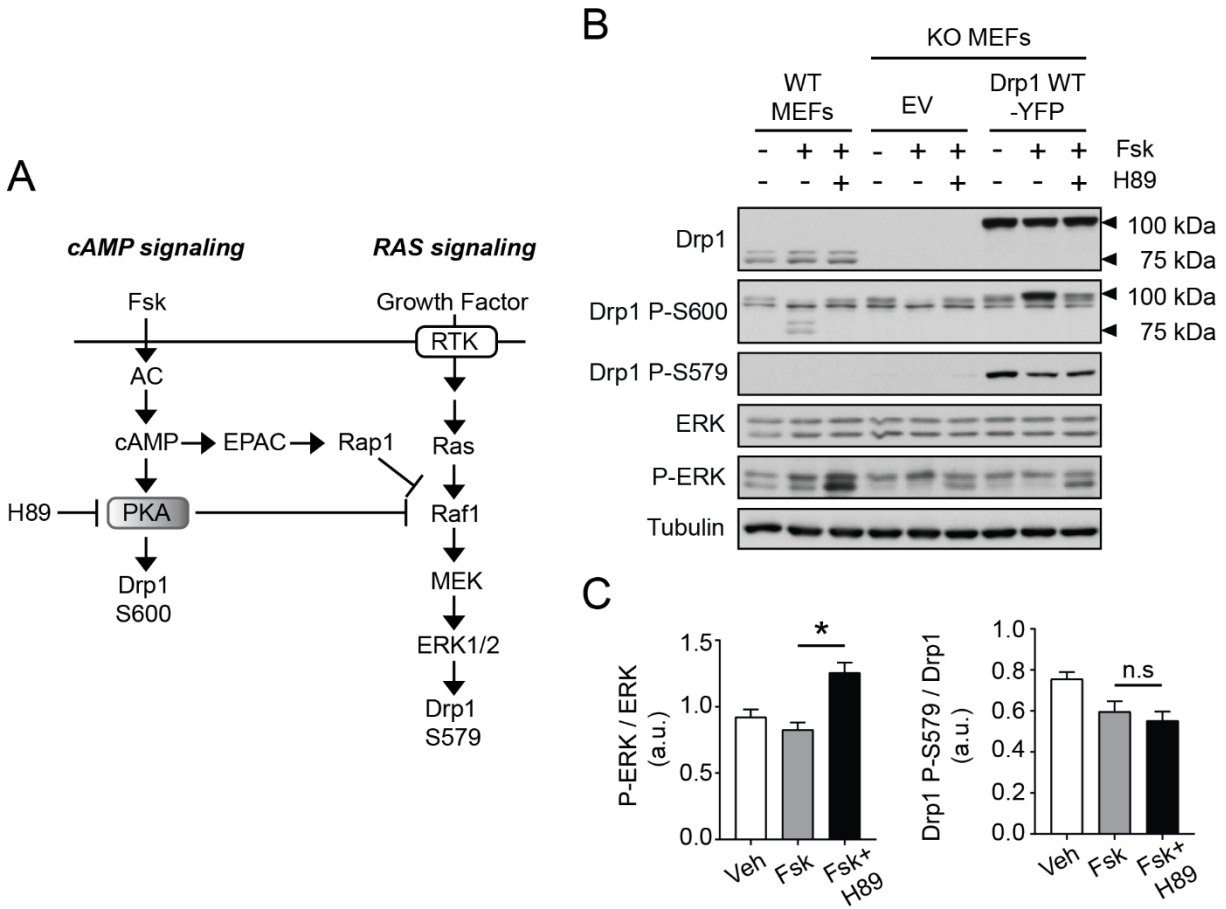
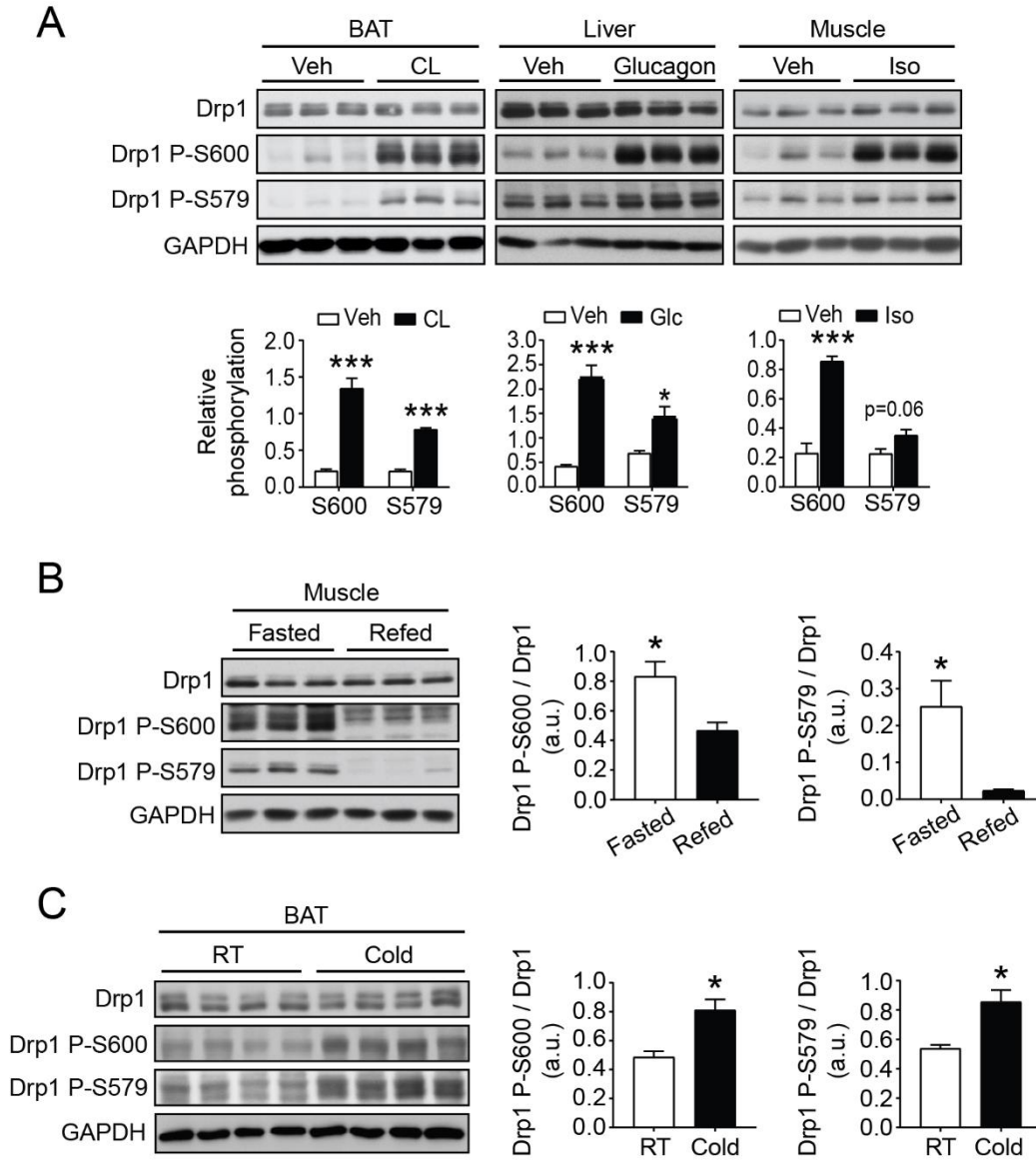


Figure 2.2. Drp1 S579 phosphorylation occurs independently of ERK.

(A) Scheme representing the crosstalk between the cAMP and MAPK pathways (adapted from Guerrero *et al.* (2002)). **(B)** Drp1KO MEFs were transfected with either empty vector (EV, pcDNA3) or with a YFP-tagged Drp1 WT plasmid. For the inhibition of PKA, cells were pre-treated with 100 μ M H89 (1h) prior to the addition of Forskolin. Otherwise, cells were treated with DMSO as a control or 20 μ M Forskolin (Fsk) (2h). Then, total protein extracts were obtained to evaluate the indicated markers. Drp1 WT MEFs were also analyzed as a measure of endogenous protein levels. Quantifications are shown in **(C)** for the P-ERK and Drp1 P-S579 levels, respectively, corresponding to the Drp1 WT-YFP transfected KO MEFs. All values are presented as mean \pm SEM. * $p < 0.05$ (two-tailed Student's t-test) statistically significant differences between the indicated groups.

Figure 2.3**Figure 2.3. Drp1 phosphorylation at S600 and S579 occur simultaneously in mouse tissues.**

(A) Control C57Bl/6NTac male mice were intraperitoneally injected with either saline (as vehicle), CL316,243 (1mg/kg; 1 hour), glucagon (1mg/kg; 15 minutes) or isoproterenol (10 mg/kg; 15 minutes) in three different experiments (n= 3 mice per condition). Then, tissues were extracted and snap frozen to evaluate Drp1 phosphorylation levels. **(B)** Control C57Bl/6NTac male mice were single housed at 9 am and fasted for 24 h. Afterwards, half of these mice were sacrificed (fasted) and some were given back food for 6 h (refed) before sacrifice. Then, muscle (quadriceps) was collected and snap frozen to analyse Drp1 phosphorylation levels (n= 3 mice per condition). **(C)** Control C57Bl/6NTac male mice were subjected to a cold challenge for 4 h (6°C; Cold). Then, BAT was collected and snap frozen to evaluate the markers indicated. These samples were compared to BAT of control WT

mice regularly housed at normal room temperature (22°C; RT) (n = 4 mice per condition). All values are presented as mean \pm SEM. *p < 0.05, **p < 0.01, ***p < 0.001, (two tailed Student's t-test) statistically significant differences between the indicated groups.

Chapter 3. Drp1 S600 phosphorylation boosts S579 activation to promote mitochondrial fragmentation

In this Chapter, we generated and characterized Drp1 phospho-mimetic plasmids, containing point mutations in the Serine 579 and Serine 600 residues. For instance, a Serine to Alanine (A) mutation prevents the site from activation and thus mimics a constitutive dephosphorylation. Conversely, a Serine to Glutamate (E) or Aspartate (D) mutation imitates the phosphorylation of the residue, in which case the site will be “activated” in the absence of stimuli. We thus aimed to simulate the previous paradigm observed in mouse tissues by inducing S600 activation and analyzing whether S579 phosphorylation could occur independently of PKA. Moreover, we used similar phospho-mutant plasmids attached to the fluorescent photoactivable mtDsRED tag to evaluate the impact on mitochondrial morphology.

3.1 P-S600 protects against Drp1 S579 dephosphorylation

Given that S579 does not meet the consensus sequence to be a direct PKA target and is not phosphorylated by PKA in *in vitro* assays (Chang & Blackstone, 2007) (Chang & Blackstone, 2010), we aimed to understand how S579 phosphorylation is influenced by PKA stimulation. We initially wanted to test whether the increase in S579 phosphorylation was due to the activation of a kinase from the PKA signaling pathway or, alternatively, to the fact that S600 phosphorylation could alter the conformation of the Drp1 protein favoring the interaction with enzymes regulating S579 phosphorylation. For this, we transfected Drp1 knock-out (KO) mouse embryonic fibroblasts (MEFs) with plasmids encoding for either a WT Drp1 form, a S600 phospho-null form (S600A) or a S600 phospho-mimetic form (S600E), and then analyzed P-S579 levels. In line with the observations in mouse tissues, the Drp1 phospho-mimetic S600E form resulted in increased Drp1 S579 phosphorylation levels compared to the WT or phospho-null forms (Figure 3.1A). The increase in Drp1 P-S579 in cells overexpressing the Drp1 S600E form, however, was not related to altered Cdk1 activity, since markers such as P-Cdk1 or the phosphorylation of the retinoblastoma (Rb) protein, a canonical Cdk1 substrate, were unaltered in Drp1 S600E transfected cells

(Figure 3.1B). Similarly, we also observed increased Drp1 P-S579 levels when an alternative phospho-mimetic form, S600D, was used (Figure 3.1C and Figure 3.1D). Interestingly, we did not observe any significant change in Drp1 P-S600 levels when using a phospho-mimetic form of Drp1 S579 (Drp1 S579E and Drp1 S579D) (Figure 3.1E). This indicates that Drp1 S600 phosphorylation promotes the phosphorylation of S579, but not vice versa.

Next, we evaluated how the S600E-induced phosphorylation of S579 was influenced by the activity of putative kinases for the S579 site, particularly CDKs and ERK. For this, we initially tested the effectiveness of a panel of CDK inhibitors (RO336 and Roscovitine) and ERK inhibitors (PD98059 and PD0325901) and analyzed whether there was a response in S579 activation (Figure 3.2). RO336 did not manage to inhibit Cdk1 activation after the effective 6 h of treatment (Figure 3.2A). On the other hand, both ERK-specific MAPK inhibitors reduced ERK activation, though with no apparent signs of Drp1 P-S579 impairment (Figure 3.2B). This again suggests that ERK is not directly involved in Drp1 S579 phosphorylation in our system. Roscovitine, a small molecule that arrests the cell cycle of treated cells through direct competition at the ATP-binding site of CDKs, was the most effective at inhibiting Cdk1. Indeed, Roscovitine led to a large reduction not only in the activation of canonical targets, such as Cdk1 and Rb, but also of Drp1 S579 phosphorylation (Figure 3.2A).

Therefore, we next used Roscovitine for a time-course experiment and evaluated P-S579 response upon S600 dephosphorylation (S600A) or constitutive activation (S600E). Drp1KO MEF cells transfected with Drp1 S600A and treated with Roscovitine displayed a marked decrease in Drp1 S579 phosphorylation (Figure 3.1F). In contrast, Drp1 P-S579 levels were highly sustained when Drp1KO cells were transfected with Drp1 S600E (Figure 3.1F). Importantly, P-Cdk1 and P-Rb levels decreased to a similar extent after Roscovitine treatment in both S600A and S600E transfected cells, indicating that the S600E form did not alter the inhibitory effect of the drug on CDK activity. These results suggest that Drp1 S600 phosphorylation protects against S579 dephosphorylation.

3.2 Both S579 and S600 phosphorylations are required to trigger mitochondrial fission

Given the conflicting views in the literature on the role of Drp1 phosphorylations on mitochondrial fission, we aimed to determine the impact of the Drp1 S600 and S579 phosphorylations on mitochondrial morphology in our experimental setting. For this, we performed imaging analysis of the Drp1KO MEFs expressing bicistronically mtDsRed and either Drp1 WT or phospho-mutant forms. Drp1KO MEFs

expressing the control Drp1 WT-mtDSRED plasmid displayed an intermediate mitochondrial morphology, suggesting the recovery of a regulated balance in the fission and fusion states (Figure 3.3). We observed increased mitochondrial fragmentation when expressing Drp1 S600E-mtDsRED (Figure 3.3A and Figure 3.3C). The expression of the double phospho-mimetic Drp1 S600E/S579E increased mitochondrial fragmentation to a similar extent to that observed in cells expressing the S600E-mtDsRED form (Figure 3.3A and Figure 3.3C). Of note, the Drp1 S579E-mtDSRED form also led to mitochondrial fragmentation, although to a lesser extent to that observed with the Drp1 S600E and Drp1 S600E/S579E forms (Figure 3.3A and Figure 3.3C).

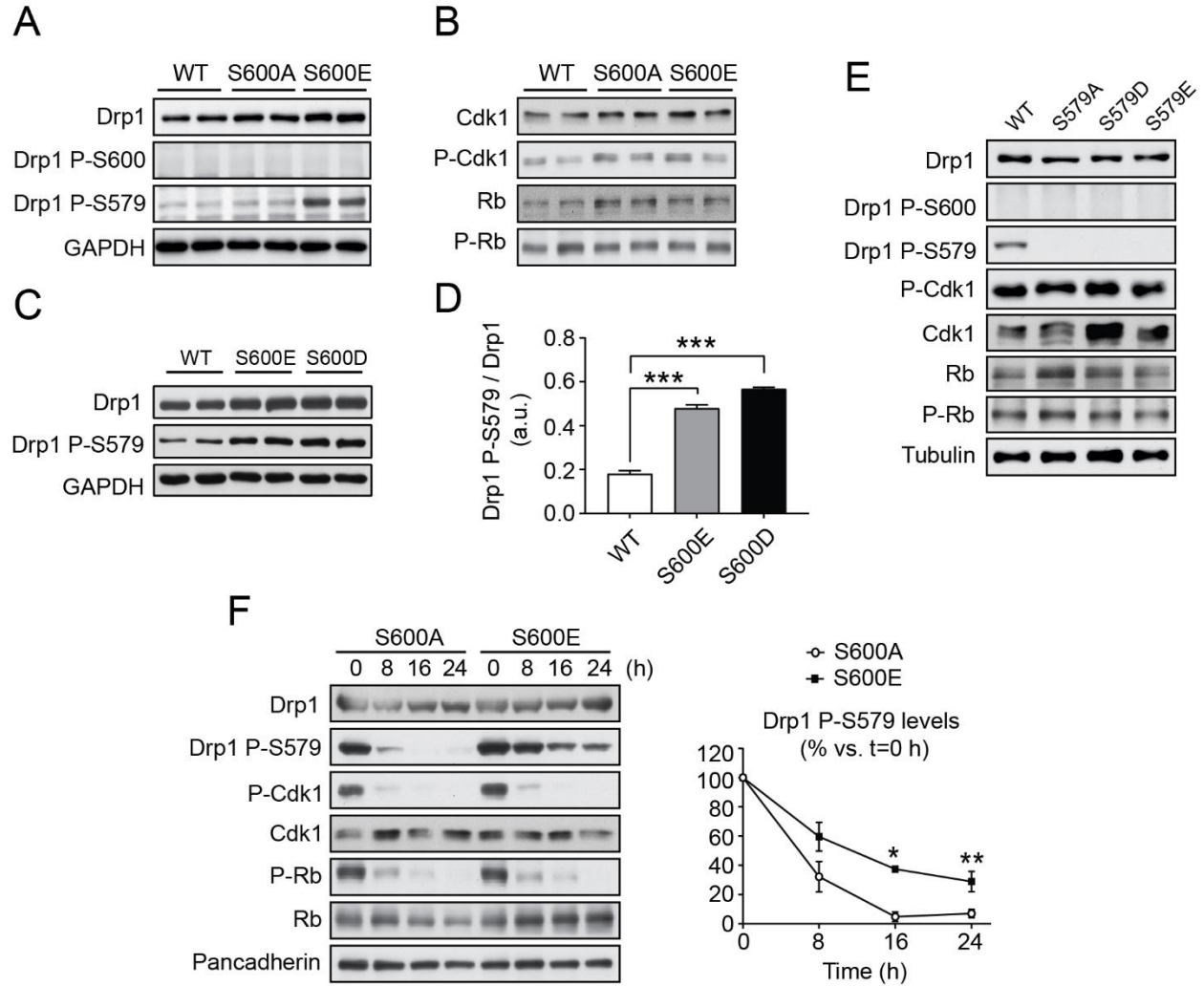
Given that the phosphorylation at Drp1 S600 triggers S579 activation, we aimed to elucidate whether S600 phosphorylation could promote mitochondrial fragmentation independently of the S579 site. For that, we generated a plasmid encoding for a Drp1 S600E/S579A-mtDsRED form. Contrarily to the marked mitochondrial fission observed with the S600E and S600E/S579E plasmids, respectively, we observed a rather predominant mitochondrial tubulation for the Drp1KO cells expressing the S600E/S579A-mtDsRED plasmid (Figure 3.3B and Figure 3.3D). Similarly, we also observed mitochondrial elongation for cells expressing the single mutated S579A and S600A plasmids (Figure 3.3B and Figure 3.3D).

Since starvation has been demonstrated to promote mitochondrial elongation in cultured cells, we finally assessed whether the phosphorylation of S600 and/or S579 residues is critical for the effects of fasting. In line with previous research (Gomes *et al.*, 2011) (Rambold *et al.*, 2011), cells expressing the Drp1 WT-mtDsRED form presented higher mitochondrial elongation when shifted to starvation media (HBSS) (Figure 3.4A and Figure 3.4B). Cells expressing Drp1 S600E or Drp1 S600E/S579E forms also underwent mitochondrial elongation when cultured on starvation media, but to a lesser degree than cells transfected with Drp1 WT (Figure 3.4A and Figure 3.4B). In contrast, the Drp1 S579E-mtDSRED cells did show comparable percentages of elongated mitochondria to those observed in cells expressing the Drp1 WT form (Figure 3.4A and Figure 3.4B). These results indicate that Drp1 phosphorylation at either S600 or S579 cannot fully oppose fasting-induced mitochondrial fusion.

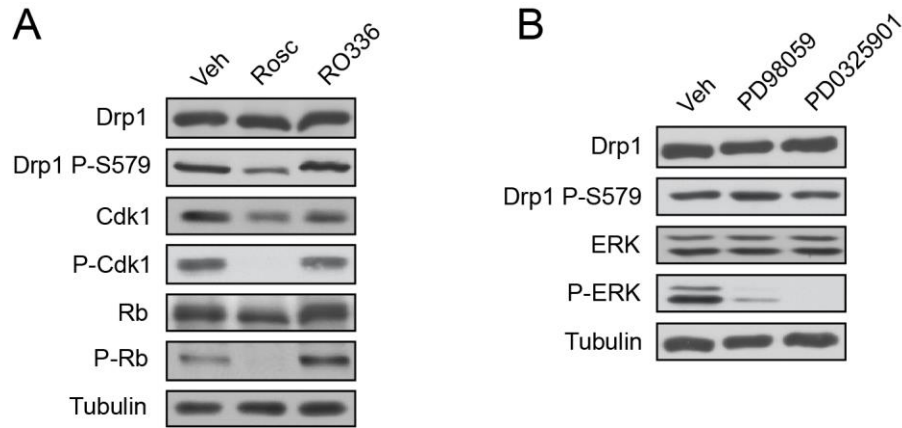
3.3 Conclusions

Overall, these results suggest that the phosphorylation of Drp1 S600 is an upstream event for the activation at S579. Inhibiting Cdk1 activity by impairing the cell cycle led to different outcomes on Drp1 S579 phosphorylation depending on whether the S600 was activated or inactivated. In this way, Drp1 S600 constitutive phosphorylation in the Drp1 S600E phospho-mimetic plasmid protected against Drp1 S579

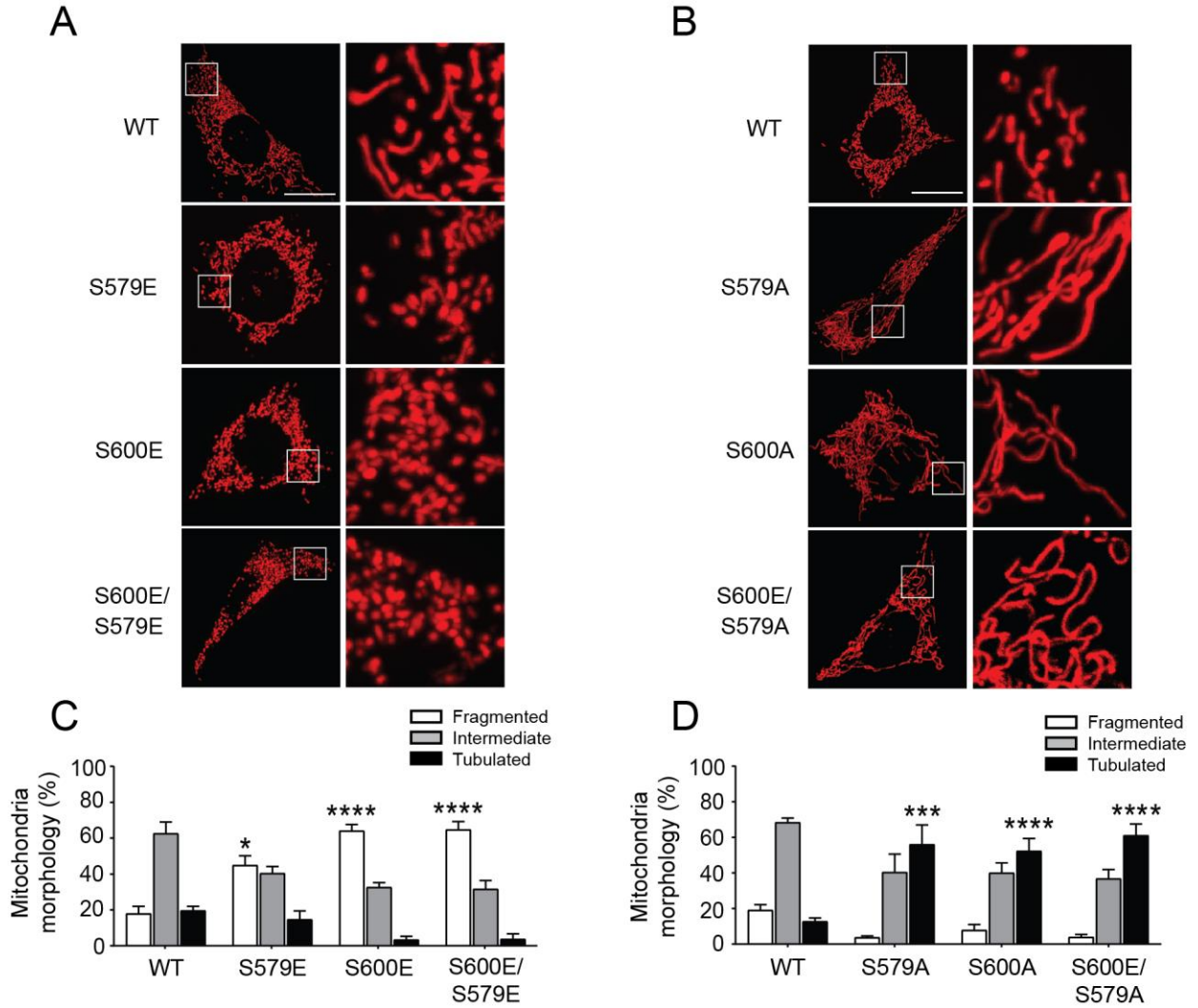
dephosphorylation. The double Drp1 phosphorylation event that we observed in our cell culture system, as well as in mouse tissues, serves to promote mitochondrial fission. Testified by the imaging analysis of the double phospho-mutant Drp1 S600E/S579A plasmid, the activation of the S600 site is not sufficient to induce mitochondrial fragmentation and thus, promotes the phosphorylation of the Drp1 S579 residue, which is the ultimate effector of mitochondrial fission. Therefore, our observations indicate that maximal Drp1-related mitochondrial fission activity is only achieved when the two residues are phosphorylated.

Figure 3.1**Figure 3.1. Drp1 S600 phosphorylation protects against S579 dephosphorylation.**

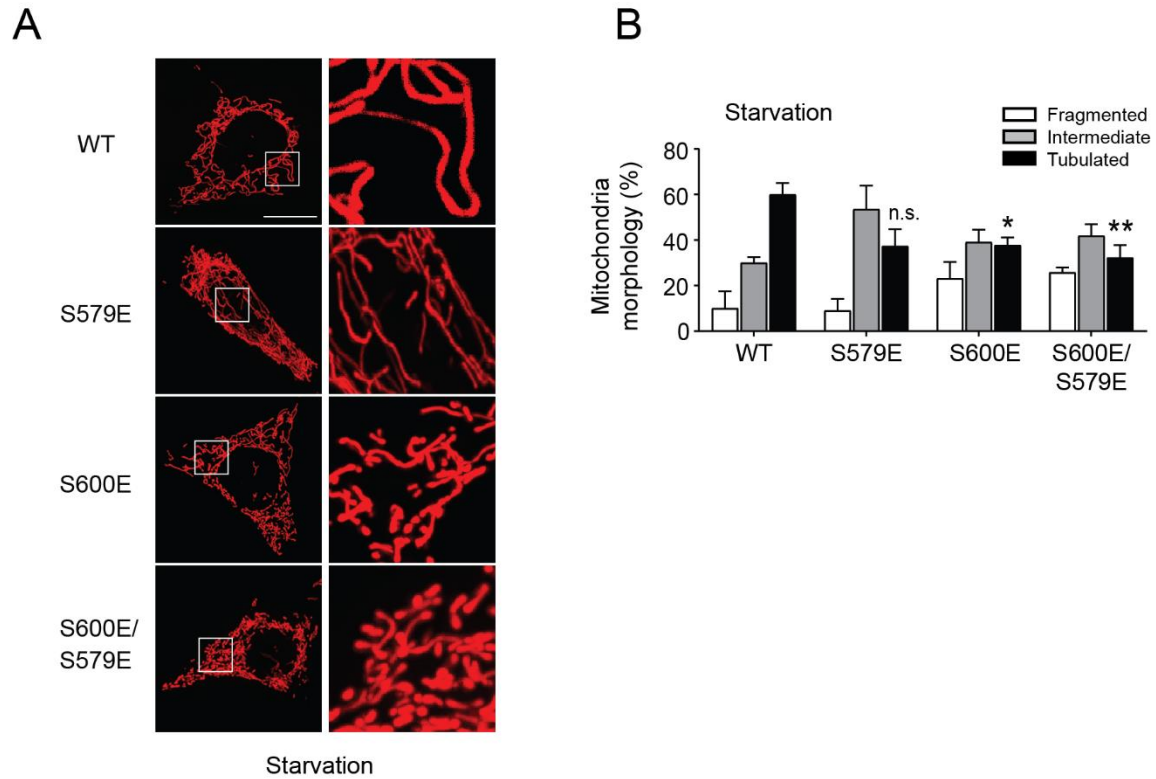
(A-B) Drp1KO MEFs were transfected with either WT, S600A or S600E forms of Drp1. After 48 hrs, protein extracts were obtained to evaluate Drp1 phosphorylation levels **(A)** or the cell-cycle markers Cdk1/P-Cdk1 and Rb/P-Rb **(B)**. **(C)** Drp1KO MEFs were transfected with either WT Drp1 or the phospho-mimetic Drp1 S600E and S600D forms. After 48 hours, total protein extracts were obtained to evaluate Drp1 P-S579 levels. **(D)** Quantifications for Drp1 P-S579 normalized by total Drp1 levels from experiment in (C). **(E)** Drp1KO MEFs were transfected with WT Drp1 or with S579A, S579D or S579E mutant forms. Total protein extracts were obtained to evaluate the indicated markers. **(F)** Drp1KO MEFs were transfected with either Drp1 S600A or S600E forms. Then, cells were treated with 60 μ M Roscovitine for the indicated time-course points and protein samples were collected to examine the indicated markers. The percentage of decreased Drp1 P-S579 levels are representative of $n = 3$ independent experiments. * $p < 0.05$, ** $p < 0.01$, *** $p < 0.001$, (two tailed Student's t-test) statistically significant differences between the indicated groups.

Figure 3.2**Figure 3.2. Efficiency of CDK and ERK inhibitors.**

Drp1KO MEFs were transfected with a Flag-tagged Drp1 WT plasmid and, after 48 h, cells were treated with the indicated compounds to measure the inhibition of CDKs and ERK, respectively. **(A)** To analyze CDK inhibition, cells were treated with DMSO (vehicle), Roscovitine (Rosc, 40 μ M) or RO336 (10 μ M) for 6 h. After treatment, protein lysates were collected to examine the indicated markers. **(B)** To analyze ERK inhibition, cells were treated with DMSO (vehicle), PD98059 (50 μ M) or PD0325901 (1 μ M) for 2 h. Then, protein lysates were collected to evaluate the indicated markers.

Figure 3.3**Figure 3.3. Both S579 and S600 phosphorylations are required for mitochondrial fragmentation.**

Drp1KO MEFs were transfected with the Drp1 S579E, S600E, S600E/S579E phospho-mimetic plasmids **(A)** or with the Drp1 S579A, S600A phospho-null **(B)** plasmids tagged to mtDsRed. The double mutant S600E/S579A form was also evaluated and is presented in **(B)**. After 24h, mitochondrial morphology was measured by live fluorescence imaging (scale bar applies to all images: 20 μ m). Quantifications are shown in **(C)** and **(D)** for the imaging in **(A)** and **(B)**, respectively, as the mean of $n=3$ independent experiments, counting approximately 50 different cells per experiment. Statistically significant difference is indicated vs. the respective fragmented **(C)** or tubulated **(D)** WT group. All values are presented as mean \pm SEM. * $p < 0.05$, *** $p < 0.001$, **** $p \leq 0.0001$ (two-tailed Student's t-test) statistically significant differences between the indicated groups.

Figure 3.4**Figure 3.4. Starvation shapes mitochondrial morphology differently upon Drp1 phosphorylation.**

(A) Drp1KO MEFs were transfected with the indicated phospho-mimetic plasmids tagged to mtDsRed. After 24h, starvation was induced in cells by the incubation with HBSS media for 2 h prior to imaging (scale bar applies to all images: 20 μ m). Quantifications are shown in **(B)** for the imaging in (A) as the mean of $n=3$ independent experiments, counting approximately 50 different cells per experiment. Statistically significant difference is indicated vs. the respective tubulated WT group. All values are presented as mean \pm SEM. * $p < 0.05$, ** $p < 0.01$ (two-tailed Student's t-test) statistically significant differences between the indicated groups.

Chapter 4. Drp1 S600A KI mice display higher lipid utilization and respiratory capacity

Beyond its role as a key regulator of mitochondrial dynamics, Drp1 is also critically important for cellular and organismal homeostasis. Since Drp1 function is influenced by phosphorylations, alterations in the Drp1 phosphorylation crosstalk might hamper systemic metabolic regulation. Yet, the physiological impact and interrelation of Drp1 phosphorylations *in vivo* remains unknown. In the previous Chapters, we have described that phosphorylation at Drp1 S600 acts as an upstream event that determines the activation of Drp1 S579. Importantly, the Drp1 S600 phosphorylation site is conserved in all metazoans, emphasizing the essential role of this residue on mitochondrial function among species. Based on these observations, we decided to generate and characterize a mouse model where the Drp1 S600 site is prevented from phosphorylation, the Drp1 S600A knock-in (KI) mouse model.

We then subjected Drp1 S600A KI mice to a thorough metabolic phenotyping under a control low-fat diet to characterize the implications of Drp1 S600 phosphorylation in metabolic and nutrient homeostasis under basal conditions.

4.1 Generation of a Drp1 S600A knock-in mouse model

To evaluate the regulation and functional consequences of Drp1 phosphorylations *in vivo*, and based on the governance of S600 over S579 phosphorylation, we generated a whole-body Drp1 knock-in (Drp1 KI) mutant mouse model harbouring a site-specific serine (S) to alanine (A) mutation at S600. This was achieved by developing a targeting vector aimed to place a loxP site flanking exons 17 to 20 of the native *Dnm1l* gene, followed by a duplication containing the desired mutation in *Dnm1l* exon 18 (Figure 4.1A; more information in the methods section). An additional polyadenylation signal (hGHpA; human Growth Hormone polyadenylation signal) was inserted between the 3' UTR and the distal loxP site in order to prevent downstream transcription of the duplicated exons 17-20 including the desired mutation (Figure 4.1A). Upon successful recombination and insertion of the targeting vector in ES cells, these were used to

generate the conditional Drp1 KI model. Finally, the whole-body Drp1 KI mouse was obtained by crossing our floxed animals with a Cre-Deleter mouse model (Otto *et al.*, 2009), leading to the deletion of the WT exons 17 to 20 and the hGHpA signal, so that the resulted allele encoded for the mutated S600A protein (Figure 4.1A). The resulting mice were then bred to remove the expression of the Cre-recombinase.

The Drp1 KI mice were viable and fertile and showed no developmental abnormalities. Analysis of total Drp1 protein levels revealed that the S600A mutation did not lead to changes in total Drp1 protein levels in the different tissues examined (Figure 4.1B). Interestingly, we could observe a differential expression of Drp1 among tissues, being highly expressed in heart, BAT, skeletal muscle and liver, and with poor expression in white adipose tissue and kidney (Figure 4.1B). Differences between tissue-specific Drp1 isoforms could also be detected. Indeed, the neuron-specific Drp1 isoform 1 exhibits a higher molecular weight when analysed by Western Blot, whereas Drp1 isoform 3 is smaller and is ubiquitously expressed in tissues including BAT, liver or muscle (Appendix 2). Moreover, the S600 mutation did not alter Drp1 localization on basal conditions (Figure 4.1C). We also analysed the protein levels in BAT of the other proteins involved in mitochondrial dynamics, namely Mfn1, Mfn2 and Opa1, though no differences were observed between Drp1 KI and control mice (Figure 4.1D). Complementarily, the protein levels of the mitochondrial receptors Mff and Fis1 did not differ between genotypes (Figure 4.1D). Based on the role of Drp1 in promoting peroxisomal fission, we analysed the expression levels of the peroxisome markers Pex3 and Pex5, which have been previously associated to Drp1 function (Tanaka *et al.*, 2019). However, the Drp1 S600A mutation did not alter the protein expression levels of Pex3 and Pex5, indicating that peroxisomal biogenesis is overtly affected in the Drp1 KI mice (Figure 4.1D).

4.2 The Drp1 S600A mutation blunts Drp1 P-S579 levels

Similar to our previous results, treating control WT mice with the β 3-specific adrenergic receptor agonist CL316,243 led to increased Drp1 S600 phosphorylation in BAT, and this was linked to an upregulation of Drp1 P-S579 levels (Figure 4.2A and Figure 4.2B). However, the phosphorylation of S600 was absolutely blunted in the BAT of Drp1 KI mice (Figure 4.2A and Figure 4.2B). Importantly, P-S579 was compromised in Drp1 KI mice after CL treatment (Figure 4.2A and Figure 4.2B). In order to discard any tissue-specific effects, we also analysed the response to cAMP induction in the liver of our Drp1 KI mice, by treatment with glucagon. Similar to BAT, glucagon treatment increased Drp1 P-S600 and Drp1 P-S579 levels in control mice, but prevented the phosphorylation at Drp1 S600 in the KI mice (Figure 4.2C and Figure 4.2D). This, in turn, significantly decreased the levels of Drp1 P-S579 (Figure 4.2C and Figure 4.2D). Moreover,

we also characterized Drp1 phosphorylations in muscle, for which we first selected the muscle type that displayed the best response to cAMP induction, by treatment with isoproterenol. To do this, we analysed Drp1 total and Drp1 phosphorylation levels in quadriceps, soleus and EDL, from WT mice (Appendix 3A). Quadriceps showed higher levels of total Drp1 and a better response to treatment as compared to soleus and EDL, thus we selected this tissue for the characterization of the Drp1 KI (Appendix 3A). A similar tendency in the Drp1 phosphorylation crosstalk was observed in the Drp1 KI muscle upon cAMP stimuli (Appendix 3B and Appendix 3C) as in the case of BAT and liver. Altogether, these observations confirm the effectiveness of our knock-in strategy and serves as a complementary proof-of-concept that phosphorylation of S600 acts upstream of S579 phosphorylation.

Based on these results, we also tried to evaluate whether this phosphorylation crosstalk could be reproduced in primary cultures from WT and Drp1 KI tissues. Primary cultures from liver (Appendix 4A and Appendix 4B), muscle (Appendix 4C) and BAT (Appendix 4D) responded properly to cAMP stimuli. However, the results on the Drp1 S579 and S600 phosphorylation interplay were not necessarily aligned with those observed in mouse tissues. This suggests once more that *in vitro* analyses, even in primary cultures from mice, do not reflect the *in vivo* interplay observed physiologically in mouse tissues. Hence, we continued using mouse tissues as our main working model. Also, it must be clarified that the analyses in primary cultures are very preliminary (n=1 in some cases) and should be further validated with more experimental replicates.

4.3 Drp1 KI mice display a tendency towards mitochondrial elongation

Since Drp1 phosphorylation influences mitochondrial shape, we next aimed to characterize the impact of the Drp1 S600A mutation on mitochondrial architecture *in vivo*. To address this, we performed electron microscopy (EM) analyses on BAT from control and Drp1 KI mice (Figure 4.3A). EM pictures showed an increased number of elongated mitochondrial profiles in the Drp1 KI BAT (Figure 4.3A and Figure 4.3B). Indeed, mitochondrial length rates were significantly different between genotypes as measured by Bonferroni test (****p < 0.0001) (Figure 4.3B). This goes in line with our previous observations in cultured cell lines with the Drp1 S600A form, where we also observed increased mitochondrial elongation. Nevertheless, the mitochondrial population was heterogeneous and we still identified mitochondria with fragmented shapes in the Drp1 KI BAT, suggesting that Drp1 phosphorylation acts as amplification rather than a switch for Drp1 fission-related activity. Further, we also performed EM analyses on BAT from control mice treated with CL, which showed an increased number of fragmented mitochondria (Appendix

5A and Appendix 5B). This is consistent with previous publications using primary brown adipocytes, which reported that Drp1 S600 phosphorylation triggered mitochondrial fission after norepinephrine treatment (Wikstrom *et al.*, 2014). These observations go in line with the higher mitochondrial elongation observed in the BAT of our Drp1 KI mice.

4.4 Glucose metabolism is not altered in Drp1 KI mice on LFD

Next, we aimed to characterize the metabolic implications of the Drp1 S600A mutation. Under a normal low fat diet (LFD) Drp1 KI mice were physically undistinguishable from the control counterparts in terms of body weight (Figure 4.4A) and body composition (Figure 4.4B). The weights of tissues from the Drp1 KI mice, such as BAT, liver, WAT (eWAT and scWAT) and heart, were similar to that of control mice (Figure 4.4C). Furthermore, Drp1 KI mice displayed normal daily activity (Figure 4.4D) and food intake (Figure 4.4E). Glucose tolerance and insulin responsiveness were also similar between genotypes (Figure 4.4F and Figure 4.4G, respectively).

4.5 Drp1 KI mice on LFD exhibit increased mitochondrial respiration and lipid oxidation rates

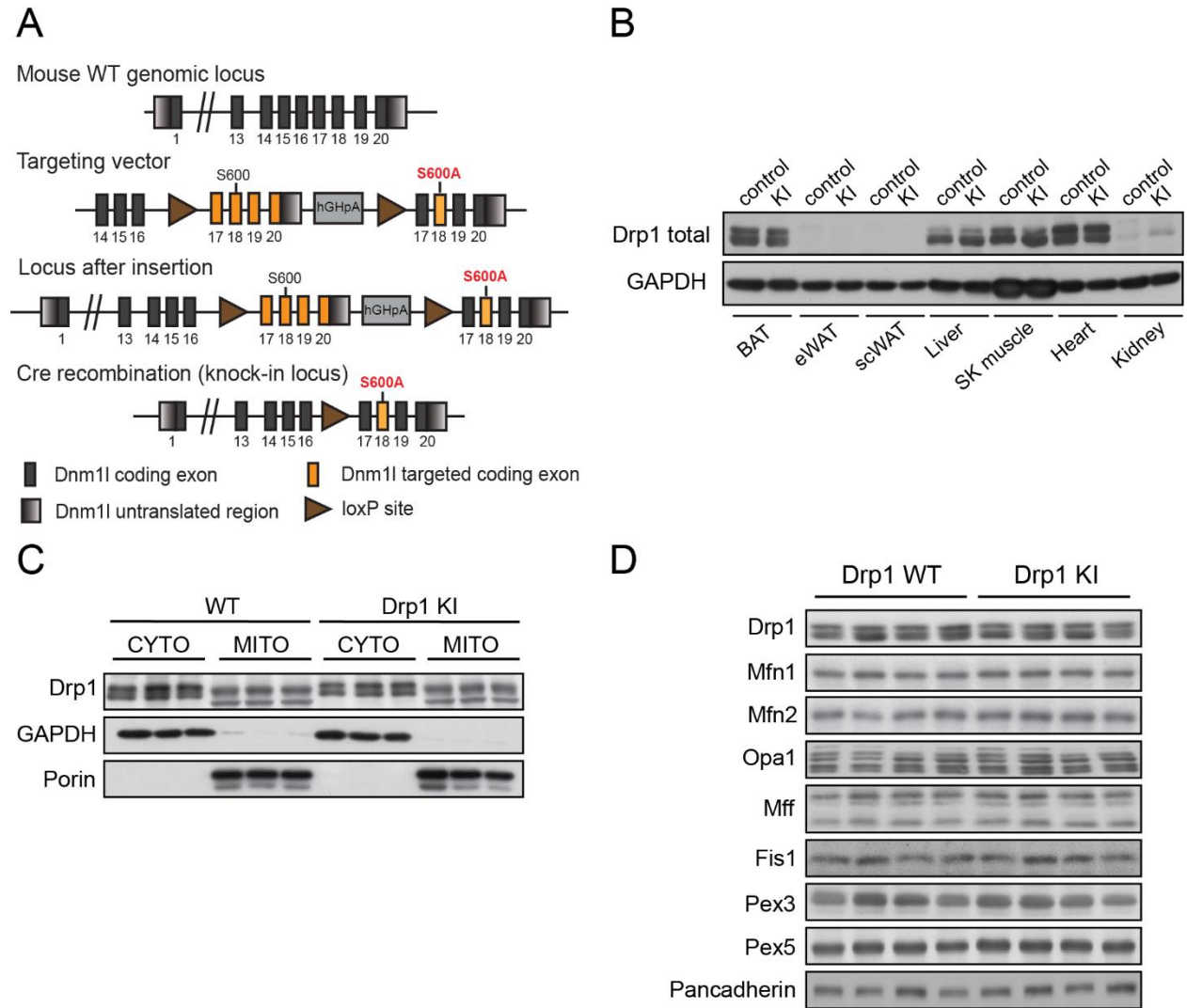
Despite these similarities between Drp1 KI mice and wild-type counterparts, we could still identify some interesting differences. First, we observed increased mitochondrial respiration in the liver and BAT from Drp1 KI mice (Figure 4.5A and Figure 4.5B, respectively), measured by high-resolution respirometry from tissue homogenates. Moreover, indirect calorimetry analyses revealed similar VO_2 consumption rates (Figure 4.5C). However, the respiratory exchange ratio (RER), defined as the ratio between the amount of CO_2 produced in metabolism and the O_2 used, was lower in Drp1 KI mice, particularly during the dark phase (Figure 4.5D). An RER close to 0.7 indicates that fat is the predominant fuel source, while a value of 1.0 is indicative of a preferential use of carbohydrates (Simonson & DeFronzo, 1990). Therefore, our observations suggest a preferential use of lipids as a fuel source for the Drp1 KI mice, possibly facilitated by a higher mitochondrial respiratory capacity.

4.6 Conclusions

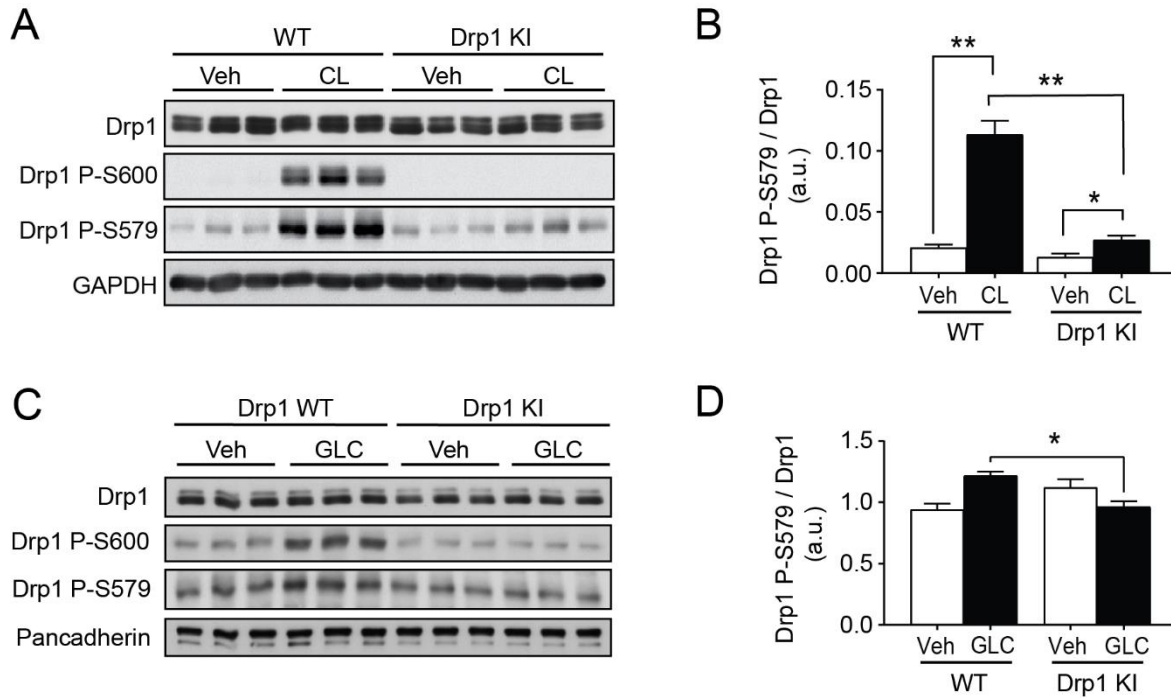
Altogether, we generated a Drp1 S600A knock-in mouse model aimed to define the relation between Drp1 phosphorylations *in vivo* and their physiological impact in metabolic adaptation. Our data suggest that impairment of the upstream Drp1 S600 phosphorylation blunts S579 activation in mouse tissues, which

complements our results with the Drp1 phospho-mutant forms in cultured cells. Moreover, our imaging analysis from mouse BAT revealed that the absence of Drp1 S600 phosphorylation tilts mitochondrial architecture towards a higher elongation.

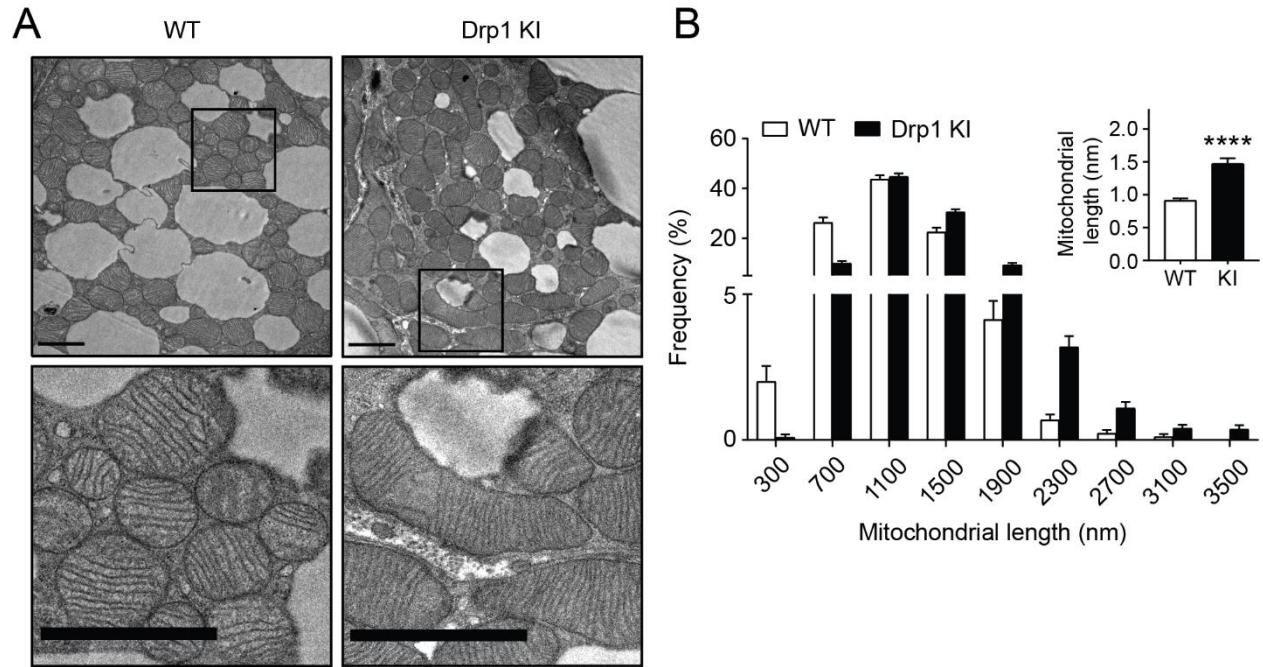
We did not observe any significant differences between control and Drp1 KI mice in body weight, body composition or glucose homeostasis under a low-fat diet. However, we observed a preferential use of lipids as energy source, testified by the indirect calorimetry analyses. Moreover, high-resolution respirometry analysis revealed an increased maximal mitochondrial respiration in BAT and liver from the Drp1 KI mice. Based on these results, it will be interesting to evaluate whether this phenotype could protect Drp1 KI mice when challenged on a fat-based caloric diet.

Figure 4.1**Figure 4.1. Generation of the Drp1 KI mouse model.**

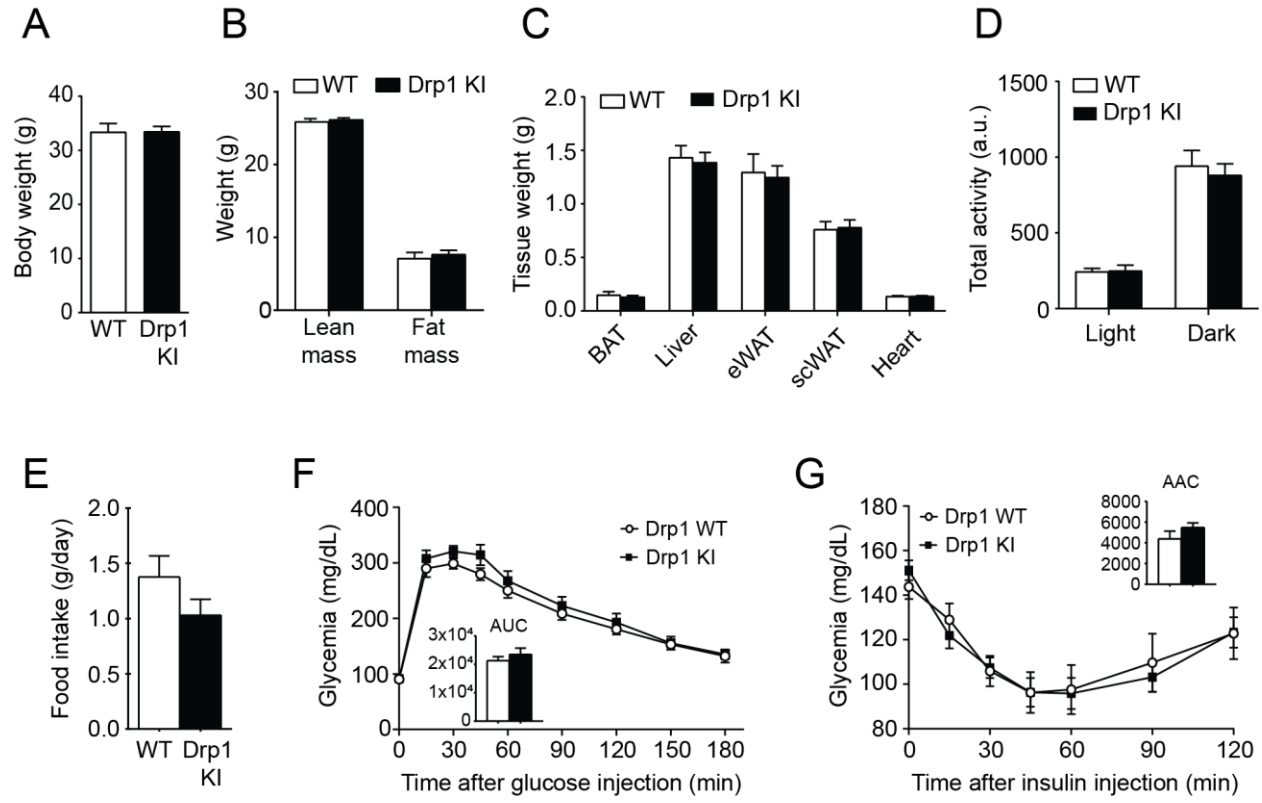
(A) Scheme of the Drp1-targeting vector, the locus after insertion, and the Drp1 KI model after CRE recombination. hGHpA; human Growth Hormone polyadenylation signal. **(B)** Tissue samples from wild-type (control) and Drp1 KI mice were collected and used to evaluate Drp1 protein levels in the indicated tissues. **(C)** Mitochondria were isolated from BAT of WT and Drp1 KI mice, and then Drp1 localization was analyzed in the cytosolic (CYTO) and mitochondrial (MITO) fractions. GAPDH and porin were used as cytosolic and mitochondrial markers, respectively ($n = 3$ mice per genotype). **(D)** Mitochondrial dynamics (Drp1, Mfn1, Mfn2, Opa1), mitochondrial receptors (Mff and Fis1) and peroxisomal proteins (Pex3, Pex5) were analyzed in total homogenates from BAT of WT and Drp1 KI mice ($n = 4$ mice per genotype).

Figure 4.2**Figure 4.2. The Drp1 KI mouse model presents impaired S579 phosphorylation.**

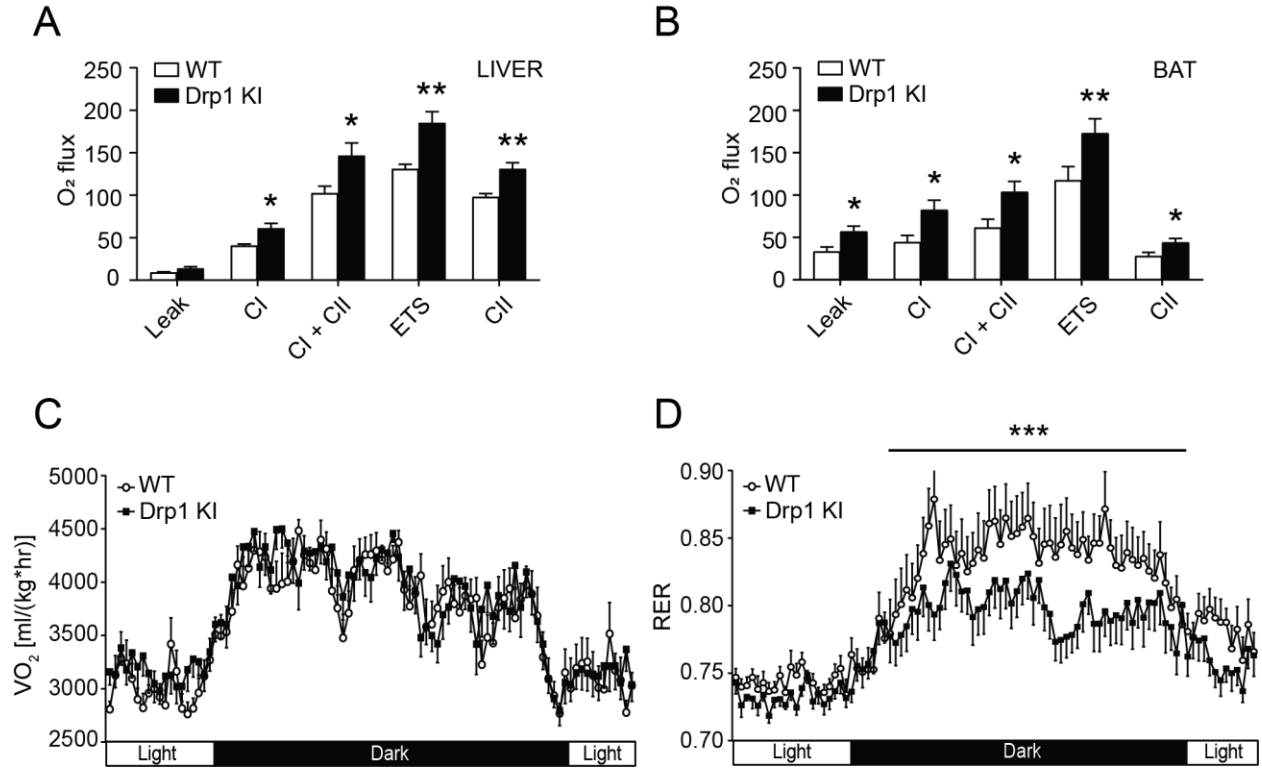
(A) WT and Drp1 KI mice were treated with CL316,243 (1 mg/kg) for 1 h before collecting BAT and evaluating the protein lysates for Drp1 total and Drp1 phosphorylation levels. **(B)** Drp1 P-S579 quantifications from the experiments in (A) ($n=3$ per condition) normalized to Drp1 total levels. **(C)** WT and Drp1 KI mice were fasted for 2 h and then treated with glucagon (1 mg/kg) for 15 min before collecting liver and evaluating the protein lysates for Drp1 total and Drp1 phosphorylation levels ($n=3$ mice per condition). **(D)** Quantifications of Drp1 P-S579 levels normalized to total Drp1 from the experiment in (C). Values are presented as mean \pm SEM from 3 mice/group. * and ** indicate statistically significant difference at $p < 0.05$ and $p < 0.01$, respectively (two-tailed Student's t-test).

Figure 4.3**Figure 4.3. The Drp1 KI mouse model displays increased mitochondrial elongation.**

(A) Electron microscopy (EM) images from BAT (scale bar: 2 μ m) of 10-week old WT and Drp1 KI mice. **(B)** Mitochondrial length was measured, and frequency distributions were calculated from EM images of the experiment in (A), corresponding to 20 independent images per BAT sample ($n = 4$ mice per genotype). Bonferroni test, **** $p < 0.0001$. All values are presented as mean \pm SEM.

Figure 4.4**Figure 4.4. Drp1 KI mice fed on a LFD do not exhibit differences in glucose homeostasis.**

(A-B) Control and Drp1 KI mice fed on a low-fat diet were used to analyze body weight **(A)** and composition **(B)** through EchoMRI. **(C)** Tissues from WT and Drp1 KI mice were collected after sacrifice and weighted. **(D-E)** Total activity **(D)** and food intake **(E)** were measured during indirect calorimetry tests using a comprehensive laboratory animal monitoring system (CLAMS). **(F)** Intraperitoneal glucose tolerance test (ipGTT) performed on WT and Drp1 KI mice fasted for 12 h. Glycemia was measured for the indicated times. **(G)** Intraperitoneal insulin tolerance test (ipITT) performed on WT and Drp1 KI mice fasted for 6h. Insulin (0.5 U/kg) was injected and glycemia was recorded for the timepoints indicated. All data are presented as mean \pm SEM of $n=12$ mice per group. Differences between two groups were analyzed using a Student's two-tailed t-test in (A-E). Linear mixed-effect models were used in (F-G) to assess time*group interaction effects, subsequent comparisons were performed with Tukey's Honest Significant Difference post-hoc test.

Figure 4.5**Figure 4.5. Drp1 KI mice display higher rates of lipid utilization and mitochondrial respiration.**

(A-B) Respirometry analyses of uncoupled respiration (leak), Complex I respiration (CI), Complex I + Complex II respiration (CI + CII), maximal electron transfer system (ETS) capacity, and maximal Complex II driven respiration (CII) in liver **(A)** and BAT **(B)** homogenates from WT and Drp1 KI mice. **(C-D)** Total VO₂ **(C)** and RER **(D)** of WT and Drp1 KI mice was measured through indirect calorimetry. All data are presented as mean \pm SEM of $n=12$ mice per group. * $p < 0.05$, ** $p < 0.01$, *** $p < 0.001$, represent statistically significant differences between the indicated groups. Differences between two groups were analyzed using a Student's two-tailed t-test in (A-B). Linear mixed-effect models were used in (C-D) to assess time*group interaction effects, subsequent comparisons were performed with Tukey's Honest Significant Difference post-hoc test.

Chapter 5. Drp1 KI mice are protected against high-fat-diet-induced insulin resistance

In recent times, the prevalence of obesity has become a major health problem worldwide, reaching pandemic proportions. Obesity occurs when dietary energy intake exceeds energy expenditure, often propelled by the prevalence of high-caloric diets and the decline in physical activity in industrialized societies. One of the main health consequences of obesity is the development of the metabolic syndrome, characterized by an occurrence of metabolic disturbances such as glucose intolerance, insulin resistance, dyslipidaemia and hypertension. Patients with metabolic syndrome are at higher risk of developing type 2 diabetes mellitus (T2DM), cardiovascular disease, cancer or non-alcoholic fatty liver disease. Thus, there's a strong interest in developing therapeutic strategies to palliate the metabolic alterations associated to obesity. The mouse model of diet-induced obesity has become one of the most important tools for understanding the interplay of high-fat Western diets and the development of obesity. Indeed, the metabolic abnormalities of C57BL/6 mice fed *ad libitum* with a high-fat diet closely parallel the human metabolic derangements linked to obesity and the metabolic syndrome (Wang & Liao, 2012).

In this Chapter, we studied how alterations in Drp1 phosphorylation contribute to the onset of obesity and insulin resistance, thus establishing a link between mitochondrial dynamics and metabolic disorders. For that, we challenged Drp1 KI mice and control littermates on a lard-based, high-fat diet (HFD; 60% fat, 20% carbohydrate, 20% protein; Research Diets, D12492i) and performed a comprehensive metabolic phenotyping.

5.1 Drp1 KI mice display improved insulin sensitivity

Given that Drp1 KI mice displayed higher lipid oxidation rates and that lipid accumulation constitutes a key driver of metabolic disease, we next aimed to understand how the Drp1 KI mice handled dietary lipid overload in the shape of a high-fat diet (HFD). WT and Drp1 KI mice fed a HFD gained similar body weight (Figure 5.1A). Food intake (Figure 5.1B) and daily activity (Figure 5.1C) were also similar between genotypes, suggesting a similar feeding behavior. Moreover, there were no changes in total energy

expenditure (Figure 5.1D). Strikingly, while glucose tolerance was comparable between control and Drp1 KI mice when fed a low-fat diet (Figure 4.4F), HFD-fed Drp1 KI mice displayed a less pronounced glucose excursion compared to control mice upon glucose administration (Figure 5.1E). Plasma insulin levels were similar between groups during the glucose tolerance test, suggesting that the higher glucose tolerance was not due to increased insulin secretion (Figure 5.1F). Rather, HFD-fed Drp1 KI mice were more responsive to insulin, as testified by the insulin tolerance test (Figure 5.1G).

In line with the better glucose tolerance and insulin sensitivity, Drp1 KI mice displayed lower levels of a number of circulating inflammatory markers, including ANGPT-L3, C-Reactive Protein (CRP), ICAM-1 or RBP4 (Figure 5.2A), while other hormones, such as leptin, remained unchanged (Figure 5.2B). Of note, Fgf21, which has been proposed as a marker of mitochondrial dysfunction (Suomalainen, 2013) (Boutant *et al.*, 2017), is also notably reduced in the plasma of Drp1 KI mice (Figure 5.2C). Moreover, plasma biochemistry analysis showed that the Drp1 KI mice had increased free fatty acids (FFA), while no differences were observed for cholesterol or triglyceride (TG) content (Figure 5.2D).

We next carried out a series of tests aimed to evaluate tissue-specific function. Since muscle and heart are tissues with high-energy demand and high mitochondrial content, it is possible that the Drp1 S600A mutation exerts a particular effect leading to changes in tissue performance. To study muscle function, we carried out treadmill and grip strength tests. However, we observed no differences in the running distance or duration during the treadmill test (Figure 5.2E and Figure 5.2F, respectively) or the four-paw grip strength (Figure 5.2G). To evaluate heart function, we performed a non-invasive blood pressure (NIBP) test. In this case, we observed no differences in the systolic pressure between Drp1 KI and control mice fed a HFD (Figure 5.2H). In line with this, heart tissue weight was similar between genotypes upon sacrifice (WT: 170 mg \pm 0.019; KI: 180 mg \pm 0.021), suggesting that the Drp1 S600A mutation might not notably impair heart function.

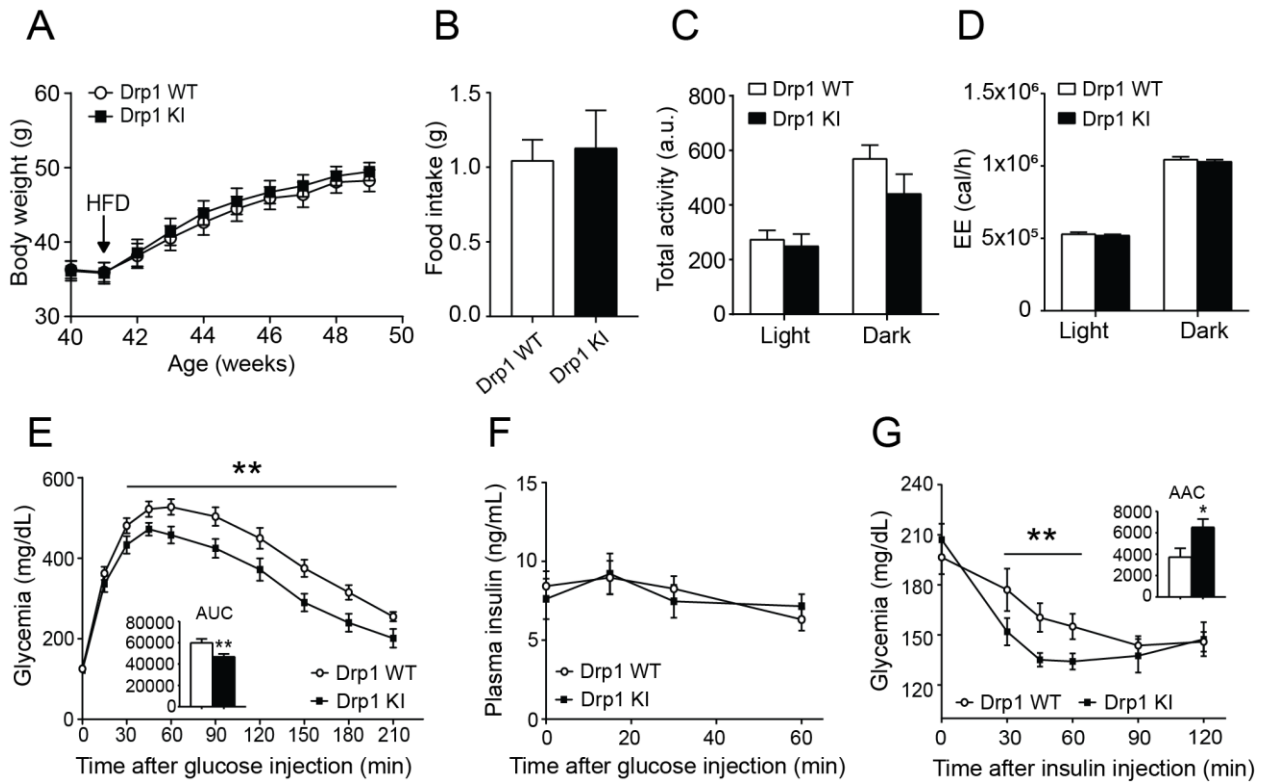
5.2 Drp1 KI mice exhibit increased thermogenesis

Next, we assessed BAT thermogenic function by subjecting mice to a 4 h cold challenge. While no differences in core body temperature were observed at baseline (WT: 38.20°C \pm 0.12; KI: 38.41°C \pm 0.10), Drp1 KI mice were better protected against the drop in body temperature throughout the test than WT mice (Figure 5.3A), which suggested a higher thermogenic capacity in BAT. In line with this, we observed an increase in *Ucp1* transcription levels in the BAT of the HFD-fed Drp1 KI mice, while no differences were observed in the browning marker *Prdm16* (Figure 5.3B). Interestingly, *Pgc1 α* , which is a direct regulator

of UCP1-mediated thermogenesis in BAT (Sharma *et al.*, 2014), was also elevated in the Drp1 KI mice (Figure 5.3B). As the response to cold-exposure can be influenced by multiple factors, we next aimed to assess in a more direct manner BAT thermogenic function in the Drp1 KI mice. For this, we measured whole-body O₂ consumption after β 3-adrenergic stimulation in anesthetized mice. While Drp1 KI and control littermates showed similar O₂ consumption rates at baseline, the increase in O₂ consumption triggered by the β 3-adrenergic receptor agonist CL326,243 (CL) was higher in the Drp1 KI mice (Figure 5.3C and Figure 5.3E), further supporting increased BAT thermogenic capacity. When a similar experiment was performed after housing the mice for 4 weeks at thermoneutrality (30°C) in order to blunt the thermogenic function of the BAT, the differences between genotypes were abrogated (Figure 5.3D and Figure 5.3E). Therefore, these observations point out to an improved response to cold exposure of the Drp1 KI mice due to the increased thermogenesis of their BAT.

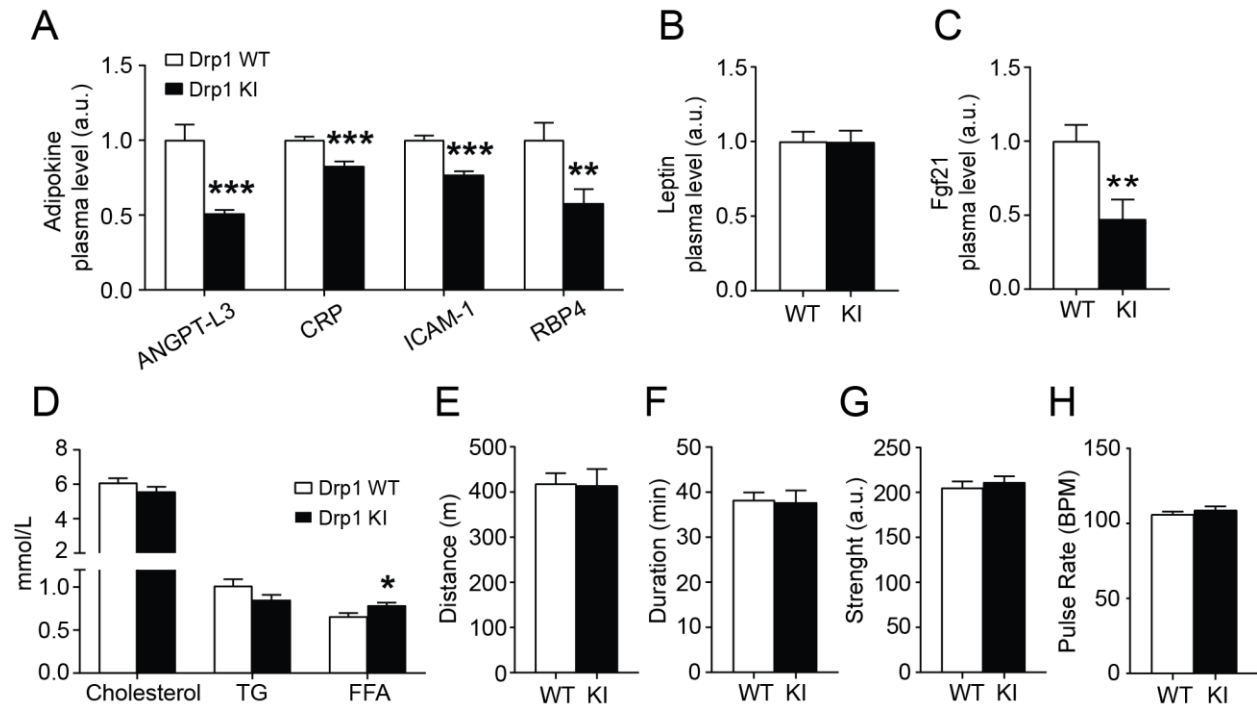
5.3 Conclusions

Altogether, we described in this Chapter the impact of the Drp1 S600A mutation in the protection against glucose intolerance and insulin resistance associated to metabolic disease, by means of challenging Drp1 KI mice to a high-fat feeding. Interestingly, the HFD-fed Drp1 KI mice demonstrated improved systemic glucose homeostasis, testified by their higher glucose tolerance and insulin sensitivity as compared to the HFD-fed control littermates. Thus, these results indicate of a protective effect of the Drp1 S600A mutation against the onset of the metabolic syndrome. While there were no apparent differences in heart and muscle function in the Drp1 KI mice as compared to the control counterparts, we had some insights from the brown adipose tissue function. We observed that HFD-fed Drp1 KI mice displayed an increased thermogenic capacity, due to the enhanced adrenergic tone of their BAT. Pointing out in this direction, the Drp1 KI mice exhibited increased whole-body O₂ consumption after β 3-adrenergic stimulation. When these mice were placed at thermoneutrality, which blunts the thermogenic capacity of the BAT, the higher O₂ consumption of the Drp1 KI animals was completely neutralized. Overall, these results point out towards an important role for the BAT in controlling systemic energy homeostasis in the Drp1 KI mice.

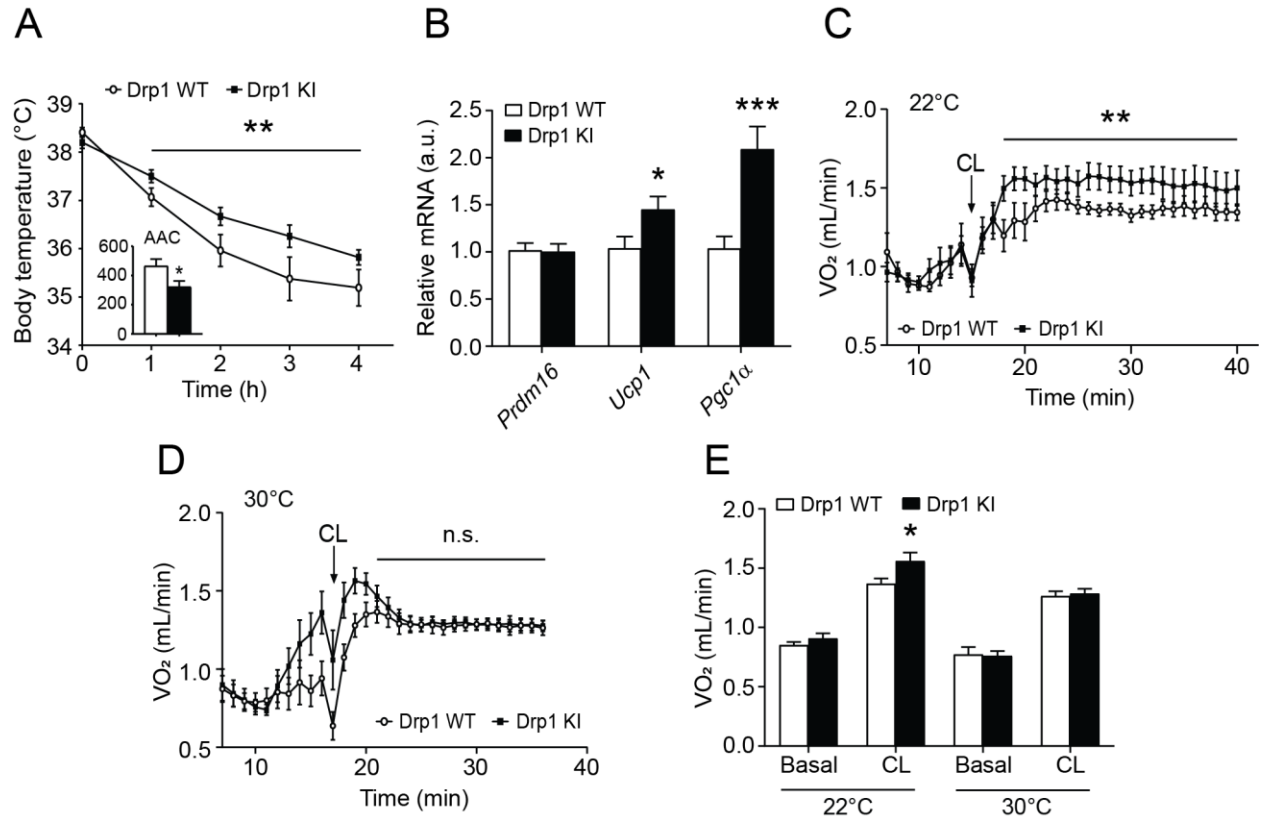
Figure 5.1**Figure 5.1. Drp1 KI mice are protected against diet-induced glucose intolerance and insulin resistance.**

(A) Body weight evolution during the HFD-feeding period of Drp1 KI and control mice. **(B-D)** Food intake **(B)**, total activity **(C)**, and energy expenditure (EE) **(D)** were measured during indirect calorimetry tests using a comprehensive laboratory animal monitoring system (CLAMS) on HFD-fed control and Drp1 KI mice. **(E)** Intraperitoneal glucose tolerance test (ipGTT) performed on HFD-fed WT and Drp1 KI mice. Mice were fasted for 12 hours prior to the injection of 2 g/kg glucose. **(F)** Plasma insulin concentration was measured for the indicated times during the glucose tolerance test in **(E)**. **(G)** Intraperitoneal insulin tolerance test (ipITT) performed on HFD-fed WT and Drp1 KI mice fasted for 6h. Insulin (1 U/kg) was injected and glycemia was recorded for the timepoints indicated. All values are presented as mean \pm SEM of, unless otherwise stated, $n = 12$ mice for each genotype. ** indicate statistically significant difference between control (white bars and white circles) and Drp1 KI mice (black bars and black squares) at $p < 0.01$. Differences between the two groups were analyzed using a Student's two-tailed t-test in **(B-D)**. Linear mixed-effect models were used in **(A)** and **(E-G)** to assess time*group interaction effects, subsequent comparisons were performed with Tukey's Honest Significant Difference post-hoc test.

Figure 5.2

**Figure 5.2. Muscle and heart performance are not impaired in Drp1 KI mice.**

(A) Plasma levels of the indicated cytokines in HFD-fed WT and Drp1 KI mice after a 12 hour fast. **(B-C)** Circulating leptin **(B)** and Fgf21 **(C)** levels in plasma from WT and Drp1 KI mice after a 12 hour fast. **(D)** Plasma biochemistry of HFD-fed Drp1 KI and control mice. Blood samples were collected during sacrifice, after 12 hours of fasting. TG – triglycerides, FFA – free fatty acids. **(E-G)** Muscle performance in WT and Drp1 KI mice was evaluated by carrying out a treadmill test and evaluating the running distance **(E)** and duration **(F)** before exhaustion, as well as a grip test **(G)** to evaluate muscle strength. **(H)** Heart function was evaluated by performing a non-invasive blood pressure test and measuring systolic heart pressure. All values are presented as mean \pm SEM of, unless otherwise stated, $n = 12$ mice for each genotype. *, ** and *** stand for statistical difference vs. the WT group at $p < 0.05$, $p < 0.01$ and $p < 0.001$, respectively (two tailed Student's T-test). WT mice are represented as white bars, while Drp1 KI mice are presented as black bars.

Figure 5.3**Figure 5.3. Drp1 KI mice have increased thermogenic function.**

(A) Thermogenic capacity was evaluated by placing WT and Drp1 KI mice at 6°C and measuring body temperature for 4 h. (B) BAT from HFD-fed control and Drp1 KI mice was collected upon sacrifice and mRNA levels were measured for the indicated genes. (C) Non-shivering thermogenesis in HFD-fed WT and Drp1 KI mice kept at regular housing temperature (22°C) was evaluated by measuring baseline and CL (1 mg/kg) -induced O₂ consumption in anesthetized mice (n = 10 mice per genotype). Immediately after the experiment in (C), the mice were housed at thermoneutrality (30-33°C) for 4 weeks. (D) Then, non-shivering thermogenesis was measured as in (C). (E) Total O₂ consumption at 22°C and 30°C for HFD-fed WT and Drp1 KI mice. All values are presented as mean ± SEM of, unless otherwise stated, n = 12 mice for each genotype. *, ** and *** indicate statistically significant difference between control (white bars and white circles) and Drp1 KI mice (black bars and black squares) at p < 0.05, p < 0.01, p < 0.001, respectively (two-tailed Student's t-test). Differences between the two groups were analyzed using a Student's two-tailed t-test in (B) and (E). Linear mixed-effect models were used in (A) and (C-D) to assess time*group interaction effects, subsequent comparisons were performed with Tukey's Honest Significant Difference post-hoc test.

Chapter 6. Drp1 KI mice display a unique BAT-specific phenotype

Our previous experiments on mice challenged on a high-fat diet (HFD) indicated an increased thermogenic function of the brown adipose tissue (BAT) from the Drp1 KI mice. Contrarily, we did not observe any apparent alterations in muscle or heart performance in these mice. Mitochondrial dynamics play a key role in maintaining mitochondrial function in the BAT. For instance, a previous study from our lab demonstrated that the adipose tissue-specific deletion of the mitochondrial fusion factor Mfn2 greatly impaired BAT thermogenic function, while conferring Mfn2-adKO mice protection against HFD-induced insulin resistance (Boutant *et al.*, 2017). While we and others have contributed to remarkable insights of how Mfn1 or Mfn2 modulates mitochondrial dynamics in BAT function, little is known about the role of Drp1 in BAT.

Mitochondrial function is also influenced by its communication with other cellular organelles, including the endoplasmic reticulum (ER), lipid droplets or the lysosomes (Gordaliza-Alaguero *et al.*, 2019). For instance, mitochondria physical interaction with the ER has many functional implications, including calcium exchange or lipid transfer, but also targets the ER as one of the first sites when mitochondrial function is altered (Valera-Alberni & Canto, 2018). The disruption of ER function causes an accumulation of misfolded and unfolded proteins in the ER lumen, which triggers the unfolded protein response (UPR). In mammals, the UPR is initiated by three ER transmembrane proteins: Inositol-Requiring Enzyme 1 (IRE1), PKR-like ER kinase (PERK), and Activating Transcription Factor 6 (ATF6) (Walter & Ron, 2011). During unstressed conditions, the ER chaperone, Binding Immunoglobulin Protein (BIP) binds to the luminal domains of these master regulators keeping them inactive. Upon ER stress, BIP dissociates from these sensors resulting in their activation. The activation of the IRE1/PERK/ATF6 UPR signaling pathways regulates downstream effectors with the aim of reducing global protein synthesis and increasing the ER protein-folding capacity (Walter & Ron, 2011). Because of the close proximity of the ER and mitochondria, alterations in mitochondrial function can directly elicit stress responses in the ER, and vice versa. Thus,

these stress responses act as quality control mechanisms that not only determine the function and fate of the ER and mitochondria, but also define cellular homeostasis.

In this Chapter, we aimed to further characterize the morphological and functional features of the Drp1 KI BAT, in parallel to results in white adipose tissue and liver, in order to study patterns of fat utilization in these tissues. Moreover, we also evaluated the contribution of the *in vivo* Drp1 S600A mutation in inducing the unfolded protein response by the analysis of ER stress markers.

6.1 Drp1 KI BAT displays enhanced fatty acid oxidation and mitochondrial function

We first evaluated the morphological features of the BAT from the Drp1 KI mice by histology. H&E staining revealed a decrease in the lipid droplet (LD) area in the BAT from the Drp1 KI mice (Figure 6.1A). Indeed, almost 40% of the LDs measured in WT samples were large ($>1000 \mu\text{m}^2$), while only 13% of LDs reached this size in Drp1 KI mice (Figure 6.1B). In contrast, neither the epididymal white adipose tissue (eWAT) (Figure 6.2A) nor the liver (Figure 6.3A) displayed altered lipid deposition, suggesting that this phenotype was rather specific to the BAT.

Next, we explored whether this altered lipid deposition in the BAT was due to variations in either lipogenic or lipolytic processes. The lower lipid accumulation in the BAT of Drp1 KI mice was unlikely caused by impaired lipogenesis, as the mRNA levels for lipogenic markers were increased in the Drp1 KI mice (Figure 6.4A). This was the case for sterol regulatory element-binding proteins 1 and 2 (SREBP1c and SREBP2), key transcriptional regulators of fatty acids biosynthesis, or the acetyl-CoA carboxylases 1 and 2 (ACC1 and ACC2), enzymes catalyzing the carboxylation of acetyl-CoA to malonyl-CoA, the main building block for *de novo* fatty acid synthesis (Figure 6.4A). We additionally evaluated global ACC phosphorylation, a critical negative determinant of ACC activity. As suggested by the mRNA data, ACC protein levels were higher in Drp1 KI mice by 27%, while ACC phosphorylation was increased by 50% when normalized to total ACC levels (Figure 6.4B and Figure 6.4C), although these differences were not statistically significant. This might indicate that whereas ACC is upregulated at the transcriptional level, its activity is fine-tuned by different post-translational modifications. Despite the fact that alterations in *de novo* lipogenesis are not seemingly the source of the small lipid droplet size in the Drp1 KI BAT, we cannot discard possible changes in other lipogenesis processes, such as the direct esterification of fatty acids.

We reasoned that the altered lipid handling could be also linked to changes in lipid catabolism. This led us to explore possible alterations in fatty acid mobilization and oxidation enzymes. Indeed, fatty acid oxidation (FAO) markers, particularly of the carnitine-palmitoyl transferase enzymes CPT1B and CPT2, increased at the mRNA level (Figure 6.1C). These differences were specific to the BAT, since the expression of FAO-related genes were unchanged between groups in eWAT or liver (Figure 6.2B and Figure 6.3B, respectively). Moreover, we performed untargeted metabolomics analyses by liquid chromatography–mass spectrometry (LC-MS), which identified a marked increase of a family of up to 12 acyl-carnitines in the BAT of Drp1 KI mice (Figure 6.1D). Despite the fact that the liver is the most active tissue for endogenous carnitine synthesis and metabolism (Simcox *et al.*, 2017), we did not observe any significant differences in acyl-carnitines between Drp1 KI and control mice in this tissue (Figure 6.3C). We also performed untargeted metabolomics analyses from muscle of the HFD-fed Drp1 KI mice and, as in the case of liver, we did not detect any significant changes in the acyl-carnitine levels (Appendix 3D).

In line with the increase in acyl-carnitines in the BAT, we detected by gas chromatography–mass spectrometry (GC-MS) a significant increase of two species of long chain fatty acids in the Drp1 KI mice, namely FA(18:1) and FA(18:2) (Figure 6.4D). These observations further suggest an increased lipid mobilization in the Drp1 KI BAT. The analysis by GC-MS also uncovered a significant decrease in glutamic acid and urea in the BAT from the Drp1 KI mice (Figure 6.4E), possibly indicating alterations in ammonia metabolism or an increase in the citric acid cycle in this tissue. The levels of asparagine, which is biosynthesized from aspartic acid and ammonia, were upregulated in the Drp1 KI BAT (Figure 6.4E). Nevertheless, future experiments will be required to understand the metabolic implications around the changes in these metabolites.

One critical determinant of lipid oxidation is mitochondrial oxidative phosphorylation capacity. Given that higher respiration was observed in Drp1 KI tissues on low-fat diet, we next evaluated mitochondrial respiratory capacity in HFD-fed Drp1 KI mice. In line with the higher *Ucp1* transcription levels (Figure 5.3B), uncoupled (leak) respiration was increased in the BAT of the Drp1 KI mice (Figure 6.1E). Coupled respiration through either Complex I (CI) or Complex I + Complex II (CI + CII) was also increased in total BAT homogenates from the Drp1 KI mice compared to the control mice (Figure 6.1E). Similarly, maximal electron transport system (ETS) capacity of the respiratory chain was enhanced (Figure 6.1E). The higher mitochondrial respiratory capacity in the BAT of the Drp1 KI mice was not linked to an increase in mitochondrial content as evaluated by the quantification of protein levels of the mitochondrial respiratory complexes (Figure 6.1F) and mitochondrial DNA (Figure 6.1G). However, intrinsic changes in respiratory

properties were observed using isolated mitochondria. In particular, state 4 respiration of Complex I, triggered by malate and glutamate, was higher in the isolated mitochondria from the Drp1 KI (Figure 6.1H).

While mitochondrial respiration in the eWAT was similar between genotypes (Figure 6.2C), increased mitochondrial respiration was detected in liver homogenates from HFD-fed Drp1 KI mice (Figure 6.3D), where lipid content was unaltered (Figure 6.3A). Thus, the maximal mitochondrial respiratory capacity in the Drp1 KI tissues is maintained regardless of the diet.

Overall, we demonstrate that the BAT of the HFD-fed Drp1 KI mice displays specific features that are not reproduced in liver or white adipose tissue, and that the lower lipid deposition in the BAT is correlated to an increased lipid oxidation and mitochondrial function.

6.2 Drp1 KI BAT exhibits increased ER stress

We next aimed to evaluate how these changes impact ER function by analyzing markers of ER stress in the Drp1 KI mouse tissues. The unfolded protein response (UPR) in mammals is monitored through the ATF6, IRE1 and PERK mechanisms, respectively (Figure 6.5A). Each mechanism regulates a set of downstream effectors aimed to promote clearance of unwanted proteins or, alternatively, to inhibit protein translation and prevent further accumulation of unfolded proteins (Figure 6.5A).

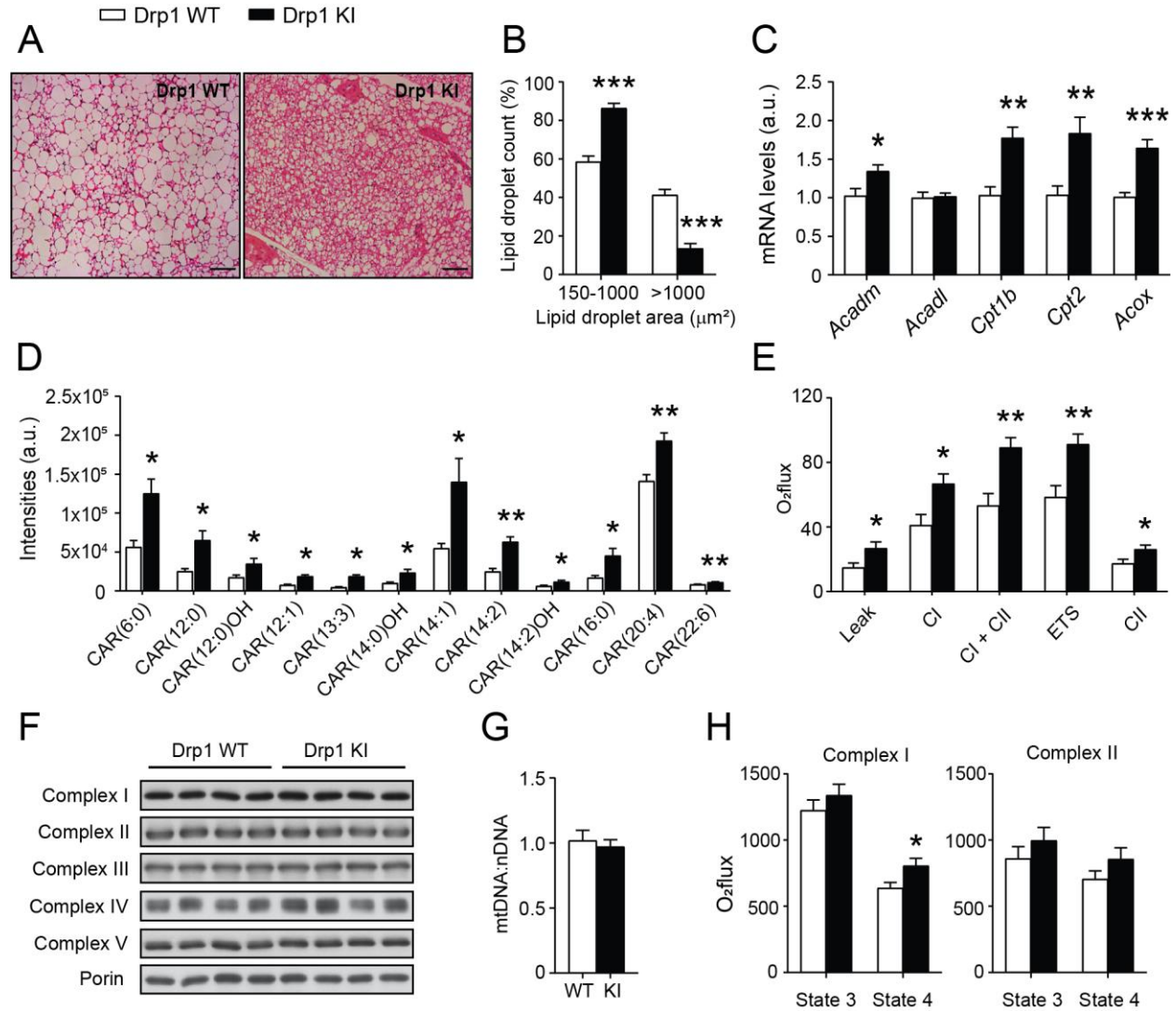
The analysis of UPR markers in the BAT of the HFD-fed Drp1 KI mice indicated a marked increase in the mRNA levels of *Atf4*, *Atf6* and *Bip* as compared to the control mice (Figure 6.5B), while no differences were observed in liver (Figure 6.5C) or eWAT (Figure 6.5D). The transcription of *Atf4* is a downstream event from the activation of the PERK signaling, in parallel to the activation of EIF2 α , whose function is to decrease the synthesis of new proteins (Figure 6.5A). In line with this, the phosphorylation levels of EIF2 α were significantly higher in the BAT of the Drp1 KI mice (Figure 6.5E and Figure 6.5F). Unfortunately, the commercial antibody used against phospho-PERK did not work in our experimental setting. However, the simultaneous increase of *Atf4* transcription levels and EIF2 α phosphorylation suggests that the PERK/ATF4/EIF2 α axis of the UPR is altered in the Drp1 KI mice. Furthermore, the phosphorylation of IRE1 was also increased in the Drp1 KI BAT (Figure 6.5E and Figure 6.5F), indicating that multiple molecular pathways shaping the UPR are activated in the BAT of HFD-fed Drp1 KI mice.

6.3 Conclusions

Altogether, our data suggest that impaired Drp1 S600 phosphorylation in mice leads to increased lipid oxidation rates in the BAT, testified by the reduced lipid droplet size and the increased expression of FAO-related enzymes. In line with this, upregulation of the acyl-carnitine transporters CPT1B and CPT2 were correlated to an increase in acyl-carnitine levels.

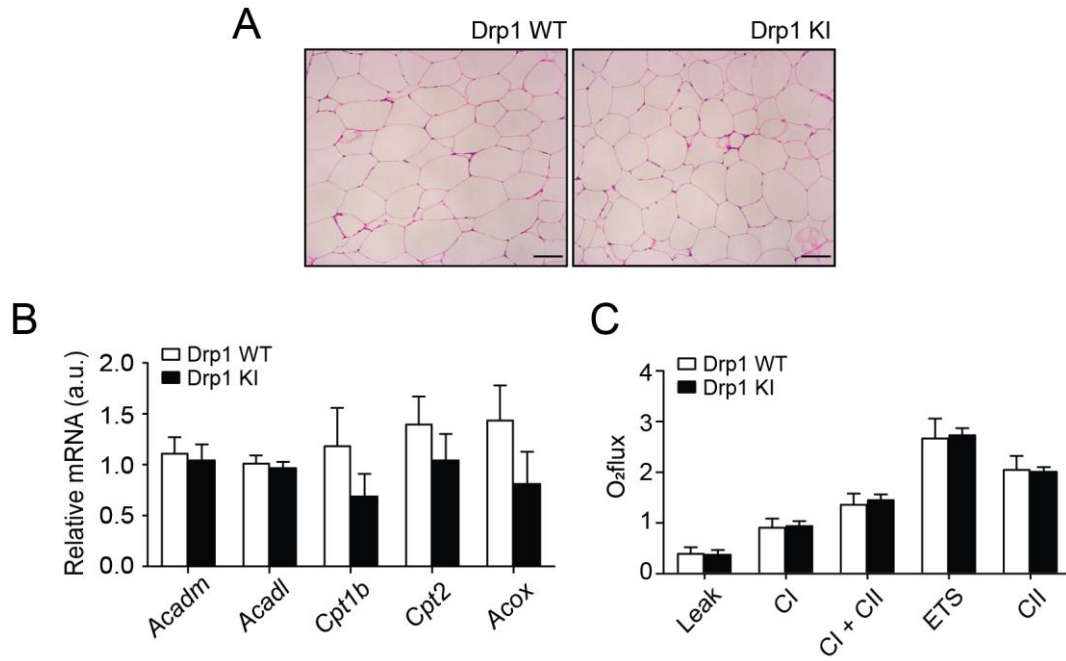
Moreover, our results indicate that the unfolded protein response in the endoplasmic reticulum (ER) was increased specifically in the brown adipose tissue of the Drp1 KI mice on HFD, via the upregulation of the three signaling mechanisms of the UPR: ATF6, IRE1 and PERK/ATF4. These findings notably remark the communicative behavior of mitochondria with other cellular organelles to signal alterations in their morphology and/or function. However, further analyses are required to evaluate how the increase in the UPR impacts on the ER structure in our Drp1 KI mouse model, by evaluating ER morphology in mouse tissues. This will allow us to define why the improved mitochondrial function in the Drp1 KI mice is linked to enhanced ER stress, and why these changes are specific to the BAT. These observations go in line with previous work indicating that higher ER stress can occur in the context of insulin sensitivity (Boutant *et al.*, 2017), although opposing views exist (Salvadó *et al.*, 2015). Importantly, ER stress is highly influenced by variations in lipid metabolism and, particularly, in lipid droplet homeostasis (Han & Kaufman, 2016) (Jarc & Petan, 2019). Conversely, activation of the UPR pathways can modulate lipid metabolism by controlling the transcriptional regulation of lipogenesis (Basseri & Austin, 2012). In this regard, the increased ER stress of the Drp1 KI BAT would provide a plausible explanation for the enhanced lipogenesis markers, notably of the ER-bound SREBP-1c and SREBP2. Overall, these results give a notion of the impact of the Drp1 S600 mutation *in vivo*, although further experiments will be needed to evaluate the mitochondria-ER crosstalk in maintaining cellular homeostasis.

Finally, we did not observe any lipid oxidation or ER-stress marker upregulation in other Drp1 KI tissues such as the liver or the white adipose tissue, which define the BAT as the main tissue affected upon the whole-body Drp1 S600A mutation in mice. Further approaches will be needed to evaluate the role of the BAT in the phenotype observed in the Drp1 KI mice.

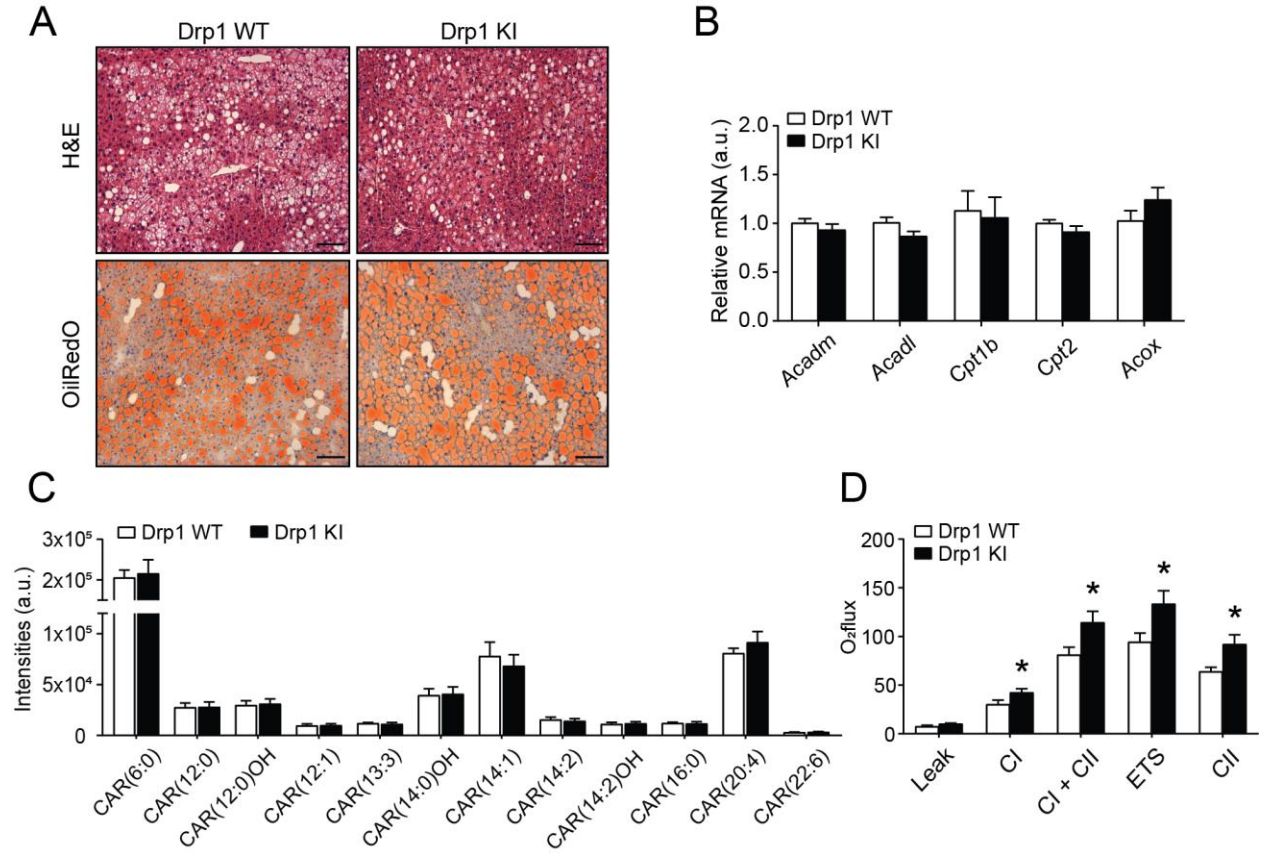
Figure 6.1**Figure 6.1. Increased fatty acid oxidation capacity in the BAT of Drp1 KI mice.**

BAT from HFD-fed WT and Drp1 KI mice was extracted at the end of the phenotyping and the following tests were performed. **(A)** Hematoxylin/eosin staining of BAT (scale bar: 100 μm). **(B)** Lipid droplet size quantification from histology images in (A), corresponding to 20 independent images per BAT section (n = 5 samples per genotype). **(C)** mRNA levels of markers of fatty acid oxidation (FAO) were analyzed by qPCR. **(D)** Acyl-carnitine levels were measured by liquid chromatography and mass-spectrometry (LC-MS) from BAT of HFD-fed mice (n = 12 WT and 9 KI). **(E)** Respirometry analyses of uncoupled respiration (leak), Complex I respiration (CI), Complex I + Complex II respiration (CI + CII), maximal electron transfer system (ETS) capacity, and maximal Complex II driven respiration (CII) in BAT homogenates from HFD-fed WT and Drp1 KI mice (n = 8 per genotype). **(F)** Mitochondrial complexes were evaluated by analyzing protein levels in total homogenates from BAT. **(G)** Total DNA was extracted and the ratio between mitochondrial encoded and nuclear encoded genes (mtDNA:nDNA) was measured by RT-qPCR (n = 8 per genotype).

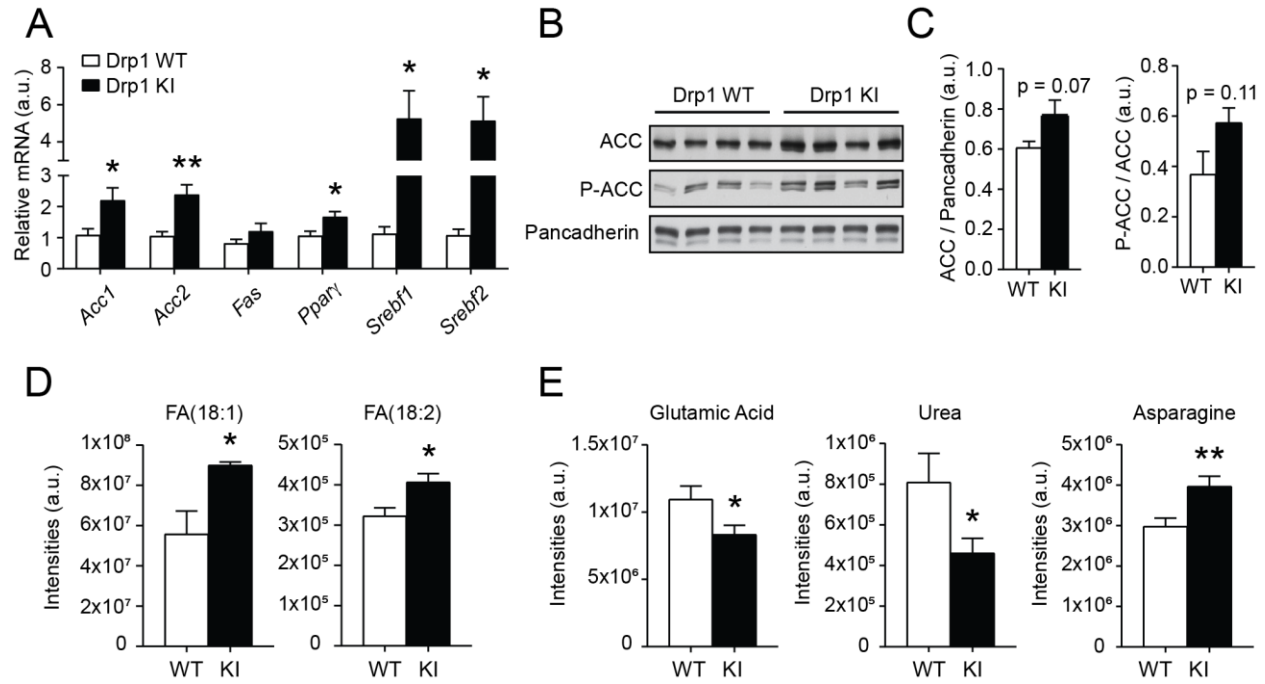
(H) Respirometry analyses were performed in isolated mitochondria from BAT of control and Drp1 KI mice (n = 8 per genotype). On the left, malate (2 mM) and glutamate (10 mM) were used to stimulate Complex I, and State 3, State 4 respiration were evaluated. On the right, succinate (10 mM) and rotenone (0.5 μ M) were used to evaluate Complex II, and State 3, State 4 respiration were measured. Through the figure, white bars represent WT mice, while black bars represent the Drp1 KI mice. All data is expressed as mean \pm SEM. *, ** and *** indicate statistical difference at $p < 0.05$, $p < 0.01$ and $p < 0.001$ vs. the respective WT group (two tailed Student's T-test).

Figure 6.2**Figure 6.2. Characterization of eWAT from HFD-fed Drp1 KI mice.**

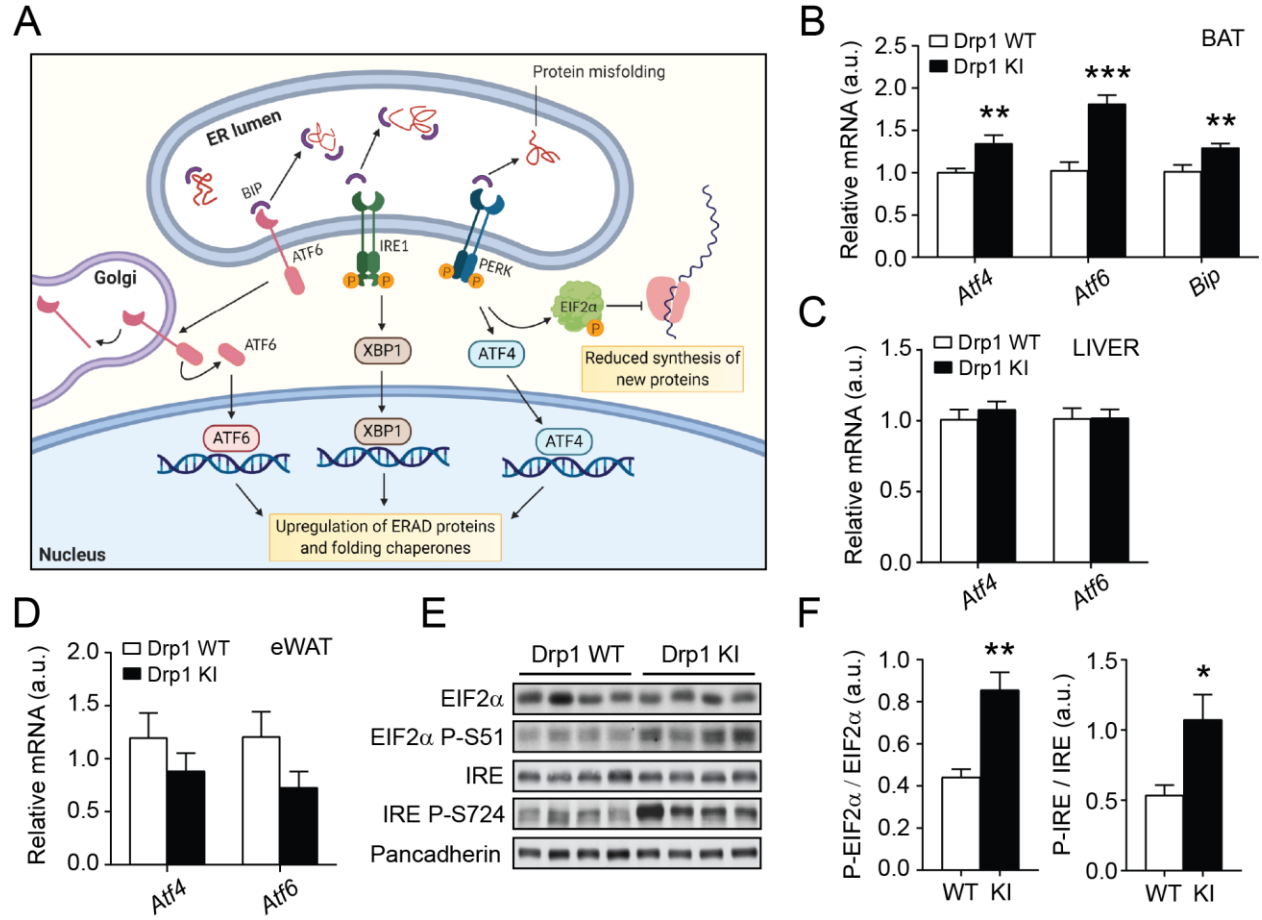
(A) H&E staining of eWAT from control and Drp1 KI HFD-fed mice (scale bar: 100 μ m). **(B)** mRNA levels from fatty acid oxidation (FAO) markers in eWAT of HFD-fed WT and Drp1 KI mice. **(C)** Respirometry analyses of uncoupled respiration (leak), Complex I respiration (CI), Complex I + Complex II respiration (CI + CII), maximal electron transfer system (ETS) capacity, and maximal Complex II driven respiration (CII) in eWAT homogenates from HFD-fed WT and Drp1 KI mice. Through the figure, white bars represent WT mice, while black bars represent the Drp1 KI mice. All values are presented as mean \pm SEM of n=8-10 mice per genotype.

Figure 6.3**Figure 6.3. Characterization of liver from HFD-fed Drp1 KI mice.**

(A) H&E staining and Oil Red'O staining of liver from HFD-fed mice (scale bar: 100 μ m). **(B)** mRNA levels from fatty acid oxidation markers. **(C)** Acyl-carnitine levels were measured by liquid chromatography and mass-spectrometry (LC-MS) from liver of HFD-fed mice ($n = 12$ WT and 9 KI). **(D)** Respirometry analyses of uncoupled respiration (leak), Complex I respiration (CI), Complex I + Complex II respiration (CI + CII), maximal electron transfer system (ETS) capacity, and maximal Complex II driven respiration (CII) in liver homogenates from HFD-fed WT and Drp1 KI mice. Through the figure, white bars represent WT mice, while black bars represent the Drp1 KI mice. All values are presented as mean \pm SEM of $n=8-10$ mice per genotype. * indicates statistical difference vs. the respective WT group at $p<0.05$ (two-tailed Student's T-test).

Figure 6.4**Figure 6.4. Supplementary BAT-specific features of the HFD-fed Drp1 KI mice.**

(A) mRNA levels of lipogenesis markers from BAT of WT and Drp1KI mice on HFD. **(B)** Protein levels of ACC and phospho-ACC (Ser79) were measured by Western blot from BAT total homogenates. **(C)** Quantifications of ACC and phospho-ACC levels from the experiment in (B). **(D-E)** Gas chromatography - mass-spectrometry (GC-MS) measurements detected two species of long-chain fatty acids (FA) **(D)** as well as various ammonium-related metabolites **(E)** from BAT of Drp1 KI and control HFD-fed mice (n = 12 WT and 9 KI). Through the figure, white bars represent WT mice, while black bars represent the Drp1 KI mice. All data is expressed as mean \pm SEM. * and ** indicate statistical difference at p < 0.05 and p < 0.01 vs. the respective WT group (two tailed Student's T-test).

Figure 6.5**Figure 6.5. Drp1 KI BAT exhibits increased ER stress-induced unfolded protein response.**

(A) Schematic showing the unfolded protein response (UPR) signaling pathways initiated during ER stress. Protein folding efficiency is impaired during ER stress and results in the accumulation of misfolded proteins in the ER lumen. In order to relieve ER stress and restore ER homeostasis, the cell activates three different signaling mechanisms (ATF6, IRE1 and PERK) which promote the expression of ER-associated degradation (ERAD) proteins and chaperones that aid correct protein folding, or inhibit the synthesis of new proteins to reduce the working load in the ER (Adapted from Todd *et al.* (2008)). **(B-D)** Tissues from HFD-fed Drp1 KI and control mice were collected at the end of the phenotyping and mRNA was extracted to measure the indicated ER-stress markers in BAT **(B)**, liver **(C)** and epididymal WAT **(D)** ($n=8$ mice per genotype). **(E)** Protein levels of total and phosphorylated EIF2 α and IRE, respectively, were measured from tissue homogenates of BAT of HFD-fed Drp1 KI and control mice. **(F)** Quantifications of the phosphorylation levels of EIF2 α and IRE, respectively, from the experiment in (E). All data is expressed as mean \pm SEM. *, ** and *** indicate statistical difference at $p<0.05$, $p<0.01$ and $p<0.001$ vs. the respective WT group (two tailed Student's T-test).

Chapter 7. Thermoneutrality blunts the phenotype of the Drp1 KI mice

In the previous Chapters, we described the metabolic phenotype of the Drp1 S600A KI mice under low-fat and high-fat diet. Remarkably, we observed that the constitutive dephosphorylation of the Drp1 S600 site granted Drp1 KI mice protection against diet-induced insulin resistance and glucose intolerance. We also observed a set of metabolic features specific to the brown adipose tissue (BAT), such as reduced adiposity linked to increased lipid oxidation and mobilization rates. Moreover, the BAT of the Drp1 KI mice displayed increased thermogenesis, testified by direct calorimetry analysis as well as by cold challenge.

Importantly, the BAT is greatly influenced by the environmental temperature which, in turn, affects systemic metabolic rates in humans and in mice. Laboratory mice have a thermoneutral zone at around 30°C but are normally housed at the standard temperature of thermal comfort for humans, at 22-25°C (Cannon & Nedergaard, 2011) (Maloney *et al.*, 2014). Therefore, laboratory mice are constantly under cold stress, and thus need to produce extra heat to defend their body temperature, which leads to substantially increased metabolic rates as compared to those housed at thermoneutrality (Fischer *et al.*, 2018).

Therefore, we next aimed to assess the contribution of the BAT thermogenic function to the insulin sensitivity phenotype of the Drp1 KI mice. For this, we reasoned that if the higher BAT thermogenic function of Drp1 KI mice can be trumped by housing at thermoneutrality, this should allow us to evaluate the contribution of BAT to the glucose tolerance phenotype.

7.1 Thermoneutrality blunts the BAT-specific features of the Drp1 KI mice

We fed WT and Drp1 KI mice with a high-fat diet for 8 weeks at thermoneutrality (TN, 30°C). We initially aimed to validate the effectiveness of our thermoneutrality protocol by comparing the BAT of WT mice housed at normal temperature to samples of mice housed at thermoneutrality. Protein analyses revealed a sharp reduction of UCP1 levels in control mice at thermoneutrality, as compared to control mice at

normal housing conditions (RT, 22-25°C) (Figure 7.1A and Figure 7.1B). Interestingly, we also observed a decrease in Drp1 S600 and S579 phosphorylation levels, respectively, in agreement with a much lower β -adrenergic tone in the BAT of mice housed at thermoneutrality (Figure 7.1A and Figure 7.1B).

After validating our thermoneutrality protocol, we evaluated parameters of BAT function. Interestingly, the smaller lipid droplet (LD) size of the HFD-fed Drp1 KI mice housed at RT was completely abolished at thermoneutrality, testified by the H&E staining that revealed comparable LD size between genotypes (Figure 7.2A and Figure 7.2B). Moreover, the higher *Ucp1* mRNA levels (Figure 7.2C), as well as those of fatty acid oxidation and lipogenesis genes (Figure 7.2D) observed in the BAT of Drp1 KI mice at normal housing conditions were abrogated at thermoneutrality. Similarly, the transcription levels of the ER-stress markers *Atf4*, *Atf6* and *Bip*, which indicated an upregulation of the unfolded protein response in the Drp1 KI BAT, were unchanged between genotypes at thermoneutrality (Figure 7.2D).

We next measured mitochondrial oxidative phosphorylation capacity, which was increased in BAT and liver of Drp1 KI mice at RT. Due to the reduced β -adrenergic tone of the BAT at thermoneutrality, the mitochondrial respiratory capacity was largely blunted in BAT homogenates from TN-housed mice (Figure 7.2E). Of note, Drp1 KI mice exhibited undistinguishable respiratory profiles from those of control mice in BAT (Figure 7.2E). Importantly, the higher respiratory capacity in the liver of Drp1 KI mice was still observed in mice housed at thermoneutrality (Figure 7.2F), testifying for the BAT-specific effect of the protocol.

Altogether, these results suggest that the increased thermogenesis of the BAT from the Drp1 KI mice is at the root of their increased lipid oxidation rates, and that this eventually monitors mitochondrial respiratory capacity.

7.2 Thermoneutrality prevents the improved insulin sensitivity of the Drp1 KI mice

We next aimed to evaluate whether the blunted BAT thermogenesis could influence glucose handling in the Drp1 KI mice. For that, we performed a glucose tolerance test (GTT) and insulin tolerance test (ITT), respectively, of HFD-fed Drp1 KI and control mice housed at thermoneutrality. Remarkably, thermoneutrality abolished the higher glucose tolerance of the Drp1 KI mice observed at normal housing conditions (Figure 7.3A). Of note, we observed that the blood glucose curve was noticeably lower for both genotypes during the GTT at thermoneutrality, where it peaked at 300 mg/dL (Figure 7.3A), as compared

to the same test in mice housed at 22°C where blood glucose was maximum at 600 mg/dL (Figure 5.1E). In line with this, glucose-stimulated plasma insulin values at thermoneutrality were 8-fold higher as compared to those at RT (Figure 7.3B and Figure 5.1F, respectively), even though basal insulin levels were comparable between both housing temperature conditions (HFD-WT at RT: 8.43 ± 0.94 ; HFD-WT at TN: 11.78 ± 2.31). Moreover, thermoneutrality blunted the higher insulin sensitivity of the Drp1 KI mice observed at normal housing conditions (Figure 7.3C and Figure 5.1G, respectively). Basal glycemia levels of Drp1 KI mice prior to the insulin tolerance test were notably higher as compared to the control mice (WT: 129.44 ± 3.14 ; KI: 142.25 ± 2.30) after 6 hours of fasting (Figure 7.3C). This could have been a unrelated event, since glycemia values measured after a 12-hour fasting indicated no differences between groups (Figure 7.3D). Overall, these observations indicate that blunting the thermogenic capacity of the BAT also neutralizes the insulin sensitivity phenotype of the Drp1 KI mice.

While the better glucose tolerance and insulin sensitivity of the Drp1 KI mice housed at room temperature were associated with lower levels of circulating inflammatory markers such as ANGPT-L3, C-Reactive Protein (CRP), ICAM-1 or RBP4, these differences were completely blunted at thermoneutrality (Figure 7.3E). This was also the case for Fgf21, which displayed no significant differences between genotypes in mice housed at thermoneutrality (Figure 7.3F).

Overall, these results suggest that the increased thermogenic capacity of the BAT from Drp1 KI mice monitors their increased systemic glucose tolerance and insulin sensitivity.

7.3 Conclusions

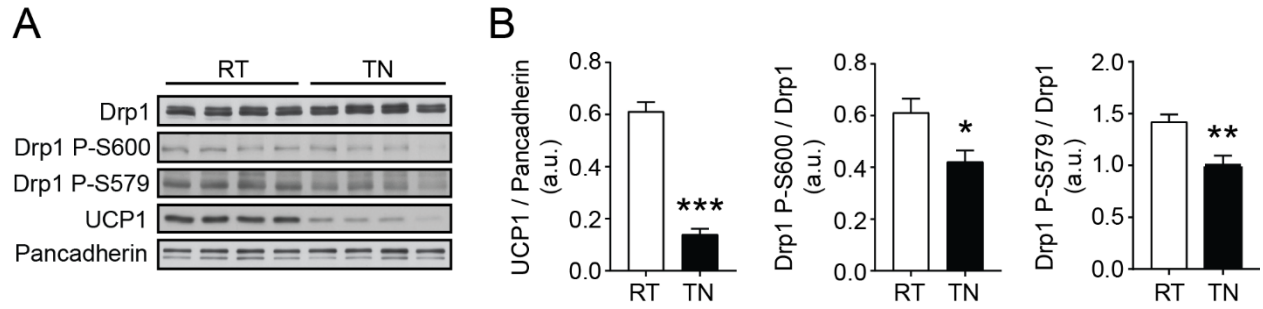
In this Chapter, we evaluated the role of the thermogenic function of the brown adipose tissue in the phenotype of the Drp1 KI mice. Of note, we demonstrate that the increased thermogenesis of the Drp1 KI BAT regulates not only its lipid oxidation rates but also is at the root of the improved insulin sensitivity and glucose tolerance observed in the Drp1 KI mice. Thus, these results provide novel insights of how Drp1 phosphorylation in the BAT influences whole-body glucose homeostasis.

Importantly, we show remarkable differences in whole-body glucose tolerance in mice housed at normal room temperature as compared to mice at thermoneutrality. Indeed, the housing temperature of laboratory mice has been reported to affect a wide range of physiological parameters, including glucose metabolism. However, research on how housing temperature affects glucose tolerance in mouse models have yielded variable results. Some of these reports show no change in glucose tolerance in mice held at

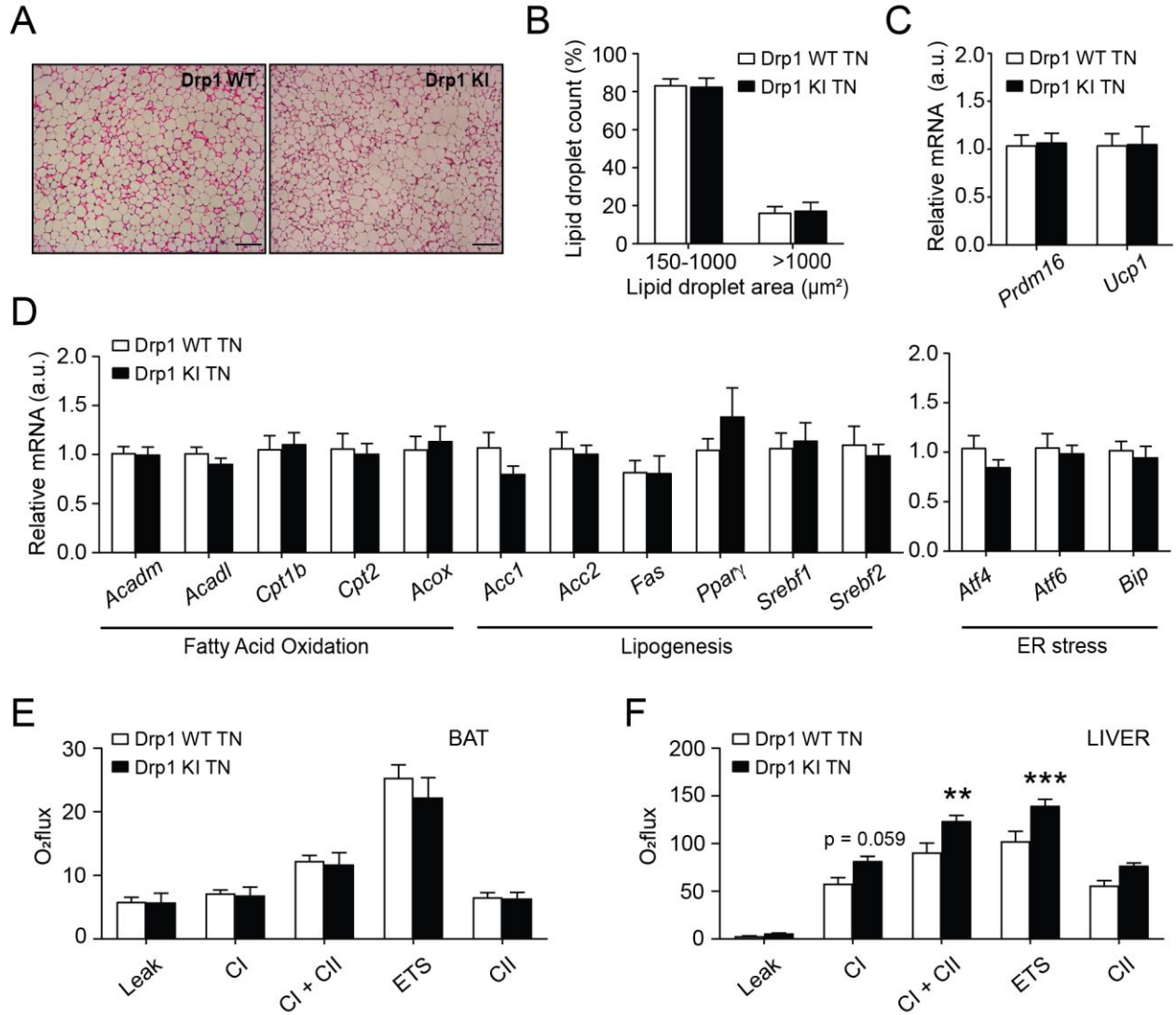
thermoneutrality compared to standard housing temperatures (Clayton & McCurdy, 2018) (Rippe *et al.*, 2000) (Cui *et al.*, 2016) (Tian *et al.*, 2016), and even similar maximum glycemia values at thermoneutrality as to those obtained at standard temperature (Ahmadian *et al.*, 2018). Contrarily, recent publications showed that thermoneutrality improved glucose tolerance in mice, validated by the noticeably lower blood glucose curve during the glucose tolerance test (McKie *et al.*, 2019) (Raun *et al.*, 2020) (Uchida *et al.*, 2010). This improved glucose tolerance was associated to a remarkable increase in glucose-stimulated plasma insulin levels in mice housed at thermoneutrality compared to RT, suggesting that housing temperature could affect β -cell function (Raun *et al.*, 2020) (Uchida *et al.*, 2010). These observations are aligned with our data, where the lower glycemia values in our GTT at TN were linked to an 8-fold increase in plasma insulin levels as compared to those at RT.

One possible explanation for the published contradictory observations regarding the influence of thermoneutrality on glucose handling could be the temperature of the thermoneutral room, as well as the time period in which the mice were acclimatized. For instance, Raun *et al.* (2020) housed the mice at 30°C for 8 weeks, similar to our approach. Conversely, other studies reduced the acclimatization time to only 10 days, as in the case of Ahmadian *et al.* (2018) and Clayton & McCurdy (2018). Thus, comparisons between these reports are difficult to draw, especially when some of these studies did not verify to what degree the thermogenic capacity of the BAT was blunted. Evaluating abolition of the BAT function could be performed, for example, by comparing UCP1 levels of control mice housed at standard conditions to those of mice housed at thermoneutrality. Indeed, we housed mice at 30°C for 8 weeks, which resulted in a 3-fold decrease in UCP1 protein levels compared to mice housed at 22°C. Based on these findings, housing temperature will be a crucial factor to take into consideration in studies analyzing whole-body glucose metabolism.

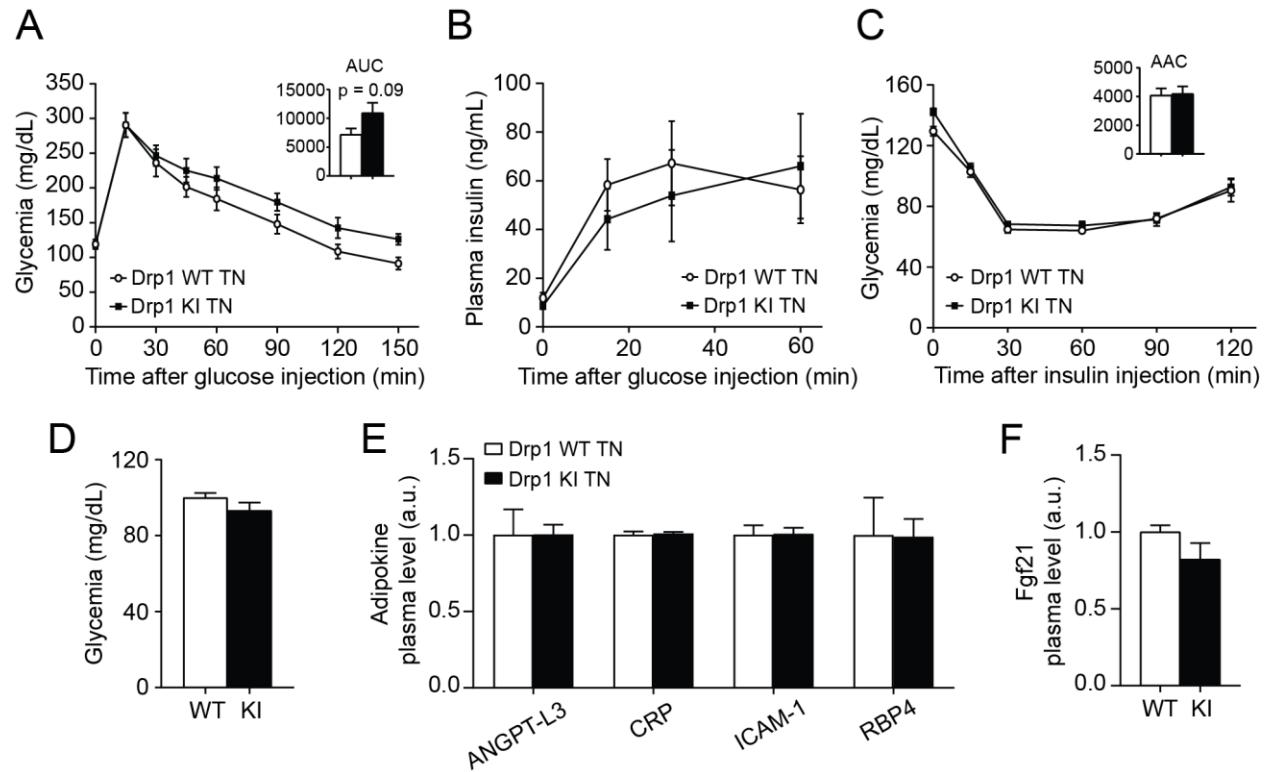
In conclusion, we provide new evidence of the role of the brown adipose tissue in the protection of Drp1 KI mice against metabolic damage. However, further research is necessary to elucidate the gene or molecular mechanism that is at the root of the increased thermogenesis in the Drp1 KI mice. Providing an explanation to this phenotype will be essential in assessing the role of Drp1 phosphorylations in BAT function and systemic metabolism, which could aid in finding new therapeutic approaches in the treatment and prevention of metabolic disease.

Figure 7.1**Figure 7.1. Housing mice at 30°C hinders BAT thermogenic tone.**

(A) Evaluation of total Drp1, Drp1 phosphorylations and UCP1 protein levels in WT mice housed either at 22°C (room temperature; RT) or at 30°C (thermoneutrality; TN) ($n = 4$ mice per condition). **(B)** Quantifications of the markers in (A). White bars represent WT mice at RT, while black bars represent WT mice at TN. All values are presented as mean \pm SEM. *, **, *** indicates statistical difference at $p < 0.05$, $p < 0.01$, $p < 0.001$, respectively, vs. the corresponding RT group (two tailed Student's T-test).

Figure 7.2**Figure 7.2. Thermoneutrality blunts the BAT-specific features of the Drp1 KI mice.**

A cohort of WT and Drp1 KI mice was challenged on a high-fat diet (4 weeks) and housed at thermoneutrality (30°C-33°C) (extra 4 weeks). **(A)** Hematoxylin/eosin staining of BAT from WT and Drp1 KI mice housed at TN (scale bar: 100 μ m). **(B)** Lipid droplet size quantification from histology images in (A), corresponding to 20 independent images per BAT section (n = 4 mice per genotype). **(C-D)** mRNA levels of BAT-specific markers **(C)**, as well as fatty acid oxidation, lipogenesis and ER-stress genes **(D)**, respectively, measured by qPCR. **(E-F)** Respirometry analyses of uncoupled respiration (leak), Complex I respiration (CI), Complex I + Complex II respiration (CI + CII), maximal electron transfer system (ETS) capacity, and maximal Complex II driven respiration (CII) in BAT **(E)** and liver **(F)** homogenates from HFD-fed WT and Drp1 KI mice housed at thermoneutrality. All values are presented as mean \pm SEM of, unless otherwise stated, n=8 mice per group. **, *** indicates statistical difference at p<0.01 and p<0.001, respectively, vs. the corresponding WT group (two tailed Student's T-test).

Figure 7.3**Figure 7.3. Thermoneutrality blunts the improved insulin sensitivity phenotype of the Drp1 KI mice.**

(A) Intraperitoneal glucose tolerance test (ipGTT) performed on HFD-fed WT and Drp1 KI mice housed at thermoneutrality. Mice were fasted for 12 hours prior to the injection of 2 g/kg glucose. (B) Plasma insulin concentration was measured for the indicated times during the glucose tolerance test represented in (A). (C) Intraperitoneal insulin tolerance test (ipITT) performed on HFD-fed WT and Drp1 KI mice housed at thermoneutrality. Mice were fasted for 6 hours after which insulin (1 U/kg) was injected and glycemia was recorded for the timepoints indicated. (D) Glycemia measured prior to sacrifice in animals after 12 hours of fasting. (E-F) Plasma levels of inflammatory cytokines (E) and Fgf21 (F) in HFD-fed WT and Drp1 KI mice housed at thermoneutrality, after a 12 hour fasting (n = 4 mice per genotype). All values are presented as mean \pm SEM of, unless otherwise stated, n=10 mice per group. Linear mixed-effect models were used in (A-C) measuring the time*group interaction effects, subsequent comparisons were performed with Tukey's Honest Significant Difference post-hoc test. Differences between the two groups were analyzed using a Student's two-tailed t-test in (D-F).

Chapter 8. Mitochondrial dynamics in the progression of the epithelial-mesenchymal transition

Cancer cells are well characterized by their ability to rewire their metabolism to support and enable rapid proliferation, continuous growth, survival in harsh conditions and resistance to cancer treatments (Phan *et al.*, 2014). Simultaneous to their metabolic rewiring, cancer cells can also alter their plasticity and motility properties by a process known as the epithelial-mesenchymal transition (EMT). The EMT is a process that occurs early in embryonic development, in which epithelial cells undergo cytoskeletal changes and lose cell-cell contacts to gain mesenchymal traits and increase their motility (Thiery *et al.*, 2009). During carcinogenesis, pathological EMT occurs to promote tumor cell invasion and metastasis (Pearson, 2019). As EMT progresses, transformed cells lose E-cadherin, an adherens junction protein that maintains cell-cell adhesion and epithelial tissue integrity. Cells then disengage from the epithelial layer where they originated, and express mesenchymal markers such as Vimentin and specific transcription factors (e.g. Snail, Slug, Twist). The acquired mesenchymal phenotype is manifested in enhanced migratory activity, invasiveness and resistance to apoptosis (Elisha *et al.*, 2018).

One of the characteristic changes in the metabolic program of cancer cells is the increased uptake of glucose, in order to build the necessary biomass required for proliferation and tumor development (Masin *et al.*, 2014). To do this, tumor cells upregulate the expression of glucose transporters, of which the facilitative glucose transporter (GLUT) family has gained most attention. In recent years, an increasing number of studies identified GLUT3 as one of the main factors in oncogenic glucose uptake and accelerated metabolism (Ancy *et al.*, 2018). Interestingly, the Meylan group described a direct correlation between the induction of the EMT and the increase in the expression of the glucose transporter GLUT3 in non-small cell lung cancer (NSCLC) cell lines (Masin *et al.*, 2014). Transduction of two low-GLUT3 expressing epithelial cell lines (H727 and H2009) with SNAIL or ZEB1 proteins, two known EMT-inducing transcription factors, led to a marked increase of the GLUT3 gene levels (Masin *et al.*, 2014).

Moreover, GLUT3 expression contributed to the proliferation of lung tumor cells and was a prognostic factor of poor overall survival in NSCLC patients (Masin *et al.*, 2014).

Progressing tumors display increased glucose uptake to sustain the high rates of glycolysis, and also to fuel the pentose phosphate pathway (PPP) for nucleic acid synthesis and glutathione reduction (Porporato *et al.*, 2018). Moreover, cancer cells are characterized by the deregulation of redox homeostasis, resulting in abnormally high levels of reactive oxygen species (ROS) and oxidative stress. Consequently, this promotes cellular damage to proteins, lipids and DNA. Particularly, permanent DNA damage, including depurination and depyrimidination, single and double-DNA breaks or base modifications, can trigger a variety of transcription and transduction pathways associated to carcinogenesis and tumor formation. Additionally, tumor cells alter mitochondrial function by modifying their sulfur-based metabolism and NADPH generation to accommodate high ROS levels (Hayes *et al.*, 2020).

Beyond the ability of cancer cells to modify mitochondrial function, tumors alter the balance in mitochondrial dynamics to promote their growth and survival (Anderson *et al.*, 2018). Moreover, there is now evidence linking alterations in mitochondrial morphology to the machinery of tumor cell motility and metastatic spreading (Altieri, 2019). However, there are opposing views on the particular role of mitochondrial fission and fusion in tumor invasiveness and the induction of the EMT. For instance, induction of the EMT in the mammary epithelial cell line MCF12A activates mitochondrial fusion via upregulation of Mfn1, which allows stem cell progeny to enhance reactive oxygen species scavenging capacity to sustain the stem cell pool (Wu *et al.*, 2019). Contrarily, depletion of Mfn1 triggered the EMT in hepatocellular carcinoma patients (HCC), and this was associated with high metastatic capacity and poor prognosis (Zhang *et al.*, 2020). Interestingly, these patients also exhibited increased Drp1 levels (Zhang *et al.*, 2020), in line with previous studies that also demonstrated a Drp1-mediated upregulation of mitochondrial fission in the promotion of breast cancer progression (Sehrawat *et al.*, 2019). Previous studies have also demonstrated that ERK1/2 phosphorylates Drp1 at S579 (as for Drp1 isoform 3, equivalent to S616 in human isoform 1) to promote mitochondrial fission, which then contributes to cell transformation and tumor growth (Kashatus *et al.*, 2015) (Serasinghe *et al.*, 2015). Thus, the abnormal activation of the RAS/MEK/ERK pathway that occurs in many human cancers will highly influence Drp1 function and activity. Indeed, the induction of Drp1 phosphorylation at S579 has been documented in several tumor types, including melanoma (Wieder *et al.*, 2015), lung cancer (Rehman *et al.*, 2012), breast cancer (Zhao *et al.*, 2013) (Han *et al.*, 2015) or pancreatic cancer (Nagdas *et al.*, 2019) (Meng *et al.*, 2019).

Therefore, altered mitochondrial dynamics can broadly impact tumor cell physiology, and vice versa. Using genetic and pharmacological profiling of cancer cell lines and human tumors, Anderson *et al.* (2018) reported that perturbations to the mitochondrial dynamics network also result in specific therapeutic vulnerabilities, which demonstrates that targeting the core proteins in mitochondrial dynamics might facilitate additional cancer therapeutic opportunities.

In light of the observation that mitochondrial morphology is frequently altered upon induction of the EMT, we collaborated with the Meylan's laboratory to evaluate the change in mitochondrial dynamics markers upon induction of the EMT in the H727 human NSCLC cell line. The findings from these experiments will provide novel knowledge on the role of mitochondrial dynamics in the proliferation and metastasis ability of lung tumor cells.

8.1 Mitochondrial dynamics proteins increase upon EMT in a NSCLC cell line

To evaluate the role of mitochondrial dynamics during the epithelial-mesenchymal transition (EMT), we worked with the lung adenocarcinoma epithelial cell line H727, which was originally transduced with lentiviruses to generate cells stably expressing the EMT-transcription factor SNAIL under the control of a doxycycline (DOX) response element. Therefore, we treated the H727-SNAIL cells with DOX, and collected mRNA and protein samples before treatment (day 0), and also after 3 and 6 days post-induction of the EMT. In line with an upregulation of *SNAIL1*, mRNA levels of the epithelial marker *Cdh1* were notably downregulated 3 days post-induction (Figure 8.1A). Accordingly, *VIM* (Vimentin) transcription levels were increased after 3 days of SNAIL expression, and notably more after 6 days (Figure 8.1A), thus indicating an efficient transition from the epithelial to the mesenchymal cellular state. In agreement with the findings from Masin *et al.* (2014), induction of the EMT led to a significant increase in the mRNA levels of the GLUT3 gene, *SLC2A3* (Figure 8.1B). Based on this successful validation of the EMT process on the H727-SNAIL cells, we next aimed to evaluate the alterations in mitochondrial dynamics markers. Overall, we observed an upregulation of the *Dnm1l* and *Mfn2* mRNA levels 3 days and 6-days post-induction, respectively, while the transcription levels of *Mfn1* and *Opa1* were downregulated after 3 days, but notably increased after 6 days of EMT induction (Figure 8.1C).

We next analyzed the protein samples to validate our results at the mRNA level. Protein analyses in three different experimental replicates indicated a significant decrease in E-cadherin expression 3 days after DOX treatment (p value = 0.0005***), where we could not detect any signal by Western Blot analysis (Figure 8.1D and Figure 8.1G). In line with this, Vimentin protein levels were increased, reaching a

maximum signal at 6 days post-induction ($p < 0.0001$ ****) (Figure 8.1D and Figure 8.1G). Despite the increase in SNAIL protein levels, differences in SNAIL expression were appreciable between the three experimental replicates, being the second replicate where the efficiency of SNAIL expression was the lowest (Figure 8.1D and Figure 8.1G). Contrarily to the observations at the mRNA level, we did not detect any change in GLUT3 expression by protein analysis (Figure 8.1E and Figure 8.1G).

Nevertheless, the analysis of the mitochondrial dynamics proteins revealed some interesting findings. On the one hand, Drp1 protein levels were significantly increased after 3 days of EMT induction, but then were decreased to almost-basal levels by day 6 (Figure 8.1F and Figure 8.1G). This gives rise to the notion that intensive mitochondrial fragmentation might be needed only at the initial stage of the EMT. Moreover, the expression levels of Mfn1 were increased after 3 days of EMT induction, and were then maintained until day 6 (Figure 8.1F and Figure 8.1G). The increased expression in Mfn1 upon EMT induction would resemble the research from Wu *et al.* (2019) on mammary cultured cells. Contrarily, we did not observe changes in Mfn2 expression. Despite the fact we did not detect any apparent changes in Opa1 protein levels, especial consideration should be given to the particular case of the Opa1 long (L-Opa1) and short (S-Opa1) forms, respectively. Indeed, Opa1 expresses 8 different isoforms divided by unprocessed long forms or the proteolytically cleaved short forms. Long forms have been demonstrated to promote mitochondrial fusion while short forms have been suggested to facilitate mitochondrial fragmentation (Del Dotto *et al.*, 2017). Western blot results suggest an increase in S-Opa1 by day 3 of EMT induction, though the protein quantifications are not significant possibly due to the variability between replicates.

Finally, we decided to briefly investigate the impact of the EMT on mitochondrial morphology in the H727 cells transiently expressing SNAIL. For this, we collected cells after 4 days of DOX treatment and performed immunostaining with a Drp1 antibody combined with Alexa488 to visualize mitochondria in green. Non-treated cells had a variable morphology, with a mixture of elongated and shortened mitochondrial shapes (Figure 8.1H). However, our mitochondrial staining would require further optimization in order to allow for proper quantifications. Imaging was improved in the samples with DOX treatment, where mitochondria presented a tendency towards increased mitochondrial fragmentation (Figure 8.1H). Due to low resolution of the control images, as well as to the fact that the imaging was only carried out for an $n = 1$, our results should be considered simply indicative.

Therefore, our observations with the H727 cell line are consistent with previous reports suggesting that the induction of the EMT leads to alterations in the mitochondrial architecture and, thus, in the levels of mitochondrial dynamics-related proteins. Nevertheless, further experiments are required to complement these findings.

8.2 Discussion and conclusions

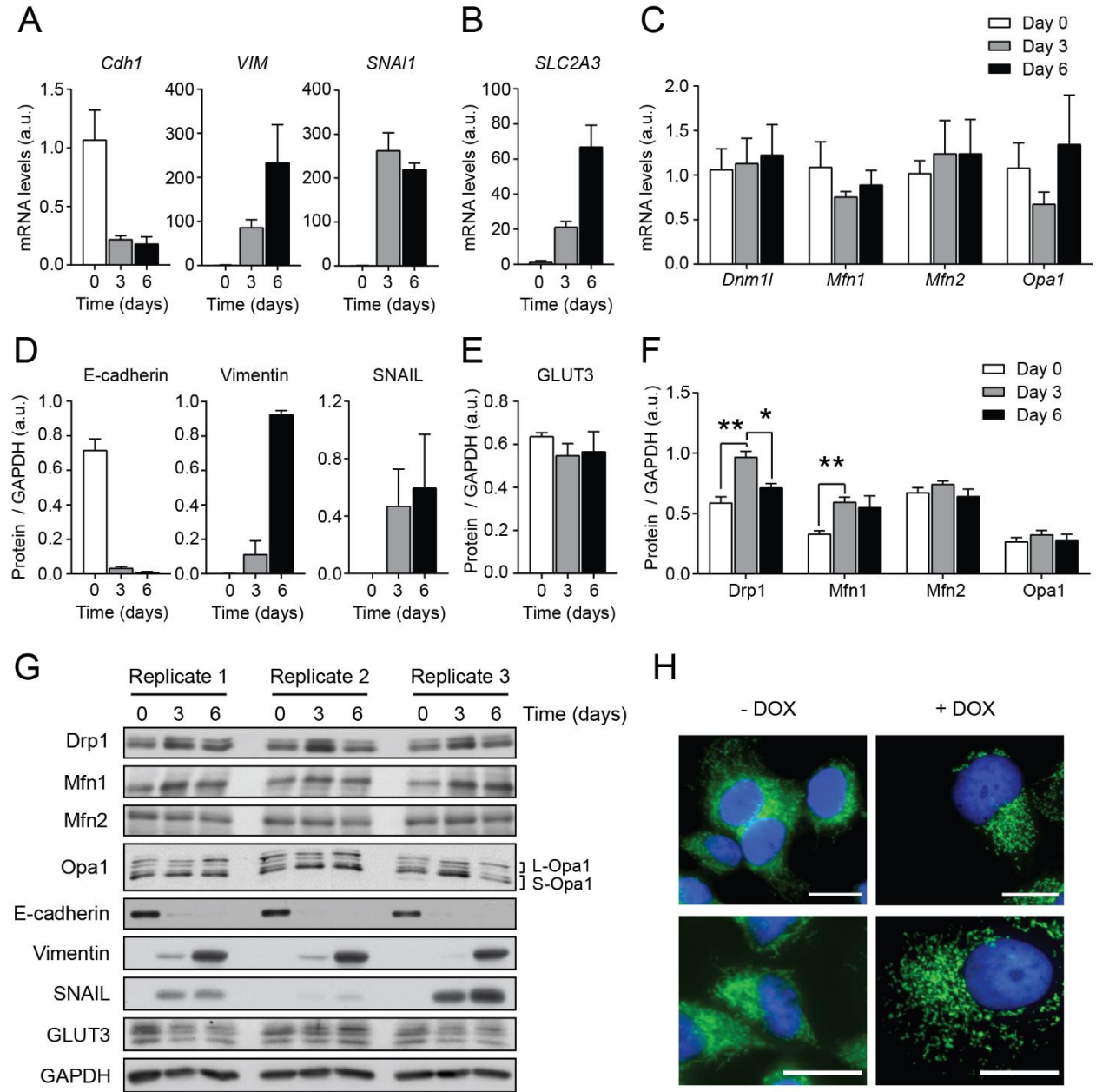
In this Chapter, we performed a series of experiments aimed to analyze the link between the epithelial-mesenchymal transition (EMT), and the components of the mitochondrial dynamics machinery. Previously, the Meylan group identified that the glucose transporter GLUT3 was induced upon EMT on human NSCLC cell lines. This high GLUT3 expression promoted glucose uptake and allowed the proliferation of mesenchymal lung tumor cells in conditions where glucose concentrations were limiting (Masin *et al.*, 2014). Therefore, we aimed to analyze how these changes were correlated to possible alterations in the balance in mitochondrial dynamics.

Overall, our mRNA analyses of mesenchymal and epithelial states indicated that our culture cell model efficiently underwent EMT transition upon doxycycline induction of SNAIL. However, there were some disagreements between the mRNA and protein data on some markers, such as GLUT3 and the mitochondrial dynamics proteins. While *SLC2A3* mRNA levels were increased, GLUT3 protein expression showed no differences throughout the time-course. This could probably be due to the low efficacy of the GLUT3 commercial antibody we used. Alternatively, changes at the mRNA level could be reflected in a low fold-change variation in GLUT3 expression due to different post-translational modification that fine-tune protein regulation. Moreover, Drp1 and Mfn1 exhibited increased protein expression by day 3 post-induction, though this was not reflected on the mRNA data. Similarly, the tendency of Opa1 expression was dubious comparing protein and mRNA data. In this regard, the variability between biological replicates could have contributed to these disparities. Thus, these results are merely indicative and should be reproduced in following experiments.

At the protein level, the progression to the mesenchymal phenotype resulted in an upregulation of Drp1 expression by day 3, which significantly decreased by day 6. One possible explanation is that the initial increase in mitochondrial fragmentation could aid in the distribution of mitochondria to the increasingly proliferating lung tumor cells. After this, the higher glucose uptake could be facilitated by the increase in Mfn1-mediated mitochondrial fusion, in order to promote ATP production via oxidative phosphorylation. Indeed, mitochondrial elongation facilitates cristae formation and assembly of respiratory complexes to

enhance oxidative phosphorylation (Li *et al.*, 2017) (Gomes *et al.*, 2011). This proved to be essential for tumor cell survival both *in vitro* and *in vivo* and predicted poor prognosis of hepatocellular carcinoma patients (Li *et al.*, 2017). Nevertheless, we would need to validate this data with further experimental approaches.

In conclusion, we propose a correlation between mitochondrial morphology and the EMT process, which complements the previous research by the Meylan group on the relationship between glucose metabolism and the EMT. These findings suggest that the EMT could modify mitochondrial function by direct alterations in the mitochondrial fission/fusion balance, and provide novel insights for the development of targeted therapies for the treatment of patients with NSCLC.

Figure 8.1**Figure 8.1. Mitochondrial dynamics upon EMT in a H727 transformed cell line.**

The H727 lung adenocarcinoma cell line was differentiated from the epithelial to the mesenchymal phenotype by treatment with Doxycycline (2 $\mu\text{g}/\text{mL}$), which activated the expression of the recombinant vector coding for the SNAIL EMT-induction factor. Trizol extraction was performed to obtain the RNA samples, while cells were lysed with RIPA buffer for protein homogenates, at day 0, and after 3 and 6 days, respectively. **(A)** mRNA levels of the epithelial marker *Cdh1*, as well as the mesenchymal markers Vimentin (*VIM*) and SNAIL (*SNAIL*) were analyzed by qPCR. **(B-C)** mRNA levels of GLUT3 gene (*SLC2A3*) **(B)** and mitochondrial dynamics components **(C)** were also measured by qPCR.

(D-F) Quantification of the protein levels for the EMT differentiation factors **(D)**, as well as GLUT3 **(E)** and mitochondrial dynamics **(F)** markers represented by Western Blot in (G) normalized to GAPDH. **(G)** EMT markers, GLUT3 and mitochondrial dynamics proteins were evaluated by analyzing protein levels in three different biological replicates at the timepoints indicated. Opa1 long (L-Opa1) and short (S-Opa1) forms are represented in the blot. **(H)** Immunostaining of H727 cells without (-DOX) and with (+DOX) Doxycycline treatment for two different sets of images. Under the microscope, the cells at (-DOX) formed groups, while at (+DOX) were placed in an isolated manner. The nucleus is stained in DAPI, and the mitochondria in Tom20 and Alexa488 (scale bar: 10 μ m). All values are presented as mean \pm SEM. * $p < 0.05$, ** $p < 0.01$ (two-tailed Student's t-test) statistically significant differences between the indicated groups.

Chapter 9. General discussion and future perspectives

Mitochondrial dynamics has emerged as a key factor in modulating cellular metabolism, including bioenergetics, macromolecular biosynthesis, nutrient catabolism or redox homeostasis. Importantly, mitochondrial dynamics maintains the balance between health and disease at the cellular and organismal level. Altered mitochondrial architecture is a feature of multiple human pathologies, as in the case of obesity, type 1 and 2 diabetes or Parkinson's and Alzheimer's disease. Considering that excessive mitochondrial fission has been implicated in the development and progression of these disorders, it is possible to envision the utility of the fission machinery, particularly Drp1, for the development of therapeutic strategies.

Drp1 function is highly dependent on the phosphorylation at specific sites, which are responsible for Drp1 activation and mitochondrial fission. Nevertheless, the interaction and co-regulation of the two main phosphorylation sites of Drp1 (i.e. S579 and S600) has never been clearly addressed. Moreover, the physiological events that influence Drp1 phosphorylation *in vivo* remain largely unknown, including how the regulation of these phosphorylations might impact metabolic and age-related pathologies.

In this work, we have provided novel insights on two different aspects of Drp1 function and, therefore, the regulation of mitochondrial fission. First, we identified a novel crosstalk relationship between Drp1 S579 and S600 phosphorylation sites, and defined how this crosstalk remodels mitochondrial shape. Second, we characterized the novel Drp1 S600A knock-in (KI) mouse model by performing a thorough phenotyping to elucidate the role of the Drp1 S600 phosphorylation in metabolic homeostasis and mitochondrial function.

9.1 Crosstalk of Drp1 phosphorylation sites

Despite the central role of Drp1 phosphorylations on regulating its function, describing the effect of Drp1 S600 phosphorylation on mitochondrial morphology has been controversial. While some reports suggested that the phosphorylation at Drp1 S600 by ROCK1 or the Ca^{2+} /calmodulin-dependent protein kinase I α (CaMKI α) promotes mitochondrial fission (Wang *et al.*, 2012b) (Han *et al.*, 2008), other studies have proposed that the phosphorylation at this same site, for instance by PKA, leads to decreased recruitment of Drp1 to mitochondria, resulting in unopposed mitochondrial fusion (Cribbs & Strack, 2007) (Chang & Blackstone, 2007). In this work, we decided to address these seemingly opposing views, and tried to elucidate the interplay between the two phosphorylations on Drp1 function.

We first demonstrated that the phosphorylation of S579 is a downstream consequence of S600 activation. Several observations point out to this direction. First, our experiments in MEF cells demonstrate that S579 phosphorylation was increased with the phospho-mimetic Drp1 S600E and Drp1 S600D forms, respectively, in the absence of cAMP stimulation. Second, the phosphorylation at the S579 site was highly upregulated in mouse tissues after pharmacological PKA activation. Similarly, physiological stimuli raising intracellular cAMP, such as fasting or a cold challenge, led to the simultaneous increase in Drp1 S579 and S600 phosphorylations in muscle and brown adipose tissue, respectively. The fact that S579 phosphorylation was blunted in the Drp1 KI mice after pharmacological PKA activation suggests that the downstream S579 phosphorylation event is dependent of the prior S600 phosphorylation rather than PKA activation. These observations go in line with previous reports demonstrating that PKA fails to phosphorylate the S579 residue in *in vitro* assays (Cribbs & Strack, 2007) (Chang & Blackstone, 2007).

So, how does S600 influence S579 phosphorylation? Our observations suggest that S600 phosphorylation protects against S579 dephosphorylation. In line with the literature linking Cdk1/cyclin B with the Drp1 S579 site (Taguchi *et al.*, 2007), inhibiting cell cycle-dependent Cdk1 activity led to a decay of Drp1 S579 phosphorylation. In contrast, Drp1 P-S579 levels were highly sustained when Drp1KO cells were transfected with Drp1 S600E. This was not directly linked to Cdk1, since we did not observe changes in Cdk1 activity when cells were transfected with our phospho-mimetic Drp1 S600 forms. One possible explanation is that S600 activation induces a conformational change on Drp1 that blocks the access of a phosphatase that decreases P-S579 levels or, contrarily, that allows the access of S579 to a constitutively active kinase. Similar cases are known in the literature. For example, 5'-AMP binding to AMP-activated protein kinase (AMPK) promotes a conformational change that blocks the access of phosphatases, leading to an overall increase in its phosphorylation and activity (Woods *et al.*, 2003). In this sense, it is often

overseen that multiple proteins undergo a constant cycle of active phosphorylation/dephosphorylation and that the overall balance can be determined by changes in either phosphorylation rates, dephosphorylation rates, or both.

One striking feature we observed in this work was the seemingly contradictory results in cultured cells compared to mouse tissues regarding the potential crosstalk of S600 and S579. While Drp1 phospho-S600 and phospho-S579 were inversely correlated upon cAMP activation in MEF cells, they occurred simultaneously *in vivo*. However, it is essential to keep in mind that most cultured systems derive from immortalized cell lines or tumors. Given that S579 phosphorylation is heavily influenced by the cell cycle, this residue might be highly phosphorylated in the basal state in immortalized cultured cells, as compared to differentiated tissues. Similarly, most drugs aimed to increase intracellular cAMP levels and activate PKA act as potent cell cycle inhibitors in cultured cells (Chen *et al.*, 1998). Accordingly, Forskolin was found to decrease proliferation in A172 cells and induced transient dephosphorylation of phospho-Rb, substrate of Cdk1, in human Reh cells (Chen *et al.*, 1998) (Gütschow *et al.*, 2002). Thus, the reduced levels of Drp1 phospho-S579 observed in our Drp1 overexpressing MEFs treated with Forskolin could be explained from the inhibition of Cdk activity caused by Forskolin. Given the high basal Cdk activity in immortalized MEFs, the decrease in Cdk activity prompted by Forskolin can probably mask and override the effects of S600 phosphorylation on the accessibility of phosphatase and kinase enzymes. Supporting this view, when instead of Forskolin we used a phospho-mimetic S600E or S600D form, which do not alter Cdk activity, we consistently observed an increase in S579 phosphorylation. Finally, differentiated tissues also harbor much less Cdk activity than immortalized MEFs, allowing to unveil the impact of S600 phosphorylation on S579. All in all, careful considerations should be taken when comparing observations on the regulation of Drp1 S579 phosphorylation between immortalized cell lines and differentiated tissues.

Paradoxical views exist on the functional outcome of the S600 phosphorylation on mitochondrial morphology. Our results support that S600 phosphorylation favors mitochondrial fission, testified by experiments with the Drp1 S600 phospho-mimetic mutant in cultured cells and the tendency towards mitochondrial tubulation in the BAT from our Drp1 S600A KI mice. This goes in line with the elongated mitochondrial network of podocytes from a parallel Drp1 S600 KI mouse model (Galvan *et al.*, 2019), or the increased mitochondrial fragmentation upon Drp1 S600 phosphorylation in brown adipocytes from mice exposed to cold temperatures (Wikstrom *et al.*, 2014), which overall supports a pro-fission role of Drp1 S600 phosphorylation. Similarly, Drp1 S600 phosphorylation has been reported to induce mitochondrial fission in human podocytes and endothelial cells (Wang *et al.*, 2012b). Contrarily,

phosphorylation of the same site led to mitochondrial fusion in cardiomyocytes and vascular smooth muscle cells (Zaja *et al.*, 2014). Of particular interest is the case of neurons, where Drp1 phosphorylation at S600 by CaMKI α induces mitochondrial fission (Han *et al.*, 2008), whereas the phosphorylation at the same site by PKA/AKAP1 increases mitochondrial length (Dickey & Strack, 2011). Therefore, the effects of S600 phosphorylation could be highly cell-type and/or stimulus specific. These specific effects could be based on the expression of the different Drp1 isoforms. Indeed, mammalian cells express 9 distinct isoforms of Drp1 that arise from the alternative splicing of its single gene-encoded pre-mRNA transcript (Macdonald *et al.*, 2016) (Rosdah *et al.*, 2020). These Drp1 isoforms differ in their tissue abundance (Strack *et al.*, 2013), their ability to engage into mitochondrial fission (Macdonald *et al.*, 2016) and their subcellular localization (Itoh *et al.*, 2018) (Strack *et al.*, 2013). For example, the mouse Drp1 long isoform 1 (comprising 742 amino acids) is highly enriched in neurons, and its recruitment to mitochondria is highly dependent on the mitochondrial receptor mitochondrial fission factor (Mff) and cardiolipin abundance (Macdonald *et al.*, 2016). Contrarily, the shorter isoform 3 (only ranging 699 aa) is expressed ubiquitously, and is able to perform substantial mitochondrial fission in the absence of Mff (Macdonald *et al.*, 2016). Since our work is based on tissues such as BAT, liver or muscle, we would be mainly describing Drp1 mouse isoform 3. Nevertheless, previous studies relating Drp1 S600 phosphorylation with mitochondrial elongation focused on the neuron-specific isoform 1 (Cereghetti *et al.*, 2008) (Flippo & Strack, 2017).

Importantly, the impact of Drp1 S600 phosphorylation on mitochondrial morphology depends on the capacity to promote downstream S579 phosphorylation (Figure 9.1). In the impossibility of S579 activation, S600 phosphorylation leads to mitochondrial elongation, as demonstrated in our imaging experiments using the Drp1 S600E/S579A form. This, in turn, could explain some of the discrepancies in the literature, suggesting that, in addition to isoform-specific differences, the different outputs of S600 phosphorylation could be linked to the basal S579 phosphorylation state of the cell lines tested. Altogether, these observations suggest that Drp1 S600 would act as the activator site while S579 is the effector in promoting mitochondrial fragmentation (Figure 9.1).

In conclusion, in this first part of our work we provide novel insights on the crosstalk between Drp1 phosphorylations. Until now, the vast majority of research documenting Drp1 S579 and S600 phosphorylations was based on cultured cell lines, which do not mimic the physiological conditions involving the intervention of multiple organs. In higher models such as rodents or humans, only one of these phosphorylations is reported in most of the cases. For example, increased Drp1 S579 phosphorylation levels have been documented in various human cancers (Breitzig *et al.*, 2018). Thus, it

would be highly interesting to analyze whether tumor samples from patients display enhanced Drp1 S600 phosphorylation in parallel to that of S579. Of note, our observations that Drp1 S579 phosphorylation is dependent on the prior S600 activation provide an attractive therapeutic strategy where the Drp1 S600 site could be targeted in human cancer. We also provide a plausible explanation on the contradictory views on whether the Drp1 S600 site promotes mitochondrial fragmentation or elongation, which has been a subject of debate over the last decades in the exploration of Drp1 function.

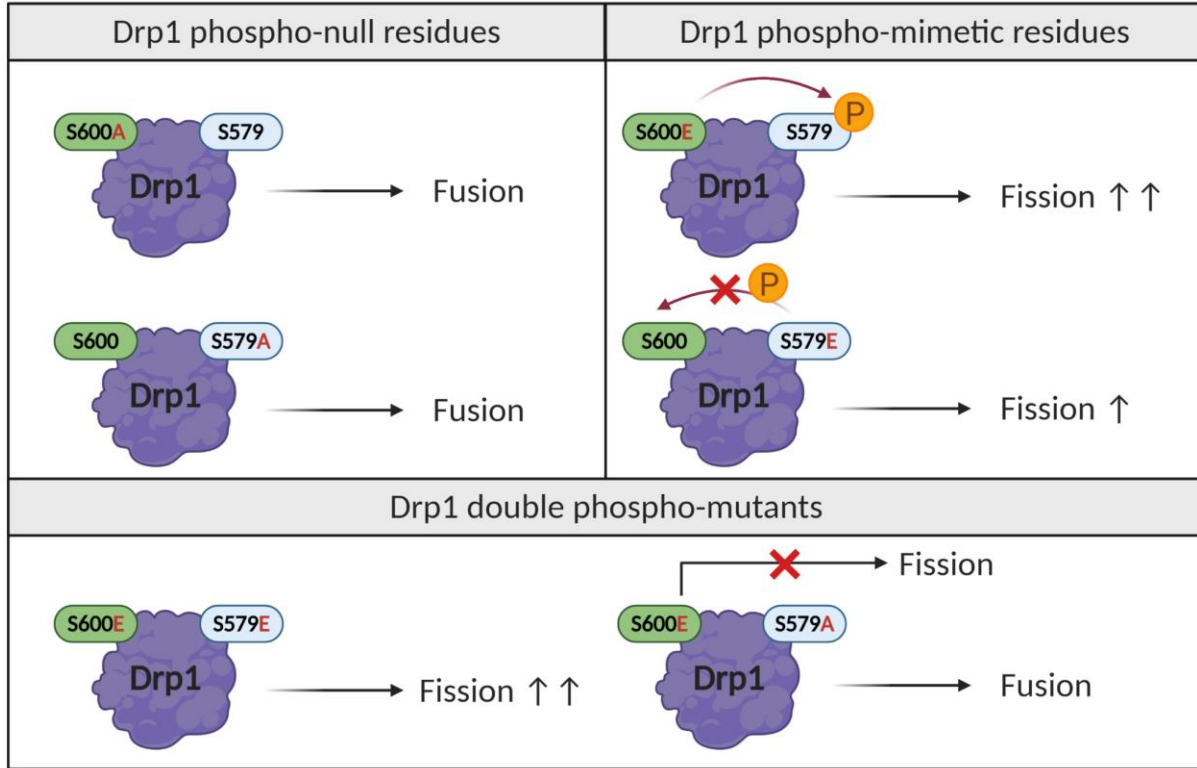


Figure 9.1. Crosstalk between Drp1 S579 and Drp1 S600 phosphorylation sites.

Our studies with phospho-null plasmids demonstrated that when Drp1 is prevented from being phosphorylated by mutating the Serine residues to Alanine (S→A) at either S600 or S579, the mitochondrial network exhibits a prevalence on mitochondrial tubulation (fusion). Contrarily, the change from Serine to Glutamate (S→E) mimics a constitutive phosphorylation of the site. Activation of the S600 site promotes the phosphorylation at Drp1 S579, even in the absence of stimuli. Cells expressing the Drp1 S600E form showed a marked increase in mitochondrial fragmentation (fission). Contrarily, cells expressing the Drp1 S579E form did not exhibit increased levels of phosphorylated Drp1 S600. Nevertheless, Drp1 S579E promoted mitochondrial fission, although to a lesser extent to that observed with the Drp1 S600E form. A double Drp1 S600E/S579E phospho-mutant led to maximal levels of mitochondrial fragmentation. The double Drp1 S600E/ S579A mutant displayed mitochondrial fusion, indicating that the Drp1 S600 site is not able to bypass the inhibition of the S579 site to promote fragmentation.

9.2 Role of the Drp1 S600 phosphorylation in mammalian physiology

As a key component in mitochondrial quality control, Drp1 is also critically important for organismal homeostasis and survival. Indeed, mutations that impair Drp1 function have been implicated in human encephalopathies and developmental regression (Waterham *et al.*, 2007) (Fahrner *et al.*, 2016). Moreover, the homozygote deletion of the *Dnm1* gene in mice is embryonically lethal, due to deficient synaptic formations that result in brain hypoplasia (Ishihara *et al.*, 2009) (Wakabayashi *et al.*, 2009). Therefore, the vast majority of research on Drp1 function relies on its tissue-specific deletion (Favaro *et al.*, 2019) (Wang *et al.*, 2015), which fails to reflect the impact of mutations or treatments influencing Drp1 function in different tissues. Despite the fact that it is well documented that Drp1 function is influenced by phosphorylations, the physiological impact of the Drp1 phosphorylation sites remains yet unknown.

Therefore, we decided to address these issues in the second part of this work by characterizing our Drp1 S600A knock-in (KI) mice. This is a whole-body genetic mouse model that codes for a recombinant protein harbouring a site-specific serine (S) to alanine (A) mutation at S600, therefore preventing the addition of the phosphate group and mimicking a constitutive dephosphorylation of this site. To date, there is no other literature describing this model, with the exception of the report by the Danesh group, who used a parallel Drp1 S600A KI mouse model to elucidate the role of the ROCK1-Drp1 axis specifically in kidney function (Galvan *et al.*, 2019). Contrarily, our strategy with the Drp1 KI extends to portray the impact of the Drp1 phosphorylation crosstalk on mitochondrial dynamics, as well as to define the role of the Drp1 S600 phosphorylation in whole-body metabolic adaptation.

Interestingly, one of our first observations was that kidney exhibits almost absent levels of Drp1 protein expression, as compared to high-expressing Drp1 tissues such as brain, heart or muscle. Moreover, white adipose tissue displays poor Drp1 expression, as compared to the brown adipose tissue. This reflects of the requirement for a proper balance in mitochondrial dynamics particularly in brown as opposite to white adipocytes, in order to preserve BAT function. The impact of the Drp1 S600 mutation will thus be determined by the basal levels of Drp1 expression on different tissues.

We metabolically characterized our Drp1 S600A KI mice under a low-fat diet (LFD) and high-fat diet (HFD) challenge, respectively. Drp1 KI mice on a LFD did not manifest any changes in glucose or insulin handling, yet they exhibited a tendency towards increased lipid utilization as energy source, according to indirect calorimetry analyses. Moreover, we showed that Drp1 KI tissues, such as the liver or the BAT, displayed higher Complex I and Complex II-driven mitochondrial respiration. Regarding this, mitochondrial

elongation has been previously linked to higher respiratory capacity and improved respiratory coupling in cultured cells and tissues (Gomes *et al.*, 2011) (Liesa & Shirihai, 2013). Importantly, improved mitochondrial function strongly correlates with protection against diet-induced metabolic disease (Cantó, 2018). Accordingly, our Drp1 KI mice were protected against HFD-induced glucose intolerance and insulin resistance. Drp1 KI mice also maintained better their body temperature upon cold exposure, which was related to a higher BAT thermogenic capacity. Importantly, it has been highlighted how changes in BAT activity can significantly influence whole-body metabolic homeostasis (Chouchani & Kajimura, 2019). Recent preclinical investigations have even reported that increased BAT mass and/or activity through transplantation can improve glucose metabolism and insulin sensitivity in recipients (White *et al.*, 2019). Therefore, the higher glucose utilization in the Drp1 KI mice might be used to sustain the increased thermogenic function of their BAT.

Finally, we showed that the contribution of the BAT was critical for the better insulin sensitivity of our HFD-fed Drp1 KI mice (Figure 9.2). Mainly, housing the Drp1 KI mice at thermoneutrality, which blunted the thermogenic capacity of the BAT, completely neutralized their increased glucose tolerance and insulin sensitivity, as well as the enhanced lipid oxidation rates and mitochondrial respiration of their BAT. Interestingly, the profile of adipokines that was upregulated in the Drp1 KI mice under normal housing conditions, including the marker of mitochondrial function Fgf21, was also blunted at thermoneutrality. This observation gives rise to the notion that the molecular mechanism explaining the phenotype of the Drp1 KI mice lies probably on their enhanced adrenergic signaling. Given the role of the energy sensor AMPK in modulating thermogenesis in adipose tissue, it is possible that the improved insulin sensitivity of the Drp1 KI mice is due to the increased activation of AMPK in BAT. Indeed, adipose tissue-specific AMPK KO mice fed on a HFD exhibited impaired glucose tolerance and insulin sensitivity, and also reduced β 3-adrenergic-activated energy expenditure (Wu *et al.*, 2018), in alignment to our observations in the Drp1 KI mice. Moreover, PGC1 α is a critical regulator of UCP1-mediated thermogenesis in BAT (Sharma *et al.*, 2014). Indeed, UCP1 and PGC1 α transcription levels were upregulated in the Drp1 KI BAT. Thus, the impact of adiposity and glucose homeostasis on PGC1 α expression could be an interesting venue explaining the metabolic adaptations of the Drp1 KI mice, though further research will be required to elucidate whether this is a direct or indirect cause for the Drp1 KI phenotype.

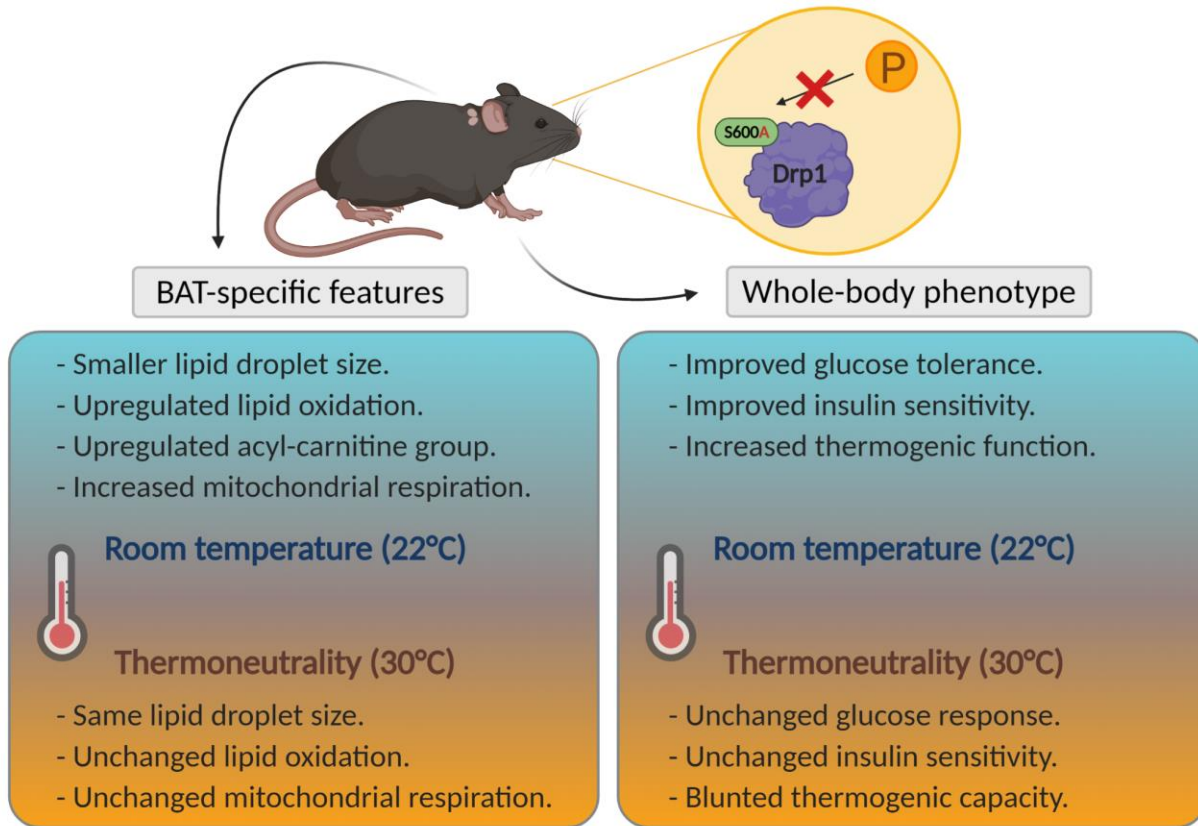


Figure 9.2. Phenotype of the Drp1 S600A KI mice.

Our Drp1 S600A KI mouse model contains a site-specific serine (S) to alanine (A) mutation at S600, therefore preventing the addition of the phosphate group and mimicking a constitutive dephosphorylation of the site. The Drp1 KI mice display a set of characteristics specific to their brown adipose tissue (BAT-specific features), which influence the whole-body phenotype. These features are dependent on the environmental temperature at which the mice have been housed. At normal room temperature (22°C), the BAT of the Drp1 KI mice displays smaller lipid droplet size, associated to an increase in lipid oxidation and mobilization enzymes, elevated levels of acyl-carnitines, as well as enhanced mitochondrial respiration. At the whole-body level, Drp1 KI mice exhibit improved glucose tolerance and insulin sensitivity, as well as increased thermogenic function. However, all these BAT-specific and systemic features, respectively, are completely blunted when the mice are housed at thermoneutrality (30°C).

9.3 Mitochondria & Co.

Mitochondria continuously communicate with other cellular organelles to carry out their function, exchanging material and transmitting signals responsible for regulating metabolism, intracellular signaling and preserve cellular homeostasis (Murley & Nunnari, 2016). This communication can be established in different ways, such as vesicular transport, the exchange of metabolites or signaling molecules or directly,

via physical contacts (Soto-Herederro *et al.*, 2017). The most studied membrane contact sites are those between mitochondria and the endoplasmic reticulum (ER), termed mitochondria-associated membranes (MAMs), which also regulate the events in mitochondrial dynamics (Friedman *et al.*, 2011). MAMs regulate the exchange between both organelles of lipids, calcium, and reactive oxygen species (ROS), allowing adaptations of cellular bioenergetics and cell fate depending of cellular needs or physiological stresses. In our model, the BAT of HFD-fed Drp1 KI mice displayed upregulated levels of the ER stress markers, testifying for the increase in the unfolded protein response (UPR). In agreement, increased ER-mitochondria coupling was shown to promote mitochondrial respiration and bioenergetics during early phases of ER stress (Bravo *et al.*, 2011). This observation would go in line with the higher mitochondrial respiration observed in the BAT of the Drp1 KI mice.

Although the UPR was originally described to maintain the protein homeostasis in the ER, a number of studies suggest that the UPR also play crucial roles in lipogenesis and the regulation of lipid metabolism. For example, ablation of ATF4 in mouse liver attenuates hepatic steatosis caused by high caloric diets through the inhibition of SREBP1c, ACC and FAS (Li *et al.*, 2011) (Xiao *et al.*, 2013). Similarly, ER stress modulates the expression levels of enzymes involved in lipid synthesis in peripheral tissues such as skeletal muscle, pancreas and heart (see reviews by Han & Kaufman (2016) and Basseri & Austin (2012) for more information on this topic). In our system, the levels of the lipogenesis enzymes ACC1, ACC2 or SREBP1c and SREBP2, were specifically upregulated in the BAT of the Drp1 KI mice, in agreement with the higher expression of the UPR markers in this tissue.

Notably, a direct role of ER-mitochondria contact sites in the control of insulin signaling pathway has been recently suggested, supporting the role of MAMs in the control of glucose homeostasis (Rieusset, 2018). Indeed, several proteins of the insulin signaling pathway locate in the MAM interface, including the protein kinase AKT, the protein phosphatase 2A (PP2A) or the mammalian target of rapamycin complex 2 (mTORC2). Insulin signaling was demonstrated to stimulate the localization of mTORC2 to MAMs (Betz *et al.*, 2013). Accordingly, mouse fibroblasts deficient in AKT or mTORC2 exhibited impaired mitochondrial function, associated to a reduction in ER-mitochondrial contacts (Betz *et al.*, 2013). Thus, it would be interesting to analyze the contribution of the mitochondria-ER communication in the phenotype of our Drp1 KI mice.

Mitochondria also communicate with peroxisomes to monitor the degradation of fatty acids and ROS detoxification (Lismont *et al.*, 2015) (Schrader & Yoon, 2007). Remarkably, peroxisomes and mitochondria also share components of the fission machinery, including Drp1 (Koch *et al.*, 2003) (Li & Gould, 2003).

Indeed, expression of a dominant-negative Drp1 mutant deficient in GTP hydrolysis inhibited peroxisomal fission and caused peroxisomal tubulation (Koch *et al.*, 2003). Recently Tanaka *et al.* (2019) showed that the genetic ablation of the peroxisomal factors *Pex3* or *Pex5*, which are essential for peroxisome biogenesis, resulted in mitochondrial fragmentation in MEF cells. In fact, *Pex3* KO MEFs displayed increased colocalization of Drp1 with mitochondria due to an increase in Mff expression. Nevertheless, we did not observe any apparent alterations in *Pex3* or *Pex5* protein expression in the BAT of our Drp1 KI mice, suggesting that the Drp1 S600 phosphorylation does not affect peroxisomal biogenesis. Alternatively, further analysis by electron microscopy of the peroxisomal morphology in the Drp1 KI tissues could complement these results. Of note, experiments in 293T cells overexpressing the Drp1 S600A form showed no differences in peroxisome morphology as compared to Drp1 WT expressing cells, endorsing that the Drp1 S600 phosphorylation status does not play a major role in regulating the activity of Drp1-mediated peroxisomal fission (Yu *et al.*, 2019b). One possible explanation is that peroxisomal fission is independent of Drp1 phosphorylation, but rather relies on an alternative post-translational modification. Despite the large number of studies describing the role of post-translational modifications in regulating Drp1 function in mitochondrial dynamics, how these events affect Drp1 role in peroxisomal dynamics is yet unknown (Brocard & Hartig, 2014). Beyond Drp1, mitochondria and peroxisomes also share the receptors Fis1 and Mff for the regulation of their fission (Schrader, 2006) (Kobayashi *et al.*, 2007) (Delille *et al.*, 2009) (Camões *et al.*, 2009). Despite of this, our Drp1 KI mice did not display any changes in the protein expression of Mff or Fis1.

9.4 Future perspectives

The functional regulation of Drp1 by post-translational modifications clearly provide cells with an impressive array of regulatory mechanisms to modulate mitochondrial morphology. Despite the fact that we focused this work on Drp1 phosphorylation on the S579 and S600 sites, further research will be required to elucidate the interrelation of these phosphorylations with other Drp1 post-translational modifications, including ubiquitination, SUMOylation, S-nitrosylation, O-GlcNAcylation or acetylation (see Chapter 1, section 1.5.3). For instance, Drp1 acetylation at K642 promotes Drp1 phosphorylation at S579, which leads to Drp1 translocation to mitochondria (Hu *et al.*, 2020). Interestingly, K642 is located within the GTPase effector domain, which regulates Drp1 oligomerization and GTPase activity. Our work has established a spatiotemporal relationship whereby a post-translational modification at one site would regulate the modification of a second site to promote Drp1 function. In this sense, Drp1 acetylation might

also be an early event in Drp1 activation, triggering a conformational change that facilitates Drp1 phosphorylation at S579.

On an additional layer, further experiments will help to evaluate to what extent the Drp1 KI phenotypes are a result of the increased mitochondrial elongation, disrupted inter-organelle contacts or more intrinsic aspects of Drp1 biology. Nevertheless, our studies have identified the BAT as one of the main tissues whose function is altered by the Drp1 S600A mutation.

Despite the fact that the impaired thermogenic function of the BAT led to an ablation of the phenotype of the Drp1 KI mice, further experiments should be performed to determine the contribution of the BAT to the overall improvement in glucose tolerance observed in these animals. To do this, one possible approach would be to perform a hyperinsulinemic-euglycemic clamp, in order to define the actual site of glucose uptake in the Drp1 KI mice. Alternatively, the analysis of insulin signaling cues in different tissues could help define if the improved insulin sensitivity of the Drp1 KI mice is due to higher insulin-dependent glucose uptake. Moreover, the generation of a tissue-specific KI mutation in BAT would provide proof that the elimination of the Drp1 KI phenotype observed under thermoneutral conditions is not mediated by ambient temperature, but is specific to the BAT.

Ultimately, the relevance in humans of the findings presented in this work should be further investigated. Several reports have made exceptional effort in highlighting the implications of Drp1 phosphorylations in human metabolic disorders (Fealy *et al.*, 2014) (Pfluger *et al.*, 2015), cancer (Kashatus *et al.*, 2015) (Dai & Jiang, 2019), cardiac pathologies (Chang *et al.*, 2013) (Xu *et al.*, 2016) (Jhun *et al.*, 2018), neurodegenerative disorders (Manczak *et al.*, 2011) (Joshi *et al.*, 2017) (Oliver & Reddy, 2019) or aging (Sharma *et al.*, 2019) (Liu *et al.*, 2020b). Whereas inhibiting Drp1-mediated mitochondrial fission has been proposed as a desirable therapeutic option for targeting cytoprotection, most Drp1 inhibitors to date show inhibitory effects independent of Drp1 activity (Smith & Gallo, 2017) (Dai *et al.*, 2020). This might partially be explained by the differential effect of these inhibitors on Drp1 isoforms specific to particular cell types or tissues. Since the two Drp1 S579 and S600 phospho-sites are conserved among all Drp1 isoforms (Rosdah *et al.*, 2020), targeting Drp1 phosphorylation might overcome the off-target effects associated to the pharmacological Drp1 inhibition strategies.

Altogether, this work unveils the regulation of Drp1 S579/S600 phosphorylation sites and demonstrates that S600 phosphorylation influences whole body nutrient utilization. Therefore, these findings pave the

way for therapeutic approaches where modulating Drp1 function by targeting its phosphorylations could improve human pathophysiological states.

Chapter 10. Materials & Methods

10.1 Materials

All chemicals and reagents used are listed in *Annex 1. Table of materials*. Working concentrations and time of treatment are indicated within the corresponding experiment.

10.2 Plasmid generation

The plasmids used in the manuscript have been generated from the pcDNA3.1(+) Drp1 plasmid kindly gifted by David Chan. The introduction of a FLAG tag to the Drp1 product was achieved through regular cloning molecular biology methods using KOD polymerase (Merck). The resulting PCR products were digested with Bamh1-Not1 or Bgl2-Not1 and ligated into a pcDNA3.1 vector (V79020), in which the Not1 site was in frame with the coding regions to provide a C-terminal Flag tag on the proteins. Additionally, plasmids with point mutations were created by PCR site-directed mutagenesis to generate enzymatically inactive (S → A) or active (S→E/D) versions with the primers indicated in *Annex 2. Primers for site-directed mutagenesis*. The mito-DsRed plasmid was kindly gifted by the Antonio Zorzano group (Liesa *et al.*, 2008) and was cloned from pWPXL-mt-DsRed. The generation of Drp1 mito-DsRed bicistronic plasmids was achieved in two steps: first, the introduction of the mito-DsRed plasmid into the multiple cloning site 1 (MCS1) of the pViro2 plasmid by digestion with BamH1-Xho1 or BamH1-Sal1, respectively; second, the mouse Drp1 – Flag plasmids obtained by site-directed mutagenesis were ligated into the multiple cloning site 2 (MCS2) of the resulting pViro2-mtDsRed plasmid by digestion with BamH1-Xho and Bgl2-Xho1, respectively. Plasmid purification was done using NucleoSpin columns and following the manufacturer's instructions. The sequences of all the clones have been verified in-house using the BigDye Terminator 3.1 kit and 3500XL Genetic analyzer (Applied Biosystems). The primers used for site directed mutagenesis can be found in *Annex 2. Primers for site-directed mutagenesis*.

10.3 Cell culture

Drp1KO MEFs and their WT counterparts were kindly provided by Prof. Katsuyoshi Mihara. The 3T3 line comes from ATCC. All lines were tested for mycoplasma contamination using MycoProbe™ Mycoplasma Detection Kit (R&D cat. CUL001B). Unless otherwise specified, all cell culture reagents were obtained from Gibco (ThermoFisher Scientific Inc.). Cells were cultured in DMEM (4.5 g/L glucose) supplemented with 10% FBS, Penstrep (1%), nonessential amino acids (1%), sodium pyruvate (1%), and L-glutamine (1%). For overexpression experiments, cells were transfected with 5 µg of plasmid DNA using Lipofectamine 2000 (Thermo Fisher) according to manufacturer's instructions. Alternatively, the JetPrime transfection was applied with 2 µg of DNA, according to manufacturer's instructions. Treatments and subsequent collection of cell protein lysates were performed 48 hours post-transfection.

10.4 Live imaging

For the imaging of the Drp1 phospho-mutant plasmids, 8×10^3 Drp1KO cells were seeded in 4-well Lab-Tek™ chambers (ThermoFisher Scientific Inc.) and, after 24 hours, transfected using 0.8 µg of DNA and 2 µL of Lipofectamine 2000 with plasmids expressing the different forms of Drp1 and, bicistronically, a mitochondrially targeted mito-DsRed protein. 24 hours after the transfection, cells were imaged using a Zeiss AxioObserver Z1 confocal spinning-disk microscope coupled to a CO₂ station. Approximately 50 different cells were imaged in at least three different biological replicates, and the orthogonal projection of each cell was taken as the final imaging result. For the starvation conditions, cells were incubated with Hank's balanced salt solution (HBSS) media for 2 h prior to imaging. Nuclei were stained with Hoechst 33342 by treating cells with 1:2,000 dilution in PBS for 10 min. Mitochondrial elongation/fragmentation rates were analyzed using the Mitochondrial Network Analysis (MiNA) macro of Fiji (Valente *et al.*, 2017). For the analysis of the mitochondrial morphology from each cell, we used a pre-processing step with the following parameters: unsharp mask (radius: 1 pixel; mask weight: 0.6), CLAHE (127, 256, 3) and median (1). The parameters of the MiNA interface were the following: ridge detection, high contrast (75), low contrast (5), line width (1), minimum line length (5). We performed an initial training of the tool to obtain the classification into fragmented/tubulated mitochondria. The classification was kept as follows: fragmented < 8 µm, intermediate 8-12 µm, tubulated >12µm

10.5 Generation of the Drp1 knock-in mice

The Drp1 knock-in (KI) mice (C57BL/6NTac-Dnm1^{ltn3143(S643A)}Arte) were generated by Taconic Farms Inc. The targeting strategy we used allowed the generation of a constitutive whole body point mutation in the *Dnm1* gene, based on the Ensembl transcript ENSMUST00000047122. Exon 1 in the mouse genomic locus contains the translation initiation codon. The targeting vector contains exons 17 to 20, including the splice acceptor site of intron 16, which were inserted downstream of the distal loxP site. The S600A mutation was introduced into the duplicated exon 18. An additional polyadenylation signal (hGHpA: human Growth Hormone polyadenylation signal) was inserted between the 3' UTR and the distal loxP site in order to prevent downstream transcription of the mutated *Dnm1* exon 18. The size of the loxP-flanked region of the targeting vector was of approximately 7.0 kb. The targeting vector was generated using BAC clones from the C57BL/6J RPCIB-731 BAC library which were then transfected into the TaconicArtemis C57BL/6N Tac ES cell line. The constitutive knock-in (KI) locus is obtained after Cre-mediated deletion of wildtype exons 17 to 20 and the hGHpA. This KI allele expresses the mutated Drp1 S600A protein. The remaining recombination sites are located in non-conserved regions of the genome. In the document, Drp1^{loxP/loxP}-Drp1S600A^{CRE} mice will be called Drp1 S600A knock-in (or Drp1 KI). Mice breedings were carefully controlled to distinguish control (WT) from Drp1 S600A^{CRE} cohorts.

10.6 Animal care

Unless otherwise specified, mice were kept in a standard temperature- and humidity-controlled environment with a 12h:12h light-dark cycle. Mice had nesting material and *ad libitum* access to water and commercial LFD and HFD (D12450J and D12492i, respectively, from Research Diets Inc.). Only male mice were used for the experiments, unless indicated otherwise. All animal experiments were carried out according to national Swiss and EU ethical guidelines and approved by the local animal experimentation committee under license VD 3118.

10.7 Animal phenotyping

All clinical tests were performed according to standard operational procedures established within the Eumorphia program (<http://empress.har.mrc.ac.uk/>). Animals were systematically randomized for the tests, ensuring similar numbers per genotype in the cohorts. All phenotyping tests were performed in aged-matched cohorts, while mice were between 30-50 weeks of age. Mice that showed any sign of severity, predefined by the Veterinary Office of the Canton of Vaud, were euthanized. These animals,

together with those who died spontaneously during the experiments, were excluded from the data analyses. Body composition was determined by Echo-MRI (Echo Medical Systems, Houston, TX, USA). Oxygen consumption (VO_2 and VCO_2), food intake, and activity were monitored by indirect calorimetry using the comprehensive laboratory animal monitoring system (CLAMS; Columbus Instruments, Columbus, OH, USA). Energy expenditure (EE) was estimated using VO_2 and VCO_2 values from indirect calorimetry, using the following equation $\text{EE (in kJ/h)} = (15.818 \times \text{VO}_2) + (5.176 \times \text{VCO}_2)$ (Virtue & Vidal-Puig, 2013). Food intake and activity were also monitored using the CLAMS during a 24 h period. Glucose tolerance was analyzed by measuring blood glucose after an intraperitoneal injection of 2 g/kg glucose after an overnight fast. Insulin tolerance was measured by injecting 0.5 U/kg insulin for LFD-fed mice, or 1 U/kg insulin for HFD-fed mice, after 6 h fasting. Insulinemia was measured on plasma samples with an ELISA kit (EMD Millipore Corp.). Cold test experiments were performed by placing mice in a cold chamber kept at 6°C and measuring rectal body temperature every hour. At the end of the phenotyping, animals were sacrificed after isoflurane inhalation at 8 a.m. after a 12 h fast, in order to stabilize systemic parameters and to allow the measurement of blood biochemistry in the fasting state. Blood samples were collected in EDTA-coated tubes, and plasma was isolated after centrifugation (2000g, 15 min, 4°C). For fasting/refeeding experiment, food was removed for 24 hours. Then, a “Fasted” group was sacrificed, and the “Refed” group was kept with access to food for another 6 hours. Tissues were collected upon sacrifice and flash-frozen in liquid nitrogen.

10.8 *In vivo* measurement of brown adipose tissue activity

In order to evaluate non-shivering thermogenesis (BAT function), we measured whole-body O_2 consumption in response to a specific β_3 -adrenergic agonist, CL, in anesthetized mice as previously described (Cannon & Nedergaard, 2011). Briefly, mice, housed either at 22°C or 30°C for at least 1 month, were anesthetized using pentobarbital (60 mg/kg) and placed on a calorimetric chamber at 30°C. After 30 min of adaptation, CL was subcutaneously injected (1 mg/kg) and mice were placed back in the chamber to follow up O_2 consumption measurements.

10.9 Electron microscopy on mouse brown adipose tissue

Brown adipose samples were cut in pieces smaller than 1mm^3 and fixed in glutaraldehyde solution (EMS, Hatfield, PA, US) 2.5% in Phosphate Buffer (PB 0.1M pH7.4) (Sigma, St Louis, MO, US) during 2h at room temperature (RT). Then, pieces were rinsed 3 times for 5 minutes in PB buffer and post-fixed by a fresh mixture of osmium tetroxide 1% (EMS, Hatfield, PA, US) with 1.5% of potassium ferrocyanide (Sigma, St

Louis, MO, US) in PB buffer during 2 h at room temperature. The samples were then washed three times in distilled water and dehydrated in acetone solution (Sigma, St Louis, MO, US) at graded concentrations (30%-1h30; 70%-1h30; 100%-2h; 100%-4h). This was followed by infiltration in Spurr resin (EMS, Hatfield, PA, US) at graded concentrations (Spurr 1/3 acetone-4h; Spurr 3/1 acetone-4h, Spurr 1/1-8h; Spurr 1/1-24h) and finally polymerized for 48 h at 60°C in the oven. Ultrathin sections of 50 nm were cut on a Leica Ultracut (Leica Mikrosysteme GmbH, Vienna, Austria) and picked up on copper slot grid 2x1mm (EMS, Hatfield, PA, US) coated with a polystyrene film (Sigma, St Louis, MO, US). Sections were poststained with uranyl acetate (Sigma, St Louis, MO, US) 2% in H₂O for 10 minutes, rinsed several times with H₂O followed by incubation with Reynolds lead citrate for 10 minutes and rinsed several times with H₂O.

Micrographs with a pixel size of 6.86nm were taken with a transmission electron microscope Philips CM100 (Thermo Fisher Scientific, Waltham, MA USA) at an acceleration voltage of 80kV with a TVIPS TemCam-F416 digital camera (TVIPS GmbH, Gauting, Germany). A total of 20 EM-sections were imaged and used for quantification from 4 control and 4 KI animals.

10.10 Histology

H&E and Oil Red O stainings were performed using the fully automated Ventana Discovery XT (Roche Diagnostics, Rotkreuz, Switzerland). All steps were performed on the machine with Ventana solutions. A total of 5 control and 5 Drp1 KI mice were compared for histology analyses, by imaging and quantifying approximately 10 sections per mouse tissue using ImageJ.

10.11 Respirometry studies on mouse tissue homogenates

Respirometry studies were performed in fresh mouse tissue homogenates using high-resolution respirometry (Oroboros Oxygraph-2k, Oroboros Instruments) as described previously (Canto & Garcia-Roves, 2015). All respirometry experiments were performed on fresh tissues immediately after dissection. Liver and adipose tissues were homogenized in amino acid-depleted respirometry medium (0.5 mM EGTA, 3 mM MgCl₂, 60 mM K-lactobionate, 10 mM KH₂PO₄, 20 mM HEPES, and 110 mM sucrose, pH 7.1) and 2 mg of wet tissue were added to the experimental chamber.

All the tissues were assessed in respirometry medium. Oxygen flux (denoted as “Leak” in figures) was measured by adding malate (final concentration 2 mM) pyruvate (10 mM) and glutamate (20 mM) in the absence of ADP. Complex I-driven oxidative phosphorylation (“CI”) was quantified by the addition of ADP (5 mM). This was followed by the addition of succinate (10 mM) for electron flow through both complex I

and II measurement ("CI+CI"). Subsequently, carbonylcyanide-4-(trifluoromethoxy)-phenyl-hydrazine (FCCP) was titrated to achieve maximum flux through the electron transfer system ("ETS"). Finally, electron transport through complex I ("CI") and complex III was inhibited by the sequential addition of rotenone (0.1 μM) and antimycin A (2.5 μM), respectively. The remaining O_2 flux after inhibition with antimycin A (O_2 flux independent of the electron transfer system) was subtracted from all the values from the previous steps. Oxygen flux values are expressed relative to tissue wet weight per second ($\text{pmol O}_2 \times \text{mg}^{-1} \text{s}^{-1}$).

10.12 Respirometry studies on isolated mitochondria

For respirometry analyses on isolated mitochondria, 200 μg of isolated mitochondrial protein were used (in a 2 ml chamber) and the incubations were done at 30 °C. State 2 respiration defines the steady-state respiration achieved after the addition of substrates for Complex I (malate and glutamate; 2 and 10 mM respectively) or Complex II (succinate 10 mM) in the absence of ADP. For analyses aimed to specifically evaluate Complex II, rotenone (0.5 μM) was added in addition to succinate, in order to inhibit Complex I. State 3 respiration was evaluated by adding ADP (250 μM or 5 mM, as indicated in the figure legends). Respiratory Control (RC) was calculated as the State 3 / State 2 ratio obtained at this stage. Maximal respiration was explored by titrating FCCP at 0.5 μM steps until maximum effects were reached. Antimycin A (2.5 μM) was used to inhibit Complex III and verify the complete abrogation of respiration in our samples. Isolated mitochondria preparations were routinely tested for the integrity of the outer mitochondrial membrane by adding Cytochrome c (10 μM) during State 3 respiration. All studies in isolated mitochondria used exclusively samples where Cytochrome c addition increased respiration by less than 5%. Similarly, mitochondrial preparations with an RC below 4 (upon Complex I stimulation) were discarded.

10.13 Mitochondria isolation

Mitochondria were isolated from frozen mouse BAT as previously described (Jha *et al.*, 2016). Mitochondria isolation from frozen tissues allowed the preservation of Drp1 phosphorylations. Upon thawing, one BAT pad was placed in a glass potter with 2 mL of freshly prepared ice-cold mitochondrial isolation buffer (IB) (250 mM sucrose, 10 mM Tris-MOPS and 0.1 mM EGTA/Tris; adjusted to pH=7.4; 1 tablet of protease and phosphatase inhibitors each were added). Pieces of tissue were homogenized at 4°C using a Teflon pestle rotating at 1600 rpm (4 strokes). The homogenate was then transferred to a 2 mL Eppendorf tube and centrifuged at 600g for 10 min at 4°C. This step separates the cell debris from the

mitochondrial extract. After this, the supernatant was transferred to a new 1.5 mL Eppendorf tube and centrifuged at 7000g for 10 min at 4°C. After this step the supernatant contained the cytosolic fraction and the pellet was washed twice with 1 ml of ice-cold IB and centrifuged at 7000g for 10 min at 4°C. The supernatant was then discarded and the pellet, containing mitochondria, was resuspended in 50 µl of buffer. Mitochondrial protein concentration was then determined using the BCA method.

10.14 Primary hepatocyte isolation

Hepatocytes were isolated from WT mice by continuous recirculating perfusion of the mouse liver *in situ* with collagenase digestion (Berry & Friend, 1969). Perfusion was performed in Krebs buffer (4.7 mM KCl, 0.7 mM KH₂PO₄, 10 mM HEPES, 117 mM NaCl, 24.6 mM NaHCO₃, 0.2% glucose) supplemented with 5 mM CaCl₂ and 0.5 mg/ml collagenase (Worthington, type IV) for 10 min with 5 ml/min flow. Cells were seeded in M199 containing 100 U/ml penicillin G, 100 µg/ml streptomycin, 0.1 % (w/v) BSA, 10 % (v/v) FBS, 10 nM insulin, 200 nM triiodothyronine and 100 nM dexamethasone. Post attachment (4-5 h), cells were cultured overnight in M199 supplemented with antibiotics and 100 nM dexamethasone and used for experiments the following morning. Primary hepatocytes were treated with DMSO or with 20 µM of Forskolin for 2 hours, after which total protein lysates were collected.

10.15 Primary muscle culture

Muscles (quadriceps, tibialis, EDL, gastrocnemius, soleus) were excised from hind limbs of mice and mulched into a smooth pulp, which was then digested by adding 6 mL of warm collagenase/Dispase II/CaCl₂ solution. The digestion mix was incubated for 10 min at 37°C, after which it was homogenized and placed again in the incubator for another 17 min. Homogenization allows the mixture to disaggregate any remaining muscle fibers. Then, 50 µL of myoblast growth media were added to the mixture to stop the digestion. The cell suspension was then filtered by means of a 70 µm filter in a 50 mL falcon tube, and centrifuged at 1200 rpm for 5 min. The pellet was then resuspended in 4 mL of complete myoblast growth medium (79% Hams F10, 20% FBS, 2.5 ng/mL rhFGF, 1% Pen/Strep) and plated onto a non-coated 10 cm plate for 2 hours. This step allows fibroblasts to adhere to the place, while myoblasts will remain in suspension. At the end of the incubation, media was transferred to 6 cm collagen-coated petri dishes. Four cell passages are recommended before performing experiments. Passage 1 to 3 are used as maintenance for the cells to expand and get rid of remaining fibroblasts; passage 4 to 10 is recommended for experiments. Upon 80% confluence media was replaced with differentiation media (DMEM

supplemented with 5% Horse Serum, 1% Pen/Strep) every two days for a total of 1 week when myotubes are observed (Figure 10.1).

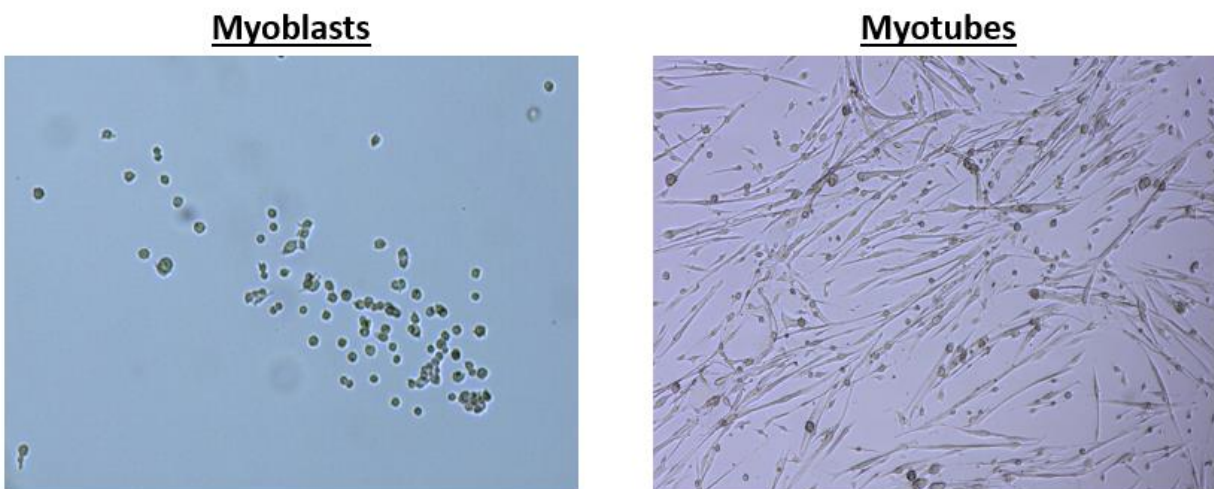


Figure 10.1. Primary muscle culture.

Left, myoblasts from WT mice plated onto collagen-coated plates. Right, myotubes were formed after 6 days of differentiation.

10.16 Primary brown adipocyte isolation

Primary brown adipocytes were collected from the interscapular BAT of mice (10 BAT/genotype are recommended for optimal cell yield). Ten individual BAT pads were added into a 5 mL Eppendorf tube containing 1 mL of warm collagenase solution (1M Glucose, 7.5% BSA, 1M CaCl_2 in Krebs buffer + 1 mg/mL collagenase type IV) and mulched. Then, 4 mL of collagenase solution were added to a 50 mL Falcon tube alongside 1 mL of the BAT mixture and placed in a 37°C shaker at 300 rpm for 40 min. It is recommended to vortex this mixture every 10 min to ensure digestion. After, 10 mL of base media (DMEM supplemented with 1% Pen/Strep, 2 mM Glutamine, 10% FCS, 20 mM Hepes) were added to stop the digestion. The cell suspension was then filtered through a 100 μm filter into a clean falcon and centrifuged for 10 min at 100 g: preadipocytes will be collected in the pellet while mature adipocytes will form a lipid layer on top of the solution. Then, the pellet was resuspended in 10 mL of base media and the cell suspension was transferred to a new 15 mL Falcon tube, and centrifuged for 10 min at 100 g. After centrifugation, the pellet was incubated in 1 mL of erythrocyte lysis buffer (0.5 M EDTA, 0.5 M KH_2PO_4 , 0.5 M NH_4Cl) at room temperature for 4 min. Then, 9 mL of base media were added to the falcon to stop the reaction and the falcon was centrifuged for 10 min at 100 g. The resulting pellet was washed with 10 mL base media and

centrifuged at 100 g for 10 min. Finally, the final pellet was resuspended in base media and plated in a collagen-coated 12 well plate. After 4 hours, media was changed to BAT culture media (base media supplemented with 1.72 mM insulin and 1 mM Triiodothyronine (T3)). Upon maximal confluence, media was replaced with differentiation media (DMEM supplemented with 0.02 μ M Insulin, 1.5 nM T3, 0.5 μ M dexamethasone, 1 μ M rosiglitazone, 0.125 μ M indomethacin, 0.5 mM isobutylmethylxanthine (IBMX)) for 7 days. After this, cells were cultivated in growth medium until day 6 of differentiation (Figure 10.2) (Boutant *et al.*, 2015).

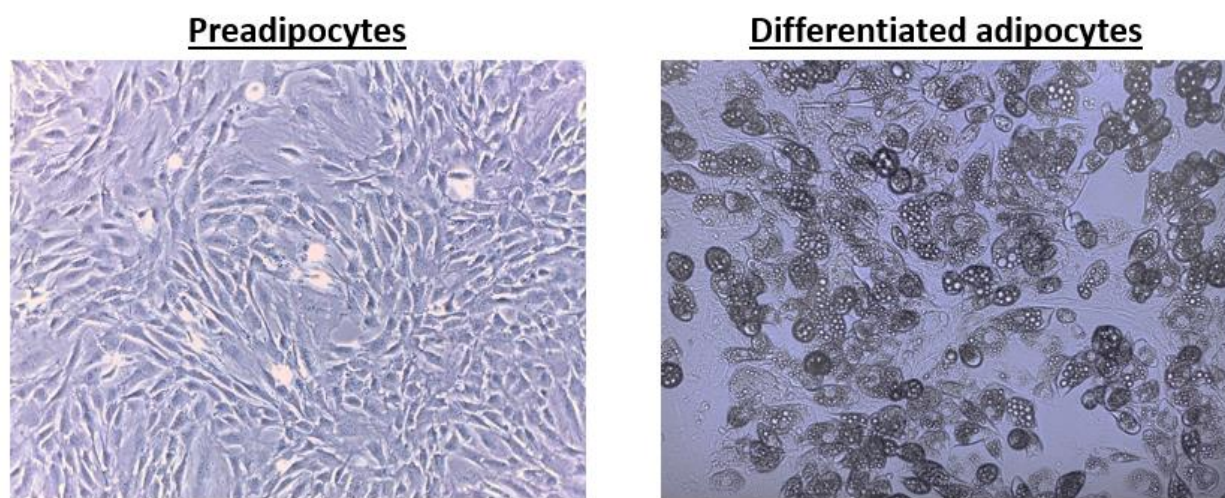


Figure 10.2. Primary BAT isolation and culture.

Left, confluent pre-adipocytes before differentiation. Right, adipocytes were differentiated for 6-7 days, when lipid droplet maturation can be observed.

10.17 Antibody generation

The rabbit polyclonal antibody against total Drp1, Drp1 phospho-Ser600 and Drp1 phospho-Ser579 were generated by rabbit injections (Yenzym antibodies, CA, USA), followed by affinity purification using standard protocols. The antibody for total Drp1 was raised against the peptide GLMNNNIEEQRRNRLARE, which covers amino acids 506-523 of the Isoform 3 of the mouse Drp1 protein. The antibody against phospho-S579 was raised against the peptide KPIPIMPA- pS- PQKGH, while the one for phospho-S600 was raised against the peptide sequence CVPVARKL-pS-AREQRD.

10.18 Protein extraction and Western Blotting

For protein extraction from cell lines, cells were initially washed twice with cold PBS and lysed in lysis buffer (50 mM Tris-HCL pH7.5, 150 mM NaCl, EDTA 5 mM, NP40 1%, protease and phosphatase inhibitors),

followed by centrifugation at 13,000 g for 10 min at 4°C. Protein extracts from mouse tissues were isolated with the TissueLyser (Qiagen®) system following manufacturer's instructions. Proteins were quantified using a BCA assay (Pierce). For western blotting, proteins were separated by SDS-PAGE and transferred onto nitrocellulose membranes. Membranes were blocked for 1 hour with 5% BSA in TBS-Tween followed by an overnight incubation at 4°C with primary antibody dilution in TBS-Tween with 0.5% BSA. The primary antibodies used are listed in *Annex 3. Table of antibodies*. Secondary antibodies were used in 1:20000 dilution for 1 hour incubation. Membranes were then developed by enhanced chemiluminescence (Amersham). For quantification, the intensity of each band was determined by densitometry using ImageJ software.

10.19 RNA extraction and qPCR

Total mRNA from all studied tissues or cells was extracted using TRIzol (Life Technologies) according to manufacturer's instructions. RNA concentrations were measured with Nanodrop 1000 (Thermo Scientific). Reverse transcription was performed using SuperScript II (Life Technologies) with oligo dT plus, random hexamer primers and RNAsin (Roche) according to the manufacturer's protocol. Quantification of mRNA expression was performed using SYBR Green real time PCR technology (Roche). Reactions were performed in duplicate in a 384-well plate using the Light Cycler (Roche). Gene expression was normalized with *b2-microglobulin* and *cyclophilin* as housekeeping genes. Relative gene expression between genotypes was assessed using the $\Delta\Delta C_t$ method. Primer sequences are listed in *Annex 4. Primers for qPCR*. Mitochondrial number was assessed by using mitochondrial DNA – nuclear DNA ratio. Total DNA was extracted using the DNeasy Blood & Tissue Kit (Qiagen, reference #69504) and mitochondrial DNA was quantified as described in Quiros *et al.* (2017). UCP2 and HK2 primers were used as endogenous control for nuclear DNA, while COX2 and 16S as marker for mitochondrial DNA.

10.20 Measurement of acyl-carnitines in BAT

Metabolites were extracted from the brown adipose tissue (BAT) by mixing 400µl of acetonitrile, methanol and water in a 4:4:2 proportion to the lyophilized and pulverized matrix. After mixing the sample with a vortex, the mixture was frozen under liquid nitrogen for 10-20s, then sonicated for 20-30s and vortexed 20s for homogenizing the mixture. These steps were repeated for a total of three complete cycles. The untargeted LC/MS data was generated using a UHPLC system (1200 series, Agilent Technologies) coupled to a G6550A ESI-qToF MS (Agilent Technologies) operated in positive electrospray ionization (ESI+) mode. Metabolites were separated by hydrophilic interactions using an InfinityLab

Poroshell 120 HILIC-Z, 2.1 x 100 mm, 2.7 μm (PEEK lined) (Agilent Technologies) column. Mobile phase A was water (50 mM ammonium acetate) and mobile phase B was acetonitrile. The separation of the extracts was conducted under the following gradient: 0-2 min 98% of B; 2-10 min decrease to 40% of B; 10-10.5 min raise to 98% of B; 10.5-15 min 98% of B. The parameters for the electrospray ionization source (ESI) were as follow: gas temperature, 200 $^{\circ}\text{C}$; drying gas, 14 l min⁻¹; nebulizer, 35 psig; fragmentor, 175 V; and skimmer, 65 V. The m/z acquisition range was set between 50 and 1100 Da, acquiring 3 spectra/s. In order to identify compounds, MS/MS data was generated in targeted mode and instrument was set to acquire spectra over the m/z range from 50 to 600, with a narrow width of 1.3 m/z. Several collision energies (CE) were tested between 10 and 40V.

Data generated in the LC/MS instrument was processed and analyzed using the xcms R package (version 3.4.4) to detect and align mzRT features. The xcms R package data analysis output is a matrix containing the integrated peak area, the retention time and the m/z value of each feature for each sample. A pool of each sample extract was created and used as quality control sample (QC), injected at the beginning and periodically through the worklist to correct the instrument drift, these samples are used to assess instrumental variability. Untargeted metabolomics data analysis involved feature filtering based on average intensity, variability and sample consistency, followed by PQN and tissue weight normalization. Filtered and normalized features were statistically tested using Welch's T-test, those significant were putatively annotated using LIPID MAPS Lipidomics Database and Human Metabolome Database.

10.21 Adipokine profiling

Adipokines were measured from 100 μL of plasma samples from WT and Drp1 KI mice by using the Mouse Adipokine Array kit (ARY013, R&D systems), following manufacturer's instructions. The intensity of each dot was measured by the Protein Array Analyzer plugin for ImageJ.

10.22 Plasma Biochemistry

Blood samples were collected in EDTA-coated tubes, and plasma was isolated after centrifugation (2000g, 15 min). Plasma parameters (cholesterol, triglycerides, free fatty acid) were measured using Dimension[®] Xpand Plus (Siemens Healthcare Diagnostics AG, Dudingen, Switzerland).

10.23 Statistical Analyses

Statistical analyses were performed with Prism software (GraphPad). The sample size was estimated based on the known variability of the assays. *In vitro* analyses were performed as minimum in duplicates in three separate experiments. For mouse time-series experiments, differences between two groups were analyzed using linear mixed effect models, with time and treatment groups as fixed effects, and animal id as a random effect. Models were fitted using restricted maximum likelihood approaches. Two types of models were performed, models testing the time*group interaction effects; and models testing time+group additive effects. Posthoc analyses were performed using Tukey's Honest Significance Differences. Data are expressed as means \pm SEM.

Annex 1. Table of materials

Product	Supplier	Catalog No.
Oligomycin	Sigma	#1404-19-9
FCCP	Sigma	#370-86-5
Rotenone	Sigma	#83-79-4
Antimycin A	Sigma	#1397-94-0
CL316,243	Sigma	#C5976
Glucagon	Novo Nordisk	#0169-7065-15
Isoproterenol hydrochloride	Sigma	#I6504
Glucose	Gibco	#15023021
Insulin (100U/mL)	NovoRapid	#058610
Roscovitine	Cell Signaling Technology	#9885
KOD Hot Start DNA Polymerase	Merck/SigmaAldrich	#71086
T4 DNA ligase	Fermentas/Thermofisher	#EL0016
BamH1	Fermentas/Thermofisher	#FD0055
Not1	Fermentas/Thermofisher	#ER0592
Dpn1	Fermentas/Thermofisher	#ER1702
Proteome Profiler Mouse Adipokine Array Kit	R&D Systems	#ARY013
DNeasy Blood & Tissue Kit	Qiagen	#69504
BigDye Terminator 3.1 kit	Applied Biosystems	

Annex 2. Primers for site-directed mutagenesis

Mutation	Primer	Sequence 5' to 3'
Drp1 S579A	F	CCAATTATGCCAGCAGCTCCACAGAAAGGC
	R	GCCTTTCTGTGGAGCTGCTGGCATAATTGG
Drp1 S600A	F	GTTGCAAGAAAAGCTGGCTGCCCAGAACAG
	R	CTGTTCTCGGGCAGCCAGTTTTCTTGCAAC
Drp1 S579D	F	CCAATTATGCCAGCAGATCCACAGAAAGGC
	R	GCCTTTCTGTGGATCTGCTGGCATAATTGG
Drp1 S600D	F	GTTGCAAGAAAAGCTGGATGCCCAGAACAG
	R	CTGTTCTCGGGCATCCAGTTTTCTTGCAAC
Drp1 S579E	F	CCAATTATGCCAGCAGAACCACAGAAAGGC
	R	GCCTTTCTGTGGTTCTGCTGGCATAATTGG
Drp1 S600E	F	GTTGCAAGAAAAGCTGGAAGCCCAGAACAG
	R	CTGTTCTCGGGCTTCCAGTTTTCTTGCAAC

Annex 3. Table of antibodies

Protein	Manufacturer	Catalog No.	Species	Working dilution
Drp1	YenZym	YZ6212	Rabbit	1:1000
Drp1 phospho-Ser600	YenZym	YZ5447	Rabbit	1:2000
Drp1 phospho-Ser579	YenZym	YZ6213	Rabbit	1:1000
Mfn1	YenZym	YZ5443	Rabbit	1:2000
Mfn2	YenZym	YZ5445	Rabbit	1:2000
OPA1 (Clone 18/OPA1)	BD Biosciences	612606	Mouse	1:2000
MFF	ProteinTech	17090-1-AP	Rabbit	1:1000
FIS1	Thermo Fisher	PA1-41082	Rabbit	1:500
Pex3	ProteinTech	10946-1-AP	Rabbit	1:1000
Pex5	ProteinTech	12545-1-AP	Rabbit	1:1000
GAPDH (Clone 14C10)	Cell Signaling	2118	Rabbit	1:2000
Pan-cadherin	Cell Signaling	4068	Rabbit	1:1000
Rb (D20)	Cell Signaling	9313	Rabbit	1:1000
phospho-Rb (Ser780)	Cell Signaling	9307	Rabbit	1:1000
Cdk1	Abcam	ab133327	Rabbit	1:1000
phospho-Cdk1 (Tyr15)	Millipore	219440	Rabbit	1:500
ERK	Cell Signaling	4695	Rabbit	1:1000
phospho-ERK (Thr202/Tyr204)	Cell Signaling	9101	Rabbit	1:1000
VDAC1 / Porin	Abcam	ab14734	Mouse	1:5000
NDUFA9 (Clone 20C11)	Abcam	ab14713	Mouse	1:2000
SDHA (Clone 2E3)	Abcam	ab14715	Mouse	1:5000
UQCRC1	Abcam	ab110252	Mouse	1:2000
MTCO1	Abcam	ab14705	Mouse	1:1000
ATP5A	Abcam	ab14748	Mouse	1:5000
UCP1	Abcam	ab10983	Rabbit	1:5000
IRE1	Abcam	ab37073	Rabbit	1:1000
phospho-IRE1 (S724)	Abcam	ab104157	Rabbit	1:500
eIF2 α	Cell Signaling	5324	Rabbit	1:1000
phospho-eIF2 α (Ser51)	Cell Signaling	3398	Rabbit	1:500
ACC	Cell Signaling	3676	Rabbit	1:1000
phospho-ACC (Ser 79)	Millipore	07-303	Rabbit	1:500
GLUT3	Millipore	400062	Rabbit	1:1000
E-Cadherin	Cell Signaling	3195	Rabbit	1:1000
Vimentin	Cell Signaling	5741	Rabbit	1:1000
SNAIL	Cell Signaling	3879	Rabbit	1:1000

Annex 4. Primers for qPCR

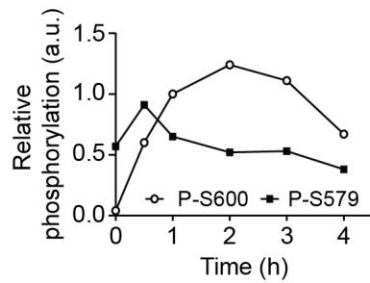
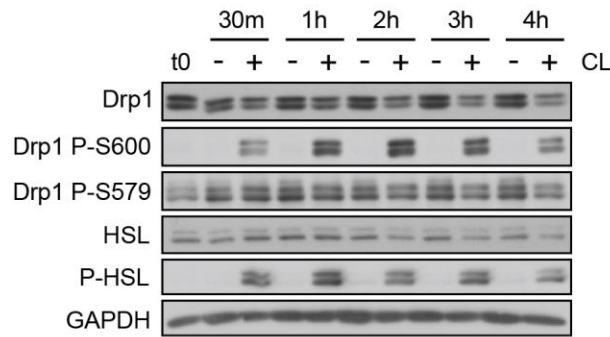
Species	Gene	Forward primer (5' to 3')	Reverse primer (5' to 3')
Mouse	B-2 microglobulin	ATGGGAAGCCGAACATACTG	CAGTCTCAGTGGGGGTGAAT
	Cyclophilin	CAGGGGAGATGGCACAGGAG	CGGCTGTCTGTCTTGGTGCTCTCC
	Ucp1	CTTTGCCTCACTCAGGATTGG	ACTGCCACACCTCCAGTCATT
	Prdm16	TGGCCTTCATCACCTCTCTGAA	TTTCTGATCCACGGCTCCTGTGA
	Pgc1 α	AAGTGTGGAAGTCTCTGGAAGTCTG	GGGTTATCTTGGTTGGCTTTATG
	Acadm (Mcad)	GGCCATTAAGACCAAAGCAGA	GTGTCGGCTTCCACAATGAAT
	Acadl (Lcad)	GTAGCTTATGAATGTGTGCAACTC	GTCTTGCATCAGCTCTTTCATTA
	Cpt1b	CCCATGTGCTCCTACCAGAT	CCTGAAGAAGCGACCTTTG
	Cpt2	AGCCAGTTCAGGAAGACAGA	GACAGAGTCTCGAGCAGTTA
	Aco2	ACCGCCTATGCCTTCCACTTTC	GCAAGCCATCCGACATTCTTCG
	Ppar γ	ATGGGTGAAACTCTGGGAGATTCT	CTTGGAGCTTCAGGTCATATTGTA
	Acc1	GACAGACTGATCGCAGAGAAAG	TGGAGAGCCCCACACACA
	Acc2	CCCAGCCGAGTTTGTCCT	GGCGATGAGCACCTTCTCTA
	Fas	TTCCAAGACGAAAATGATGC	AATTGTGGGATCAGGAGAGC
	Srebf1 (Srebp1c)	GGAGCCATGGATTGCACATT	GCTTCCAGAGAGGAGGCCAG
	Srebf2 (Srebp2)	GCGTTCTGGAGACCATGGA	ACAAAGTTGCTCTGAAAACAAATCA
	16s	CCGCAAGGGGAAAGATGAAAGAC	TCGTTTGGTTTCGGGGTTTC
	Cox2	GTTGATAACCGAGTCGTTCTGC	CCTGGGATGGCATCAGTTTT
	Hk2	TCTGGCTCTGAGATCCATCTTCA	CCGGCCTCTTAACCACATTCC
	Ucp2	CTACAGATGTGGTAAAGGTCCGC	GCAATGGTCTTGTAGGCTTCG
	Atf4	CCTGAACAGCGAAGTGTTGG	TGGAGAACCCATGAGGTTTCAA
	Atf6	AACCGAGAGTCTGCTTGTC	AGCCTCTGGTTCTCTGACAC
	Bip	GACTGCTGAGGCGTATTTGG	AGCATCTTTGGTTGCTTGTCG

Species	Gene	TaqMan ID
Human	18S	Hs99999901_s1
	CDH1	Hs01023894_m1
	Drp1	Hs01552605_m1
	GAPDH	Hs02758991_g1
	Mfn1	Hs00966851_m1
	Mfn2	Hs00208382_m1
	Opa1	Hs01047018_m1
	SLC2A3	Hs00359840_m1
	SNAIL1	Hs00195591_m1
	VIM	Hs00185584_m1

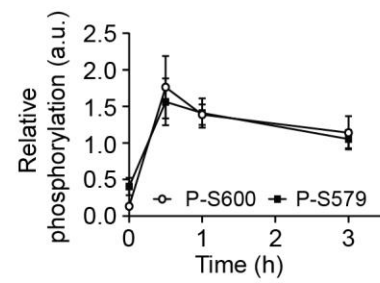
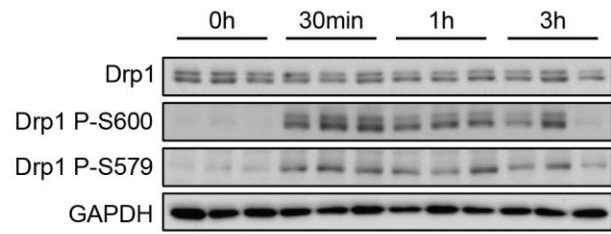
Appendices

Appendix 1

A



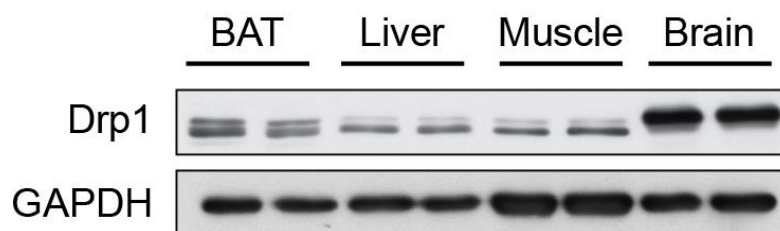
B



Appendix 1. Time-course for Drp1 phosphorylations *in vitro* and *in vivo*.

(A) Total protein lysates were evaluated by Western blot from differentiated brown adipocytes non-treated (-) or treated (+) with CL316,243 at times 0, 30 min, 1h, 2h, 3h or 4h. GAPDH was used as a loading control and HSL/P-HSL was utilized as control for the differentiation process. Quantification of the variation with time of the phosphorylation levels for both S600 and S579 residues in the differentiated adipocytes are represented in the graph below (n = 1 experiment). **(B)** WT control mice were treated with CL316,243 (1mg/kg) for the indicated time points, after which brown adipose tissue was collected and protein homogenates were evaluated by Western blot for Drp1 total and Drp1 phosphorylations (n = 3 mice per time point). Quantification of the variation with time of the phosphorylation levels for both S600 and S579 residues from the BAT samples are represented in the graph below. All values are presented as mean +/- SEM.

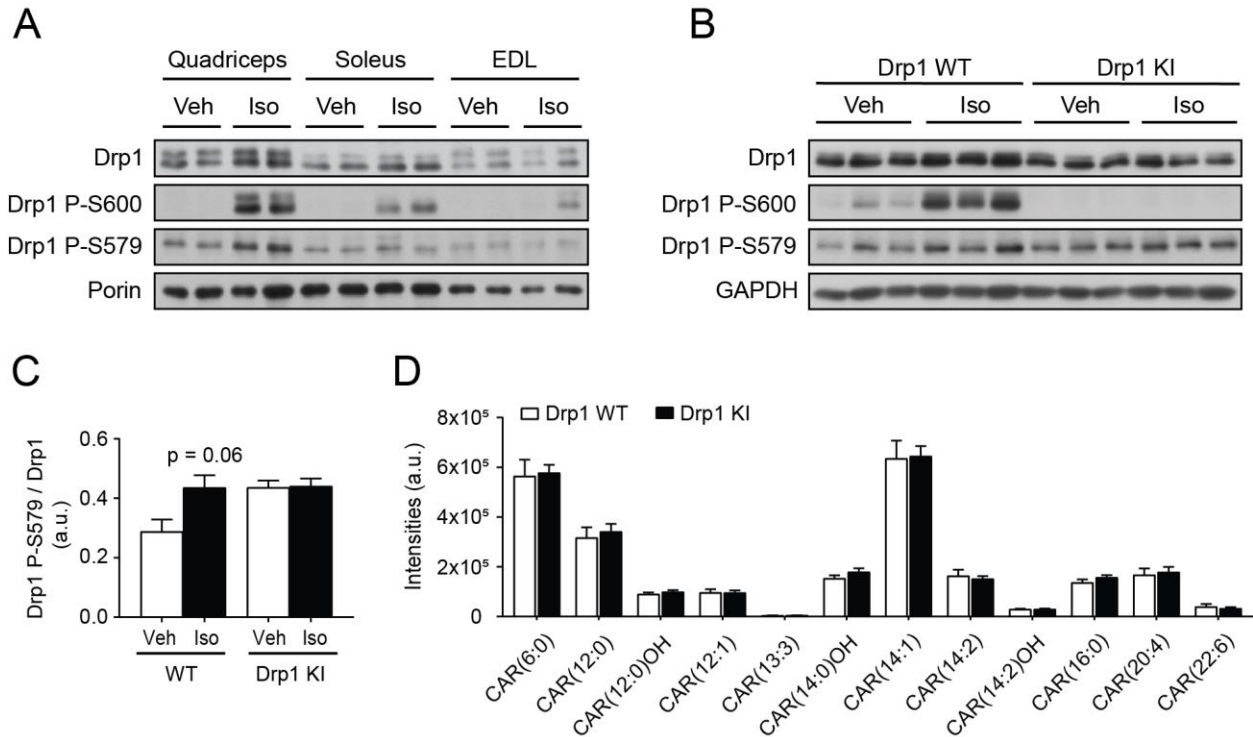
Appendix 2



Appendix 2. Drp1 isoforms in different tissues.

BAT, liver, muscle and brain from two control mice were collected and protein homogenates were used to evaluate Drp1 levels. Neuron-specific isoform 1 contains the B-insert within Drp1 structure, whereas Drp1 isoform 3, present in BAT, liver and muscle, lacks it. Thus, Drp1 isoform 1 in brain displays a slightly higher molecular weight on the Western Blot.

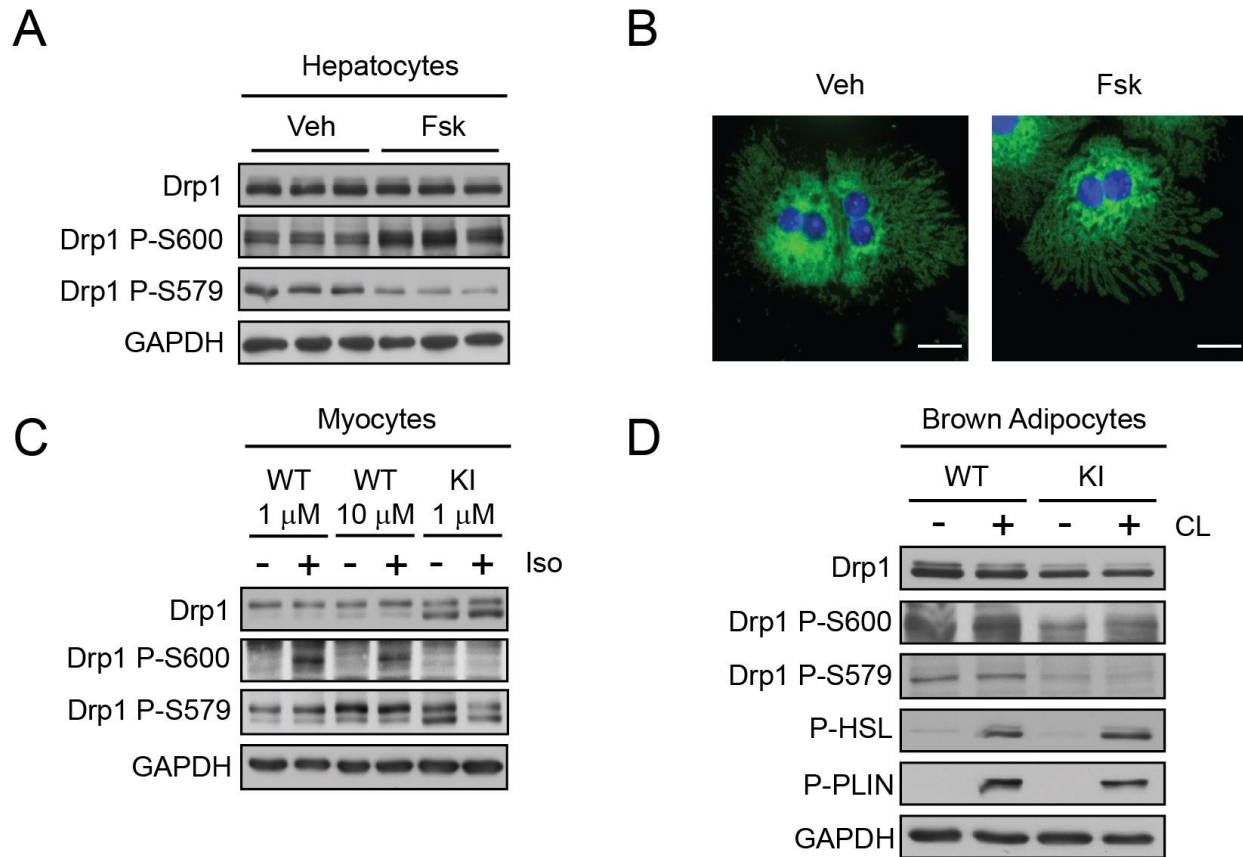
Appendix 3



Appendix 3. Muscle data from the Drp1 KI mice.

(A) Muscle samples from wild type mice were collected and used to compare Drp1 total and Drp1 phosphorylation levels between Quadriceps, Soleus and EDL after treatment with Vehicle (Veh, PBS) or Isoproterenol (Iso, 10 mg/kg) for 15 min (n=2 mice per condition). **(B)** WT and Drp1 KI mice were injected with Isoproterenol (10 mg/kg) for 15 min before collecting muscle (quadriceps) and evaluating the protein lysates for Drp1 total and Drp1 phosphorylation levels (n=3 mice per condition). **(C)** Quantifications of Drp1 P-S579 levels normalized to total Drp1 from the experiment in (B). **(D)** Acyl-carnitine levels were measured by liquid chromatography and mass-spectrometry (LC-MS) from quadriceps of HFD-fed mice (n = 12 WT and 9 KI). Values are presented as mean +/- SEM.

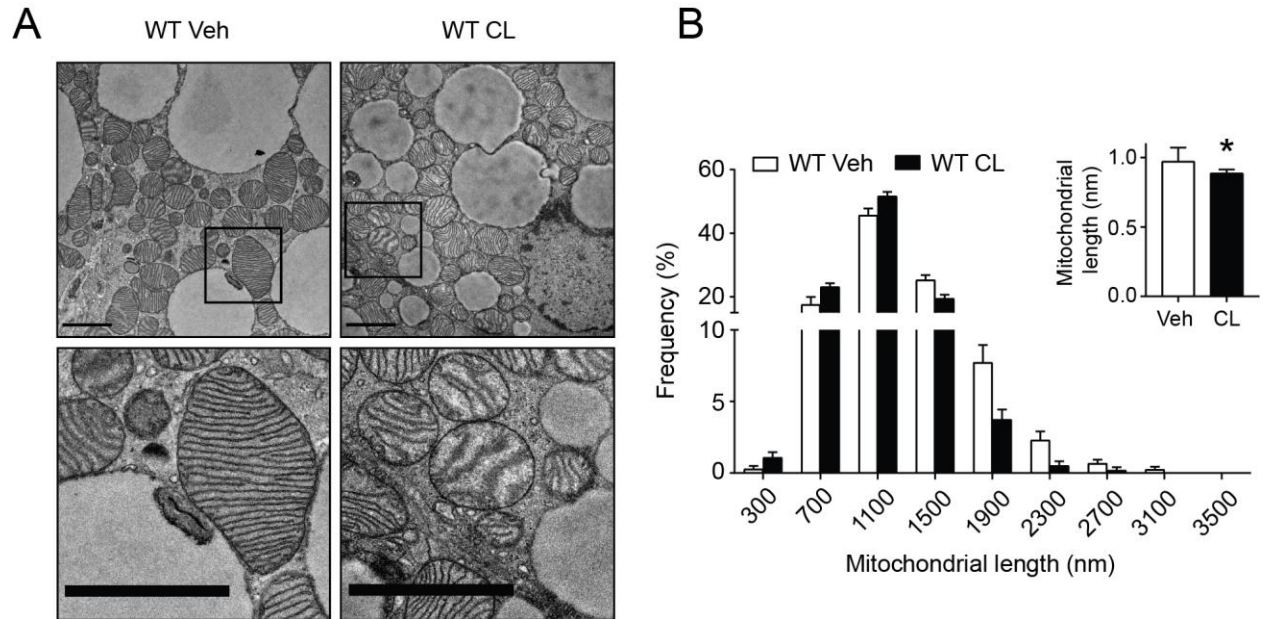
Appendix 4



Appendix 4. Primary cultures of liver, muscle and BAT.

(A) Primary hepatocytes were isolated from 10-20 week old wild type mice and treated with vehicle (Veh, DMSO) or 20 μ M Forskolin (Fsk) for 2 hours ($n = 3$ mice per condition as separate replicates). After this, total protein extracts were obtained to evaluate Drp1 total and Drp1 phosphorylation levels. **(B)** Immunofluorescence of primary hepatocytes from the experiment in (A) staining mitochondria with Alexa 488 (green) and nuclei with Dapi (blue). **(C)** Primary myoblasts were isolated from hind leg muscles of 5 week old wild type (WT) and Drp1 KI (KI) mice ($n = 1$ mouse per genotype). Then, cultured myoblasts were differentiated into myocytes. WT myocytes were treated with 1 μ M or 10 μ M Isoproterenol (Iso, +), respectively, to assess concentration effects, while KI myocytes were treated with 1 μ M Isoproterenol. Treatment duration was of 30 min. PBS was used as vehicle (-). **(D)** Primary brown adipocytes were isolated from brown adipose tissue of 4-5 week old wild type (WT) and Drp1 KI (KI) mice and differentiated into mature adipocytes ($n = 10-12$ mice per genotype as one replicate). Prior to treatment, differentiated brown adipocytes were serum starved for 3 hours in phenol red-free, serum-free media. Then, cells were treated with vehicle (-, PBS) or 1 μ M CL316,243 (+) for 3 hours. Total protein extracts were collected to evaluate the markers indicated.

Appendix 5



Appendix 5. Adrenergic stimuli in brown adipose tissue leads to mitochondrial fragmentation.

(A) Electron microscopy (EM) images from BAT (scale bar: 2 μ m) of 27 week old WT mice injected with PBS (Vehicle, Veh) or CL316,243 (+) (1mg/kg) for 1 hour. **(B)** Mitochondrial length was measured, and frequency distributions were calculated from EM images of the experiment in (A), corresponding to 20 independent images per BAT sample (n = 1 per condition). Bonferroni test, *p < 0.05. All values are presented as mean \pm SEM.

References

- Achiriloaie M, Barylko B, Albanesi JP (1999) Essential role of the dynamin pleckstrin homology domain in receptor-mediated endocytosis. *Molecular and cellular biology* 19: 1410-1415
- Adachi Y, Itoh K, Yamada T, Cervený KL, Suzuki TL, Macdonald P, Frohman MA, Ramachandran R, Iijima M, Sesaki H (2016) Coincident Phosphatidic Acid Interaction Restrains Drp1 in Mitochondrial Division. *Mol Cell* 63: 1034-1043
- Ahmadian M, Liu S, Reilly SM, Hah N, Fan W, Yoshihara E, Jha P, De Magalhaes Filho CD, Jacinto S, Gomez AV *et al* (2018) ERR γ Preserves Brown Fat Innate Thermogenic Activity. *Cell Rep* 22: 2849-2859
- Aldridge AC, Benson LP, Siegenthaler MM, Whigham BT, Stowers RS, Hales KG (2007) Roles for Drp1, a dynamin-related protein, and mltin, a kinesin-associated protein, in mitochondrial segregation, unfurling and elongation during *Drosophila* spermatogenesis. *Fly* 1: 38-46
- Alexander C, Votruba M, Pesch UE, Thiselton DL, Mayer S, Moore A, Rodriguez M, Kellner U, Leo-Kottler B, Auburger G *et al* (2000) OPA1, encoding a dynamin-related GTPase, is mutated in autosomal dominant optic atrophy linked to chromosome 3q28. *Nature genetics* 26: 211-215
- Altieri DC (2019) Mitochondrial dynamics and metastasis. *Cellular and Molecular Life Sciences* 76: 827-835
- Ameka M, Markan KR, Morgan DA, BonDurant LD, Idiga SO, Naber MC, Zhu Z, Zingman LV, Grobe JL, Rahmouni K *et al* (2019) Liver Derived FGF21 Maintains Core Body Temperature During Acute Cold Exposure. *Scientific Reports* 9: 630
- Anand R, Wai T, Baker MJ, Kladt N, Schauss AC, Rugarli E, Langer T (2014) The i-AAA protease YME1L and OMA1 cleave OPA1 to balance mitochondrial fusion and fission. *J Cell Biol* 204: 919-929
- Ancey P-B, Contat C, Meylan E (2018) Glucose transporters in cancer – from tumor cells to the tumor microenvironment. *The FEBS Journal* 285: 2926-2943
- Anderson AJ, Jackson TD, Stroud DA, Stojanovski D (2019) Mitochondria: hubs for regulating cellular biochemistry: emerging concepts and networks. *Open Biology* 9: 190126
- Anderson CA, Blackstone C (2013) SUMO wrestling with Drp1 at mitochondria. *EMBO J* 32: 1496-1498
- Anderson GR, Wardell SE, Cakir M, Yip C, Ahn Y-r, Ali M, Yllanes AP, Chao CA, McDonnell DP, Wood KC (2018) Dysregulation of mitochondrial dynamics proteins are a targetable feature of human tumors. *Nature Communications* 9: 1677
- Arimura S-i, Yamamoto J, Aida GP, Nakazono M, Tsutsumi N (2004) Frequent fusion and fission of plant mitochondria with unequal nucleoid distribution. *Proc Natl Acad Sci U S A* 101: 7805
- Ashrafian H, Docherty L, Leo V, Towilson C, Neilan M, Steeples V, Lygate CA, Hough T, Townsend S, Williams D *et al* (2010) A mutation in the mitochondrial fission gene Dnm1l leads to cardiomyopathy. *PLoS genetics* 6: e1001000
- Ayanga BA, Badal SS, Wang Y, Galvan DL, Chang BH, Schumacker PT, Danesh FR (2016) Dynamin-Related Protein 1 Deficiency Improves Mitochondrial Fitness and Protects against Progression of Diabetic Nephropathy. *Journal of the American Society of Nephrology : JASN* 27: 2733-2747

- Bach D, Naon D, Pich S, Soriano FX, Vega N, Rieusset J, Laville M, Guillet C, Boirie Y, Wallberg-Henriksson H *et al* (2005) Expression of Mfn2, the Charcot-Marie-Tooth neuropathy type 2A gene, in human skeletal muscle: effects of type 2 diabetes, obesity, weight loss, and the regulatory role of tumor necrosis factor alpha and interleukin-6. *Diabetes* 54: 2685-2693
- Bach D, Pich S, Soriano FX, Vega N, Baumgartner B, Oriola J, Dugaard JR, Lloberas J, Camps M, Zierath JR *et al* (2003) Mitofusin-2 Determines Mitochondrial Network Architecture and Mitochondrial Metabolism: A NOVEL REGULATORY MECHANISM ALTERED IN OBESITY. *Journal of Biological Chemistry* 278: 17190-17197
- Baker MJ, Lampe PA, Stojanovski D, Korwitz A, Anand R, Tatsuta T, Langer T (2014) Stress-induced OMA1 activation and autocatalytic turnover regulate OPA1-dependent mitochondrial dynamics. *EMBO J* 33: 578-593
- Barsoum MJ, Yuan H, Gerencser AA, Liot G, Kushnareva Y, Gräber S, Kovacs I, Lee WD, Waggoner J, Cui J *et al* (2006) Nitric oxide-induced mitochondrial fission is regulated by dynamin-related GTPases in neurons. *EMBO J* 25: 3900-3911
- Basseri S, Austin RC (2012) Endoplasmic reticulum stress and lipid metabolism: mechanisms and therapeutic potential. *Biochem Res Int* 2012: 841362-841362
- Basu K, Lajoie D, Aumentado-Armstrong T, Chen J, Koning RI, Bossy B, Bostina M, Sik A, Bossy-Wetzel E, Rouiller I (2017) Molecular mechanism of DRP1 assembly studied in vitro by cryo-electron microscopy. *PLoS One* 12: e0179397-e0179397
- Beale EG (2013) Insulin signaling and insulin resistance. *Journal of investigative medicine : the official publication of the American Federation for Clinical Research* 61: 11-14
- Bereiter-Hahn J (1978) Intracellular motility of mitochondria: role of the inner compartment in migration and shape changes of mitochondria in XTH-cells. *J Cell Sci* 30: 99-115
- Beręsewicz M, Charzewski Ł, Krzyśko KA, Kochański A, Zabłocka B (2018) Molecular modelling of mitofusin 2 for a prediction for Charcot-Marie-Tooth 2A clinical severity. *Scientific Reports* 8: 16900
- Berry MN, Friend DS (1969) High-yield preparation of isolated rat liver parenchymal cells: a biochemical and fine structural study. *The Journal of cell biology* 43: 506-520
- Berthet A, Margolis EB, Zhang J, Hsieh I, Zhang J, Hnasko TS, Ahmad J, Edwards RH, Sesaki H, Huang EJ *et al* (2014) Loss of Mitochondrial Fission Depletes Axonal Mitochondria in Midbrain Dopamine Neurons. *The Journal of Neuroscience* 34: 14304-14317
- Betz C, Stracka D, Prescianotto-Baschong C, Frieden M, Demareux N, Hall MN (2013) mTOR complex 2-Akt signaling at mitochondria-associated endoplasmic reticulum membranes (MAM) regulates mitochondrial physiology. *Proceedings of the National Academy of Sciences* 110: 12526-12534
- Bleazard W, McCaffery JM, King EJ, Bale S, Mozdy A, Tieu Q, Nunnari J, Shaw JM (1999) The dynamin-related GTPase Dnm1 regulates mitochondrial fission in yeast. *Nat Cell Biol* 1: 298-304
- Boutant M, Joffraud M, Kulkarni SS, Garcia-Casarrubios E, Garcia-Roves PM, Ratajczak J, Fernandez-Marcos PJ, Valverde AM, Serrano M, Canto C (2015) SIRT1 enhances glucose tolerance by potentiating brown adipose tissue function. *Molecular metabolism* 4: 118-131
- Boutant M, Kulkarni SS, Joffraud M, Ratajczak J, Valera-Alberni M, Combe R, Zorzano A, Cantó C (2017) Mfn2 is critical for brown adipose tissue thermogenic function. *EMBO J* 36: 1543-1558

- Brandt T, Cavellini L, Kühlbrandt W, Cohen MM (2016) A mitofusin-dependent docking ring complex triggers mitochondrial fusion in vitro. *Elife* 5: e14618
- Bravo R, Vicencio JM, Parra V, Troncoso R, Munoz JP, Bui M, Quiroga C, Rodriguez AE, Verdejo HE, Ferreira J *et al* (2011) Increased ER–mitochondrial coupling promotes mitochondrial respiration and bioenergetics during early phases of ER stress. *Journal of Cell Science* 124: 2143
- Breitzig MT, Alleyn MD, Lockey RF, Kolliputi N (2018) A mitochondrial delicacy: dynamin-related protein 1 and mitochondrial dynamics. *American Journal of Physiology-Cell Physiology* 315: C80-C90
- Brocard PC, Hartig A (2014) *Molecular Machines Involved in Peroxisome Biogenesis and Maintenance*
- Camões F, Bonekamp NA, Delille HK, Schrader M (2009) Organelle dynamics and dysfunction: A closer link between peroxisomes and mitochondria. *Journal of inherited metabolic disease* 32: 163-180
- Cannon B, Nedergaard J (2004) Brown adipose tissue: function and physiological significance. *Physiological reviews* 84: 277-359
- Cannon B, Nedergaard J (2011) Nonshivering thermogenesis and its adequate measurement in metabolic studies. *The Journal of experimental biology* 214: 242-253
- Cantó C (2018) Mitochondrial Dynamics: Shaping Metabolic Adaptation. *International review of cell and molecular biology* 340: 129-167
- Canto C, Garcia-Roves PM (2015) High-Resolution Respirometry for Mitochondrial Characterization of Ex Vivo Mouse Tissues. *Current protocols in mouse biology* 5: 135-153
- Cereghetti GM, Stangherlin A, Martins de Brito O, Chang CR, Blackstone C, Bernardi P, Scorrano L (2008) Dephosphorylation by calcineurin regulates translocation of Drp1 to mitochondria. *Proc Natl Acad Sci U S A* 105: 15803-15808
- Chandel NS (2014) Mitochondria as signaling organelles. *BMC Biol* 12: 34-34
- Chang C-R, Manlandro CM, Arnoult D, Stadler J, Posey AE, Hill RB, Blackstone C (2010) A lethal de novo mutation in the middle domain of the dynamin-related GTPase Drp1 impairs higher order assembly and mitochondrial division. *The Journal of biological chemistry* 285: 32494-32503
- Chang CR, Blackstone C (2007) Cyclic AMP-dependent protein kinase phosphorylation of Drp1 regulates its GTPase activity and mitochondrial morphology. *The Journal of biological chemistry* 282: 21583-21587
- Chang CR, Blackstone C (2010) Dynamic regulation of mitochondrial fission through modification of the dynamin-related protein Drp1. *Annals of the New York Academy of Sciences* 1201: 34-39
- Chang YW, Chang YT, Wang Q, Lin JJ, Chen YJ, Chen CC (2013) Quantitative phosphoproteomic study of pressure-overloaded mouse heart reveals dynamin-related protein 1 as a modulator of cardiac hypertrophy. *Molecular & cellular proteomics : MCP* 12: 3094-3107
- Chen H, Detmer SA, Ewald AJ, Griffin EE, Fraser SE, Chan DC (2003) Mitofusins Mfn1 and Mfn2 coordinately regulate mitochondrial fusion and are essential for embryonic development. *J Cell Biol* 160: 189-200
- Chen TC, Hinton DR, Zidovetzki R, Hofman FM (1998) Up-regulation of the cAMP/PKA pathway inhibits proliferation, induces differentiation, and leads to apoptosis in malignant gliomas. *Laboratory investigation; a journal of technical methods and pathology* 78: 165-174

- Chen Z, Ma Y, Yang Q, Hu J, Feng J, Liang W, Ding G (2020) AKAP1 mediates high glucose-induced mitochondrial fission through the phosphorylation of Drp1 in podocytes. *Journal of Cellular Physiology*
- Cheng Z, Almeida FA (2014) Mitochondrial alteration in type 2 diabetes and obesity: an epigenetic link. *Cell Cycle* 13: 890-897
- Cho DH, Nakamura T, Fang J, Cieplak P, Godzik A, Gu Z, Lipton SA (2009) S-nitrosylation of Drp1 mediates beta-amyloid-related mitochondrial fission and neuronal injury. *Science* 324: 102-105
- Chou C-H, Lin C-C, Yang M-C, Wei C-C, Liao H-D, Lin R-C, Tu W-Y, Kao T-C, Hsu C-M, Cheng J-T *et al* (2012) GSK3 β -mediated Drp1 phosphorylation induced elongated mitochondrial morphology against oxidative stress. *PLoS One* 7: e49112-e49112
- Chouchani ET, Kajimura S (2019) Metabolic adaptation and maladaptation in adipose tissue. *Nature metabolism* 1: 189-200
- Claude A (1946) Fractionation of mammalian liver cells by differential centrifugation : I. Problems, methods, and preparation of extract. *J Exp Med* 84: 51-59
- Clayton ZS, McCurdy CE (2018) Short-term thermoneutral housing alters glucose metabolism and markers of adipose tissue browning in response to a high-fat diet in lean mice. *American Journal of Physiology-Regulatory, Integrative and Comparative Physiology* 315: R627-R637
- Cribbs JT, Strack S (2007) Reversible phosphorylation of Drp1 by cyclic AMP-dependent protein kinase and calcineurin regulates mitochondrial fission and cell death. *EMBO Rep* 8: 939-944
- Cui X, Nguyen NL, Zarebidaki E, Cao Q, Li F, Zha L, Bartness T, Shi H, Xue B (2016) Thermoneutrality decreases thermogenic program and promotes adiposity in high-fat diet-fed mice. *Physiological reports* 4
- Dai W, Jiang L (2019) Dysregulated Mitochondrial Dynamics and Metabolism in Obesity, Diabetes, and Cancer. *Frontiers in Endocrinology* 10
- Dai W, Wang G, Chwa J, Oh ME, Abeywardana T, Yang Y, Wang QA, Jiang L (2020) Mitochondrial division inhibitor (mdivi-1) decreases oxidative metabolism in cancer. *British Journal of Cancer* 122: 1288-1297
- Dar S, Pucadyil TJ (2017) The pleckstrin-homology domain of dynamin is dispensable for membrane constriction and fission. *Mol Biol Cell* 28: 152-160
- Davies VJ, Hollins AJ, Piechota MJ, Yip W, Davies JR, White KE, Nicols PP, Boulton ME, Votruba M (2007) Opa1 deficiency in a mouse model of autosomal dominant optic atrophy impairs mitochondrial morphology, optic nerve structure and visual function. *Human molecular genetics* 16: 1307-1318
- de Brito OM, Scorrano L (2008) Mitofusin 2 tethers endoplasmic reticulum to mitochondria. *Nature* 456: 605-610
- Del Dotto V, Mishra P, Vidoni S, Fogazza M, Maresca A, Caporali L, McCaffery JM, Cappelletti M, Baruffini E, Lenaers G *et al* (2017) OPA1 Isoforms in the Hierarchical Organization of Mitochondrial Functions. *Cell Rep* 19: 2557-2571
- Delettre C, Lenaers G, Griffoin JM, Gigarel N, Lorenzo C, Belenguer P, Pelloquin L, Grosgeorge J, Turc-Carel C, Perret E *et al* (2000) Nuclear gene OPA1, encoding a mitochondrial dynamin-related protein, is mutated in dominant optic atrophy. *Nature genetics* 26: 207-210
- Delille HK, Alves R, Schrader M (2009) Biogenesis of peroxisomes and mitochondria: linked by division. *Histochemistry and Cell Biology* 131: 441-446

- Deus CM, Yambire KF, Oliveira PJ, Raimundo N (2020) Mitochondria-Lysosome Crosstalk: From Physiology to Neurodegeneration. *Trends in Molecular Medicine* 26: 71-88
- Dickey AS, Strack S (2011) PKA/AKAP1 and PP2A/B β 2 Regulate Neuronal Morphogenesis via Drp1 Phosphorylation and Mitochondrial Bioenergetics. *The Journal of Neuroscience* 31: 15716-15726
- Dorn GW, 2nd (2015) Gone fission...: diverse consequences of cardiac Drp1 deficiency. *Circ Res* 116: 225-228
- Edwards G, Perkins GA, Kim K-Y, Kong Y, Lee Y, Choi S-H, Liu Y, Skowronska-Krawczyk D, Weinreb RN, Zangwill L *et al* (2020) Loss of AKAP1 triggers Drp1 dephosphorylation-mediated mitochondrial fission and loss in retinal ganglion cells. *Cell death & disease* 11: 254
- Ehse S, Raschke I, Mancuso G, Bernacchia A, Geimer S, Tondera D, Martinou JC, Westermann B, Rugarli EI, Langer T (2009) Regulation of OPA1 processing and mitochondrial fusion by m-AAA protease isoenzymes and OMA1. *J Cell Biol* 187: 1023-1036
- Elgass KD, Smith EA, LeGros MA, Larabell CA, Ryan MT (2015) Analysis of ER-mitochondria contacts using correlative fluorescence microscopy and soft X-ray tomography of mammalian cells. *Journal of Cell Science* 128: 2795
- Elisha Y, Kalchenko V, Kuznetsov Y, Geiger B (2018) Dual role of E-cadherin in the regulation of invasive collective migration of mammary carcinoma cells. *Scientific Reports* 8: 4986
- Ephrussi B (1950) The interplay of heredity and environment in the synthesis of respiratory enzymes in yeast. *Harvey lectures Series* 46: 45-67
- Ernster L, Schatz G (1981) Mitochondria: a historical review. *Journal of Cell Biology* 91: 227s-255s
- Fahrner JA, Liu R, Perry MS, Klein J, Chan DC (2016) A novel de novo dominant negative mutation in DNM1L impairs mitochondrial fission and presents as childhood epileptic encephalopathy. *American journal of medical genetics Part A* 170: 2002-2011
- Favaro G, Romanello V, Varanita T, Andrea Desbats M, Morbidoni V, Tezze C, Albiero M, Canato M, Gherardi G, De Stefani D *et al* (2019) DRP1-mediated mitochondrial shape controls calcium homeostasis and muscle mass. *Nature Communications* 10: 2576
- Fealy CE, Mulya A, Lai N, Kirwan JP (2014) Exercise training decreases activation of the mitochondrial fission protein dynamin-related protein-1 in insulin-resistant human skeletal muscle. *Journal of Applied Physiology* 117: 239-245
- Ferré M, Amati-Bonneau P, Tourmen Y, Malthiery Y, Reynier P (2005) eOPA1: an online database for OPA1 mutations. *Hum Mutat* 25: 423-428
- Ferretta A, Maida I, Guida S, Azzariti A, Porcelli L, Tommasi S, Zanna P, Cocco T, Guida M, Guida G (2016) New insight into the role of metabolic reprogramming in melanoma cells harboring BRAF mutations. *Biochimica et Biophysica Acta (BBA) - Molecular Cell Research* 1863: 2710-2718
- Figuroa-Romero C, Iñiguez-Lluhí JA, Stadler J, Chang C-R, Arnoult D, Keller PJ, Hong Y, Blackstone C, Feldman EL (2009) SUMOylation of the mitochondrial fission protein Drp1 occurs at multiple nonconsensus sites within the B domain and is linked to its activity cycle. *FASEB J* 23: 3917-3927
- Fischer AW, Cannon B, Nedergaard J (2018) Optimal housing temperatures for mice to mimic the thermal environment of humans: An experimental study. *Molecular Metabolism* 7: 161-170

- Flippo KH, Strack S (2017) Mitochondrial dynamics in neuronal injury, development and plasticity. *J Cell Sci* 130: 671-681
- Fonseca TB, Sánchez-Guerrero Á, Milosevic I, Raimundo N (2019) Mitochondrial fission requires DRP1 but not dynamins. *Nature* 570: E34-E42
- Francy CA, Clinton RW, Fröhlich C, Murphy C, Mears JA (2017) Cryo-EM Studies of Drp1 Reveal Cardiolipin Interactions that Activate the Helical Oligomer. *Scientific Reports* 7: 10744
- Frederic J, Chevremont M (1952) [Investigations on the chondriosomes of living cells by phase contrast microscopy and microcinematography]. *Archives de biologie* 63: 109-131
- Friedman JR, Lackner LL, West M, DiBenedetto JR, Nunnari J, Voeltz GK (2011) ER tubules mark sites of mitochondrial division. *Science* 334: 358-362
- Fröhlich C, Grabiger S, Schwefel D, Faelber K, Rosenbaum E, Mears J, Rocks O, Daumke O (2013) Structural insights into oligomerization and mitochondrial remodelling of dynamin 1-like protein. *EMBO J* 32: 1280-1292
- Gall JM, Wang Z, Liesa M, Molina A, Havasi A, Schwartz JH, Shirihai O, Borkan SC, Bonaglio RGB (2012) Role of mitofusin 2 in the renal stress response. *PLoS One* 7: e31074-e31074
- Galvan DL, Long J, Green N, Chang BH, Lin JS, Schumacker P, Truong LD, Overbeek P, Danesh FR (2019) Drp1S600 phosphorylation regulates mitochondrial fission and progression of nephropathy in diabetic mice. *The Journal of clinical investigation* 129: 2807-2823
- Gammie AE, Kurihara LJ, Vallee RB, Rose MD (1995) DNM1, a dynamin-related gene, participates in endosomal trafficking in yeast. *Journal of Cell Biology* 130: 553-566
- Gandre-Babbe S, van der Bliek AM (2008) The novel tail-anchored membrane protein Mff controls mitochondrial and peroxisomal fission in mammalian cells. *Mol Biol Cell* 19: 2402-2412
- Gawlowski T, Suarez J, Scott B, Torres-Gonzalez M, Wang H, Schwappacher R, Han X, Yates JR, 3rd, Hoshijima M, Dillmann W (2012) Modulation of dynamin-related protein 1 (DRP1) function by increased O-linked- β -N-acetylglucosamine modification (O-GlcNAc) in cardiac myocytes. *The Journal of biological chemistry* 287: 30024-30034
- Gegg ME, Cooper JM, Chau KY, Rojo M, Schapira AH, Taanman JW (2010) Mitofusin 1 and mitofusin 2 are ubiquitinated in a PINK1/parkin-dependent manner upon induction of mitophagy. *Human molecular genetics* 19: 4861-4870
- Gerber S, Charif M, Chevrollier A, Chaumette T, Angebault C, Kane MS, Paris A, Alban J, Quiles M, Delettre C *et al* (2017) Mutations in DNM1L, as in OPA1, result in dominant optic atrophy despite opposite effects on mitochondrial fusion and fission. *Brain : a journal of neurology* 140: 2586-2596
- Gomes LC, Di Benedetto G, Scorrano L (2011) During autophagy mitochondria elongate, are spared from degradation and sustain cell viability. *Nat Cell Biol* 13: 589-598
- Gordaliza-Alaguero I, Cantó C, Zorzano A (2019) Metabolic implications of organelle-mitochondria communication. *EMBO Rep* 20: e47928
- Gouspillou G, Hepple RT (2016) Editorial: Mitochondria in Skeletal Muscle Health, Aging and Diseases. *Front Physiol* 7: 446-446

- Guerrero C, Pesce L, Lecuona E, Ridge KM, Sznajder JJ (2002) Dopamine activates ERKs in alveolar epithelial cells via Ras-PKC-dependent and Grb2/Sos-independent mechanisms. *American journal of physiology Lung cellular and molecular physiology* 282: L1099-1107
- Guo C, Hildick KL, Luo J, Dearden L, Wilkinson KA, Henley JM (2013) SENP3-mediated deSUMOylation of dynamin-related protein 1 promotes cell death following ischaemia. *EMBO J* 32: 1514-1528
- Gützkow KB, Naderi S, Blomhoff HK (2002) Forskolin-mediated G1 arrest in acute lymphoblastic leukaemia cells: phosphorylated pRB sequesters E2Fs. *Journal of cell science* 115: 1073-1082
- Hales KG, Fuller MT (1997) Developmentally regulated mitochondrial fusion mediated by a conserved, novel, predicted GTPase. *Cell* 90: 121-129
- Han J, Kaufman RJ (2016) The role of ER stress in lipid metabolism and lipotoxicity. *Journal of lipid research* 57: 1329-1338
- Han X-J, Lu Y-F, Li S-A, Kaitsuka T, Sato Y, Tomizawa K, Nairn AC, Takei K, Matsui H, Matsushita M (2008) CaM kinase I α -induced phosphorylation of Drp1 regulates mitochondrial morphology. *J Cell Biol* 182: 573-585
- Han XJ, Yang ZJ, Jiang LP, Wei YF, Liao MF, Qian Y, Li Y, Huang X, Wang JB, Xin HB *et al* (2015) Mitochondrial dynamics regulates hypoxia-induced migration and antineoplastic activity of cisplatin in breast cancer cells. *International journal of oncology* 46: 691-700
- Harder Z, Zunino R, McBride H (2004) Sumo1 conjugates mitochondrial substrates and participates in mitochondrial fission. *Current biology : CB* 14: 340-345
- Hatch AL, Gurel PS, Higgs HN (2014) Novel roles for actin in mitochondrial fission. *Journal of Cell Science* 127: 4549
- Haun F, Nakamura T, Shiu AD, Cho DH, Tsunemi T, Holland EA, La Spada AR, Lipton SA (2013) S-nitrosylation of dynamin-related protein 1 mediates mutant huntingtin-induced mitochondrial fragmentation and neuronal injury in Huntington's disease. *Antioxidants & redox signaling* 19: 1173-1184
- Hayes JD, Dinkova-Kostova AT, Tew KD (2020) Oxidative Stress in Cancer. *Cancer cell*
- Head B, Griparic L, Amiri M, Gandre-Babbe S, van der Bliek AM (2009) Inducible proteolytic inactivation of OPA1 mediated by the OMA1 protease in mammalian cells. *J Cell Biol* 187: 959-966
- Hennings TG, Chopra DG, DeLeon ER, VanDeusen HR, Sesaki H, Merrins MJ, Ku GM (2018) In Vivo Deletion of β -Cell Drp1 Impairs Insulin Secretion Without Affecting Islet Oxygen Consumption. *Endocrinology* 159: 3245-3256
- Hermann GJ, Thatcher JW, Mills JP, Hales KG, Fuller MT, Nunnari J, Shaw JM (1998) Mitochondrial fusion in yeast requires the transmembrane GTPase Fzo1p. *J Cell Biol* 143: 359-373
- Hu Q, Zhang H, Gutiérrez Cortés N, Wu D, Wang P, Zhang J, Mattison Julie A, Smith E, Bettcher Lisa F, Wang M *et al* (2020) Increased Drp1 Acetylation by Lipid Overload Induces Cardiomyocyte Death and Heart Dysfunction. *Circulation Research* 126: 456-470
- Huang H, Gao Q, Peng X, Choi SY, Sarma K, Ren H, Morris AJ, Frohman MA (2011) piRNA-associated germline nuage formation and spermatogenesis require MitoPLD profusogenic mitochondrial-surface lipid signaling. *Developmental cell* 20: 376-387
- Huang S, Wang Y, Gan X, Fang D, Zhong C, Wu L, Hu G, Sosunov AA, McKhann GM, Yu H *et al* (2015) Drp1-Mediated Mitochondrial Abnormalities Link to Synaptic Injury in Diabetes Model. *Diabetes* 64: 1728

- Imoto M, Tachibana I, Urrutia R (1998) Identification and functional characterization of a novel human protein highly related to the yeast dynamin-like GTPase Vps1p. *Journal of Cell Science* 111: 1341
- Ishihara N, Eura Y, Mihara K (2004) Mitofusin 1 and 2 play distinct roles in mitochondrial fusion reactions via GTPase activity. *Journal of Cell Science* 117: 6535
- Ishihara N, Nomura M, Jofuku A, Kato H, Suzuki SO, Masuda K, Otera H, Nakanishi Y, Nonaka I, Goto Y *et al* (2009) Mitochondrial fission factor Drp1 is essential for embryonic development and synapse formation in mice. *Nat Cell Biol* 11: 958-966
- Itoh K, Adachi Y, Yamada T, Suzuki TL, Otomo T, McBride HM, Yoshimori T, Iijima M, Sesaki H (2018) A brain-enriched Drp1 isoform associates with lysosomes, late endosomes, and the plasma membrane. *The Journal of biological chemistry* 293: 11809-11822
- Itoh K, Murata D, Kato T, Yamada T, Araki Y, Saito A, Adachi Y, Igarashi A, Li S, Pletnikov M *et al* (2019) Brain-specific Drp1 regulates postsynaptic endocytosis and dendrite formation independently of mitochondrial division. *Elife* 8
- Jagendorf AT, Uribe E (1966) ATP formation caused by acid-base transition of spinach chloroplasts. *Proc Natl Acad Sci U S A* 55: 170-177
- James DI, Parone PA, Mattenberger Y, Martinou JC (2003) hFis1, a novel component of the mammalian mitochondrial fission machinery. *The Journal of biological chemistry* 278: 36373-36379
- Jarc E, Petan T (2019) Lipid Droplets and the Management of Cellular Stress. *The Yale journal of biology and medicine* 92: 435-452
- Jha P, Wang X, Auwerx J (2016) Analysis of Mitochondrial Respiratory Chain Supercomplexes Using Blue Native Polyacrylamide Gel Electrophoresis (BN-PAGE). *Curr Protoc Mouse Biol* 6: 1-14
- Jhun BS, J OU, Adaniya SM, Cypress MW, Yoon Y (2018) Adrenergic Regulation of Drp1-Driven Mitochondrial Fission in Cardiac Physio-Pathology. *Antioxidants (Basel)* 7
- Jiang LQ, Garcia-Roves PM, de Castro Barbosa T, Zierath JR (2010) Constitutively active calcineurin in skeletal muscle increases endurance performance and mitochondrial respiratory capacity. *American journal of physiology Endocrinology and metabolism* 298: E8-e16
- Joshi AU, Saw NL, Shamloo M, Mochly-Rosen D (2017) Drp1/Fis1 interaction mediates mitochondrial dysfunction, bioenergetic failure and cognitive decline in Alzheimer's disease. *Oncotarget* 9
- Joshi AU, Saw NL, Vogel H, Cunningham AD, Shamloo M, Mochly-Rosen D (2018) Inhibition of Drp1/Fis1 interaction slows progression of amyotrophic lateral sclerosis. *EMBO Mol Med* 10: e8166
- Kabra UD, Pfuhmann K, Migliorini A, Keipert S, Lamp D, Korsgren O, Gegg M, Woods SC, Pflugger PT, Lickert H *et al* (2017) Direct Substrate Delivery Into Mitochondrial Fission-Deficient Pancreatic Islets Rescues Insulin Secretion. *Diabetes* 66: 1247-1257
- Kalia R, Wang RY, Yusuf A, Thomas PV, Agard DA, Shaw JM, Frost A (2018) Structural basis of mitochondrial receptor binding and constriction by DRP1. *Nature* 558: 401-405
- Karbowski M, Neutzner A, Youle RJ (2007) The mitochondrial E3 ubiquitin ligase MARCH5 is required for Drp1 dependent mitochondrial division. *J Cell Biol* 178: 71-84

- Kashatus JA, Nascimento A, Myers LJ, Sher A, Byrne FL, Hoehn KL, Counter CM, Kashatus DF (2015) Erk2 phosphorylation of Drp1 promotes mitochondrial fission and MAPK-driven tumor growth. *Mol Cell* 57: 537-551
- Kennedy EP, Lehninger AL (1949) Oxidation of fatty acids and tricarboxylic acid cycle intermediates by isolated rat liver mitochondria. *The Journal of biological chemistry* 179: 957-972
- Kim DI, Lee KH, Gabr AA, Choi GE, Kim JS, Ko SH, Han HJ (2016) A β -Induced Drp1 phosphorylation through Akt activation promotes excessive mitochondrial fission leading to neuronal apoptosis. *Biochimica et Biophysica Acta (BBA) - Molecular Cell Research* 1863: 2820-2834
- Kingsbury BF (1912) Cytoplasmic fixation. *The Anatomical Record* 6: 39-52
- Kobayashi S, Tanaka A, Fujiki Y (2007) Fis1, DLP1, and Pex11p coordinately regulate peroxisome morphogenesis. *Experimental cell research* 313: 1675-1686
- Koch A, Thiemann M, Grabenbauer M, Yoon Y, McNiven MA, Schrader M (2003) Dynamin-like Protein 1 Is Involved in Peroxisomal Fission. *Journal of Biological Chemistry* 278: 8597-8605
- Koch A, Yoon Y, Bonekamp NA, McNiven MA, Schrader M (2005) A role for Fis1 in both mitochondrial and peroxisomal fission in mammalian cells. *Mol Biol Cell* 16: 5077-5086
- Koch J, Brocard C (2012) PEX11 proteins attract Mff and human Fis1 to coordinate peroxisomal fission. *Journal of Cell Science* 125: 3813
- Koch J, Feichtinger RG, Freisinger P, Pies M, Schrödl F, Iuso A, Sperl W, Mayr JA, Prokisch H, Haack TB (2016) Disturbed mitochondrial and peroxisomal dynamics due to loss of MFF causes Leigh-like encephalopathy, optic atrophy and peripheral neuropathy. *Journal of medical genetics* 53: 270-278
- Korobova F, Ramabhadran V, Higgs HN (2013) An actin-dependent step in mitochondrial fission mediated by the ER-associated formin INF2. *Science* 339: 464-467
- Koshiha T, Bashiruddin N, Kawabata S (2011) Mitochondria and antiviral innate immunity. *Int J Biochem Mol Biol* 2: 257-262
- Kulkarni SS, Joffraud M, Boutant M, Ratajczak J, Gao AW, MacLachlan C, Hernandez-Alvarez MI, Raymond F, Metairon S, Descombes P *et al* (2016) Mfn1 Deficiency in the Liver Protects Against Diet-Induced Insulin Resistance and Enhances the Hypoglycemic Effect of Metformin. *Diabetes* 65: 3552
- Küntzel H, Noll H (1967) Mitochondrial and cytoplasmic polysomes from *Neurospora crassa*. *Nature* 215: 1340-1345
- Labrousse AM, Zappaterra MD, Rube DA, van der Bliek AM (1999) *C. elegans* Dynamin-Related Protein DRP-1 Controls Severing of the Mitochondrial Outer Membrane. *Molecular Cell* 4: 815-826
- Larrea D, Pera M, Gonnelli A, Quintana-Cabrera R, Akman HO, Guardia-Laguarta C, Velasco KR, Area-Gomez E, Dal Bello F, De Stefani D *et al* (2019) MFN2 mutations in Charcot-Marie-Tooth disease alter mitochondria-associated ER membrane function but do not impair bioenergetics. *Human molecular genetics* 28: 1782-1800
- Lavine RL, Voyles N, Perrino PV, Recant L (1975) The effect of fasting on tissue cyclic cAMP and plasma glucagon in the obese hyperglycemic mouse. *Endocrinology* 97: 615-620
- Lee D-s, Kim J-E (2018) PDI-mediated S-nitrosylation of DRP1 facilitates DRP1-S616 phosphorylation and mitochondrial fission in CA1 neurons. *Cell death & disease* 9: 869

- Lee JE, Westrate LM, Wu H, Page C, Voeltz GK (2016) Multiple dynamin family members collaborate to drive mitochondrial division. *Nature* 540: 139-143
- Lee YJ, Jeong SY, Karbowski M, Smith CL, Youle RJ (2004) Roles of the mammalian mitochondrial fission and fusion mediators Fis1, Drp1, and Opa1 in apoptosis. *Mol Biol Cell* 15: 5001-5011
- Lewis MR, Lewis WH (1915) Mitochondria (and other cytoplasmic structures) in tissue cultures. *American Journal of Anatomy* 27: 339-401
- Lewis SC, Uchiyama LF, Nunnari J (2016) ER-mitochondria contacts couple mtDNA synthesis with mitochondrial division in human cells. *Science* 353: aaf5549
- Li H, Meng Q, Xiao F, Chen S, Du Y, Yu J, Wang C, Guo F (2011) ATF4 deficiency protects mice from high-carbohydrate-diet-induced liver steatosis. *The Biochemical journal* 438: 283-289
- Li J, Huang Q, Long X, Guo X, Sun X, Jin X, Li Z, Ren T, Yuan P, Huang X *et al* (2017) Mitochondrial elongation-mediated glucose metabolism reprogramming is essential for tumour cell survival during energy stress. *Oncogene* 36: 4901-4912
- Li X, Gould SJ (2003) The Dynamin-like GTPase DLP1 Is Essential for Peroxisome Division and Is Recruited to Peroxisomes in Part by PEX11. *Journal of Biological Chemistry* 278: 17012-17020
- Liesa M, Borda-d'Água B, Medina-Gómez G, Lelliott CJ, Paz JC, Rojo M, Palacín M, Vidal-Puig A, Zorzano A (2008) Mitochondrial Fusion Is Increased by the Nuclear Coactivator PGC-1 β . *PLoS One* 3: e3613
- Liesa M, Shirihaï OS (2013) Mitochondrial dynamics in the regulation of nutrient utilization and energy expenditure. *Cell metabolism* 17: 491-506
- Lismont C, Nordgren M, Van Veldhoven PP, Fransen M (2015) Redox interplay between mitochondria and peroxisomes. *Front Cell Dev Biol* 3: 35
- Liu R, Chan DC (2015) The mitochondrial fission receptor Mff selectively recruits oligomerized Drp1. *Mol Biol Cell* 26: 4466-4477
- Liu W, Duan X, Xu L, Shang W, Zhao J, Wang L, Li J-C, Chen C-H, Liu J-P, Tong C (2020a) Chchd2 regulates mitochondrial morphology by modulating the levels of Opa1. *Cell Death & Differentiation* 27: 2014-2029
- Liu X, Kim CN, Yang J, Jemmerson R, Wang X (1996) Induction of Apoptotic Program in Cell-Free Extracts: Requirement for dATP and Cytochrome c. *Cell* 86: 147-157
- Liu YJ, McIntyre RL, Janssens GE, Houtkooper RH (2020b) Mitochondrial fission and fusion: A dynamic role in aging and potential target for age-related disease. *Mechanisms of Ageing and Development* 186: 111212
- Losón OC, Song Z, Chen H, Chan DC (2013) Fis1, Mff, MiD49, and MiD51 mediate Drp1 recruitment in mitochondrial fission. *Mol Biol Cell* 24: 659-667
- Lu B, Kennedy B, Clinton RW, Wang EJ, McHugh D, Stepanyants N, Macdonald PJ, Mears JA, Qi X, Ramachandran R (2018) Steric interference from intrinsically disordered regions controls dynamin-related protein 1 self-assembly during mitochondrial fission. *Scientific Reports* 8: 10879
- Lutz AK, Exner N, Fett ME, Schlehe JS, Kloos K, Lämmermann K, Brunner B, Kurz-Drexler A, Vogel F, Reichert AS *et al* (2009) Loss of parkin or PINK1 function increases Drp1-dependent mitochondrial fragmentation. *The Journal of biological chemistry* 284: 22938-22951

- Ma R, Ma L, Weng W, Wang Y, Liu H, Guo R, Gao Y, Tu J, Xu T-L, Cheng J *et al* (2020) DUSP6 SUMOylation protects cells from oxidative damage via direct regulation of Drp1 dephosphorylation. *Science Advances* 6: eaaz0361
- Macdonald PJ, Francy CA, Stepanyants N, Lehman L, Baglio A, Mears JA, Qi X, Ramachandran R (2016) Distinct Splice Variants of Dynamin-related Protein 1 Differentially Utilize Mitochondrial Fission Factor as an Effector of Cooperative GTPase Activity. *The Journal of biological chemistry* 291: 493-507
- Maloney SK, Fuller A, Mitchell D, Gordon C, Overton JM (2014) Translating animal model research: does it matter that our rodents are cold? *Physiology (Bethesda, Md)* 29: 413-420
- Manczak M, Calkins MJ, Reddy PH (2011) Impaired mitochondrial dynamics and abnormal interaction of amyloid beta with mitochondrial protein Drp1 in neurons from patients with Alzheimer's disease: implications for neuronal damage. *Human molecular genetics* 20: 2495-2509
- Manor U, Bartholomew S, Golani G, Christenson E, Kozlov M, Higgs H, Spudich J, Lippincott-Schwartz J (2015) A mitochondria-anchored isoform of the actin-nucleating spire protein regulates mitochondrial division. *Elife* 4
- Marelli C, Amati-Bonneau P, Reynier P, Layet V, Layet A, Stevanin G, Brissaud E, Bonneau D, Durr A, Brice A (2011) Heterozygous OPA1 mutations in Behr syndrome. *Brain : a journal of neurology* 134: e169; author reply e170
- Masin M, Vazquez J, Rossi S, Groeneveld S, Samson N, Schwalie PC, Deplancke B, Frawley LE, Gouttenoire J, Moradpour D *et al* (2014) GLUT3 is induced during epithelial-mesenchymal transition and promotes tumor cell proliferation in non-small cell lung cancer. *Cancer Metab* 2: 11-11
- McKie GL, Medak KD, Knuth CM, Shamshoum H, Townsend LK, Peppler WT, Wright DC (2019) Housing temperature affects the acute and chronic metabolic adaptations to exercise in mice. *The Journal of Physiology* 597: 4581-4600
- McWilliams TG, Muqit MM (2017) PINK1 and Parkin: emerging themes in mitochondrial homeostasis. *Current opinion in cell biology* 45: 83-91
- Meng N, Glorieux C, Zhang Y, Liang L, Zeng P, Lu W, Huang P (2019) Oncogenic K-ras Induces Mitochondrial OPA3 Expression to Promote Energy Metabolism in Pancreatic Cancer Cells. *Cancers (Basel)* 12: 65
- Merkin J, Russell C, Chen P, Burge CB (2012) Evolutionary dynamics of gene and isoform regulation in Mammalian tissues. *Science* 338: 1593-1599
- Merrill RA, Dagda RK, Dickey AS, Cribbs JT, Green SH, Usachev YM, Strack S (2011) Mechanism of Neuroprotective Mitochondrial Remodeling by PKA/AKAP1. *PLOS Biology* 9: e1000612
- Mishra P, Carelli V, Manfredi G, Chan DC (2014) Proteolytic cleavage of Opa1 stimulates mitochondrial inner membrane fusion and couples fusion to oxidative phosphorylation. *Cell metabolism* 19: 630-641
- Mitchell P (1961) Coupling of Phosphorylation to Electron and Hydrogen Transfer by a Chemi-Osmotic type of Mechanism. *Nature* 191: 144-148
- Molina AJA, Wikstrom JD, Stiles L, Las G, Mohamed H, Elorza A, Walzer G, Twig G, Katz S, Corkey BE *et al* (2009) Mitochondrial networking protects beta-cells from nutrient-induced apoptosis. *Diabetes* 58: 2303-2315
- Mourier A, Motori E, Brandt T, Lagouge M, Atanassov I, Galinier A, Rappl G, Brodesser S, Hultenby K, Dieterich C *et al* (2015) Mitofusin 2 is required to maintain mitochondrial coenzyme Q levels. *J Cell Biol* 208: 429-442
- Murley A, Nunnari J (2016) The Emerging Network of Mitochondria-Organelle Contacts. *Molecular Cell* 61: 648-653

- Nagashima S, Tábara L-C, Tilokani L, Paupe V, Anand H, Pogson JH, Zunino R, McBride HM, Prudent J (2020) Golgi-derived PI4-containing vesicles drive late steps of mitochondrial division. *Science* 367: 1366
- Nagdas S, Kashatus DF (2017) The Interplay between Oncogenic Signaling Networks and Mitochondrial Dynamics. *Antioxidants (Basel)* 6: 33
- Nagdas S, Kashatus JA, Nascimento A, Hussain SS, Trainor RE, Pollock SR, Adair SJ, Michaels AD, Sesaki H, Stelow EB *et al* (2019) Drp1 Promotes KRas-Driven Metabolic Changes to Drive Pancreatic Tumor Growth. *Cell Rep* 28: 1845-1859.e1845
- Nakamura N, Kimura Y, Tokuda M, Honda S, Hirose S (2006) MARCH-V is a novel mitofusin 2- and Drp1-binding protein able to change mitochondrial morphology. *EMBO Rep* 7: 1019-1022
- Oettinghaus B, Schulz JM, Restelli LM, Licci M, Savoia C, Schmidt A, Schmitt K, Grimm A, Morè L, Hench J *et al* (2016) Synaptic dysfunction, memory deficits and hippocampal atrophy due to ablation of mitochondrial fission in adult forebrain neurons. *Cell death and differentiation* 23: 18-28
- Olichon A, Emorine LJ, Descoins E, Pelloquin L, Brichese L, Gas N, Guillou E, Delettre C, Valette A, Hamel CP *et al* (2002) The human dynamin-related protein OPA1 is anchored to the mitochondrial inner membrane facing the inter-membrane space. *FEBS letters* 523: 171-176
- Olichon A, Guillou E, Delettre C, Landes T, Arnauné-Pelloquin L, Emorine LJ, Mils V, Daloyau M, Hamel C, Amati-Bonneau P *et al* (2006) Mitochondrial dynamics and disease, OPA1. *Biochimica et Biophysica Acta (BBA) - Molecular Cell Research* 1763: 500-509
- Oliver D, Reddy PH (2019) Dynamics of Dynamin-Related Protein 1 in Alzheimer's Disease and Other Neurodegenerative Diseases. *Cells* 8
- Ormazabal V, Nair S, Elfeky O, Aguayo C, Salomon C, Zuñiga FA (2018) Association between insulin resistance and the development of cardiovascular disease. *Cardiovascular Diabetology* 17: 122
- Osellame LD, Singh AP, Stroud DA, Palmer CS, Stojanovski D, Ramachandran R, Ryan MT (2016) Cooperative and independent roles of the Drp1 adaptors Mff, MiD49 and MiD51 in mitochondrial fission. *Journal of Cell Science* 129: 2170
- Otera H, Ishihara N, Mihara K (2013) New insights into the function and regulation of mitochondrial fission. *Biochimica et Biophysica Acta (BBA) - Molecular Cell Research* 1833: 1256-1268
- Otera H, Wang C, Cleland MM, Setoguchi K, Yokota S, Youle RJ, Mihara K (2010) Mff is an essential factor for mitochondrial recruitment of Drp1 during mitochondrial fission in mammalian cells. *Journal of Cell Biology* 191: 1141-1158
- Otsuga D, Keegan BR, Brisch E, Thatcher JW, Hermann GJ, Bleazard W, Shaw JM (1998) The Dynamin-related GTPase, Dnm1p, Controls Mitochondrial Morphology in Yeast. *Journal of Cell Biology* 143: 333-349
- Otto C, Fuchs I, Kauselmann G, Kern H, Zevnik B, Andreasen P, Schwarz G, Altmann H, Klewer M, Schoor M *et al* (2009) GPR30 does not mediate estrogenic responses in reproductive organs in mice. *Biology of reproduction* 80: 34-41
- Ouellet V, Labbé SM, Blondin DP, Phoenix S, Guérin B, Haman F, Turcotte EE, Richard D, Carpentier AC (2012) Brown adipose tissue oxidative metabolism contributes to energy expenditure during acute cold exposure in humans. *The Journal of clinical investigation* 122: 545-552

- Palade GE (1953) An electron microscope study of the mitochondrial structure. *The journal of histochemistry and cytochemistry : official journal of the Histochemistry Society* 1: 188-211
- Palmer CS, Elgass KD, Parton RG, Osellame LD, Stojanovski D, Ryan MT (2013) Adaptor proteins MiD49 and MiD51 can act independently of Mff and Fis1 in Drp1 recruitment and are specific for mitochondrial fission. *The Journal of biological chemistry* 288: 27584-27593
- Palmer CS, Osellame LD, Laine D, Koutsopoulos OS, Frazier AE, Ryan MT (2011) MiD49 and MiD51, new components of the mitochondrial fission machinery. *EMBO Rep* 12: 565-573
- Patten DA, Wong J, Khacho M, Soubannier V, Mailloux RJ, Pilon-Larose K, MacLaurin JG, Park DS, McBride HM, Trinkle-Mulcahy L *et al* (2014) OPA1-dependent cristae modulation is essential for cellular adaptation to metabolic demand. *EMBO J* 33: 2676-2691
- Pearson GW (2019) Control of Invasion by Epithelial-to-Mesenchymal Transition Programs during Metastasis. *J Clin Med* 8: 646
- Pfluger PT, Kabra DG, Aichler M, Schriever SC, Pfuhlmann K, García VC, Lehti M, Weber J, Kutschke M, Rozman J *et al* (2015) Calcineurin Links Mitochondrial Elongation with Energy Metabolism. *Cell metabolism* 22: 838-850
- Phan LM, Yeung S-CJ, Lee M-H (2014) Cancer metabolic reprogramming: importance, main features, and potentials for precise targeted anti-cancer therapies. *Cancer Biol Med* 11: 1-19
- Porporato PE, Filigheddu N, Pedro JMB-S, Kroemer G, Galluzzi L (2018) Mitochondrial metabolism and cancer. *Cell Research* 28: 265-280
- Prudent J, Zunino R, Sugiura A, Mattie S, Shore Gordon C, McBride Heidi M (2015) MAPL SUMOylation of Drp1 Stabilizes an ER/Mitochondrial Platform Required for Cell Death. *Molecular Cell* 59: 941-955
- Qi X, Disatnik M-H, Shen N, Sobel RA, Mochly-Rosen D (2011) Aberrant mitochondrial fission in neurons induced by protein kinase C{delta} under oxidative stress conditions in vivo. *Mol Biol Cell* 22: 256-265
- Qi X, Qvit N, Su YC, Mochly-Rosen D (2013) A novel Drp1 inhibitor diminishes aberrant mitochondrial fission and neurotoxicity. *J Cell Sci* 126: 789-802
- Qi Z, Huang Z, Xie F, Chen L (2019) Dynamin-related protein 1: A critical protein in the pathogenesis of neural system dysfunctions and neurodegenerative diseases. *J Cell Physiol* 234: 10032-10046
- Quiros PM, Goyal A, Jha P, Auwerx J (2017) Analysis of mtDNA/nDNA Ratio in Mice. *Curr Protoc Mouse Biol* 7: 47-54
- Rambold AS, Kostecky B, Elia N, Lippincott-Schwartz J (2011) Tubular network formation protects mitochondria from autophagosomal degradation during nutrient starvation. *Proceedings of the National Academy of Sciences* 108: 10190-10195
- Raun SH, Henriquez-Olguín C, Karavaeva I, Ali M, Møller LLV, Kot W, Castro-Mejía JL, Nielsen DS, Gerhart-Hines Z, Richter EA *et al* (2020) Housing temperature influences exercise training adaptations in mice. *Nature Communications* 11: 1560
- Rehman J, Zhang HJ, Toth PT, Zhang Y, Marsboom G, Hong Z, Salgia R, Husain AN, Wietholt C, Archer SL (2012) Inhibition of mitochondrial fission prevents cell cycle progression in lung cancer. *The FASEB Journal* 26: 2175-2186

- Reinhardt F, Schultz J, Waterstradt R, Baltrusch S (2016) Drp1 guarding of the mitochondrial network is important for glucose-stimulated insulin secretion in pancreatic beta cells. *Biochemical and biophysical research communications* 474: 646-651
- Restelli LM, Oettinghaus B, Halliday M, Agca C, Licci M, Sironi L, Savoia C, Hench J, Tolnay M, Neutzner A *et al* (2018) Neuronal Mitochondrial Dysfunction Activates the Integrated Stress Response to Induce Fibroblast Growth Factor 21. *Cell Rep* 24: 1407-1414
- Rieusset J (2018) The role of endoplasmic reticulum-mitochondria contact sites in the control of glucose homeostasis: an update. *Cell death & disease* 9: 388
- Rippe C, Berger K, Böiers C, Ricquier D, Erlanson-Albertsson C (2000) Effect of high-fat diet, surrounding temperature, and enterostatin on uncoupling protein gene expression. *American Journal of Physiology-Endocrinology and Metabolism* 279: E293-E300
- Rizza S, Cardaci S, Montagna C, Di Giacomo G, De Zio D, Bordi M, Maiani E, Campello S, Borreca A, Puca AA *et al* (2018) S-nitrosylation drives cell senescence and aging in mammals by controlling mitochondrial dynamics and mitophagy. *Proceedings of the National Academy of Sciences* 115: E3388-E3397
- Romanello V, Guadagnin E, Gomes L, Roder I, Sandri C, Petersen Y, Milan G, Masiero E, Del Piccolo P, Foretz M *et al* (2010) Mitochondrial fission and remodelling contributes to muscle atrophy. *EMBO J* 29: 1774-1785
- Rosdah AA, Smiles WJ, Oakhill JS, Scott JW, Langendorf CG, Delbridge LMD, Holien JK, Lim SY (2020) New perspectives on the role of Drp1 isoforms in regulating mitochondrial pathophysiology. *Pharmacology & Therapeutics* 213: 107594
- Ruan Y, Li H, Zhang K, Jian F, Tang J, Song Z (2013) Loss of Yme1L perturbs mitochondrial dynamics. *Cell death & disease* 4: e896
- Salvadó L, Palomer X, Barroso E, Vázquez-Carrera M (2015) Targeting endoplasmic reticulum stress in insulin resistance. *Trends in endocrinology and metabolism: TEM* 26: 438-448
- Samuel VT, Shulman GI (2016) The pathogenesis of insulin resistance: integrating signaling pathways and substrate flux. *The Journal of clinical investigation* 126: 12-22
- Sano S, Inoue S, Tanabe Y, Sumiya C, Koike S (1959) Significance of Mitochondria for Porphyrin and Heme Biosynthesis. *Science* 129: 275
- Santel A, Fuller MT (2001) Control of mitochondrial morphology by a human mitofusin. *Journal of Cell Science* 114: 867
- Schmitt JM, Stork PJ (2002) PKA phosphorylation of Src mediates cAMP's inhibition of cell growth via Rap1. *Mol Cell* 9: 85-94
- Schrader M (2006) Shared components of mitochondrial and peroxisomal division. *Biochimica et biophysica acta* 1763: 531-541
- Schrader M, Yoon Y (2007) Mitochondria and peroxisomes: are the 'big brother' and the 'little sister' closer than assumed? *BioEssays : news and reviews in molecular, cellular and developmental biology* 29: 1105-1114
- Sebastián D, Hernández-Alvarez MI, Segalés J, Sorianello E, Muñoz JP, Sala D, Waget A, Liesa M, Paz JC, Gopalacharyulu P *et al* (2012) Mitofusin 2 (Mfn2) links mitochondrial and endoplasmic reticulum function with insulin signaling and is essential for normal glucose homeostasis. *Proc Natl Acad Sci U S A* 109: 5523-5528

- Segalés J, Paz JC, Hernández-Alvarez MI, Sala D, Muñoz JP, Noguera E, Pich S, Palacín M, Enríquez JA, Zorzano A (2013) A form of mitofusin 2 (Mfn2) lacking the transmembrane domains and the COOH-terminal end stimulates metabolism in muscle and liver cells. *American journal of physiology Endocrinology and metabolism* 305: E1208-1221
- Sehrawat A, Samanta SK, Hahm E-R, St Croix C, Watkins S, Singh SV (2019) Withaferin A-mediated apoptosis in breast cancer cells is associated with alterations in mitochondrial dynamics. *Mitochondrion* 47: 282-293
- Serasinghe MN, Chipuk JE (2017) Mitochondrial Fission in Human Diseases. *Handbook of experimental pharmacology* 240: 159-188
- Serasinghe MN, Wieder SY, Renault TT, Elkholi R, Ascioia JJ, Yao JL, Jabado O, Hoehn K, Kageyama Y, Sesaki H *et al* (2015) Mitochondrial division is requisite to RAS-induced transformation and targeted by oncogenic MAPK pathway inhibitors. *Molecular cell* 57: 521-536
- Sesaki H, Jensen RE (1999) Division versus fusion: Dnm1p and Fzo1p antagonistically regulate mitochondrial shape. *J Cell Biol* 147: 699-706
- Sharma A, Smith HJ, Yao P, Mair WB (2019) Causal roles of mitochondrial dynamics in longevity and healthy aging. *EMBO Rep* 20: e48395
- Sharma BK, Patil M, Satyanarayana A (2014) Negative regulators of brown adipose tissue (BAT)-mediated thermogenesis. *J Cell Physiol* 229: 1901-1907
- Shields LY, Kim H, Zhu L, Haddad D, Berthet A, Pathak D, Lam M, Ponnusamy R, Diaz-Ramirez LG, Gill TM *et al* (2015) Dynamin-related protein 1 is required for normal mitochondrial bioenergetic and synaptic function in CA1 hippocampal neurons. *Cell death & disease* 6: e1725
- Shimobayashi M, Albert V, Woelnerhanssen B, Frei IC, Weissenberger D, Meyer-Gerspach AC, Clement N, Moes S, Colombi M, Meier JA *et al* (2018) Insulin resistance causes inflammation in adipose tissue. *The Journal of clinical investigation* 128: 1538-1550
- Siekevitz P (1957) Powerhouse of the Cell. *Scientific American* 197: 131-144
- Simcox J, Geoghegan G, Maschek JA, Bensard CL, Pasquali M, Miao R, Lee S, Jiang L, Huck I, Kershaw EE *et al* (2017) Global Analysis of Plasma Lipids Identifies Liver-Derived Acylcarnitines as a Fuel Source for Brown Fat Thermogenesis. *Cell metabolism* 26: 509-522.e506
- Simonson DC, DeFronzo RA (1990) Indirect calorimetry: methodological and interpretative problems. *The American journal of physiology* 258: E399-412
- Sjostrand FS (1953) Electron microscopy of mitochondria and cytoplasmic double membranes. *Nature* 171: 30-32
- Smirnova E, Griparic L, Shurland DL, van der Bliek AM (2001) Dynamin-related protein Drp1 is required for mitochondrial division in mammalian cells. *Mol Biol Cell* 12: 2245-2256
- Smirnova E, Shurland D-L, Ryazantsev SN, van der Bliek AM (1998) A Human Dynamin-related Protein Controls the Distribution of Mitochondria. *Journal of Cell Biology* 143: 351-358
- Smith G, Gallo G (2017) To mdivi-1 or not to mdivi-1: Is that the question? *Developmental neurobiology* 77: 1260-1268

- Song Z, Chen H, Fiket M, Alexander C, Chan DC (2007) OPA1 processing controls mitochondrial fusion and is regulated by mRNA splicing, membrane potential, and Yme1L. *J Cell Biol* 178: 749-755
- Soto-Heredero G, Baixauli F, Mittelbrunn M (2017) Interorganelle Communication between Mitochondria and the Endolysosomal System. *Front Cell Dev Biol* 5: 95-95
- Stojanovski D, Koutsopoulos OS, Okamoto K, Ryan MT (2004) Levels of human Fis1 at the mitochondrial outer membrane regulate mitochondrial morphology. *J Cell Sci* 117: 1201-1210
- Strack S, Wilson TJ, Cribbs JT (2013) Cyclin-dependent kinases regulate splice-specific targeting of dynamin-related protein 1 to microtubules. *J Cell Biol* 201: 1037-1051
- Strauss M, Hofhaus G, Schröder RR, Kühlbrandt W (2008) Dimer ribbons of ATP synthase shape the inner mitochondrial membrane. *EMBO J* 27: 1154-1160
- Sugiura A, Mattie S, Prudent J, McBride HM (2017) Newly born peroxisomes are a hybrid of mitochondrial and ER-derived pre-peroxisomes. *Nature* 542: 251-254
- Suomalainen A (2013) Fibroblast growth factor 21: a novel biomarker for human muscle-manifesting mitochondrial disorders. *Expert Opinion on Medical Diagnostics* 7: 313-317
- Suzuki M, Jeong SY, Karbowski M, Youle RJ, Tjandra N (2003) The solution structure of human mitochondria fission protein Fis1 reveals a novel TPR-like helix bundle. *Journal of molecular biology* 334: 445-458
- Taguchi N, Ishihara N, Jofuku A, Oka T, Mihara K (2007) Mitotic phosphorylation of dynamin-related GTPase Drp1 participates in mitochondrial fission. *The Journal of biological chemistry* 282: 11521-11529
- Tanaka A, Kobayashi S, Fujiki Y (2006) Peroxisome division is impaired in a CHO cell mutant with an inactivating point-mutation in dynamin-like protein 1 gene. *Experimental cell research* 312: 1671-1684
- Tanaka H, Okazaki T, Aoyama S, Yokota M, Koike M, Okada Y, Fujiki Y, Gotoh Y (2019) Peroxisomes control mitochondrial dynamics and the mitochondrion-dependent apoptosis pathway. *Journal of Cell Science* 132: jcs224766
- Tezze C, Romanello V, Desbats MA, Fadini GP, Albiero M, Favaro G, Ciciliot S, Soriano ME, Morbidoni V, Cerqua C *et al* (2017) Age-Associated Loss of OPA1 in Muscle Impacts Muscle Mass, Metabolic Homeostasis, Systemic Inflammation, and Epithelial Senescence. *Cell metabolism* 25: 1374-1389.e1376
- Thiery JP, Acloque H, Huang RYJ, Nieto MA (2009) Epithelial-Mesenchymal Transitions in Development and Disease. *Cell* 139: 871-890
- Thiselton DL, Alexander C, Taanman J-W, Brooks S, Rosenberg T, Eiberg H, Andreasson S, Van Regemorter N, Munier FL, Moore AT *et al* (2002) A Comprehensive Survey of Mutations in the OPA1 Gene in Patients with Autosomal Dominant Optic Atrophy. *Investigative Ophthalmology & Visual Science* 43: 1715-1724
- Tian XY, Ganeshan K, Hong C, Nguyen KD, Qiu Y, Kim J, Tangirala RK, Tontonoz P, Chawla A (2016) Thermoneutral Housing Accelerates Metabolic Inflammation to Potentiate Atherosclerosis but Not Insulin Resistance. *Cell metabolism* 23: 165-178
- Tilokani L, Nagashima S, Paupe V, Prudent J (2018) Mitochondrial dynamics: overview of molecular mechanisms. *Essays in biochemistry* 62: 341-360

- Todd DJ, Lee AH, Glimcher LH (2008) The endoplasmic reticulum stress response in immunity and autoimmunity. *Nature reviews Immunology* 8: 663-674
- Tondera D, Santel A, Schwarzer R, Dames S, Giese K, Klippel A, Kaufmann J (2004) Knockdown of MTP18, a novel phosphatidylinositol 3-kinase-dependent protein, affects mitochondrial morphology and induces apoptosis. *The Journal of biological chemistry* 279: 31544-31555
- Touvier T, De Palma C, Rigamonti E, Scagliola A, Incerti E, Mazelin L, Thomas JL, D'Antonio M, Politi L, Schaeffer L *et al* (2015) Muscle-specific Drp1 overexpression impairs skeletal muscle growth via translational attenuation. *Cell death & disease* 6: e1663-e1663
- Trotta AP, Chipuk JE (2017) Mitochondrial dynamics as regulators of cancer biology. *Cell Mol Life Sci* 74: 1999-2017
- Twig G, Elorza A, Molina AJA, Mohamed H, Wikstrom JD, Walzer G, Stiles L, Haigh SE, Katz S, Las G *et al* (2008) Fission and selective fusion govern mitochondrial segregation and elimination by autophagy. *EMBO J* 27: 433-446
- Twig G, Shirihai OS (2011) The Interplay Between Mitochondrial Dynamics and Mitophagy. *Antioxidants & redox signaling* 14: 1939-1951
- Uchida K, Shiuchi T, Inada H, Minokoshi Y, Tominaga M (2010) Metabolic adaptation of mice in a cool environment. *Pflugers Archiv : European journal of physiology* 459: 765-774
- Vafai SB, Mootha VK (2012) Mitochondrial disorders as windows into an ancient organelle. *Nature* 491: 374-383
- Valente AJ, Maddalena LA, Robb EL, Moradi F, Stuart JA (2017) A simple ImageJ macro tool for analyzing mitochondrial network morphology in mammalian cell culture. *Acta histochemica* 119: 315-326
- Valera-Alberni M, Canto C (2018) Mitochondrial stress management: a dynamic journey. *Cell Stress* 2: 253-274
- Verhoeven K, Claeys KG, Züchner S, Schröder JM, Weis J, Ceuterick C, Jordanova A, Nelis E, De Vriendt E, Van Hul M *et al* (2006) MFN2 mutation distribution and genotype/phenotype correlation in Charcot-Marie-Tooth type 2. *Brain : a journal of neurology* 129: 2093-2102
- Verstreken P, Ly CV, Venken KJT, Koh T-W, Zhou Y, Bellen HJ (2005) Synaptic Mitochondria Are Critical for Mobilization of Reserve Pool Vesicles at Drosophila Neuromuscular Junctions. *Neuron* 47: 365-378
- Virtue S, Vidal-Puig A (2013) Assessment of brown adipose tissue function. *Front Physiol* 4: 128
- von Eyss B, Jaenicke LA, Kortlever RM, Royla N, Wiese KE, Letschert S, McDuffus LA, Sauer M, Rosenwald A, Evan GI *et al* (2015) A MYC-Driven Change in Mitochondrial Dynamics Limits YAP/TAZ Function in Mammary Epithelial Cells and Breast Cancer. *Cancer cell* 28: 743-757
- Wakabayashi J, Zhang Z, Wakabayashi N, Tamura Y, Fukaya M, Kensler TW, Iijima M, Sesaki H (2009) The dynamin-related GTPase Drp1 is required for embryonic and brain development in mice. *J Cell Biol* 186: 805-816
- Walter P, Ron D (2011) The Unfolded Protein Response: From Stress Pathway to Homeostatic Regulation. *Science* 334: 1081-1086
- Wang CY, Liao JK (2012) A mouse model of diet-induced obesity and insulin resistance. *Methods in molecular biology (Clifton, NJ)* 821: 421-433

- Wang H, Song P, Du L, Tian W, Yue W, Liu M, Li D, Wang B, Zhu Y, Cao C *et al* (2011) Parkin ubiquitinates Drp1 for proteasome-dependent degradation: implication of dysregulated mitochondrial dynamics in Parkinson disease. *The Journal of biological chemistry* 286: 11649-11658
- Wang K, Long B, Jiao JQ, Wang JX, Liu JP, Li Q, Li PF (2012a) miR-484 regulates mitochondrial network through targeting Fis1. *Nat Commun* 3: 781
- Wang L, Ishihara T, Ibayashi Y, Tatsushima K, Setoyama D, Hanada Y, Takeichi Y, Sakamoto S, Yokota S, Mihara K *et al* (2015) Disruption of mitochondrial fission in the liver protects mice from diet-induced obesity and metabolic deterioration. *Diabetologia* 58: 2371-2380
- Wang W, Wang Y, Long J, Wang J, Haudek SB, Overbeek P, Chang BH, Schumacker PT, Danesh FR (2012b) Mitochondrial fission triggered by hyperglycemia is mediated by ROCK1 activation in podocytes and endothelial cells. *Cell metabolism* 15: 186-200
- Warburg O (1925) The Metabolism of Carcinoma Cells. *The Journal of Cancer Research* 9: 148
- Waterham HR, Koster J, van Roermund CW, Mooyer PA, Wanders RJ, Leonard JV (2007) A lethal defect of mitochondrial and peroxisomal fission. *The New England journal of medicine* 356: 1736-1741
- Weidling I, Swerdlow RH (2019) Mitochondrial Dysfunction and Stress Responses in Alzheimer's Disease. *Biology* 8
- White JD, Dewal RS, Stanford KI (2019) The beneficial effects of brown adipose tissue transplantation. *Molecular Aspects of Medicine* 68: 74-81
- Whitley BN, Lam C, Cui H, Haude K, Bai R, Escobar L, Hamilton A, Brady L, Tarnopolsky MA, Dengle L *et al* (2018) Aberrant Drp1-mediated mitochondrial division presents in humans with variable outcomes. *Human molecular genetics* 27: 3710-3719
- Wieder SY, Serasinghe MN, Sung JC, Choi DC, Birge MB, Yao JL, Bernstein E, Celebi JT, Chipuk JE (2015) Activation of the Mitochondrial Fragmentation Protein DRP1 Correlates with BRAF(V600E) Melanoma. *J Invest Dermatol* 135: 2544-2547
- Wikstrom JD, Mahdavian K, Liesa M, Sereda SB, Si Y, Las G, Twig G, Petrovic N, Zingaretti C, Graham A *et al* (2014) Hormone-induced mitochondrial fission is utilized by brown adipocytes as an amplification pathway for energy expenditure. *EMBO J* 33: 418-436
- Wong YC, Kim S, Peng W, Krainc D (2019) Regulation and Function of Mitochondria-Lysosome Membrane Contact Sites in Cellular Homeostasis. *Trends in Cell Biology* 29: 500-513
- Woods A, Johnstone SR, Dickerson K, Leiper FC, Fryer LGD, Neumann D, Schlattner U, Wallimann T, Carlson M, Carling D (2003) LKB1 Is the Upstream Kinase in the AMP-Activated Protein Kinase Cascade. *Current Biology* 13: 2004-2008
- Wu L, Zhang L, Li B, Jiang H, Duan Y, Xie Z, Shuai L, Li J, Li J (2018) AMP-Activated Protein Kinase (AMPK) Regulates Energy Metabolism through Modulating Thermogenesis in Adipose Tissue. *Front Physiol* 9
- Wu MJ, Chen YS, Kim MR, Chang CC, Gampala S, Zhang Y, Wang Y, Chang CY, Yang JY, Chang CJ (2019) Epithelial-Mesenchymal Transition Directs Stem Cell Polarity via Regulation of Mitofusin. *Cell metabolism* 29: 993-1002.e1006
- Wu Y, Zhou D, Xu X, Zhao X, Huang P, Zhou X, Song W, Guo H, Wang W, Zheng S (2016) Clinical significance of mitofusin-2 and its signaling pathways in hepatocellular carcinoma. *World Journal of Surgical Oncology* 14: 179

- Xiao G, Zhang T, Yu S, Lee S, Calabuig-Navarro V, Yamauchi J, Ringquist S, Dong HH (2013) ATF4 Protein Deficiency Protects against High Fructose-induced Hypertriglyceridemia in Mice. *Journal of Biological Chemistry* 288: 25350-25361
- Xie Q, Wu Q, Horbinski CM, Flavahan WA, Yang K, Zhou W, Dombrowski SM, Huang Z, Fang X, Shi Y *et al* (2015) Mitochondrial control by DRP1 in brain tumor initiating cells. *Nature neuroscience* 18: 501-510
- Xu K, Chen G, Li X, Wu X, Chang Z, Xu J, Zhu Y, Yin P, Liang X, Dong L (2017) MFN2 suppresses cancer progression through inhibition of mTORC2/Akt signaling. *Scientific Reports* 7: 41718
- Xu S, Wang P, Zhang H, Gong G, Gutierrez Cortes N, Zhu W, Yoon Y, Tian R, Wang W (2016) CaMKII induces permeability transition through Drp1 phosphorylation during chronic β -AR stimulation. *Nature Communications* 7: 13189
- Yan J, Liu XH, Han MZ, Wang YM, Sun XL, Yu N, Li T, Su B, Chen ZY (2015) Blockage of GSK3 β -mediated Drp1 phosphorylation provides neuroprotection in neuronal and mouse models of Alzheimer's disease. *Neurobiology of aging* 36: 211-227
- Yang J, Nie J, Ma X, Wei Y, Peng Y, Wei X (2019) Targeting PI3K in cancer: mechanisms and advances in clinical trials. *Molecular Cancer* 18: 26
- Yang X, Coulombe-Huntington J, Kang S, Sheynkman GM, Hao T, Richardson A, Sun S, Yang F, Shen YA, Murray RR *et al* (2016) Widespread Expansion of Protein Interaction Capabilities by Alternative Splicing. *Cell* 164: 805-817
- Yonashiro R, Ishido S, Kyo S, Fukuda T, Goto E, Matsuki Y, Ohmura-Hoshino M, Sada K, Hotta H, Yamamura H *et al* (2006) A novel mitochondrial ubiquitin ligase plays a critical role in mitochondrial dynamics. *EMBO J* 25: 3618-3626
- Yoon Y, Krueger EW, Oswald BJ, McNiven MA (2003) The Mitochondrial Protein hFis1 Regulates Mitochondrial Fission in Mammalian Cells through an Interaction with the Dynamin-Like Protein DLP1. *Molecular and cellular biology* 23: 5409
- Yoon Y, Pitts KR, Dahan S, McNiven MA (1998) A Novel Dynamin-like Protein Associates with Cytoplasmic Vesicles and Tubules of the Endoplasmic Reticulum in Mammalian Cells. *Journal of Cell Biology* 140: 779-793
- Yoon Y, Pitts KR, McNiven MA (2001) Mammalian Dynamin-like Protein DLP1 Tubulates Membranes. *Mol Biol Cell* 12: 2894-2905
- Yu R, Jin SB, Lendahl U, Nistér M, Zhao J (2019a) Human Fis1 regulates mitochondrial dynamics through inhibition of the fusion machinery. *EMBO J* 38
- Yu R, Liu T, Ning C, Tan F, Jin S-B, Lendahl U, Zhao J, Nistér M (2019b) The phosphorylation status of Ser-637 in dynamin-related protein 1 (Drp1) does not determine Drp1 recruitment to mitochondria. *Journal of Biological Chemistry* 294: 17262-17277
- Yu T, Fox RJ, Burwell LS, Yoon Y (2005) Regulation of mitochondrial fission and apoptosis by the mitochondrial outer membrane protein hFis1. *J Cell Sci* 118: 4141-4151
- Zaja I, Bai X, Liu Y, Kikuchi C, Dosenovic S, Yan Y, Canfield SG, Bosnjak ZJ (2014) Cdk1, PKC δ and calcineurin-mediated Drp1 pathway contributes to mitochondrial fission-induced cardiomyocyte death. *Biochemical and biophysical research communications* 453: 710-721
- Zhang K, Li H, Song Z (2014) Membrane depolarization activates the mitochondrial protease OMA1 by stimulating self-cleavage. *EMBO Rep* 15: 576-585

- Zhang Z, Li T-E, Chen M, Xu D, Zhu Y, Hu B-Y, Lin Z-F, Pan J-J, Wang X, Wu C *et al* (2020) MFN1-dependent alteration of mitochondrial dynamics drives hepatocellular carcinoma metastasis by glucose metabolic reprogramming. *British Journal of Cancer* 122: 209-220
- Zhang Z, Liu L, Jiang X, Zhai S, Xing D (2016) The Essential Role of Drp1 and Its Regulation by S-Nitrosylation of Parkin in Dopaminergic Neurodegeneration: Implications for Parkinson's Disease. *Antioxidants & redox signaling* 25: 609-622
- Zhao J, Liu T, Jin S, Wang X, Qu M, Uhlén P, Tomilin N, Shupliakov O, Lendahl U, Nistér M (2011) Human MIEF1 recruits Drp1 to mitochondrial outer membranes and promotes mitochondrial fusion rather than fission. *EMBO J* 30: 2762-2778
- Zhao J, Zhang J, Yu M, Xie Y, Huang Y, Wolff DW, Abel PW, Tu Y (2013) Mitochondrial dynamics regulates migration and invasion of breast cancer cells. *Oncogene* 32: 4814-4824
- Zhu PP, Patterson A, Stadler J, Seeburg DP, Sheng M, Blackstone C (2004) Intra- and intermolecular domain interactions of the C-terminal GTPase effector domain of the multimeric dynamin-like GTPase Drp1. *The Journal of biological chemistry* 279: 35967-35974
- Züchner S, Mersiyanova IV, Muglia M, Bissar-Tadmouri N, Rochelle J, Dadali EL, Zappia M, Nelis E, Patitucci A, Senderek J *et al* (2004) Mutations in the mitochondrial GTPase mitofusin 2 cause Charcot-Marie-Tooth neuropathy type 2A. *Nature genetics* 36: 449-451
- Zunino R, Schauss A, Rippstein P, Andrade-Navarro M, McBride HM (2007) The SUMO protease SENP5 is required to maintain mitochondrial morphology and function. *J Cell Sci* 120: 1178-1188

MIRIAM VALERA- ALBERNI

Avenue de Tivoli 70 | 1007 Lausanne, Switzerland | +41 78 681 77 63 | miriam.valeraalberni@epfl.ch

EDUCATION

2016- present PhD in Molecular Life Sciences

PhD program at the École Polytechnique Fédérale de Lausanne (EPFL), Switzerland.

Funded by the EU Marie Skłodowska-Curie ITN *ChroMe* (H2020-MSCA-ITN project number 675610).

2014 - 2015 MSc Biomedicine

University of Barcelona (Spain).

Master specialization on Basic and Translational Cancer Research.

Fully funded by the Condé Nast, SA (GLAMOUR®) scholarship.

2010 –2014 BSc Biotechnology

Polytechnic University of Valencia (Spain).

Within the Advanced Performance Group (ARA).

Supported by Ramón Areces Foundation Scholarship.

COMPETENCES

Molecular and Biochemical techniques

- Molecular biology : DNA/ RNA isolation, RT-PCR and quantitative PCR, DNA amplification.
- Cell Biology : cell culture, cell transfection, cell-based assays. Mitochondrial isolation.
- Biochemistry: Western Blotting, enzymatic activity assays, ELISA, co-immunoprecipitation and binding assays (GST pull-down). Protein purification, liquid / gas chromatography.

Microscopy

- Immunofluorescence microscopy, live-imaging. Image analysis (Fiji).
- Microscopes: Zeiss AxioObserver Z1 confocal spinning-disk, Zeiss AxioImager 2, Leica TCS SP8 STED.

Animal experimentation

- Mouse genetic models: colony management, tissue dissection, injections (IP, SC).
- Metabolic assays: glucose tolerance test (GTT), insulin tolerance test (ITT), treadmill, cold test, indirect calorimetry, EchoMRI. Thermoneutrality.
- Tissue analysis: histology, immunohistochemistry, high-resolution respirometry (Oroboros).
- Primary cultures: adipocytes, muscle cells, hepatocytes, mammary glands.

Computational skills

- Statistics and data analysis: R studio. Graph Pad prism. Fiji.

Personal competences

- Highly motivated, team player, extremely organized. Ability to work independently or in a team.

RESEARCH EXPERIENCE

Sept. 2016 – Sept. 2020 **PhD student**, with Dr. Carles Cantó.

- Nestlé Institute of Health Sciences, Switzerland. Cell Biology department.
- Project: Impact of mitochondrial dynamics on metabolic adaptation through the study of Drp1.

Research internship within the PhD in the groups of:

- Dr. Oscar Yanes. Universitat Rovira i Virgili (Reus, Spain). To perform metabolomic analyses from mouse tissues. November 2018 – February 2019.
- Prof. Andreas Ladurner. Ludwig Maximilian University (Munich, Germany). To perform live-imaging experiments on mammalian cells. June 2019 – August 2019.

Sept. 2015 – June 2016 **Visiting Graduate Research Assistant**, with Dr. Martin Jechlinger.

- European Molecular Biology Laboratory (EMBL) Heidelberg. Cell Biology and Biophysics Unit.
- Project: Mechanisms of oncogene dependence and tumor relapse in breast cancer.

June 2015 – August 2015 **Research and Practical Training Program**, with Dr. Min-Liang Kuo.

- National Taiwan Hospital – College of Medicine. Cancer Stem Cell Core.
- Project: Analysis of the effect of IL-33 on a model of lung cancer metastasis.

Nov. 2014 – June 2015 **Master Thesis Project**, with Dr. Angel R. Nebreda.

- Institute for Research in Biomedicine (IRB Barcelona). Oncology; Signaling and Cell Cycle Laboratory.
- Project: Study of the mechanisms of p38 MAPK signaling and its use as a molecular target.

July 2014 – Sept. 2014 **AECC Foundation Scholarship**, with Dr. Isidro Machado.

- Valencian Institute of Oncology (IVO) hospital. Department of Anatomical Pathology.
- Project: Histological, morphometric and immunohistochemical study of prediction factors of lymph node metastasis in colorectal cancer stage pT1.

Sept. 2013 – June 2014 **Bachelor Thesis Project**, with Dr. Jerónimo Bravo.

- Valencian Institute of Biomedicine (IBV-CSIC). Signal Transduction Unit.
- Project: Characterization of the interaction between human K-Ras and Raf1 by liquid chromatography, ITC and crystallization methods.

June 2012 – August 2012 **Research Assistant**, with Dr. Deborah Burks.

- Príncipe Felipe Research Center (CIPF). Molecular Endocrinology group.
- Project: Research in diabetes and metabolic diseases: culture and analysis of islets of Langerhans from IRS2 deficient mice.

Sept. 2010 – August 2012 **Research Assistant**, with Dr. Ana María Pérez de Castro.

- Institute for Conservation and Improvement of Agrobiodiversity. Biotechnology department.
- Projects: 'Marker-assisted selection of tomato plants carrying genes conferring resistance to viral diseases' (2010- 2011) and 'Evaluating the utility of a scale of lines with resistance to Tomato Yellow Leaf Curl Disease (TYLCD)' (2011-2012).

TEACHING EXPERIENCE

- BIO-203 Integrated laboratory in Life sciences I (2nd year Bachelor, 2017/2018).
- BIO-204 Integrated laboratory in Life sciences II (2nd year Bachelor, 2016/2017, 2017/2018).
- BIOENG-433 Biotechnology Laboratory (2nd year Master, 2017/2018).

PUBLICATIONS

1. **Valera-Alberni M**, Joffraud M, Miro-Blanch J, *et al.* (2020). Crosstalk of Drp1 phosphorylation sites on mitochondrial dynamics and metabolic adaptation. *Under submission process*.
2. Sambeat A, Ratajczak J, Joffraud M, Sanchez-Garcia JL, Giner MP, Valsesia A, Giroud-Gerbetant J, **Valera-Alberni M**, Cercillieux A, Boutant M, Kulkarni SS, Moco S, Canto C. (2019) Endogenous nicotinamide riboside metabolism protects against diet-induced liver damage. *Nat Commun.*; 10(1):4291. doi: 10.1038/s41467-019-12262-x.
3. Sardon Puig, L.*, **Valera-Alberni, M.***, Cantó, C., & Pilon, N. J. (2018). Circadian Rhythms and Mitochondria: Connecting the Dots. *Frontiers in genetics*; 9, 452. doi:10.3389/fgene.2018.00452
*These authors contributed equally to this work.
4. **Valera-Alberni M** and Canto C (2018). Mitochondrial stress management: a dynamic journey. *Cell Stress*; 2(10): 253 - 274; doi: 10.15698/cst2018.10.158.
5. Boutant M, Kulkarni SS, Joffraud M, Ratajczak J, **Valera-Alberni M**, Combe R, Zorzano A, Cantó C. (2017) Mfn2 is critical for brown adipose tissue thermogenic function. *EMBO J*; 36(11):1543-1558. doi: 10.15252/embj.201694914.
6. Machado I*, **Valera-Alberni M***, Martínez de Juan F, *et al.* (2016). Histological factors predicting loco-regional lymph node metastasis in early invasive colorectal adenocarcinoma pT1. *Gastroenterol Hepatol*; 39(1):1-8. doi: 10.1016/j.gastrohep.2015.04.006.
*These authors contributed equally to this work.

PARTICIPATION IN SCIENTIFIC CONFERENCES

- **Short talk (virtual) | WebCam seminars**. 3 June 2020.
- **Short talk (virtual) | Aging Science Talks**. 24 April 2020.
- **Poster | EMBL Symposia: Metabolism meets Epigenetics**, Heidelberg, Germany. 20-23 Nov 2019.
- **Short talk | MitoChats Symposium**, Cologne, Germany. 11-12 July 2019.
- Local **organizer** at the **12th LIMNA symposium**. University Hospital of Lausanne. 12 April 2019.
- **Poster | LIMNA Symposium: Regulation of Metabolism and Feeding**, Lausanne. 8 Nov 2018.
- **Short talk | 9th World Congress on Targeting Mitochondria**, Berlin, Germany. 23-25 Oct 2018.
- **Poster | Summer School on Chromatin and Metabolism**, Spetses, Greece. 25-31 August 2018.
- **Poster | Frontiers in Metabolism Symposium**, Lausanne, Switzerland. 24-26 October 2017.
- **Poster | LIMNA Symposium: Metabolism Research**, Lausanne, Switzerland. 1 June 2017.

Complementary skills

- Certificate of attendance on the course *Communication and Management by Leadership Sculptor®* (54 training hours). Topics included Project Management, Critical Thinking or Emotional Intelligence.
- Personal interests: baking, hiking. Science communication and public outreach:
 - Member of the Voice of Young Science (VoYS).
 - Board member at the Bioscience Network Lausanne (2019-2020).
 - Organizer of the 1st Edition of *Pint of Science* Lausanne (2019).